PhD degree in Systems Medicine (curriculum in Molecular Oncology)

European School of Molecular Medicine (SEMM),

University of Milan and University of Naples "Federico II"

Settore disciplinare: BIO/10

Functional characterization of myosin VI in centrosome biology and cell cycle progression

Elisa Magistrati

IFOM, Milan

Matricola n. R11125

Supervisor: Dr. Simona Polo

IFOM, Milan

Anno accademico 2017/2018

Table of contents

List of abbreviations

3HB	Three helix bundle
AMSH-LP	AMSH-like protein
APC/C	Anaphase promoting complex
BrdU	Bromodeoxyuridine
CaM	Calmodulin
CBD	Cargo binding domain
CC	Coiled coil
CDK	Cyclin-dependent kinase
CFTR	Cystic fibrosis transmembrane conductance regulator
CHK	Checkpoint kinase
CKI	Cyclin kinase inhibitor
CRISPR	Clustered Regularly Interspaced Short Palindromic Repeats
Dab-2	Disabled homolog 2
DDR	DNA damage response
EGFR	Epidermal growth factor receptor
EMT	Epithelial to mesenchymal transition
ER	Endoplasmic reticulum
ESCRT	Endosomal sorting complex required for sorting
EV	Empty vector
FACS	Fluorescence-activated cell sorting
FL	Full length
FUCCI	Fluorescence Ubiquitination Cell Cycle Indicator
G.I.	Gini Index
GFP	Green fluorescence protein
GIPC	GAIP-interacting protein C-terminus
GST	Glutathione S-transferase
γTuRC	γ-Tubulin ring complex
H3K9me	Histone H3 lysine 9 methylation
IF	Immunofluorescence
IP	Immunoprecipitation
KD	Knock down
kDa	Kilodalton
LATS2	Large tumor suppressor kinase 2
LI	Large insert
LIR	LC3-interacting region
LMTK2	lemur tyrosine kinase-2
MAPK	Mitogen-activated protein kinase
Me-OH	Methanol
MIU	Motif interacting with ubiquitin
MS	Mass spectrometry
MTOC	Microtubule organizing center
MyUb	Myosin VI ubiquitin binding
NDP52	Nuclear dot protein 52

NGS	Next generation sequencing
Nlp	Ninein-like protein
OFD1	Oral-facial-digital syndrome 1
ORF	Open reading frame
OSE	Ovarian surface epithelium
PCM	Pericentriolar material
PCR	Polymerase chain reaction
PFA	Paraformaldehyde
PI(4,5)P2	Phosphatidylinositol 4,5-bisphosphate
Plk	Polo-like kinase
RhoA	Ras homolog gene family, member A
RNAPII	RNA polymerase II
RPE1	Retinal pigmented epithelial cells
SA-β-gal	Senescence-associated β-galactosidase
SAH	Single alpha helix
SAHF	Senescence-associated heterochromatic foci
SAS-6	Spindle assembly abnormal protein 6 homolog
SASP	Senescence-associated secretory phenotype
SDS-PAGE	Sodium Dodecyl Sulphate – PolyAcrylamide Gel Electrophoresis
SEAP	Soluble form of alkaline phosphatase
sgRNA	Single guide RNA
shRNA	Short hairpin RNA
SI	Small insert
siRNA	Short interfering RNA
STIL	SCL-interrupting locus protein
sv	Snell's Waltzer
T6BP	Traf-6 binding protein
TCGA	The Cancer Genome Atlas
TEM	Transmission electron microscopy
TGN	Trans Golgi network
TP53	Tumor suppressor gene p53
UTR	Untranslated region
WB	Western blot
WT	Wild type
YAP	Yes-associated protein

Figure index

Table index

Abstract

Myosin VI is a unique actin motor involved in multiple biological functions, such as endocytic and secretion processes, cell migration, autophagy, and in the maintenance of the Golgi complex and stereocilia. These functions are dictated by the interaction of myosin VI with different cargos, which can also regulate the ability of this protein to work as an anchor or a motor that moves along actin filaments.

Previous experiments performed in our laboratory led to the identification of a novel set of myosin VI interactors that belong to the centrosome compartment, suggesting that myosin VI could have an important and unexpected role in centrosomal processes. Therefore, in this thesis, we characterize a novel role for myosin VI in the maintenance of centrosome structure and functions, using hTERT-RPE1 cells as a model system. We found that myosin VI localizes at the centrosome, and that its depletion leads to centrosomal alterations, namely centriole amplification, separation and random orientation, leaving the ultrastructure of the centrioles unaffected. Furthermore, based on our findings, we suggest a new role for myosin VI in the maintenance of the correct positioning of the centrosome in the cell, which is usually linked to the nuclear membrane. At the molecular level, myosin VI interacts with OFD1, a centrosome and centriolar satellite protein that is important for primary cilium formation. The interaction between myosin VI and OFD1 appears to have a functional relevance as myosin VI depletion leads to the delocalization of OFD1, a reduction in the number of the centriolar satellites and defects in primary cilia formation.

In addition to centrosomal alterations, we found an unanticipated phenotype consisting in cell cycle arrest induced by myosin VI depletion in non-tumor cells. Both siRNA- and shRNA-induced depletion of myosin VI caused the cells to arrest in G0/G1, followed by senescence, due to the activation of the tumor-suppressor p53-p21 axis. Our subsequent

results suggest that the two phenotypes observed in myosin VI-depleted cells are not functionally linked, and that a DNA damage response is not activated in these cells.

To uncover the mechanism that leads to the activation of p53 and cell cycle arrest, we performed a genome-wide CRISPR/Cas9 rescue screening and discovered a potential role, yet to be validated, of the DNA methylase SETDB1 and its binding partner ATF7IP. In addition, we demonstrated that the deubiquitinase AMSH-LP plays a critical role in mediating the cell cycle arrest induced by p53-p21 activation.

Altogether, this study unveils a new role for myosin VI in centrosome biology and in the control of the cell cycle, two processes whose dysregulation is an important step during carcinogenesis.

1. Introduction

1.1. Myosin VI

1.1.1. The myosin superfamily

The cytoskeleton is a highly dynamic structure, which provides structure and organization to the cells. Actin and microtubule filaments act as tracks for the movement of vesicles, organelles and other intracellular components through molecular motors.

The molecular motors that move along the actin cytoskeleton are called myosins. Different phylogenic examination of the myosin classes, based on sequence comparison of the heavy chains, identified 35 classes. In the human genome, 40 myosin genes are present, that belong to 13 classes (Foth et al., 2006; Odronitz and Kollmar, 2007; Richards and Cavalier-Smith, 2005; Woolner and Bement, 2009). Myosin II was the first class to be identified and it has peculiar characteristics that allow it to form bipolar myosin filaments. Myosin II was thus classified as the conventional myosin, while the other classes discovered later were classified as unconventional myosins (Woolner and Bement, 2009). All characterized myosins move toward the plus-end of actin filaments except for myosin VI, which moves in the opposite direction (Wells et al., 1999). Some myosins are capable of dimerizing through a coiled-coil domain. This process is thought to be essential for the processive walking mechanism, which is a characteristic of the myosins that function as intracellular transporters (Hammer and Sellers, 2011).

Myosins are composed of three structurally and functionally different domains that are quite conserved throughout the family. The most conserved region is the motor domain at the N-terminus, which allows the movement of the protein along filaments. The N-terminus is a globular catalytic domain that couples the ATP hydrolysis cycle to the binding and release of actin such that the motor is able to perform mechanical work: with each cycle of ATP hydrolysis, the motor takes one step (Fig. 1) (Hartman and Spudich,

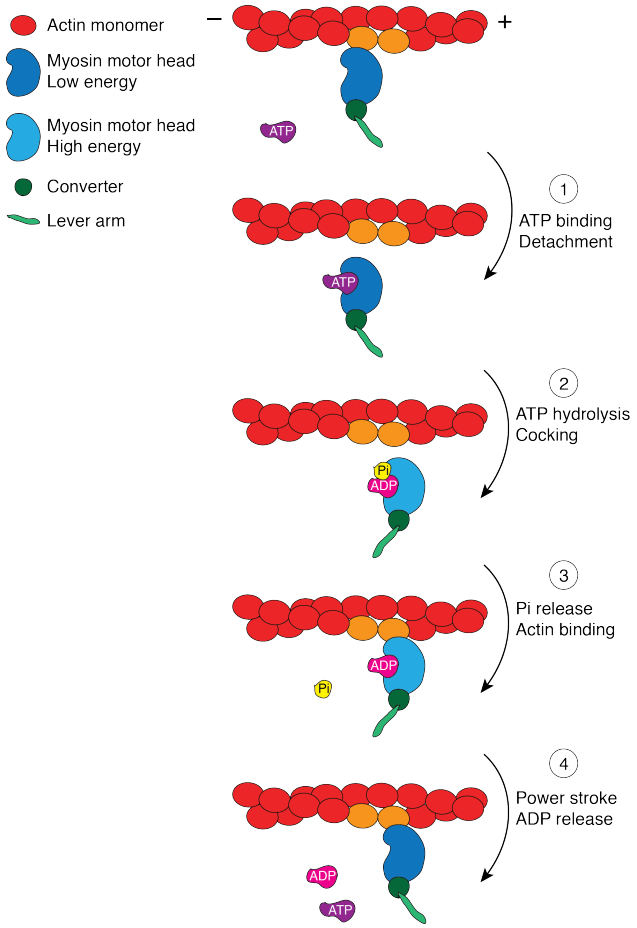

Figure 1: The myosin ATPasic cycle is coupled with its translocation on the actin filament. When the myosin head is not bound to ATP or ADP, it is linked to actin in *rigor* configuration. 1) ATP binding allows the detachment of the motor head from actin. 2) ATP hydrolysis to ADP and Pi leads to a structural rearrangement of the motor, and "cocks" the head in a high energy state. 3) The release of the Pi allows reattachment to actin and causes 4) a conformational change of the head in the tightly bound state, which is transmitted to the rest of the myosin molecule through the converter and the lever arm, thus generating the power stroke required for translocation. Then, ADP is released and the myosin head is ready to bind ATP.

2012). The C-terminal sequence of the motor domain forms a subdomain called converter that plays a role in amplifying the conformational changes that occur in the motor domain and transmitting them to the adjacent region, the lever arm.

The lever arm, also called the neck region, is composed of a variable number of successive consensus motifs, IQ domains, organized in a long α-helical segment. These IQ domains allow the binding of the myosins to myosin light chains, members of the calmodulin (CaM) and CaM-related gene families, which are required for the structural integrity of the myosins and have regulatory functions on their mechanoenzymatic activity (Heissler and Sellers, 2014; Tyska and Warshaw, 2002). The lever arm can tilt during the working stroke of the motor domain, transmitting the movement to the rest of the myosin molecule (Fig. 1). When two myosin molecules dimerize through the tail domain, as described below, the movement of the lever arm allows the reciprocal movement of the two motor heads and, consequently, directed motion. The length of the

lever arm is significantly different among the classes of myosin motors, thus generating different step sizes on the actin filaments (Baboolal et al., 2009; Terrak et al., 2005).

The C-terminal region of the myosin motors, also called tail domain, is the most divergent among the different myosin classes. The C-terminal can contain coiled-coil sequences for dimerization and extended single alpha helix (SAH) domain, followed by a C-terminal globular cargo-binding domain (CBD). The variability of the tail region is given by the presence of a wide variety of domains, which specify the binding to different cargoes (Fig.2).

Thanks to the great variability of the CBD domain and to the wide range of interactors, the different myosins can play various and specific roles in cells. The most obvious function of an actin motor is the intracellular transport of molecules, organelles and vesicles, but only few examples of these transport functions have been ascribed to myosins. In humans, myosin XIX is implicated in the transport of mitochondria in neurons (Quintero et al., 2009), a function that is pursued by myosin V and myosin VI in *Drosophila melanogaster* (Pathak et al., 2010). Some studies also identified a class V myosin-mediated transport in neurons. Within the dendritic spines, myosin Vb is

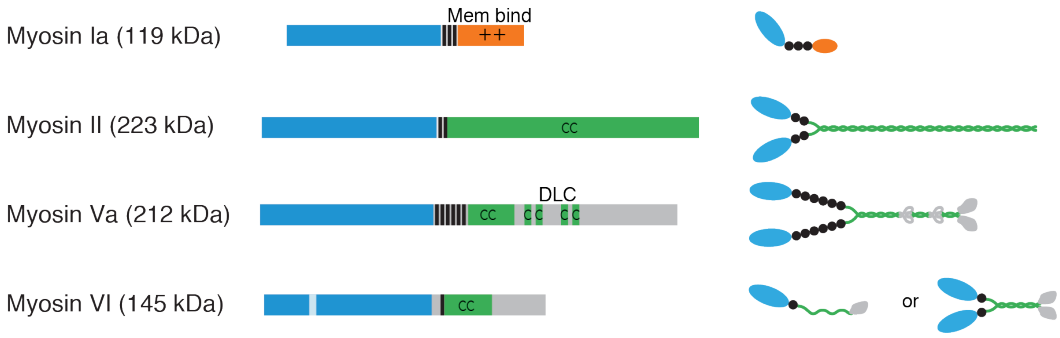

Figure 2: Domain organization of the myosins.

Scheme of the structure of representative myosins. All myosins consist of a motor head domain (blue), a neck region containing IQ motifs for the binding of myosin light chains (black), and a tail domain with coiled-coil regions (CC, green) and membrane/cargo binding domain (positively charged, ++, orange). On the right, the monomer or dimer form of the myosin is shown. DLC, presumptive dynein light chain binding domain. [Adapted from *Krendel and Moosker, Physiology Reviews, 2005*]

responsible for the transport recycling endosome membranes in response to stimulus (Wang et al., 2008), while in Purkinje neurons myosin Va is involved in pulling the ER into the dendritic spines, a process required for synaptic plasticity (Wagner et al., 2011). Furthermore, in yeast, a type V myosin plays a role in the transport of mRNA from the mother cell to the tip of the bud (Takizawa and Vale, 2000).

Myosins can also act as tethers, anchoring molecules or organelles to actin filaments. Myosin Va and Vb can anchor phagosomes and endocytic compartments, respectively, to the cell cortex, opposing the microtubule-directed movement toward the cell center. This tethering function have been proposed to be very dynamic, as the organelles can be released and transported through dynein (Al-Haddad et al., 2001; Provance et al., 2008; Woolner and Bement, 2009). Myosin Va have also been proposed as docking factor for secretory granules and melanosomes at the plasma membrane, to promote their accumulation at the actin-rich cell periphery (Desnos et al., 2007; Wu et al., 1998). Furthermore, it has been suggested that myosin XVIIIA can anchor Golgi membranes, through the Golgi protein GOLPH3, to the actin cytoskeleton, exerting a tensile force required to maintain Golgi structure (Dippold et al., 2009). Indeed, the anchoring function can be coupled to tension sensing: for example, type I myosins are capable of sensing tension and to respond to small loads by increasing their actin-attachment lifetime (Laakso et al., 2008).

A debate is still open about the extent to which myosins act as organelle transporters or dynamic tethers (Hammer and Sellers, 2011). It is worth noting that actin is usually organized as networks, instead of coherent tracks, thus not allowing the persistent movement of organelles. In fact, short-range movements of myosin Va have been identified at the cell cortex (Nelson et al., 2009), suggesting that this kind of movement could be a characteristic of myosin motors.

In addition to exploiting actin filaments for their motor or anchor activities, myosins can also influence the organization of actin itself. This is the case of Myosin I in budding yeast, that can interact with proteins that stimulate the Arp2/3 complex, promoting actin polymerization and thus providing the power for endocytosis (Kaksonen et al., 2006). Moreover, myosin X is capable of promoting F-acting bundling, thus laying a role in filopodia formation (Tokuo et al., 2007; Woolner and Bement, 2009).

1.1.2. The discovery of myosin VI and mouse models

As highlighted above, myosin VI is the only myosin motor which is able to travel towards the minus end of the actin filaments. Myosin VI is ubiquitously expressed in all multicellular eukaryotes, giving the possibility to be studied in several models. Myosin VI was first characterized in *D. melanogaster* (Kellerman and Miller, 1992) and successively identified in *Gallus gallus*, *Sus scrofa* (Hasson and Mooseker, 1994), *Mus musculus* (Avraham. et al., 1995), *Caenrohabditis elegans* (Baker and Titus, 1997) and *Homo sapiens* (Avraham et al., 1997).

Myosin VI was identified as the gene responsible for deafness in Snell's waltzer (*sv*) mice (Avraham. et al., 1995). These mice carry a spontaneous deletion in the myosin VI gene, which generates a frameshift, introducing a stop codon at the beginning of the neck region. This mutation leads to the loss of both inner and outer hair cells within the organ of Corti, which is probably due to the lack of functional stereocilia, that fuse together and lead to hair cell degeneration (Self et al., 1999). The expression of myosin VI is localized within the inner and outer hair cells of the sensory epithelium and, within these cells, it is concentrated at the base of the stereocilia that contain the negative ends of actin filaments (Avraham et al., 1997; Hasson et al., 1997). Furthermore, the *sv* mice show defects in the kidneys, with dilation of the proximal tubule and fibrosis, likely due to a

deficit in protein re-adsorption (Gotoh et al., 2010). Other phenotypes that are associated with myosin VI loss-of-function are disruption in the integrity of the intestinal brush border (Hegan et al., 2012), left ventricular hypertrophy in the heart (Hegan et al., 2015), astrogliosis in the brain and decreased synaptic density in the hippocampus (Osterweil et al., 2005).

In humans, a mutation in the myosin VI motor domain, C442Y, has been found in patients carrying a non-syndromic autosomal dominant form of deafness (Melchionda et al., 2001), and the mutation H246R has been correlated with progressive autosomal dominant sensorineural hearing loss and mild cardiac hypertrophy (Mohiddin et al., 2004), confirming a conserved role for myosin VI in the development of the auditory system.

1.1.3. The structure and mechanical properties of myosin VI

Myosin VI possesses the typical overall structure of the myosin superfamily, with some peculiar characteristics (Fig. 3A).

The motor head domain can interact with actin and ATP, and its ATPase activity is regulated by a region called insert-1 (Pylypenko et al., 2011). The hydrolysis of ATP and release of ADP and Pi cause a conformational change in the head and thus force generation, that are transmitted to the neck region through the converter. The neck region contains a peculiar insert-2, also called the reverse gear (Fig. 3A), which is an unusual CaM-binding site that is able to reposition the lever arm, conferring to myosin VI the ability to reverse the directionality of the movement and to walk towards the minus end of actin filaments (Bryant et al., 2007; Park et al., 2007). Downstream the reverse gear, the lever arm contains a single IQ motif that interacts with a second CaM molecule (Fig. 3A).

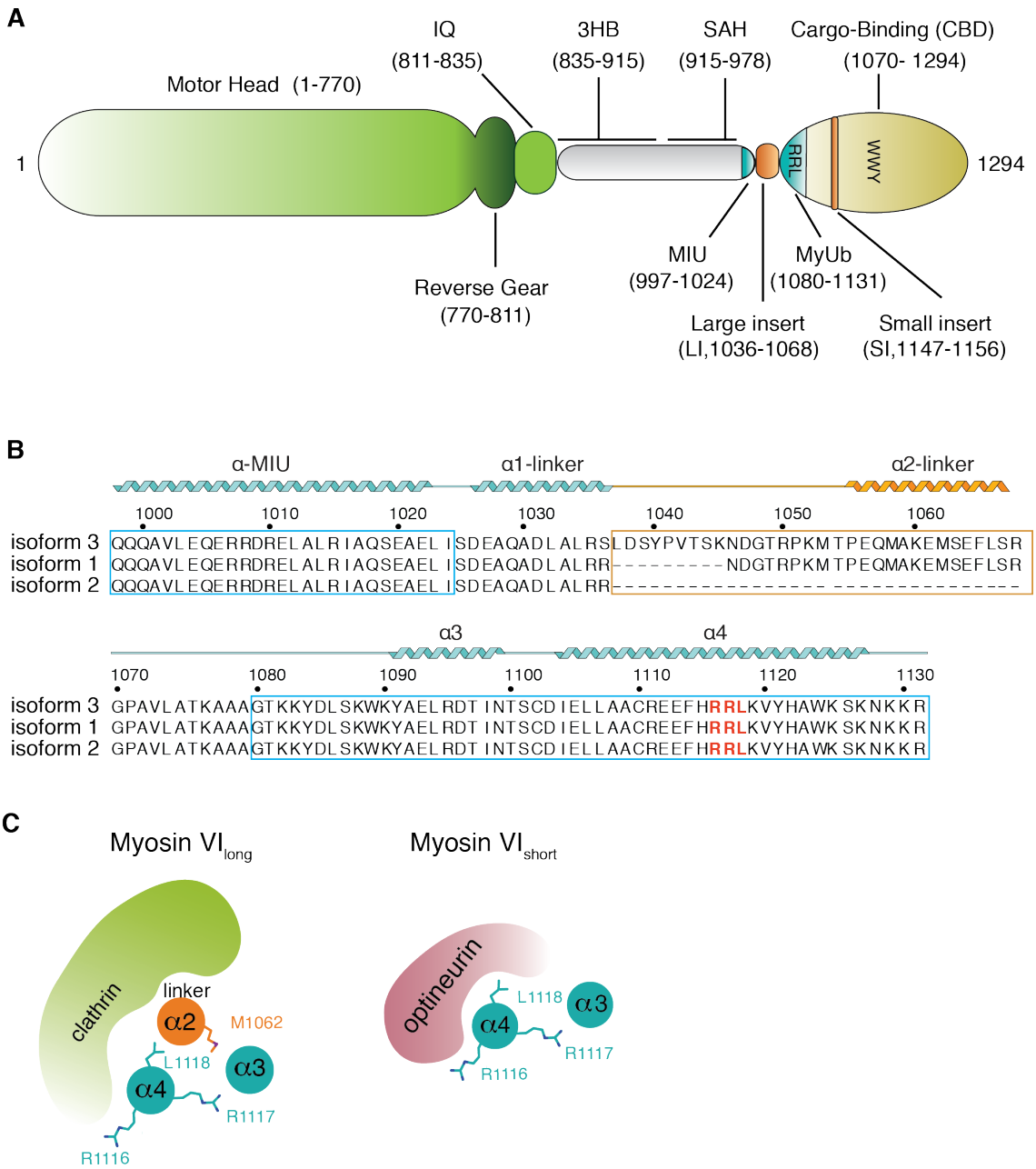

Figure 3: Structure and domain organization of myosin VI.

(A) The different functional subdomains of myosin VI are underlined in the scheme with their respective boundaries. 3HB: three-helix bundle. SAH: single alpha helix. (B) The amino acid sequence alignment of the three myosin VI isoforms is shown, covering the region between MIU and MyUb. The numbering on top of the sequence alignment refers to isoform 3. The RRL motif is highlighted in red; secondary-structure elements are depicted on the top of the sequence. The LI is boxed in orange. The ubiquitin binding domains MIU and MyUb are boxed in blue (C) A representative model of the myosin VI_{long} (left) and myosin VI_{short} (right) conformations, showing the position of the RRL motif, which in myosin VI_{long} is covered by the α2-helix (orange, part of the LI). The interaction of the myosin VI long and short isoforms with clathrin and optineurin, respectively, are reported. [Adapted from *Wollscheid et al., Nature structural and molecular biology, 2016*]

The tail region is the most divergent between myosins, and gives myosin VI some of its unique properties. The proximal part of this region, first predicted as a coiled-coil, in fact is arranged in an extensible three alpha-helix bundle (3HB) (Mukherjea et al., 2009), followed by a long single alpha-helix, namely a SAH domain (Spink et al., 2008) (Fig. 3A).

These two regions could be responsible for the large step size on actin (30-36 nm) that are a peculiar characteristic of myosin VI, as the alpha-helix bundle and the SAH domain can work as mechanical extensors of the lever arm, increasing the step size (Mukherjea et al., 2014; Mukherjea et al., 2009; Spink et al., 2008). These two regions, together with the CBD (described below), are responsible for myosin VI dimerization (described in Fig. 4). Indeed, while myosin VI is normally found in cells as a folded monomer (Lister et al., 2004; Spink et al., 2008), its dimerization can be induced by monomer clusterization at high density or by the interaction with the cargo, like its interactor optineurin (Park et al., 2006; Phichith et al., 2009; Yu et al., 2009). Dimerization is required for both anchoring and transporting functions of this motor protein (Mukherjea et al., 2014), but whether the monomeric myosin VI can have a different function is still debated.

The distal part of the tail region is the CBD, which contains the interaction surfaces required for binding with selected partners. Two well-known interaction surfaces are the "RRL" and "WWY" motifs (Fig. 3A). The RRL motif is reported to interact with several endocytic adaptors, like GAIP-interacting protein C-terminus (GIPC) (Bunn et al., 1999; Spudich et al., 2007), and autophagy receptors, such as optineurin (Sahlender et al., 2005), nuclear dot protein 52 (NDP52) and nuclear dot protein 52 (T6BP) (Morriswood et al., 2007). Instead, the WWY motif is reported to bind Tom1 (Tumbarello et al., 2012), Disabled homolog 2 (Dab-2) (Inoue et al., 2002; Spudich et al., 2007) and lemur tyrosine kinase-2 (LMTK2) (Chibalina et al., 2007). Between these two interaction sites, there is a

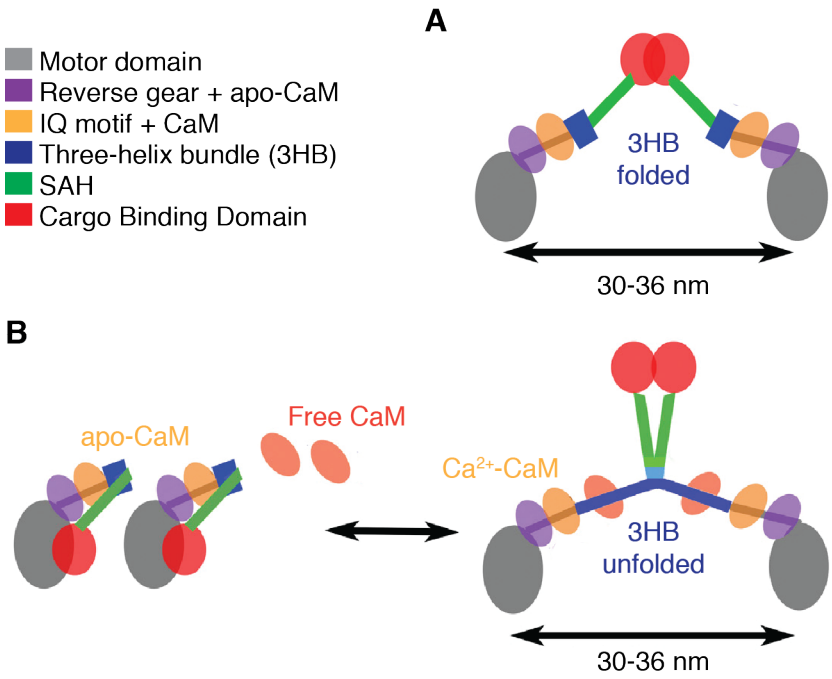

Figure 4: Dimerization models of myosin VI.

Two different models have been proposed to explain the dimerization and stepping mechanism of myosin VI. (A) The first model proposes that the dimerization occurs only via the interaction between the two CBDs, while the lever arm extension is provided by the folded three-helix bundle and the SAH domain (Spink et al., 2008). (B) The second model proposes that the three-helix bundle can unfold to work as a lever arm extension, recruiting an additional CaM to stabilize the unfolded bundle. In this latter model, the region between the lever arm extension and the SAH can dimerize, together with the CBD, while the SAH itself can act as spacer between motor and cargo or could be required for monomer folding. Indeed, the removal of the SAH domain has no impact on myosin VI step size and function (Mukherjea et al., 2009; Mukherjea et al., 2014). From the folded monomers (on the left), with the folding stabilized by interaction with the SAH (Spink et al., 2008), unfolding and dimerization could be initiated by transient Ca^{2+} increase Batters et al., 2016), or by the binding of the cargo(Phichith et al., 2009) (Phichith et al., 2009). [Adapted from *Mukherja et al., Cell Reports, 2014*].

---

phospholipid binding motif that interacts specifically and with high affinity with hosphatidylinositol 4,5-bisphosphate ($PI(4,5)P_2$) (Spudich et al., 2007).

Moreover, myosin VI CBD possesses two ubiquitin binding domains, the motif interacting with ubiquitin (MIU) domain and the myosin VI ubiquitin-binding (MyUb) domain, which contains the RRL motif (Fig. 3A) (He et al., 2016; Penengo et al., 2006). In particular, the MyUb interacts preferentially with K63-linked ubiquitin chains (He et al., 2016), which function in cell signaling and membrane trafficking event (Acconcia et al., 2009; Komander and Rape, 2012).

An important level of regulation in myosin VI is determined by the presence of the large insert (LI), a region positioned between the MIU and the MyUb that can undergo alternative splicing (Buss et al., 2001; He et al., 2016; Wollscheid et al., 2016). Alternative splicing in this region generates three isoforms: isoform 1, 2 and 3. While isoform 2 lacks completely the LI, isoform 1 and 3 contain inserts of different lengths (Fig. 3B). Interestingly, the presence of the LI reduces the ability of the MIU-MyUb to bind K63-linked ubiquitin chains, as well as affecting the interaction with other RRL-binding proteins (He et al., 2016; Wollscheid et al., 2016). This is due to the presence of an α-helix in the LI that can fold back, masking the RRL motif (Fig. 3C) (Wollscheid et al., 2016). The different conformation of the isoforms thus dictates the specificity of the binding partners. Indeed, while isoform 1 and 3 (named myosin VI_{long}) have the same interactors, among which clathrin, isoform 2 (named myosin VI_{short}) displays an interactome that is almost mutually exclusive to the one of the longer isoforms, including RRL binding proteins (Wollscheid et al., 2016).

Noteworthy, while the short isoform presents no specific expression and localization, Myosin VI_{long} isoform is specifically found in polarized epithelial cells with well-developed apical microvilli (Buss et al., 2001). Interestingly, epithelial cells can switch the isoform expression: this has been shown in non-tumor breast cells (MCF10A) and ovarian cancer cells (OVCAR-5) that display myosin VI_{short} expression when grown in sparse condition, and then switch to the expression of the long isoform after some days of confluency, when polarization has occurred (Buss et al., 2001; Wollscheid et al., 2016).

A second alternatively spliced region, known as the small insert (SI), is present in the CBD and is 9 amino acids long (Fig. 3A) (Buss et al., 2001). Even if expression and functions of the SI have not been extensively addressed, it has been shown that the myosin VI isoform containing the SI is expressed by PC12 cells, together with the isoform without inserts

(Majewski et al., 2010). In these cells, myosin VI SI isoform plays a role in the tethering of the secretory granules at the cortical actin network (Tomatis et al., 2013).

1.1.3.1. Myosin VI: motor or anchor?

As described above, myosins can act both as motor or dynamic tethers for the cargoes. Some studies have tried to clarify how myosin VI can be converted from motor and anchor and viceversa, and what are the stimuli that allow this conversion.

An interesting level of regulation of myosin VI resides on the binding to CaMs, which are further regulated by the levels of Ca^{2+}. As mentioned above, myosin VI interacts with two CaM molecules through the IQ motif and the reverse gear (Fig. 4). As suggested by the model by Batters et al., apo-CaM (Ca^{2+}-free) can keep myosin VI in a folded, and thus inactive, conformation, binding simultaneously the IQ motif and the CBD (Batters et al., 2016). When the concentration of Ca^{2+} increases, its binding to the CaM induces myosin VI unfolding, allowing the binding with the cargoes. Interestingly, this unfolded conformation is still not able to move along the actin filaments. For myosin VI conversion into a motor, Ca^{2+} levels should lower, to allow the CaM to stabilize the lever arm and gain the mechanical rigidity required for movement (Batters et al., 2016). In this picture, the recruitment of an additional CaM to the unfolded three helix bundle could help to stabilize the open conformation, allowing myosin VI to be mechanically active and translocate along the actin filaments (Mukherjea et al., 2014) (Fig. 4).

To allow myosin VI movement, dimerization is another important step. Myosin VI dimerization can be induced by an increased concentration of the cargoes, like optineurin (Phichith et al., 2009) and Dab2 which, together with PI(4,5)P2, mediates the dimerization of myosin VI on the clathrin coated pits (Spudich et al., 2007), raising the question about

the role of the cargoes in the stabilization of the unfolded myosin VI conformation, and thus in the transition to the motile form.

Interestingly, the cargoes that bind to the myosin VI tail are not only important for myosin VI dimerization, but play a role in the motor/anchor conversion. In particular, it has been proposed that myosin VI has an intrinsic force sensitivity, and it is thus able to respond to increasing loads, acting as mechanosensor (Altman et al., 2004; Chuan et al., 2011). In fact, under low loads, myosin VI could function as a processive transporter, but it can be converted to an anchor when a sufficient load is applied. This conversion is due to an increased association rate of the motor head with ADP, which promotes an actin bound state, and a decrease in the affinity with ATP, whose binding should allow the release of the head from the actin filaments (Oguchi et al., 2008). In this way, myosin VI is able to bind tightly to actin filaments when the tail is linked to structures that provide resistance.

This property could have a physiological role in the inner-ear stereocilia, where the tension at the base of the stereocilia membrane could play a role in converting myosin VI into an anchor. The anchoring of the apical cell membrane to the actin filaments at the base of the stereocilia mediated by myosin VI is important to maintain the structural integrity of the sterocilia. Indeed, myosin VI mutations that affect the ATP and ADP binding lead to fused sterocilia, impairing the hair bundle organization in inner ear cells, ultimately leading to deafness (Hertzano et al., 2008). Furthermore, it has recently been proposed that myosin VI plays an important role as sensor of the tensile stress applied to the adherens junctions. In fact, increased tensile forces at the adherens junctions could be transmitted to myosin VI by E-cadherin, which interacts with the motor protein (Mangold et al., 2012), promoting the stabilization of myosin VI at the junctions and its increased anchoring to the actin filaments. This promotes the association between E-

cadherin and Ga12 complex, which in turn activates the Rho-GEF-RhoA pathway, thus increasing the tensile strength of multicellular junctions and preserving the integrity of the epithelium under tensile stress conditions (Acharya et al., 2018).

Even if the picture of the regulation of myosin VI dimerization and motility is still incomplete, the above-mentioned studies suggest that local changes in Ca^{2+} levels could convert myosin VI from a tether to a motor protein. At the same time, by binding of different cell components, myosin VI could play a role as a transporter, in case of low loads, or as an anchor, in case of high loads. Thus, diverse stimuli could finely modulate myosin VI properties depending on the local environment.

1.1.4. The functions of myosin VI

The strong divergences in the CBD of different myosins explain the diversity of their cellular roles, thanks to specific interaction with a large variety of molecules and organelles, and the subsequent targeting to various subcellular locations. In myosin VI, another level of complexity is given by the presence of alternative splicing isoforms, that display two different and mutually exclusive sets of interactors, as discussed above. In addition to specific binding partners, myosin VI has the unique property, among all the other myosins, of travelling towards the minus end of actin filaments. Thanks to these peculiar properties, myosin VI can play a role in different cellular processes, as depicted in Fig. 5.

1.1.4.1. Myosin VI plays a dual role in endocytosis and membrane trafficking

Endocytosis is a fundamental process for the uptake of macromolecules at the plasma membrane of cells. Clathrin-mediated endocytosis is the most studied process for the internalization of a wide variety of molecules, such as nutrients, transporters, adhesion

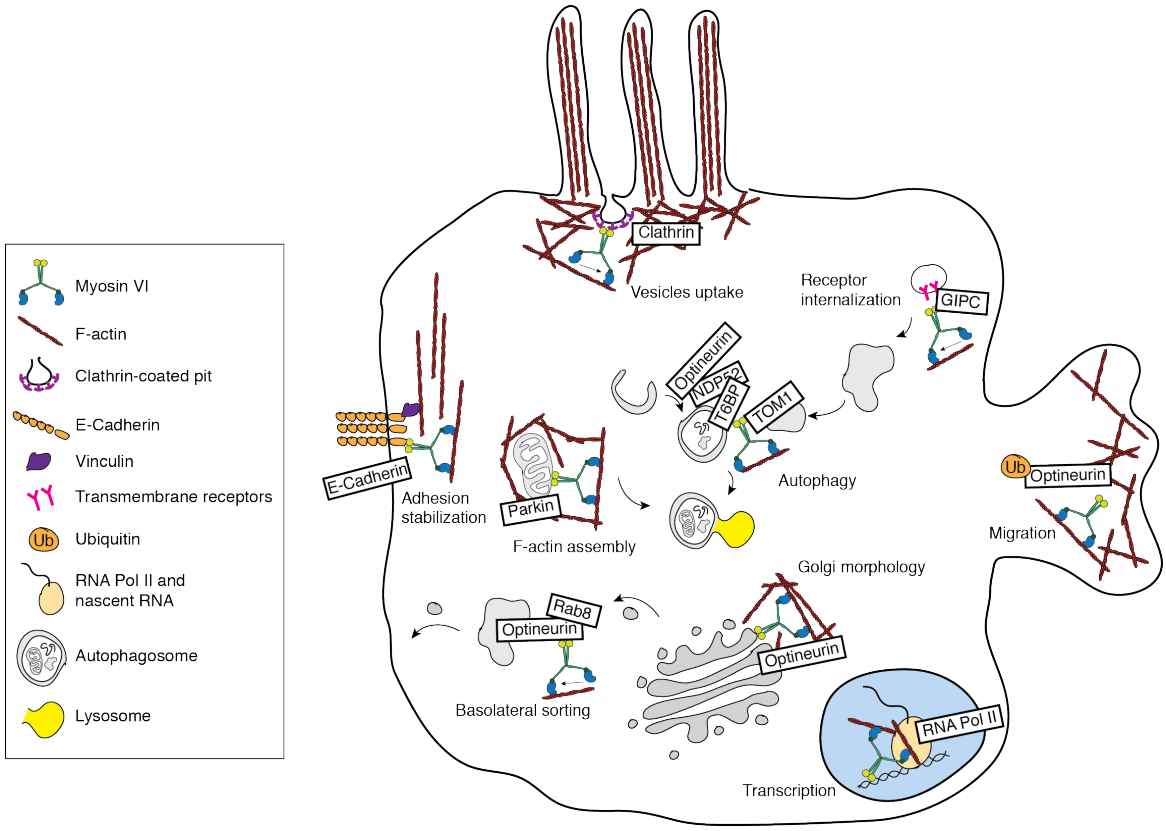

Figure 5: Myosin VI functions are directed by the interaction with multiple binding partners.

Myosin VI exerts diverse functions thanks to the interaction of its cargo binding domain with different partners (boxed), as described in detail in the text. Myosin VI plays specific roles in specialized cell types, such as polarized epithelial cells, that contain microvilli at their apical surface, and migratory cells.

---

molecules and receptors. For this process to occur, actin is normally not strictly required, but it becomes essential in locations with a dense actin network, such as apical microvilli (Mooren et al., 2012). In fact, in polarized epithelial cells with apical microvilli, actin filaments are required both for the movement and clustering of receptors and for vesicle scission (Gottlieb et al., 1993; Jackman et al., 1994; Shurety and Luzio, 1995).

As discussed above, polarized epithelial cells express mainly myosin VI_{long}, in which the α2-linker folds on the RRL motif, masking it and at the same time creating an interaction surface for clathrin (Wollscheid et al., 2016). This direct myosin VI-clathrin interaction adds on the previously described indirect interaction mediated by Dab-2 (Morris et al., 2002; Morris and Cooper, 2001). In fact, myosin VI can bind clathrin and Dab-2 through two different interaction surfaces, generating a ternary complex and thus linking clathrin-

mediated endocytosis to the actin cytoskeleton (Wollscheid et al., 2016). Indeed, myosin VI_{long} localizes at the apical membrane of polarized cells (Buss et al., 2001), at the base of the microvilli, together with the endocytic adaptors α-AP-2 and Dab2 (Collaco et al., 2010). At the apical surface, myosin VI could generate the force required for the endocytic vesicles to pass through the dense actin meshwork.

A functional role for myosin VI in the endocytosis at the apical membrane was demonstrated in cells derived from the small intestine and the airway epithelium. In these cells, cystic fibrosis transmembrane conductance regulator (CFTR), an apical-localized Cl^- channel, interacts with myosin VI, Dab-2 and clathrin, and its endocytosis requires myosin VI activity and actin filaments (Swiatecka-Urban et al., 2004). Furthermore, this process involves α-AP-2, which is part of the same complex and could be involved in directing myosin VI on CFTR for its internalization (Collaco et al., 2010). The requirement of myosin VI for CFTR endocytosis has been demonstrated also in intestinal cells derived from *sv* mice, which also present shorter microvilli compared to control mice (Ameen and Apodaca, 2007). Similarly, renal tubular cells of *sv* mice display a reduced and delayed endocytic uptake and trafficking of HRP, suggesting that myosin VI is involved both in endocytic vesicle formation and movement of endocytic vesicles toward early endosomes. Indeed, *sv* mice show renal fibrosis and proximal tubule dilation (Gotoh et al., 2010).

In addition, the complex formed by myosin VI, clathrin and Dab-2 is also important for non-canonical clathrin-mediated endocytic processes. It has been shown that the internalization of *Listeria monocytogenes* requires the recruitment of Dab-2, clathrin, HIP1R, which can promote actin polymerization, and myosin VI, which possibly provides the pulling force necessary for the uptake of the cargo (Bonazzi et al., 2012; Bonazzi et al., 2011).

While myosin VI_{long} plays a role in clathrin-mediated endocytosis in polarized cells, the short isoform is involved in later stages of the endocytic pathways. In fact, only myosin VI_{short} is able to interact with GIPC (Wollscheid et al., 2016), an endocytic adaptor that regulates receptor-mediated trafficking and, after receptor internalization, transiently associates with a pool of endocytic vesicles before the maturation into early endosomes (Varsano et al., 2006).

In non-polarized cells, myosin VI co-localizes with GIPC on uncoated transferrin-containing vesicles that are located at the periphery of the cell, before they fuse with the early endosome compartment (Aschenbrenner et al., 2003). Furthermore, the motor function of myosin VI is required for the trafficking of these vesicles, as an actin-bound myosin VI motor mutant blocks transferrin trafficking to the early endosome (Aschenbrenner et al., 2004). Interestingly, myosin VI is present in vesicles moving in and out of the cleavage furrow during cell division, where both myosin VI and GIPC are recruited and are required during cytokinesis (Arden et al., 2007).

Myosin VI plays also a role in the retention of the APPL1-positive endosomes in the cell periphery through tethering to the actin cortex. This stalled localization is important to promote continuous AKT signaling before downstream cargo processing (Masters et al., 2017).

Another adaptor molecule that associates myosin VI with the endocytic pathway is LMTK2, a transmembrane serine/threonine kinase. The interaction occurs through the WWY motif of myosin VI, and it has been shown that both proteins play a crucial role in trafficking of cargoes from the early endosomes to the endocytic recycling compartments, but a mechanistic insight is still missing (Chibalina et al., 2007).

1.1.4.2. Myosin VI is involved in autophagosome maturation

Actin and myosins play essential roles during the autophagic process (Kruppa et al., 2016). Autophagy is a catabolic process that maintains cellular homeostasis by degrading protein aggregates and damaged organelles through lysosomes. Autophagy is mediated by the autophagosomes, organelles whose formation is driven by cellular stress, such as amino acid starvation, and works as a defense mechanism against intracellular pathogens.

At the beginning of the process, the formation of a branched actin network, through Arp2/3, plays a role as a scaffold to generate the phagophore (Mi et al., 2015), and non-muscle myosin IIA is involved in the formation of actin-myosin filaments that are required for vesicle transport to the phagophore (Tang et al., 2011). During autophagosome closure and maturation, actin comet tails are thought to be formed on the autophagosomes, driving its movement. During the maturation, myosin VI plays a role in delivering the endosomal membranes to autophagosomes (Tumbarello et al., 2013; Tumbarello et al., 2012). Also in the late stage of the autophagy process, the Arp2/3 complex stimulates actin network assembly enabling the fusion of the autophagosome with the lysosome (Lee et al., 2010). During this late process, myosin IC reduces the fusion ability of autophagosomes and lysosomes, possibly by changing their lipid and cholesterol content (Brandstaetter et al., 2014).

As showed above, myosin VI can interact with several autophagy receptors, such as optineurin, NDP52 and T6BP (also called TAX1BP1). The binding to these proteins occurs through the RRL motif (Morriswood et al., 2007) and it is thus specific for the myosin VI_{short} isoform (Wollscheid et al., 2016). To exert their functions, these autophagy receptors possess a ubiquitin binding domain that allows recognition of substrates targeted for degradation, and a LC3-interacting region (LIR) deputed to the interaction

with the autophagosomal membrane. Interestingly, the ubiquitin binding site overlaps with the myosin VI binding site, suggesting that they may have a dual function (Hu et al., 2018; Tumbarello et al., 2015). Another level of regulation of the interaction of myosin VI with the autophagy receptors is given by ubiquitination. In fact, it has been shown that optineurin can be ubiquitinated, thus increasing the interaction with myosin VI_{short} (He et al., 2016).

Depletion of myosin VI leads to autophagosome accumulation due to defects in the maturation process and lysosome fusion, causing a reduced rate of protein aggregate clearance (Tumbarello et al., 2012). These phenotypes are mirrored by Tom1, a component of the ESCRT-0. Tom1 interacts with myosin VI through its WWY motif and can recruit the motor protein to the endosomal membranes where myosin VI is required for the movement and/or the fusion of the endosomes to the autophagosomes (Tumbarello et al., 2012).

Furthermore, myosin VI and TAX1BP1 are recruited to ubiquitylated Salmonella and play a key role in its clearance by autophagy. Indeed, loss of myosin VI leads to an accumulation of ubiquitylated Salmonella inside LC3-positive autophagosomes, implicating that myosin VI is a critical factor during the later maturation stage of the autophagosome (Tumbarello et al., 2015).

Interestingly, myosin VI and Tom1 were identified as proteins that associate with Parkin in response to mitochondrial damage (Sarraf et al., 2013). Myosin VI is recruited to damaged mitochondria through a Parkin-dependent mechanism by binding to ubiquitin chains. Once there, myosin VI promotes the assembly of actin cages around the fragmented mitochondria, together with CDC42 and actin nucleators, preventing their re-fusion and thus contenting the damage (Kruppa and Buss, 2018).

Given the interaction of myosin VI with Tom1 and autophagy receptors through distinct domains, a proposed model suggests that myosin VI could bring endosomes in close proximity to the autophagosomes by binding Tom1 and the autophagy adaptors through different interaction sites and by tethering them to the surrounding actin cytoskeleton (Tumbarello et al., 2015).

Thanks to all these interactions, myosin VI appears to play an important role in the autophagy of protein aggregates, as well as for the clearance of damaged mitochondria and invading pathogens.

1.1.4.3. Myosin VI interacts with optineurin at the Golgi complex

The Golgi complex is a central node of vesicle trafficking in the cell: proteins coming from the endoplasmic reticulum are modified and then sorted through secretory vesicles to the plasma membrane, organelles or the extracellular environment. Structurally, the Golgi complex is composed by packed cisternae that are functionally divided into *cis*-Golgi, more proximal to the ER, *medial*-Golgi, and *trans*-Golgi (*trans*-Golgi network, TGN), which is instead deputed to release the vesicles for cargo sorting. This system is located near the nucleus and in close connection with the centrosome, and its localization with respect to the nucleus is polarized in migrating or apico/basal polarized cells.

The maintenance of the complex Golgi structure relies on the actin and microtubule cytoskeletons, which have different roles in the Golgi complex. In fact, actin microtubule depolymerization causes Golgi complex fragmentation, whereas actin depolymerization causes Golgi complex compaction (Gurel et al., 2014). The microtubules are nucleated at the Golgi complex, where they are required for vesicle transport through kinesins and dyneins. The actin network, instead, together with many actin nucleators and multiple

myosins that are present at the Golgi complex, provide the force for the budding and the fission of vesicles, and the maintenance of cisternae shape (Gurel et al., 2014).

The first localization studies revealed that myosin VI is enriched in the Golgi apparatus, in particular at the TGN, suggesting a potential role of the motor protein connected to the Golgi complex (Buss et al., 1998). Indeed, in primary fibroblasts derived from *sv* mice, the size of the Golgi complex is 40% reduced compared to fibroblasts from wild type mice, and the secretion of a soluble form of alkaline phosphatase (SEAP) is impaired (Warner et al., 2003). The only myosin VI interactor identified at the Golgi complex is optineurin, which co-localizes with myosin VI and is essential for its targeting to the Golgi complex (Sahlender et al., 2005). The depletion of optineurin leads to fragmentation of the ribbon structure and a greatly reduced secretion of VSV-G (Sahlender et al., 2005), similar to the phenotype observed in the *sv* mice. Furthermore, optineurin interacts with Rab8, which plays an important role in the biosynthetic trafficking pathway from the Golgi complex to the plasma membrane, linking myosin VI to the protein secretion process (Sahlender et al., 2005). Later studies challenged the idea that optineurin and myosin VI played a role in vesicle formation at the TGN, as suggested by the study by Sahlender et al (Sahlender et al., 2005). In fact, the depletion of myosin VI results in no significant change in the number of vesicles travelling from the Golgi complex to the plasma membrane, but rather in a strong decrease of vesicle fusion events at the plasma membrane (Bond et al., 2010).

Other studies suggest the involvement of myosin VI in different steps of constitutive exocytosis. In fact, myosin VI seems to play a role in early stages of protein secretion, in particular in endoplasmic reticulum (ER)-to-Golgi transport (Bond et al., 2010), while in polarized epithelial cells myosin VI, optineurin and Rab8 can function together in cargo sorting specifically to the basolateral but not to the apical plasma membrane domain (Au et al., 2007). Specifically, in polarized MDCK, myosin VI and optineurin are present on a

specialized recycling compartment, which works as a sorting station for proteins delivered to the basolateral domain, suggesting that these proteins are not involved in the direct delivery from the Golgi complex to the plasma membrane, but rather in the route that involves the recycling compartment (Au et al., 2007). The myosin VI isoform involved in this exocytic pathway is the short one, since myosin VI_{long} is not present in the TGN or at the recycling endosomes, but is targeted specifically to the apical domain (Au et al., 2007). Furthermore, the other player in the basolateral protein sorting pathway is optineurin, which can bind only myosin VI_{short} (Wollscheid et al., 2016), further corroborating its involvement.

Interestingly, in neurons, the dendritic surface of the cell body is similar to the basolateral domain. Indeed, myosin VI is required for trafficking of the AMPA receptor in this domain in hippocampal neurons (Nash et al., 2010). Similarly, in polarized migrating cells, proteins with basolateral sorting motifs are transported into the leading edge. Indeed, myosin VI and optineurin are required for the polarized delivery of epidermal growth factor receptor (EGFR) into the leading edge, suggesting a role for these proteins in cell migration (Chibalina et al., 2010).

1.1.4.4. Myosin VI_{short} is involved in cancer cell migration

Early studies implicate myosin VI in the migratory potential of cancer cells (Chibalina et al., 2009). It has been shown that myosin VI is overexpressed in ovarian and prostate cancers, and its overexpression correlates with a clinically aggressive behavior (Dunn et al., 2006; Yoshida et al., 2004). Recent work from our lab have demonstrated selective isoform overexpression in cancer. Indeed, a bioinformatics analysis of isoform expression in tumor and normal samples, using data from The Cancer Genome Atlas (TCGA) database, revealed that the majority of tumor types show overexpression of myosin VI_{short}

(Wollscheid et al., 2016). Moreover, cancer cells that express only the short isoform require myosin VI for cell migration, while others that express also myosin VI_{long} do not require it for cell migration (Wollscheid et al., 2016). These observations suggest that during epithelial to mesenchymal transition, a process fundamental for cancer invasion and metastasis, the overexpression of myosin VI_{short} could confer a migratory advantage to cancer cells.

From a mechanistic point of view, it has been show that optineurin, which binds selectively to myosin VI_{short}, acts in the same pathway of myosin VI to regulate cell migration (Wollscheid et al., 2016). Furthermore, silencing of myosin VI or optineurin in A549 cells, human lung adenocarcinoma cells, affects the ability of the cells to migrate towards an EGF gradient, and this is caused by the inhibition of polarized delivery of the EGFR into the leading edge (Chibalina et al., 2010). The mechanistic details about the role played by myosin VI in migration need further elucidation, and an interesting starting point is the observation that the binding of myosin VI to optineurin is increased by optineurin ubiquitination (He et al., 2016), suggesting a potential regulatory role of ubiquitin in the context of cell migration.

In the *D. Melanogaster* ovary, myosin VI is required for border cell migration and for the formation of the membrane protrusions at the leading edge of moving cells (Geisbrecht and Montell, 2002). In these cells, myosin VI interacts with armadillo (orthologue of beta-catenin) in a complex with DE-cadherin, suggesting that through this interaction myosin VI is able to push the actin filaments towards the leading edge (Buss et al., 2002; Geisbrecht and Montell, 2002).

The regulation of the actin filament network is critical for cell migration. As described for other myosins, some evidences suggest that myosin VI could play a role in actin shaping. In fact, myosin VI is required for the proper distribution of cortactin and the arp2/3

complex at the actin cones that separate the syncytial spermatids in *D. Melanogaster* (Rogat and Miller, 2002). It has been shown that myosin VI stabilizes the branched actin network at the front of the actin cones (Noguchi et al., 2006). Myosin VI remains bound for a long time to actin cones, and its localization depends on its actin-binding activity, suggesting that myosin VI works as a structural linker (Noguchi et al., 2006). Also in mammalian cells, it has been suggested that the phosphorylation of myosin VI in the motor domain increases its tethering abilities, leading to the stabilization of actin filaments. This latter event could be due to the inhibition of depolymerization from the minus ends of the filaments (Naccache and Hasson, 2006).

1.1.4.5. Myosin VI regulates cell-cell and cell-matrix adhesion

As described above, in *D. Melanogaster*, myosin VI was found in a complex with armadillo and DE-cadherin (Geisbrecht and Montell, 2002). The same was shown also in mammals, where a direct interaction between myosin VI and E-cadherin was demonstrated (Mangold et al., 2012). Myosin VI is recruited to cell-cell contacts by E-cadherin during the maturation of the adherens junctions, where it is important for the integrity of the adhesions (Maddugoda et al., 2007). Consistent with the central role for E-cadherin function in junctional biogenesis, the depletion of myosin VI perturbs the integrity of not only cadherin adhesions, but also of tight junctions and desmosomes. Furthermore, myosin VI bridges E-cadherin and vinculin, which has been found as a downstream effector for myosin VI at the adherent junctions (Maddugoda et al., 2007).

Even if the mechanistic details of the requirement of myosin VI for the stability of the junctions has not been extensively studied, one interesting possibility is that myosin VI could work as a tether anchoring the junctions to the cortical actin cytoskeleton. In fact, a recent study showed that the increase in the tension on adherent junctions leads to an

increased anchoring of myosin VI to the actin filaments under load, and to the recruitment of myosin VI to E-cadherin. There, myosin VI mediates the activation of RhoA pathway, which helps the cell monolayer to resist to the tensile stress (Acharya et al., 2018).

Moreover, myosin VI has been localized to gap junction plaques, as well as at intercalated discs in heart sections (Karolczak et al., 2014; Piehl et al., 2007). Indeed, loss of myosin VI impairs GJ plaque formation and downregulates intracellular communication (Waxse et al., 2017).

In addition to cell-cell adhesions, myosin VI is involved in the regulation of cell-matrix junctions, together with its interactor GIPC. The depletion of myosin VI or GIPC impairs $\alpha 5\beta 1$ integrin internalization, affecting the adhesion of cells to fibronectin (Valdembri et al., 2009). These data suggest that GIPC recruits myosin VI at the sites of cell-matrix adhesions, where myosin VI could play a role as actin motor to drive the transport of endocytic vesicles containing $\alpha 5\beta 1$ integrin along the actin filaments. While isoform specificity has not been tested in this system, the integrin internalization is predicted to be clathrin-independent.

1.1.4.6. Myosin VI in the nucleus: a player in transcription

Unlike its well-described cytoplasmic function, nuclear roles of myosin VI are poorly understood. Few reports have suggested that myosin VI is present not only in the cytoplasm, but also in the nucleus, where it associates with the RNA polymerase II (RNAPII) transcription machinery at active genes (Fili et al., 2017; Majewski et al., 2018; Vreugde et al., 2006). The isoform involved in the interaction with the RNAPII seems to be myosin VI_{short}, which has been proposed to act as tethering factor or auxiliary motor connecting the DNA and the actin present on the polymerase (Fili et al., 2017). A role for

myosin VI in transcription has also been shown in T-cells, in which nuclear myosin VI regulates the switch between poised and elongating RNAPII, following TCR re-stimulation (Zorca et al., 2015). Further studies are needed to uncover other possible functions of myosin VI in the nucleus.

1.2. Centrosomes

The centrosome is the main microtubule organizing center (MTOC) of the cell and it plays important roles in many different cell processes, such as migration, adhesion, cell polarity and organization of the mitotic spindle (Nigg and Raff, 2009). The MTOC is composed of a pair of centrioles surrounded by the pericentriolar material (PCM), a proteinaceous matrix that contains hundreds of proteins, among which microtubule nucleators and proteins involved in microtubule organization, as well as cell cycle regulators and signaling molecules (Alves-Cruzeiro et al., 2014; Andersen et al., 2003). The centrioles function not only in the assembly of the centrosomes, but are also fundamental for the formation of the primary cilium, an important center for cellular signaling (Kim and Dynlacht, 2013).

1.2.1. Centriole structure and the duplication cycle

The centrioles are cylindrical microtubule organelles with a nine-fold symmetry, 500 nm long and 200 nm in diameter. These structures are composed of nine triplets of microtubules, which become doublets in the distal part of the centriole (Fig. 6) (Paintrand et al., 1992). This nine-fold symmetry is established during centriole biogenesis, in which the centrioles are assembled around a cartwheel structure that displays a nine-fold symmetrical arrangement (Kitagawa et al., 2011). The new daughter centriole (procentriole) is assembled during the S phase on the side of the mother, at 90° angle,

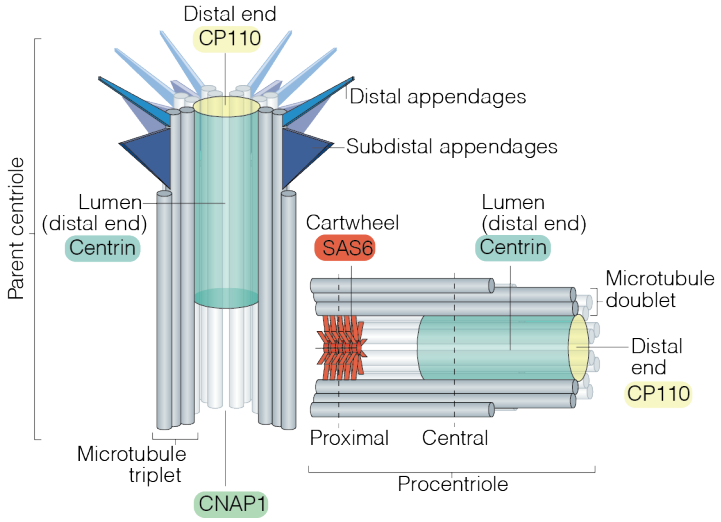

Figure 6: The structure of the centrioles.

The scheme represents the structure of a parent centriole and the engaged procentriole. The mother centriole is characterized by the presence of distal and subdistal appendages. The procentriole is assembled on the side of the parent centriole using SAS6 cartwheel as template. The CP110 forms a cap to the distal end of the centriole. The two centrioles remain engaged in this configuration until the end of mitosis when the two centrioles disengage and remain bound through a proteinaceous linker that is connected to the proximal part of the centriole through c-Nap1. [Adapted from *Nigg and Holland, Nature Reviews Molecular Cell Biology, 2018*]

---

and it remains in this "engaged" configuration until the late stages of mitosis. During mitosis, the two duplicated centrioles separate and migrate at the poles of the cell, forming the mitotic spindle, a process coordinated by the kinesin Eg5, and segregate into one of the daughter cells. At the end of mitosis, the parent centriole and the newly-formed procentriole are separated, or "disengaged", and the procentriole mature to be able to duplicate and to organize its own PCM, in a process called centriole-to-centrosome conversion (Nigg, 2007). The two separated centrioles remain connected through a proteinaceous linker that is maintained during centriole duplication in interphase and is abolished upon entry into mitosis to allow centriole separation (Bahe et al., 2005; Faragher and Fry, 2003; Fry et al., 1998; Yang et al., 2006b). After mitosis and disengagement, the oldest (mother) centriole acquires additional structures, the distal and subdistal appendages, which are involved in anchoring microtubules and in the

docking of the centriole at the plasma membrane for ciliogenesis (Bettencourt-Dias and Glover, 2007). The centriole duplication cycle is summarized in Fig. 7.

1.2.1.1. Centriole biogenesis

Studies in *C. elegans* and in *D. melanogaster* have been seminal in uncovering the mechanism of centriole formation. The essential proteins required for the initiation of centriole duplication are Polo-like kinase 4 (Plk4), SCL-interrupting locus protein (STIL) and Spindle assembly abnormal protein 6 homolog (SAS-6) (Arquint and Nigg, 2016; Bettencourt-Dias et al., 2005; Leidel et al., 2005; Loncarek and Bettencourt-Dias, 2018; Vulprecht et al., 2012). During the centriole biogenesis, the first component observed at the site of procentriole formation is SAS-6, which forms the cartwheel structure onto which the centriole is assembled. This structure is composed of nine homodimers of SAS-6 that interact to generate a ring-like central hub organized in a nine-fold symmetric structure (Kitagawa et al., 2011; Leidel et al., 2005). The stacking of this ring structure generates a cartwheel (Guichard et al., 2012). Despite the well-established importance of SAS-6 for centriole assembly, recent studies showed that it is dispensable for *de novo* centriole formation, and that the cartwheel architecture also depends critically on the assembly of the microtubule wall (Hilbert et al., 2016; Wang et al., 2015b).

During the G1 phase, STIL and SAS-6 are not present, as they are degraded by the anaphase-promoting complex (APC/C) (Arquint et al., 2012; Strnad et al., 2007), while Plk4 forms a ring around each centriole (Arquint et al., 2015; Kleylein-Sohn et al., 2007; Ohta et al., 2014). At the G1-S transition, SAS-6 is transiently recruited to the lumen of the mother centriole, where it assembles into a cartwheel-like structure through the interaction with the luminal wall (Fong et al., 2014; Keller et al., 2014).

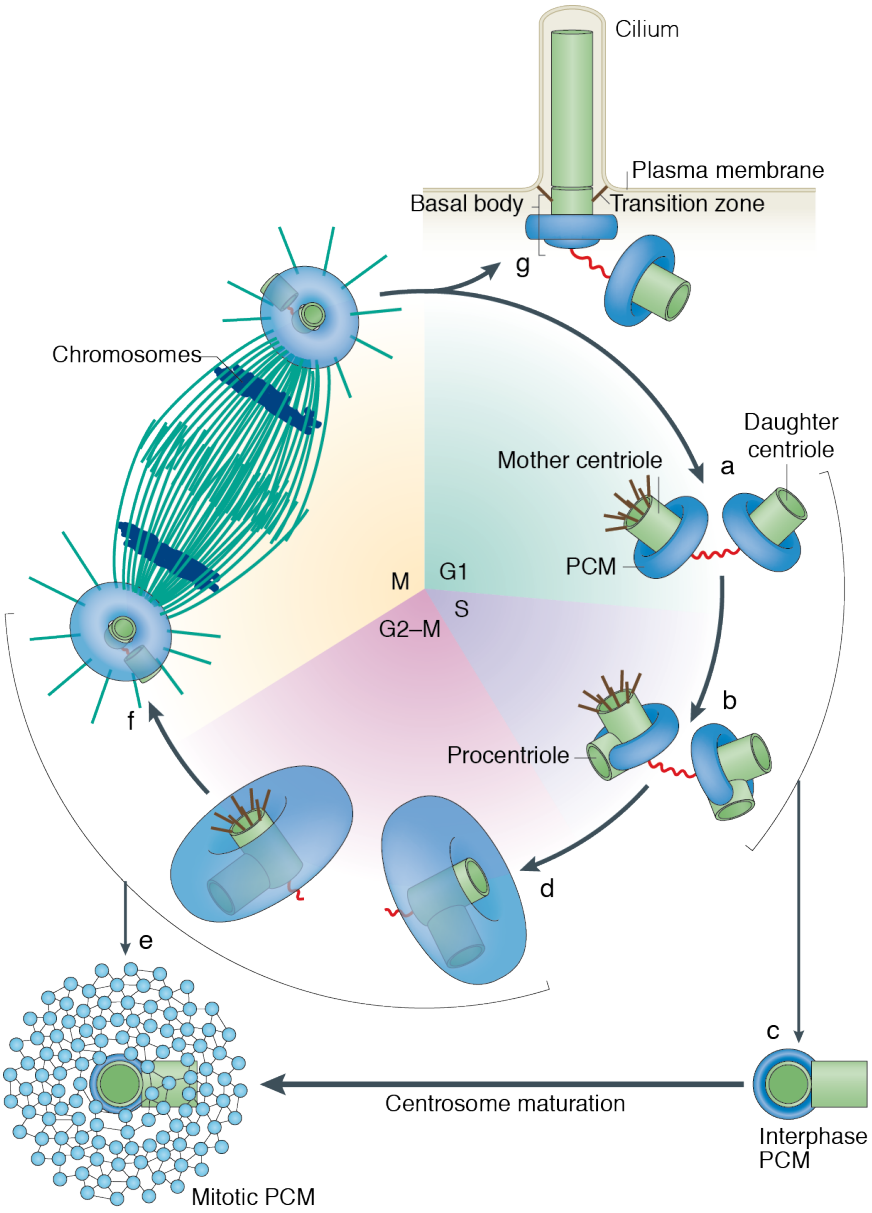

Figure 7: The centriole duplication cycle.

A scheme of the duplication cycle of the centrioles. (a) In the G1 phase, cells have two centrioles, a mother centriole with distal appendages (brown) and a daughter centriole, connected by a proteinaceous linker (red) and surrounded by the PCM. (b) At the G1/S transition, each of the two centrioles start its duplication, driving the assembly of a procentriole engaged to the parent centriole. Only the parent centriole is able to assemble the PCM (c). (d) When the cells start mitosis, the linker between the two centrioles is dissolved and the two centrosomes can separate and migrate to the cell poles, building the mitotic spindle (f). During this process, the parent centriole recruits a large amount of PCM proteins (centrosome maturation), which play a role in mitotic spindle assembly and positioning (e). (f) When the cells exit mitosis, the two centriole pairs segregate in two daughter cells and the mother and daughter cells disengage but remaining connected through the G1-G2 tether. (g) In cells that exit from the cell cycle and arrest in the G0 phase, the mother centriole docks to the plasma membrane through the distal appendages, becoming a basal body from which the primary cilium extends. [Adapted from *Conduit et al., Nature Reviews Molecular Cell Biology, 2015*]

To initiate procentriole assembly, STIL binds Plk4, releasing Plk4 autoinhibition and leading to the activation of its autophosphorylation on one side of the centriole (Arquint et al., 2015; Dzhindzhev et al., 2014; Kratz et al., 2015; Moyer et al., 2015; Ohta et al., 2014). The phosphorylation of Plk4 also triggers its ubiquitination and degradation by the $SCF^{slimb/\beta TrCP}$ ubiquitin ligase (Guderian et al., 2010; Holland et al., 2012; Holland et al., 2010; Sillibourne et al., 2010). Thus, the site of centriole duplication is likely defined by STIL, which protects activated Plk4 from degradation (Arquint et al., 2015; Ohta et al., 2018), even if the site of procentriole growth is still a matter of debate. Then, Plk4 phosphorylation of STIL promotes the recruitment of SAS-6 to STIL (Dzhindzhev et al., 2014; Ohta et al., 2014), leading to the repositioning of SAS-6 to the site of procentriole formation (Fong et al., 2014). Once the cartwheel is established, CPAP, Cep120 and SPICE1 promote the assembly of the microtubules at the end of the cartwheel spokes, possibly by recruiting the γ-Tubulin ring complex (γTuRC) that nucleates the microtubules and thus initiates the formation of a new centriolar wall (Comartin et al., 2013; Guichard et al., 2010; Lin et al., 2013; Mahjoub et al., 2010). The length of the centrioles is then dictated by CP110, which may act as a physical barrier for elongation, forming a cap at the distal end of the procentriole (Kleylein-Sohn et al., 2007).

Centrioles are stabilized by linkers between the microtubules and by tubulin post-translational modifications, like detyrosination, acetylation and glutamylation, that make centrioles resistant to depolymerization (Janke, 2014; Kochanski and Borisy, 1990; Winey and O'Toole, 2014).

1.2.1.2. Regulation of centriole duplication

The regulation of centriole duplication is finely controlled in space and time to ensure that only one procentriole can be formed at each mother centriole, and that only one round of duplication is occurring during each cell cycle.

The regulation of the centriole initiating factors, Plk4, STIL and SAS-6, is essential for the control of procentriole formation. Indeed, their overexpression leads to the formation of multiple procentrioles in a flower-like shape around the mother centriole (Habedanck et al., 2005; Kleylein-Sohn et al., 2007; Leidel et al., 2005; Vulprecht et al., 2012).

The block of the formation of more than one centriole per each mother is an intrinsic property of the centrosomes, as only unduplicated mother centrioles can initiate duplication (Wong and Stearns, 2003). In particular, the presence of the engaged daughter inhibits the formation of additional procentrioles, as its removal allows another round of duplication (Loncarek et al., 2008).

Thus, the disengagement of the centrioles at the end of mitosis is a licensing step that allows the duplication to occur. It has been suggested that centriole-associated cohesin is required for engagement, and separase is needed to cut this protein to allow disengagement. However, the exact role of cohesin and separase is still a matter of debate, as contradictory studies exist about their involvement (Schockel et al., 2011; Tsou et al., 2009). Recent studies also show that separase can cleave pericentrin, a scaffold protein of the PCM, at the exit of mitosis, and that this cleavage step is essential for disengagement (Lee and Rhee, 2012; Matsuo et al., 2012). Furthermore, Plk1 activity is known to be essential for disengagement (Tsou et al., 2009; Wang et al., 2011), even if its role has not been fully clarified. A suggested model is that Plk1 may promote the disengagement through phosphorylation and subsequent degradation of components of the PCM, like pericentrin (Seo et al., 2015). At the end of mitosis, the cartwheel is

removed from the centrioles in a process mediated by Cyclin-dependent kinase 1 (CDK1), allowing reduplication of the centriole (Arquint and Nigg, 2014; Kim et al., 2016).

The disengagement of the centrioles at the end of mitosis allows also the fully elongated procentriole to mature, acquiring the ability to duplicate, in a process that is called centriole to centrosome conversion. This process is dependent on CDK1 and Plk1 (Novak et al., 2016; Wang et al., 2011), and requires the loading of Cep135, Cep195 and Cep152 to the centriole, then allowing the recruitment of Plk4 followed by that of the PCM (Fu et al., 2016).

The proteinaceous linker that connects the two centrioles after disengagement is composed of several coiled coil proteins, including rootletin, LRRC45 and CEP68, that are docked to the proximal end of the centrioles by C-Nap1, CEP135 and centlein (Bahe et al., 2005; Flanagan et al., 2017; Fry et al., 1998; Mayor et al., 2000; Yang et al., 2006b). At the G2/M transition, Plk1 activates Nek2A, which phosphorylates the linker filaments, thus promoting the disjunction of the two centrosomes and allowing their separation and the assembly of the mitotic spindle (Agircan et al., 2014; Bahe et al., 2005; Fry et al., 1998; Helps et al., 2000; Mardin et al., 2011).

1.2.1.3. De novo centriole formation

Centrioles can be assembled in the cells even in the absence of precursor centrioles, in a process called *de novo* centriole formation. In particular, this pathway is silenced by centrosomes, occurring only in the absence of any other centriole in the cell and without any restriction on the number of formed centrioles (Khodjakov et al., 2002; La Terra et al., 2005; Uetake et al., 2007). The *de novo* centriole formation uses the same molecular network used by canonical centriole duplication, involving Plk4, STIL, SAS-6 and CPAP (Rodrigues-Martins et al., 2007). What triggers centriole formation is a high local

concentration of Plk4. Upon achieving a critical threshold, Plk4 becomes active and recruits STIL and in turn SAS-6, starting centriole biogenesis (Lopes et al., 2015; Zitouni et al., 2016). Indeed, Plk4 is able to self-assemble into condensates, that in turn act as scaffolds by recruiting components important for MT nucleation (Gouveia et al., 2018). In this view, mother centrioles act as concentrators of Plk4 activity, triggering the signaling cascade for procentriole formation, while in the cytoplasm the concentration of Plk4 is too low to allow centriole assembly (Loncarek and Bettencourt-Dias, 2018; Lopes et al., 2015; Zitouni et al., 2016). This *de novo* pathway is used by a variety of organisms to trigger centriole formation in acentriolar cells in precise time-frames. For example, in mice, the zygote initially divides without centrioles, which are formed at the blastomere stage (Courtois et al., 2012; Gueth-Hallonet et al., 1993), even if the entire process is not completely understood yet.

Another process in which centriole formation does not depend only on the mother centriole is the assembly of hundreds of centrioles in multi-ciliated cells. These cells need to sustain a massive production of centrioles, which are then converted into basal bodies to produce hundreds of cilia. For this massive production, cells develop an electron-dense structure called deuterosome, which is responsible for the nucleation of the centrioles (Meunier and Azimzadeh, 2016; Zhao et al., 2013). The deuterosome is formed from the wall of the daughter centriole, and this pathway rely on Deup1, a specific deuterosome-forming factor, paralog of Cep63 (Spassky and Meunier, 2017). Deup1 associates with the deuterosome, recruiting Cep152 and then Plk4 together with the factors belonging to the canonical centriole assembly pathway, allowing centrioles production (Klos Dehring et al., 2013; Zhao et al., 2013). Furthermore, around 10% of the centrioles are formed from the centrioles in a deuterosome-independent pathway that requires Cep63 (Spassky and Meunier, 2017).

1.2.1.4. Cell cycle control of centriole duplication

The centrosome duplication cycle and the cell cycle occur in a coordinated manner and share key regulators.

At the G1/S transition, the cell cycle kinase Cdk2, in complex with cyclin E and cyclin A, is required for both centrosome duplication and DNA replication (Hinchcliffe et al., 1999; Lacey et al., 1999; Meraldi et al., 1999). Indeed, S phase arrest by hydroxyurea treatment of CHO cells leads to the inhibition of Cdk2 activity, with subsequent block of centrosome duplication (Matsumoto et al., 1999; Meraldi et al., 1999). The precise role of Cdk2 in the duplication cycle is not clear yet, but several centrosomal proteins have been identified as Cdk2 substrates. One of these proteins is nucleophosmin, whose phosphorylation by Cdk2-cyclin E and Plk2 promote its removal from the centrosome, thus allowing centriole duplication (Krause and Hoffmann, 2010; Okuda et al., 2000). Another centrosomal substrate of Cdk2 is Mps1, a kinase involved in the regulation of the mitotic spindle assembly checkpoint, while its requirement at the centrosome for centriole duplication is still controversial (Fisk et al., 2003; Fisk and Winey, 2001; Pike and Fisk, 2011; Stucke et al., 2002). A role in centrosome duplication is also played by Orc1, a subunit of the origin recognition complex. During early S-phase, cyclin A promotes Orc1 centrosomal localization, which in turn prevents cyclin E–dependent centriole reduplication (Hemerly et al., 2009). These studies suggest that Cdk2 activation ensures that centrosome duplication is in phase with DNA replication, allowing only one round of centriole duplication per each cell cycle.

Also at the mitotic entry, at G2/M transition, the coordination between centrosome duplication cycle and cell cycle is fundamental. Indeed, Cdk1-cyclin B associates with the centrosomes together with its modulator checkpoint kinase 1 (CHK1). At the onset of mitosis, CHK1 displaces from the centrosome, thus releasing Cdk1-cyclin B activation.

(Jackman et al., 2003; Kramer et al., 2004). Furthermore, Aurora-A phosphorylates CDC25B at the centrosome during mitosis, contributing to the activation of CDK1 (Dutertre et al., 2004). These studies suggest that the centrosomes participate in the temporal and spatial regulation of mitotic entry.

Finally, at the end of mitosis, APC/C might regulate the levels of different proteins important for centriole biogenesis. Indeed, STIL and SAS-6 are targeted by APC/C, leading to the disassembly of the cartwheel (Arquint and Nigg, 2014; Arquint et al., 2012; Puklowski et al., 2011; Strnad et al., 2007; Tang et al., 2009).

1.2.1.5. Centrosome nuclear association

During most stages of the cell cycle, centrosomes are localized at the cell center between the nucleus and the Golgi complex. In particular, in most cells, centrosomes are closely associated with the nuclear envelope (Bornens, 1977; Starr, 2009) and they remain attached to each other upon mild homogenization (Nadezhdina et al., 1979), thus a structural link was proposed to mediate their interaction. This connection would be useful to maintain the nucleus-centrosome axis and to determine the polarity of interphase cells, on top of ensuring correct spindle assembly.

Few reports suggest a role for actin in the nucleus-centrosome interaction. In fact, actin and Arp2/3 have been found at the centrosome, and actin depolymerization affects the interaction between the two organelles (Hubert et al., 2011; Shay et al., 1974). However, the exact role of actin filaments in this process remains unknown.

In the G2 phase, the mother centriole is attached to the nuclear pore complex, and some mechanisms have been described for this connection. First, it has been shown that dynein-dynactin is recruited at the nuclear pore complex, keeping centrosomes tethered to the nucleus. This connection occurs through the interaction of dynein-dynactin with

the adaptor Bicaudal D (BICD), that in turn is recruited to the nuclear envelope by a component of the nuclear pore complex, Nup358 (Splinter et al., 2010). Dynein can also interact with a complex formed by NudE/NudEL and CENP-F, localized at the nuclear pore through interaction with the nuclear pore complex protein Nup133 (Bolhy et al., 2011).

Furthermore, the nuclear envelope has been shown to interact with the centrosome through the LINC complex, a protein complex that spans both nuclear membranes, composed of SUN proteins in the inner membrane and KASH in the outer membrane. The cytoplasmic domains of the KASH proteins nesprin-1 and nesprin-2 can interact with dynein and kinesin complexes and thus mediate the interaction with the centrosome (Zhang et al., 2009).

Another protein that has been found to connect the nucleus and the centrosome is emerin, a transmembrane protein localized both at the inner and outer nuclear membrane (Salpingidou et al., 2007). The depletion or deletion of emerin leads to increased nucleus-centrosome distance, as well as to a decrease in nuclei and centrosome co-sedimentation ratio, indicating that centrosomes are detached from the nucleus (Salpingidou et al., 2007). Emerin interacts directly with microtubules, and both are required for the association of the centrosome with the nuclear envelope (Salpingidou et al., 2007). Emerin also interacts with nesprin-2, further complicating the picture (Zhang et al., 2005).

1.2.2. The PCM

The PCM is the region of the centrosome that is responsible for the nucleation of the microtubules, and it is composed of a matrix of proteins that allows this process to occur. In animal cells, several hundreds of proteins belong to the centrosome and most of these localize to the PCM (Jakobsen et al., 2011).

One of the best-known components of the PCM is γTuRC, which is deputed to microtubule nucleation. Interestingly, it has been suggested that γTuRC is not the only complex involved in microtubule nucleation: α/β tubulin can be concentrated at the PCM through binding proteins such as TOG and S-CAP complexes, driving spontaneous nucleation. In this picture, γTuRC would be needed to stabilize the microtubules and to protect them from depolymerization (Wiese and Zheng, 2006; Woodruff et al., 2014). Interestingly, centrosomes can act also as actin nucleation centers. In fact, Arp2/3 and WASH were found at the centrosomes, where they promote actin nucleation (Farina et al., 2016).

During the interphase, the PCM is a layered structure that is formed by scaffold proteins. These proteins contain coiled coil domains, which are thought to mediate robust intermolecular interactions required for the assembly of a lattice-like network. The main component of this matrix is pericentrin, which forms fibrils emanating from the mother centriole (Lawo et al., 2012; Mennella et al., 2012; Salisbury, 2003).

Before the onset of mitosis, the PCM undergoes a process called maturation, consisting in a large increase in size and the recruitment of additional proteins. This process is important for the organization of the large number of microtubules needed for mitotic spindle formation. Upon maturation, the PCM does not show the layered organization of the interphase centrosome, but forms a network with interspersed γ-tubulin (Sonnen et al., 2012). PCM maturation is mainly driven by Plk1, which is also required to maintain PCM structure during mitosis (Lane and Nigg, 1996; Mahen et al., 2011). In fact, Plk1 phosphorylates some centrosomal proteins, such as pericentrin, to promote their recruitment to the PCM and initiate its expansion (Conduit et al., 2014; Lee and Rhee, 2011). Plk1 is activated by Aurora A at the G2/M transition (Macurek et al., 2008; Seki et al., 2008), and Aurora A has also a role in the enrichment of centrosomal factors at the

centrosome (Barros et al., 2005; Giet et al., 2002; Kinoshita et al., 2005; Mori et al., 2007; Terada et al., 2003).

During the mitotic exit, together with centriole disengagement, the PCM must be disassembled. This process has not been extensively addressed, but some studies indicate that the dephosphorylation of key scaffold proteins, achieved through Plk1 inactivation and phosphatase activity, could contribute to PCM dissolution (Woodruff et al., 2014). Furthermore, studies performed in flies and worms indicate that MT-dependent forces could ensure the rapid disassembly of PCM during the mitotic exit (Krueger et al., 2010; Megraw et al., 2002; Woodruff et al., 2014).

1.2.3. Centrosome alterations and the effects on the cell cycle

The number of centrioles is tightly controlled during the cell cycle, but alterations in centriole number can occur, leading to pathologies such as cancer (described in the next section). Indeed, cells can respond to centriole number alterations, by activating pathways that ultimately lead to arrest of the cell cycle (Fig. 8) (Nigg and Holland, 2018).

In the absence of centrosomes, obtained by laser ablation, bipolar mitotic spindles form in vertebrates and cell division can proceed (Khodjakov et al., 2000), but acentriolar daughter cells then arrest in the G1 phase (Khodjakov and Rieder, 2001). This G1 arrest that follows centrosome loss is due to the activation of p53 (Lambrus et al., 2015; Wong et al., 2015), which instead leads to apoptosis in the mouse embryo (Bazzi and Anderson, 2014). To understand which is the pathway that activates p53 following centrosome loss, recent studies used genome-wide CRISPR/Cas9 knock-out screenings (Fong et al., 2016; Lambrus et al., 2016; Meitinger et al., 2016). In this kind of screening, a genome-wide library of knock-out cells was generated and centrosomes were removed from these cells to induce G1 arrest. Centrosome deletion was achieved through Plk4 inhibition, with the

use of different strategies, such as the specific Plk4 inhibitor centrinone. Once the knock-out cell library was arrested in the G1 phase, the deletion of proteins required for cell cycle arrest gave a growth advantage to cells that were able to rescue the p53-dependent block of cell proliferation. These cells were analyzed through next-generation sequencing (NGS), leading to the identification of the genes involved. By this method, three independent studies identified a USP28–53BP1–p53–p21 signaling axis, which was later called the “mitotic surveillance pathway” (Fig. 8) (Fong et al., 2016; Lambrus et al., 2016; Meitinger et al., 2016).

Mechanistically, it has been suggested that 53BP1 acts as a scaffold to facilitate USP28‑dependent deubiquitylation and activation of p53 (Cuella-Martin et al., 2016), leading to cell cycle arrest. How centrosome loss can trigger the activation of this pathway is still unknown, but it probably depends on the prolonged duration of mitosis due to the absence of centrosomes. Indeed, acentriolar spindle assembly is less efficient compared to centrosome-dependent assembly, leading to an increase in the time required for cell division, and in particular of prometaphase (Bazzi and Anderson, 2014). When this time overcomes a threshold, called the “mitotic timer”, the USP28–53BP1–p53 axis is activated and cell cycle arrest occurs (Fong et al., 2016; Lambrus et al., 2016; Meitinger et al., 2016; Nigg and Holland, 2018).

Interestingly, these screenings have identified also the E3-ubiquitin ligase TRIM37 as a potential candidate for cell cycle arrest after centrosome loss. It has been shown that the deletion of TRIM37 enables the formation of extra-centrosomal microtubule organizing centers, thus reducing the duration of mitosis and allowing the cell to bypass cell cycle arrest caused by centrosome loss (Fong et al., 2016).

Moreover, also centrosome amplification leads to cell cycle arrest in the G1 phase in a p53-depended manner that does not rely on 53BP1–USP28. Two pathways have been

described so far that link centrosome amplification to p53 activation and cell cycle arrest. First, it has been shown that tetraploid cells, which contain twice the normal number of centrioles, are arrested in the G1 phase through the activation of the Hippo pathway (Ganem et al., 2014). In particular, the activation of the Large tumor suppressor kinase 2 (LATS2) leads to the inhibition of Mdm2 and stabilization of p53. Furthermore, LATS2 can phosphorylate the transcription factor Yes-associated protein (YAP), which gets inactivated and translocates to the cytoplasm, thus inhibiting proliferation (Fig. 8) (Ganem et al., 2014).

Recently, another mechanism was described for p53 activation after centrosome amplification, which involves the activation of the multiprotein complex PIDDosome. When the PIDDosome is activated, it causes the activation of caspase-2, which in turn can cleave Mdm2 thus leading to the stabilization of p53 (Fig. 8) (Fava et al., 2017).

Interestingly, also centrosome structure alterations can lead to p53–mediated cell cycle arrest. These structural defects may be caused by the depletion of several centrosomal proteins, which generate similar defects, like centrosome fragmentation (Mikule et al., 2007). It was already reported that the depletion of PCM-1, a protein of the centriolar satellites, or centriolin, a protein of the subdistal appendages, causes G1 arrest (Dammermann and Merdes, 2002; Gromley et al., 2003). Irrespective of the protein being depleted, the structural defects appear to lead to the activation of a p38-MAPK-mediated stress response pathway, in which activated p38-MAPK phosphorylates p53, leading to its activation (Mikule et al., 2007), but the validity of these findings is still controversial (personal communication).

Given the importance of a correct centrosome structure and number for a faithful chromosome segregation, the mechanisms described in these studies act as defense

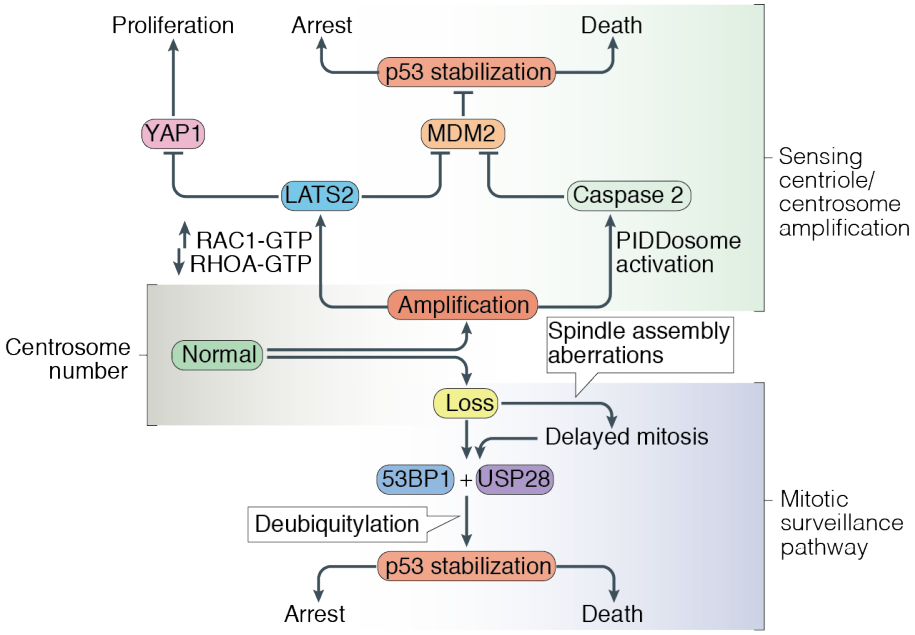

Figure 8: Cells can detect alterations in centrosome number, leading to the stabilization of p53 and subsequent cell cycle arrest.

The scheme describes the pathways that are activated upon centrosome amplification (top) or loss (bottom). Cells can sense increased centrosome number through two pathways. One pathway involves the activation of LATS2, due to downregulation of RhoA deriving from centrosome amplification. LATS2 in turn inhibits Mdm2, resulting in p53 stabilization, and, at the same time, it inactivates YAP1. The secondpathway involves the activation of the PIDDosome, which leads to Caspase2 activation and subsequent Mdm2 cleavage. On the other hand, the mitotic surveillance pathway detects centrosome loss and the subsequent increased duration of mitosis by relying on 53BP1 and USP28 that stabilize p53, thus leading to cell cycle arrest or apoptosis. [Adapted from *Nigg and Holland, Nature Reviews Molecular Cell Biology, 2018*]

---

mechanisms, protecting the cells from the result of an inaccurate chromosomes inheritance after cell division.

1.2.4. Centrosome defects and cancer

As discussed above, centriole formation and duplication are tightly controlled, since centrosome aberrations could contribute to human diseases, such as cancer. In fact, centrosome abnormalities have been described in a variety of tumors, such as breast, prostate, colon, ovarian and pancreatic cancer, but can also be detected in early disease (Godinho and Pellman, 2014). A recent report showed that centrosome amplification and

centrioles excessive length are recurrent features of cancer cells, and are associated with aggressive carcinomas (Marteil et al., 2018).

Centrosome anomalies can derive from structural defects or numerical alterations (Godinho and Pellman, 2014). The role of structural defects in the onset or progression of cancer has been poorly studied. These defects likely derive from alterations in the levels or activity of centrosome proteins. Indeed, it has recently been shown that the overexpression of Ninein-like protein (Nlp) leads to the formation of structurally aberrant centrosome-related bodies, impacting epithelial architecture and causing an increased proliferation of MCF10A cells (Schnerch and Nigg, 2016).

On the other hand, numerical anomalies have been extensively associated with cancer development and progression. Extra centrosome acquisition can be due to different mechanisms. One such mechanism derives from the deregulation of the centriole duplication cycle, which is due to an increased or decreased expression of centrosome proteins, like Plk4 (Chan, 2011; Nigg and Holland, 2018; Nigg and Raff, 2009). On the contrary, cell cycle perturbations can induce alterations in the centriole duplication cycle. For example, G2 arrest, that can derive from DNA damage, leads to Plk1 activation, centriole disengagement and their premature reduplication (Douthwright and Sluder, 2014; Inanc et al., 2010; Loncarek et al., 2010). Failure of cytokinesis causes the cell to retain two nuclei and a double set of centrosomes. These tetraploid cells have pro-tumorigenic properties, derived from their altered karyotype and can eventually lead to growth advantage (Ganem et al., 2007).

Centrosome amplification has detrimental effects on cell viability due to the formation of multipolar spindles, leading to extensive chromosome missegregation and inviable progeny (Ganem et al., 2009). Somatic cells can deal with centrosome amplification to ensure a correct division by clustering or inactivating extra centrosomes, allowing the

formation of bipolar spindles to correctly segregate the chromosomes (Basto et al., 2008; Kwon et al., 2008; Quintyne et al., 2005). Nevertheless, during these processes, multipolar intermediates can form, leading to merotelic chromosome attachment to the spindle and, thus, chromosome missegregation and aneuploidy (Ganem et al., 2009; Silkworth et al., 2009). This mechanism has been shown to be sufficient to promote tumorigenesis in mice (Levine et al., 2017). Since centrosome amplification leads to p53 activation and subsequent cell cycle arrest, it is expected that tumors harboring centrosome defects also show some impairment of the p53 pathway. Indeed, spontaneous lymphomas that develop in mice with centrosome amplification show a downregulation of p53 target genes (Levine et al., 2017).

In addition to the impact on cell division, centrosome amplification can contribute to cancer progression through other mechanisms. In fact, centrosome amplification promotes cell invasion through the activation of the small GTPase Rac1 (Godinho and Pellman, 2014; Godinho et al., 2014). Moreover, supernumerary centrosomes can drive increased or decreased formation of primary cilia, impacting on its signaling capacity and thereby contributing to tumor progression (Coelho et al., 2015; Han et al., 2009; Mahjoub and Stearns, 2012; Wong et al., 2009).

1.2.5. The primary cilium

The primary cilium is a single, usually non-motile organelle that extends from the cell surface in quiescent mammalian cells. It functions as a sensory organ of the cell and it has a major role in several signaling pathways essential for growth and differentiation (Berbari et al., 2009). Primary cilia are made of an axoneme emanating by a basal body derived from the mother centriole, surrounded by a specialized domain of the plasma membrane called ciliary membrane. The axoneme is composed of nine microtubule

doublets, which can have a central pair of microtubules in case of motile cilia, specialized structures present only in a subset of cells (Satir et al., 2010).

The formation of the primary cilium is a highly regulated multistep process. When cells are quiescent, in G1 or G0 phase, primary ciliogenesis begins. Two routes have been described for the formation of the primary cilium. In polarized cells, the basal body can directly dock to the plasma membrane through the distal appendages, from which the primary cilium then protrudes. Alternatively, in non-polarized cells the basal body associates with ciliary vesicles in the cytoplasm, and the axoneme grows inside these vesicles. The fusion of the vesicles with the plasma membrane allows a partial release of the cilium at the cell surface (Benmerah, 2013; Sorokin, 1968). Finally, at the onset of S phase, the cilium is readsorbed and the basal body is detached from the plasma membrane to allow its duplication (Fu et al., 2015; Satir et al., 2010).

For ciliogenesis to occur, the centriole cap proteins CP110 and Cep97 have to be removed from the distal end of the mother centriole (Schmidt et al., 2009). For this process, an essential protein is the kinase TTBK2, which is also involved in the recruitment of Ift proteins (Goetz et al., 2012). Ift proteins direct the anterograde and retrograde movement of other proteins along the ciliary axoneme and are, thus, fundamental for its elongation and for the movement of signaling proteins towards the cell (Pedersen and Rosenbaum, 2008). Another group of proteins important for the transport of proteins in the primary cilium is the BBSome, a group of eight proteins that act in membrane extension by the activation of Rab8 and mediate trafficking of integral membrane proteins to the ciliary membrane (Nachury et al., 2007). Once elongated, the axoneme is stabilized by post-translational modifications, like acetylation and glutamylation, to ensure its stability (Westermann and Weber, 2003).

The presence of the distal appendages that are docked to the plasma membrane generates separate membrane compartments. In fact, the membrane domain surrounding the cilium is called ciliary membrane and is separated from the plasma membrane thanks to the distal appendages (Fig. 9). Docked distal appendages are called transition fibers and act as diffusion barrier, limiting the exchanges between different membrane compartments (Benmerah, 2013). Furthermore, the primary cilium of different cell lines is partially intracellular, since the basal body is docked at the bottom of an invagination (Fig. 9) (Barnes, 1961; Sorokin, 1962). The portion of plasma membrane going from the transition fibers to the region where the axoneme emerges from the cell membrane is called ciliary pocket (Fig. 9) (Molla-Herman et al., 2010). The ciliary pocket has functional characteristics that are distinct from the plasma membrane and the ciliary

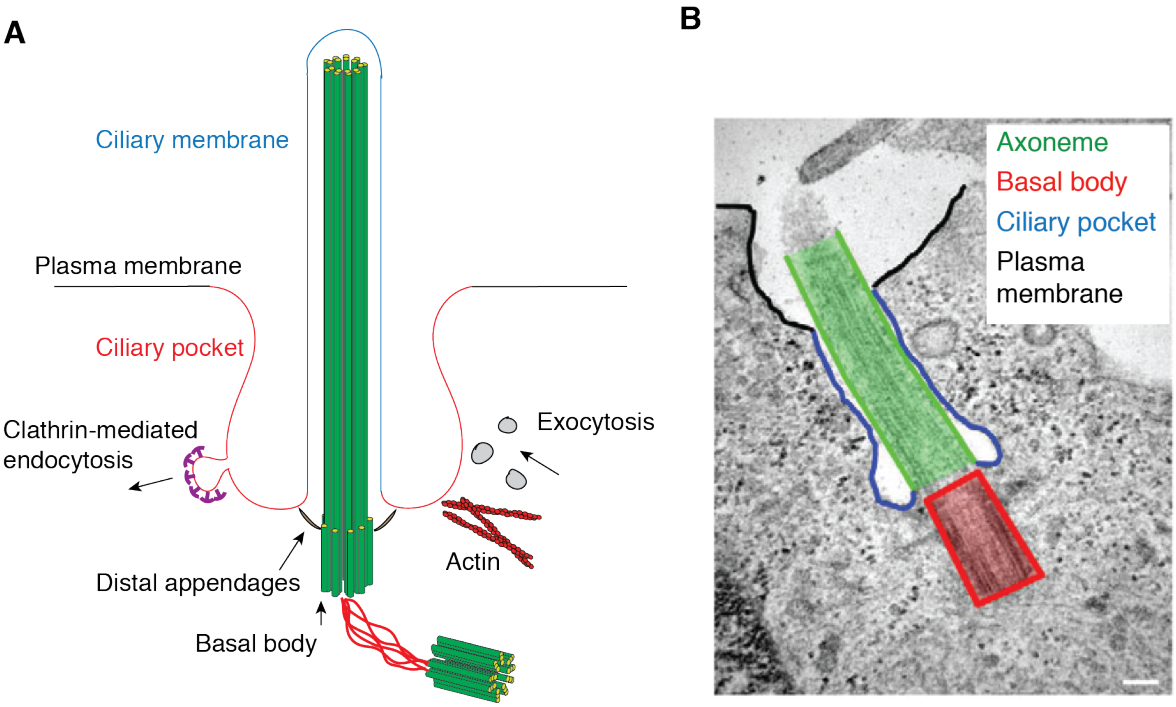

Figure 9: The structure of the primary cilium.

(A) The primary cilium is composed of an axoneme emanating from the basal body that is docked to the plasma membrane through the distal appendages. The ciliary pocket membrane (purple) is the region of the membrane from the distal appendages until the membrane emerges to the extracellular environment. Both clathrin-mediated endocytosis and secretion processes occur at the ciliary pocket. (B) TEM images of hTERT-RPE1 cells showing the different membrane and ciliary compartments. Scale bar: 100 nm. [Adapted from *Molla-Herman et al., Journal of Cell Science, 2010*]

membrane. In fact, it is characterized by an enrichment in clathrin-coated pits, suggesting that it acts as a specialized endocytic compartment (Molla-Herman et al., 2010). In addition, this membrane domain is a docking site for actin cables that could act as structural element and aid vesicle trafficking. Actin fibers surrounding the ciliary pocket can also act as sensors of mechanical stress (Ghossoub et al., 2011; Molla-Herman et al., 2010).

When the cells exit from quiescence or G1 phase to enter into S phase, the primary cilium is readsorbed and the basal body dissociates from the plasma membrane. This process is driven by components of the cell cycle and is reported to occur in two waves (Pugacheva et al., 2007). The first wave occurs at the G1/S transition and is regulated by Aurora A. This kinase induces cilium disassembly through phosphorylation and subsequent activation of HDAC6, which deacetylates axoneme tubulin, a process required for its resorption (Pugacheva et al., 2007). The inhibition of Aurora A or HDAC6 not only inhibits cilia disassembly, but also the onset of S-phase, suggesting that the cilia have an inhibitory effect on cell cycle progression (Fu et al., 2015; Li et al., 2011). A second wave of cilia resorption occurs in G2 and is dependent on the phosphorylation of HDAC6 by Plk1, again promoting tubulin deacetylation (Wang et al., 2013).

1.2.6. Centriolar satellites

Electron microscopy studies identified electron dense granules clustered around the centrosomes named centriolar satellites. Centriolar satellites are numerous non-membrane particles of around 70-100 nm in diameter and can vary in molecular composition, abundance and localization, and are detectable in almost all mammalian cell types (Kubo and Tsukita, 2003).

The main component of centriolar satellites is pericentriolar material 1 protein (PCM1), a scaffold protein. PCM1 is not only able to self-interact and aggregate, but its coiled–coil domains mediate the interaction with other satellites proteins. To date, studies about satellite protein composition identified more than 100 proteins involved in various functions of the cell, such as ciliogenesis, microtubule organization and centrosome duplication (Gupta et al., 2015; Hori and Toda, 2017; Tollenaere et al., 2015).

One of the main functions of the satellites is to maintain centrosome protein homeostasis. Indeed, thanks to their physical coupling with microtubule-associated motor proteins, they are required to ensure the centrosomal recruitment of proteins like ninein, centrin, pericentrin and Nek2A (Dammermann and Merdes, 2002; Hames et al., 2005). On the contrary, the localization of some proteins at the centrosome is increased upon satellites disruption (Kim and Rhee, 2011; Oshimori et al., 2009; Stowe et al., 2012), suggesting that the satellites can act as storage sites, while the levels of other proteins such as oral-facial-digital syndrome 1 (OFD1) are unaffected (Lopes et al., 2011). Interestingly, satellites are only present during interphase and undergo dissolution during mitosis, tuning the centrosome composition during spindle formation and chromosome segregation (Dammermann and Merdes, 2002; Lopes et al., 2011; Tollenaere et al., 2015).

The importance of centriolar satellites for the maintenance of centrosome homeostasis is supported by the fact that PCM1 depletion, which is used to disrupt the satellites, leads to centriole fragmentation or loss, accompanied by the activation of the p38MAPK-p53 signaling axis and G1 arrest (Mikule et al., 2007; Srsen et al., 2006). Interestingly, satellites proteins are required for the centrosomal localization of Cdk2, a kinase involved in centriole duplication (Kodani et al., 2015; Meraldi et al., 1999).

Even if a complete picture of satellites functions has not been described yet, some studies indicate that they can also play a role in ciliogenesis, autophagy and actin filament

organization. Indeed, satellites are involved in the assembly of the BBSome, since BBS4 recruitment to the basal body depends on these organelles, thus regulating cilium assembly (Chamling et al., 2014). Furthermore, satellites play a role in the timing of cilium re-adsorption, as PCM1 can be phosphorylated by Cdk1, an event important for Plk1 localization at the PCM and cilium disassembly (Wang et al., 2013). PCM1 can also be phosphorylated by Plk4, thus promoting ciliogenesis (Hori et al., 2016), suggesting a cell cycle-dependent regulation of PCM1 phosphorylation and cilium assembly/disassembly (Hori and Toda, 2017).

The interplay between satellites and cilium rely also on the OFD1 protein. OFD1 localizes to centrosomes, basal bodies and satellites, and it is required for primary cilium formation (Corbit et al., 2008; Ferrante et al., 2006; Lopes et al., 2011; Singla et al., 2010; Tang et al., 2013). Interestingly, OFD1 at the centriolar satellites is degraded by autophagy and its degradation promotes primary ciliogenesis (Tang et al., 2013).

Interestingly, a functional interaction between satellites and autophagy has been proposed. In fact, it has been shown that PCM1 interacts with GABARAP, a subfamily of Atg8 proteins required for starvation-induced autophagy (Joachim et al., 2017; Szalai et al., 2015). PCM1 is required for GABARAP stability and centrosome localization, thus regulating autophagosomes formation (Joachim et al., 2017).

1.3. p53 and senescence

To monitor the successful completion of cell cycle events, cells have evolved checkpoints that prevent the precocious progression of the cell cycle in the presence of abnormalities, such as DNA damage or lack of nutrients. At the checkpoints, the cell cycle can be arrested until the previous phase is successfully completed, ensuring thus the fidelity of

cell division (Barnum and O'Connell, 2014). Indeed, the loss of these checkpoints can lead to the onset of tumors (Gabrielli et al., 2012).

Several checkpoints have been identified: the G1 checkpoint, the intra-S checkpoint, the G2/M checkpoint and the mitosis-associated spindle-assembly checkpoint (Bower et al., 2017). The G1-S transition is a critical decision point, called "restriction point": cells choose between committing to replicate and duplicate the genome or to enter a resting stage called G0, in which cellular damage can be repaired or the cells can differentiate. The decision to enter into a G0 phase can result in irreversible cell cycle exit in case the damage cannot be repaired, thus acting as a tumor-suppressor mechanism (Campisi, 2011; Malumbres and Barbacid, 2001). The master regulator of the transition from the G1 to the S phases is the transcription factor E2F, that is able to activate genes that drive DNA replication and cell-cycle progression. E2F is regulated by Rb, a tumor-suppressor protein that binds and inhibit E2F in the absence of mitogenic stimuli and in cells that are arrested at the restriction point. The cell cycle progression is thus regulated by the activation of CDKs: during G1, CDK4/6 and CDK2 phosphorylate Rb, which releases E2F. The absence of CDK activity leads to the repression of cell cycle progression. As an example, DNA damage leads to the targeting of the CDKs, thus impeding the progression of the cell cycle to allow DNA repair, as described below (Dick and Rubin, 2013; Giacinti and Giordano, 2006).

1.3.1. p53 modulation and the cellular response: an overview

p53 is one of the most important transcription factors that control the cell cycle and is well known as a tumor suppressor gene that induces apoptosis, cell cycle arrest and senescence in response to stress signals. p53 protein levels have to be tightly regulated to

ensure that the cell cycle can occur in normal condition and that, instead, a proper response to cellular stress inhibits tumor formation.

The major role in this regulation is performed by MDM2, a E3 ubiquitin ligase that targets p53 to degradation in unstressed cells, thus impeding its stabilization and accumulation (Haupt et al., 1997; Kubbutat et al., 1997). The destruction of the interaction between p53 and MDM2 after stress induction occurs through a number of different mechanisms. p53 can be phosphorylated on several sites, disrupting its interaction with MDM2 and thus promoting p53 stabilization (Ashcroft et al., 1999; Shieh et al., 1997). MDM2 can also be targeted for post-translational modifications, like acetylation, that disrupt the interaction with p53 (Wang et al., 2004). Alternatively, MDM2 can be sequestered in the nucleolus by ARF (Weber et al., 1999) or degraded through self-ubiquitination (Hu et al., 2006; Song et al., 2008). These different mechanisms of p53 activation are downstream of different triggers. For example, after DNA damage, p53 is phosphorylated on Ser15 and Ser20 by the DNA damage response kinases (Appella and Anderson, 2001). Instead, hyperproliferative signals, like oncogene activation, function by liberating the E2F transcription factor, which can stimulate ARF transcription and thus MDM2 sequestration (Bates et al., 1998; DeGregori et al., 1997).

The most studied stimuli that leads to p53 activation and cell cycle arrest is DNA damage response (DDR) activation, a complex signaling cascade that is activated by DNA breaks and transiently arrests the cell cycle to allow DNA repair (Ciccia and Elledge, 2010; Polo and Jackson, 2011). Failure in DNA damage repair, and thus prolonged DDR activation, leads to apoptosis or cellular senescence, thus preventing the propagation of altered genomic information to daughter cells.

The DDR is triggered by DNA damage sensors, including the MRN complex, the Ku proteins and the RPA complex that recognize DNA breaks and single-stranded DNA. In

turn, the sensors recruit three key kinases: ATM and DNA-PK in response to double strand breaks, and ATR in response to single strand DNA (Blackford and Jackson, 2017). One of the crucial targets of these apical kinases is the histone variant H2AX, whose phosphorylated form is called γH2AX (Iacovoni et al., 2010; Rogakou et al., 1998), that recruits DNA damage mediators (MDC1, 53BP1, BRCA1). These mediators sustain DDR signaling by enhancing ATM activation (Sulli et al., 2012). Finally, the activated apical kinases phosphorylate the diffusible downstream kinases CHK2 (by ATM) and CHK1 (by ATR), which diffuse in the nucleus and spread the signal to several effectors responsible for the DNA damage checkpoint activation (Sulli et al., 2012). In G1, CHK2 and CHK1 activate the phosphatase CDC25A that inhibits CDK2, preventing the transition to S phase. Moreover, these downstream kinases target p53 and MDM2, inhibiting p53 nuclear exportation and its degradation (Sancar et al., 2004). p53 accumulation in the nucleus leads to the activation of its targets, among which p21, which contributes to cell cycle arrest.

Besides DNA damage and oncogene activation, p53 responds to many other signals, such as nutrient deprivation, hypoxia, oxidative stress, ribosomal stress, adhesion loss and centrosome alterations (Horn and Vousden, 2007; Levine et al., 2006; Nigg and Holland, 2018). These signals use different and independent pathways to stabilize and activate p53, many of which are still not completely understood. Reduced amounts of nutrients, for example, result in the inactivation of the AKT-mTOR pathway, with subsequent MDM2 inactivation and AMPK activation, which directly phosphorylate and activate p53 (Jones et al., 2005; Mayo et al., 2002; Okoshi et al., 2008). MDM2 can also be inactivated by the binding of ribosomal proteins, leading to p53 activation after ribosomal stress (Dai and Lu, 2004; Lindstrom et al., 2007; Zhang et al., 2003). Both hypoxia and oxidative stress,

instead, have been proposed to activate p53 thanks to their capability to induce DNA damage (Vousden and Ryan, 2009).

The different nature, duration and intensity of the cellular stress that cause p53 activation hava an impact on the response, which is in fact highly variable, and depends also on the cell type (Murray-Zmijewski et al., 2008). In response to low levels of stress, p53 leads to temporary cell cycle arrest to allow the cells to repair the damage. Instead, when the stress is prolonged or severe, p53 activation leads to senescence or apoptosis.

p53 can trigger apoptosis through the transcriptional induction of pro-apoptotic genes, such as BAX, PUMA, FAS, NOXA (Riley et al., 2008; Zilfou and Lowe, 2009).

On the contrary, p21 activation by p53 promotes cell cycle arrest and senescence. In fact, p21, being a CDK inhibitor, is a negative regulator of the cell cycle (Xiong et al., 1993). p21 inhibits the activity of the CDK2 and CDK4/6 complexes, regulating cell cycle progression during G1/S phases (Harper et al., 1995; He et al., 2005). In fact, the inhibition of the CDK4-cyclinD complex prevents pRB phosphorylation, which is necessary for the activation of E2F, a transcription factor that promotes cell cycle progression (Bartek et al., 1996). Furthermore, p21 blocks the transition between G1 and S phases by inhibiting the S-phase promoting complex CDK2 (Brugarolas et al., 1999; Harper et al., 1995), which is important for the firing of replication origins and for the initiation of DNA synthesis. Interestingly, p21 can target CDK1, leading to growth arrest in the G2 phase (Bunz et al., 1998; Malumbres and Barbacid, 2009). The inactivation of the CDKs is a fundamental step required for senescence (Herbig et al., 2004; Zalzali et al., 2015).

Even though the main programs regulated by p53 are cell cycle arrest and apoptosis, an increasing number of studies suggests that p53 can modulate other pathways, such as autophagy, metabolism, genome integrity and cellular plasticity (Aylon and Oren, 2016). Despite the attempt to identify all the genes that are regulated by p53, the events

downstream p53 are variable and depend on cell type, differentiation state, stress conditions and environmental signals (Kastenhuber and Lowe, 2017).

1.3.2. Senescence

The first description of senescence comes from the definition of the Hayflick's limit, which describes the loss of proliferative ability of cells due to telomere shortening (Hayflick, 1965). But senescence can be induced also by a variety of other conditions, that lead to what is called "premature cellular senescence". Premature senescence can be caused by several stimuli, most of them leading to DNA damage, like oncogenes activation, loss of tumor suppressors, UV or ionizing radiation, and other kinds of stress, like oxidative environments (Kuilman et al., 2010).

Despite the variety of stimuli that can induce senescence, senescent cells display several common characteristics (Kuilman et al., 2010). The central and indispensable characteristic of senescent cells is the long-term exit from the cell cycle that cannot be reverted by mitogenic stimuli, while in quiescent cells can. This growth arrest is sustained and maintained by two major tumor suppressor pathways: the p53/p21 and the p16INK4a/pRB pathways (Beausejour et al., 2003; Campisi and d'Adda di Fagagna, 2007).

Senescent cells usually show a transformation towards a large and flat morphology (Chen and Ames, 1994; Cho et al., 2004; Serrano et al., 1997) or a spindle-shape morphology (Chan et al., 2005; Michaloglou et al., 2005). Another characteristic of senescent cells, which is frequently used as a marker, is the induction of senescence-associated β-galactosidase (SA-β-gal) (Debacq-Chainiaux et al., 2009; Dimri et al., 1995), which is likely only a consequence of the expansion of the lysosomal compartment in senescent cells that leads to increased β-gal activity (Kurz et al., 2000; Lee et al., 2006; Yang and Hu, 2005). Senescence is also associated with an altered chromatin structure, which shows

the presence of heterochromatic foci (SAHF, senescence-associated heterochromatic foci) (Narita et al., 2003). Heterochromatic-associated proteins are found in the promoters of E2F target genes in senescent cells, thus impeding the cell cycle, and the reduction of SAHFs is associated with the abrogation of senescence (Chan et al., 2005; Kuilman et al., 2008; Ye et al., 2007; Zhang et al., 2007). Furthermore, senescent cells change their secretome, starting the secretion of cytokines, chemokines and proteases, thus called senescence-associated secretory phenotype (SASP) (Campisi, 2005; Coppe et al., 2008; Kuilman and Peeper, 2009; Rodier et al., 2009). The production of SASP can reinforce the senescence phenotype in an autocrine and paracrine manner (Acosta et al., 2013; Acosta et al., 2008; Hubackova et al., 2012; Kuilman et al., 2008), and promote the clearance of senescent cells by the immune system (Xue et al., 2007), but some studies also claim a protumorigenic effect (Dilley et al., 2003; Krtolica et al., 2001; Yang et al., 2006a).

Cells in which senescence was induced by persistent DNA damage also show the presence of senescence-associated DNA damage foci, called DNA-SCARS (DNA segments with chromatin alterations reinforcing senescence). These relatively stable structures contain DDR proteins accumulated at the sites of the damage and are important for growth arrest and SASP (Rodier and Campisi, 2011; Rodier et al., 2011).

None of these markers, taken alone, can uniquely identify senescent cells, as not all senescent cells display all of the described markers, but the combination of one or more of these markers with the activation of cell cycle inhibitors like p53, p21 and p16 are commonly used to indicate senescent cells (Kuilman et al., 2010).

2. Aim of the thesis

Previous results obtained in the lab showed that myosin VI interacts with centrosomal proteins (as described in the Appendix). The binding of centrosomal proteins by myosin VI does not seem to be mediated by a specific splicing isoform of the motor protein, as revealed by the use of cell lines expressing either myosin VI_{short} or myosin VI_{long}. Since the interaction with different cargoes can dictate the localization and function of myosin VI, the binding of centrosomal proteins possibly dictates the localization and potential function of myosin VI at this organelle.

The main aim of this study was to characterize a new potential role of myosin VI at the centrosome. To this end, we used the hTERT-RPE1 cell line, which is widely used for investigations regarding the centrosome.

During the course of our study, thanks to the use of this non-tumor cell line, we uncovered a role of myosin VI also in cell cycle arrest and senescence. Therefore, the second aim of this study was to investigate the mechanism behind the requirement of myosin VI for cell cycle progression in non-tumor cells.

3. Materials and methods

3.1. Buffers

3.1.1. Phosphate-buffered saline (PBS)

NaCl	137 mM
KCl	2.7 mM
Na_2HPO_4	10 mM
KH_2PO_4	2 mM

3.1.2. Tris-buffered saline - Tween (TBS-T)

NaCl	137 mM
KCl	2.7 mM
Tris-HCl pH 7.4	25 mM
Tween-20	0.1%

3.1.3. 10X Sodium Dodecyl Sulphate – PolyAcrylamide Gel Electrophoresis (SDS-PAGE) running buffer

Glycine	192 mM
Tris-HCl pH 8.3	250 mM
SDS	1%

3.1.4. 50X Tris-Acetate-EDTA (TAE)

Tris base	2 M
Acetic acid	1 M
EDTA pH 8	10 mM

3.1.5. 1X JS buffer

Hepes pH 7.4	50 mM
NaCl	150 mM
Glycerol	10%
Triton X-100	1%
$MgCl_2$	1.5 mM
EGTA	5 mM

500X protease inhibitor cocktail from Calbiochem, sodium pyrophosphate pH 7.5 20 mM, sodium fluoride 250 mM, PMSF 2 mM and sodium orthovanadate 10 mM were added to the buffer immediately before usage.

3.1.6. Laemmli buffer

SDS	8%
Tris-HCl pH 6.5	200 mM
Glycerol	40%
DTT	400 mM
Bromophenol blue	0.4%

The Laemmli buffer was prepared as a 4X or 2X stock solution and stored at -20°C.

3.2. Reagents

3.2.1. siRNAs

Protein	siRNA sequence 5'-3'	Source
Myosin VI (siRNA #3)	GAGGCTGCACTAGATACTTTGCTAA	Invitrogen
Myosin VI (siRNA #4)	GAGCCTTTGCCATGGTACTTAGGTA	Invitrogen
p53	CCAGUGGUAAUCUACUGGGACGGAA	Invitrogen
53BP1	GAAGGACGGAGUACUAAUA	Life Technologies
USP28	CCAUGAAGCUCUGAAGGCCAGUAAU	Invitrogen
STAMBPL1	UGCCCUAAGCAAGCUUGGUUGUAAU	Invitrogen

3.2.2. Primary antibodies

Protein	Species	Use	Identifier	Source
Myosin VI	Rabbit	IP, IF (1:400)	1295	Generated by EUROGENTEC S.A.
Myosin VI	Rabbit	IP, IF (1:400), WB (1:2000)	1296	Generated by EUROGENTEC S.A.
p53	Mouse	WB (1:1000)	DO-1	Santa-Cruz Biotechnologies
p21	Rabbit	WB (1:1000)	12D1	Cell Signaling
Acetylated Tubulin	Mouse	IF (1:1000)	6-11B-1	Sigma
Pericentrin	Mouse	IF (1:200)	28144	Abcam
PCM1	Mouse	IF (1:200)	SAB1406228	Sigma
OFD1	Rabbit	IF (1:200)	HPA031103	Sigma
YAP	Mouse	IF (1:100)	Sc-101199	Santa-Cruz Biotechnology

		WB (1:1000)		
P-YAP (Ser127)	Rabbit	WB (1:1000)	4911	Cell Signaling
p38MAPK	Rabbit	WB (1:1000)	9228	Cell Signaling
P-p38MAPK (T180/Y182)	Mouse	WB (1:1000)	3D7 - 9215	Cell Signaling
P-p53 (Ser15)	Mouse	WB (1:1000)	16G8 - 9286	Cell Signaling
P-p53 (Ser20)	Rabbit	WB (1:1000)	9287	Cell Signaling
γH2AX	Mouse	WB (1:1000)	JBW301	Millipore
pH3 (Ser10)	Rabbit	WB (1:1000)	06570	Upstate
CyclinA	Mouse	WB (1:1000)	H432-sc751	Santa-Cruz Biotechnology
Vinculin	Mouse	WB (1:5000)	V9131	Sigma
GAPDH	Mouse	WB (1:5000)	sc-32233	Santa-Cruz Biotechnology
H3	Rabbit	WB (1:1000)	1791	Abcam
Flag	Mouse	WB (1:2000)	M2	Sigma
GFP	Rabbit	IF (1:400) WB (1:5000)		Generated by EUROGENTEC S.A.
Giantin	Mouse	IF (1:1000)	PRB-114C	Babco
BrdU	Mouse	IF (1:5)	B44	BD Biosciences

3.2.3. Secondary antibodies

Antibody	**Use**	**Identifier**	**Source**
Donkey anti-Mouse Alexa 488	IF (1:400)	A-21202	Thermo Fischer Scientific
Donkey anti-Mouse Cy3	IF (1:400)	715-165-150	Jackson lab
Donkey anti-Mouse Alexa 647	IF (1:400)	A-31571	Thermo Fischer Scientific
Donkey anti-Rabbit Alexa 488	IF (1:400)	A-21206	Thermo Fischer Scientific
Donkey anti-Rabbit Cy3	IF (1:400)	711-165-152	Jackson lab
Donkey anti-Rabbit Alexa 647	IF (1:400)	A-31573	Thermo Fischer Scientific
Donkey anti-Goat Alexa 647	IF (1:400)	A-21447	Thermo Fischer Scientific
Anti-Mouse HRP	WB (1:5000)	GENA931	GE Healthcare
Anti-Rabbit HRP	WB (1:5000)	GENA934	GE Healthcare

3.3. Molecular biology techniques

3.3.1. Agarose gel electrophoresis

DNA samples were loaded on 0.8%-2% agarose gels along with DNA markers (1kb or 100bp DNA Ladder, NEB). The gels were made in TAE buffer containing Syber Safe (Thermo Fisher Scientific), according to the manufacturer's instructions, and run at 80 V until desired separation was achieved. The DNA bands were visualized under a UV lamp.

3.3.2. Large scale plasmid preparation

Cells containing transfected DNA were expanded into 250 ml cultures overnight. Plasmid DNA was isolated from these cells using the Macherey-Nagel Maxi-prep kit according to the manufacturer's instructions.

3.3.3. Constructs and plasmids

pcDNA CMV-10 3xFlag-OFD1 was kindly provided by Brunella Franco.

pBABE GFP-H2B was kindly provided by the IFOM Imaging Facility.

ES-FUCCI (Fluorescence Ubiquitination Cell Cycle Indicator) construct was a gift from Pierre Neveu (Addgene plasmid #62451) (Sladitschek and Neveu, 2015).

pSLIK NEO MyoVI shRNA ORF#9 and pSLIK NEO MyoVI shRNA UTR#4 were previously generated in our laboratory. The shRNA sequences are:

- ORF#9: 5'- AGTAATTCAGCACAATATTCCAA - 3'
- UTR#4: 5'- AGAAACATCAGAATATGCCCAT- 3'

3.4. Cell culture

3.4.1. Cell lines

3.4.1.1. Commercial cell lines

hTERT-RPE1 cells (ATCC) were maintained in Dulbecco's Modified Eagle Medium: Nutrient Mixture F-12 (DMEM/F12, Gibco), supplemented with 10% fetal bovine serum (FBS), 2 mM L-glutamine, 0.5 mM Na-Pyruvate, 15mM Hepes pH 7.5.

BJ-hTERT cells (ATCC) cells were maintained in DMEM + Medium199 (4:1), supplemented with 10% FBS and 2 mM L-glutamine.

HEK-293T cells (ICLC) were maintained in DMEM, supplemented with 10% FBS and 2 mM L-glutamine.

HCT-116 GFP-MyoVI cells were kindly provided by Hans-Peter Wollscheid. In brief, GFP-coding DNA was added at the 3' end of the MYO6 gene through CRISPR/Cas9 mediated knock-in in HCT-116 cells. These cells were maintained in DMEM, supplemented with 10% FBS and 2 mM L-glutamine.

All cell lines were authenticated at each batch freezing by STR profiling (StemElite ID System, Promega). All cell lines were tested for mycoplasma at each batch freezing with both PCR and a biochemical test (MycoAlert, Lonza).

3.4.1.2. Generated cell lines

For inducible myosin VI KD, hTERT-RPE1 cells were generated with a pSLIK NEO vector bearing the following shRNA under a doxycycline-inducible promoter:

- shORF (targeting open reading frame): 5' – AGCGCTGGAATATTGTGCTGAATTACTA GTGAAGCCACAGATGTAGTAATTCAGCACAATATTCCAA-3'
- shUTR (targeting untranslated region): 5' – AGCGCTGGGCATATTCTGATGTTTCTTAG TGAAGCCACAGATGTAAGAAACATCAGAATATGCCCAT-3'

Cells were transduced with lentiviral particles containing pSLIK NEO shORF, shUTR or empty vector (EV) as control. After selection with neomycine, to obtain homogeneous cell populations, single cell cloning was performed from bulk populations. A bulk population was used for EV cells. Clones were tested to assess the depletion of myosin VI after induction with doxycycline. For all experiments shown, clone #3 of shORF and clone #3 of shUTR were used.

To generate the hTERT-RPE1 FUCCI cell line, hTERT-RPE1 cells were transfected with the ES-FUCCI construct. mCherry-positive and YFP-positive single cells were sorted by

fluorescence-activated cell sorting (FACS) in 96-well plates for the generation of single cell clones. Clones were tested for the expression of mCherry and YFP. Clone #6 was chosen to be used for the experiments.

To generate the hTERT-RPE1 H2B-GFP cell line, hTERT-RPE1 cells were transduced with the pBABE H2B-GFP construct. Two weeks after transduction, GFP-positive cells were FACS-sorted by fluorescence-activated cell sorting and pooled.

For the genome-wide CRISPR/Cas9 screening, hTERT-RPE1 cells stably expressing Cas9 (kindly provided by Andrew Holland, (Lambrus et al., 2016)) were transduced with pSLIK NEO shUTR (as described above). After selection with neomycine, to obtain homogeneous cell population, single cell cloning was performed from bulk populations. Clones were tested to assess myosin VI depletion after induction with doxycycline. For all experiments shown, clone #8 of shUTR was used.

All of the hTERT-RPE1 cell lines containing a doxycycline-inducible construct were maintained in DMEM/F12, supplemented with 10% tetracycline-free FBS, 2 mM L-glutamine, 0.5 mM Na-Pyruvate and 15mM Hepes pH 7.5.

3.4.2. Transfection and transduction

3.4.2.1. siRNA transfection

siRNA transfections were performed using the LipofectAMINE RNAi MAX reagent from Invitrogen, according to the manufacturer's instructions. Cells were subjected to a single transfection in suspension, using 8 nM siRNA. For transfection of two siRNAs, each siRNA was transfected at a concentration of 8 nM. Mock-treated cells were subjected to the same procedure, without siRNA in the transfection mixture. Cells were incubated overnight at 37°C with the transfection mixture and the culture medium was changed one day after the transfection.

3.4.2.2. DNA transfection

DNA transfections were performed using the calcium phosphate transfection method. HEK-293T cells were plated on 10 cm cell culture dishes in order to achieve a 50% confluency on the day of transfection. The DNA/$CaPO_4$ complex was formed by mixing 10 µg of DNA and 240 mM $CaCl_2$ with the HBS solution. The solution containing the DNA/$CaPO_4$ complex was added to the cell culture medium. Cells were incubated overnight at 37°C with the transfection mixture and the culture medium was changed one day after the transfection. For immunoprecipitation assays, cells were lysed 48 hours after the transfection.

3.4.2.3. DNA transduction

For the generation of cell lines that stably incorporate exogenous DNA, DNA transduction through lentiviruses or retroviruses was performed.

For DNA transduction through lentiviruses, HEK-293T cells were transfected with 10 µg of the transfer DNA together with plasmids encoding for GAG, POL, ENV (VSVG) and REV retroviral proteins, through the calcium phosphate transfection method. For DNA transduction through retroviruses, Phoenix cells were transfected with 10 µg of the transfer DNA through the calcium phosphate transfection method. One day after the transfection, the medium was replaced with 5.5 ml of fresh medium to concentrate the virus. After 24 hours, the viral supernatant was collected and passed through PVDF 0.45 µm Millipore filters. The supernatant was used to infect target cells after adding 8 µg/ml polybrene. For retrovirus transfection, an additional infection step was performed 6 hours after the first one. 48 hours after the infection, selection of infected hTERT-RPE1 cells was performed by adding 450 µg/ml neomycin or 3.5 µg/ml puromycin.

3.5. Polymerase chain reaction (PCR)

3.5.1. Real Time PCR

Cells were collected and RNA was extracted using Maxwell® RSC simplyRNA tissue kit (Promega). Concentration and purity was determined by measuring optical density at 260 and 280 nm using a Nanodrop spectrophotometer. cDNA was generated from 1µg of RNA using the Applied Biosystems™ High-Capacity cDNA Reverse Transcription Kit (Thermo Fisher Scientific). Samples were analyzed by the Real Time PCR facility through the TaqMan method with MYO6:hs00192265_m1, STAMBPL1:hs00697414_m1, TP53:hs00153349_m1, CDKN1A:hs00355782_m1 probes (Applied Bioscience). The amplicon expression in each sample was normalized to GAPDH and GUSP mRNA content.

3.6. Protein procedures

3.6.1. Cell lysis

After washing with 1X PBS, cells were pelleted and the dry pellet was either frozen at -80°C or directly processed. Cell pellets were lysed in JS buffer and incubated for 20 minutes on ice. Lysates were cleared by centrifugation at 16 000 g for 20 minutes at 4°C. Protein concentration was measured by the Bradford assay (Biorad) following the manufacturer's instructions.

3.6.2. SDS-Polyacrylamide gel electrophoresis (SDS-PAGE) and Western blot (WB)

Proteins were denatured by adding 4X Laemmli Buffer and by boiling at 95°C for 5 minutes. Proteins were then separated on precast gradient gels (4–20% TGX precast gel, Bio-Rad) by SDS-PAGE and transferred to nitrocellulose membranes by Transblot Turbo (BIO-RAD). Ponceau staining was used to determine the efficiency of the protein transfer

onto the membrane. Membranes were blocked for 1 hour (or overnight) in 5% milk in TBS supplemented with 0.1% Tween (TBS-T). After blocking, the filters were incubated with the primary antibody, diluted in TBS-T 5% milk, for 1 hour at room temperature (RT), or overnight at 4°C. After washes, the membranes were incubated with the appropriate horseradish peroxidase (HRP)-conjugated anti-mouse or anti-rabbit secondary antibodies (GE Healthcare) diluted in TBS-T for 30 minutes at room temperature. After washes, the bound secondary antibody was detected with ECL (GE Healthcare). Western blots were visualized using films (GE Healthcare) or Chemidoc (Bio-Rad).

3.6.3. Immunoprecipitation (IP)

HEK-293T cells were transfected with the indicated constructs. After 48 hours, the cells were lysed in JS buffer and incubated for 20 minutes on ice. Lysates were cleared by centrifugation at 16 000 g for 20 minutes at 4°C.

Anti-Flag IP was performed by incubating 1 mg lysate with anti-Flag M2 conjugated beads (Sigma) for 2 hours at 4°C. For anti-myosin VI IP, 1 mg lysate was incubated with anti-myosin VI antibodies (1295 and 1296) or anti-GST rabbit antibody as negative control. After 2 hours of incubation at 4°C, protein A sepharose beads were added to the IP and the mixture was incubated for an additional hour. For anti-GFP IP, 1 mg lysate was incubated with anti-GFP lama conjugated beads (home-made) for 2 hours at 4°C. Precipitated immunocomplexes were washed, loaded on a precast gradient gel (4–20% TGX precast gel, Bio-Rad) and analyzed by WB.

3.7. Cell assays

3.7.1. Immunofluorescence (IF)

For immunostaining, cells were plated on coverslips coated with 0.2% gelatine. Cells were rinsed twice with 1X PBS and fixed with 4% paraformaldehyde (PFA) for 10 minutes at room temperature, or in methanol (Me-OH) 100% at -20°C for 10 minutes. After fixation with PFA, the cells were rinsed three times in 1X PBS and permeabilized with 1X PBS 1% bovine serum albumin (BSA) – 0.1% Triton for 10 minutes. In order to minimize aspecific antibodies interactions, the coverslips were incubated with 1X PBS-T 2% BSA (Blocking solution) for 30 minutes. Primary antibodies were diluted in 1X PBS 1% BSA and the incubation was performed for 1 hour at RT. After three washes in 1X PBS, the cells were incubated with secondary antibodies conjugated with fluorophores or with Phalloidin-TRITC (Sigma-Aldrich, cat. P1951) to visualize actin, diluted in 1X PBS 1% BSA for 30 minutes at RT. The cells were then washed three times in 1X PBS. To label the nuclei, DAPI (Sigma-Aldrich, cat. D9542), diluted 1:5000 in 1X PBS, was added to the cells for 10 minutes at RT. The coverslips were mounted on glass slides using Mowiol Mounting Medium (Calbiochem) or glycerol solution (20% glycerol, 50 mM Tris pH=8.4) to avoid mechanical deformation of the samples.

For anti-acetylated tubulin staining, microtubule depolymerization was induced by incubating the cells in PBS at +4°C for 1 hour before fixation with Me-OH.

For OFD1 and PCM-1 staining, cells fixed with Me-OH were incubated with Saponin blocking buffer (0.5% BSA, 0.05% saponin, 50 mM ammonium chloride, 0.02% sodium azide in PBS) for 20 minutes. The anti-OFD1 antibody was diluted in Saponin blocking buffer, in which the cells were incubated for 2 hours. The anti-rabbit Cy3 secondary antibody, diluted in Saponin blocking buffer, was added, followed by incubation for 45

minutes. DAPI staining was used to label the nuclei. The coverslips were mounted on glass slides using Mowiol Mounting Medium (Calbiochem).

Widefield images were collected using an Olympus BX61 upright microscope equipped with Photometrics Coolsnap EZ black & white camera and 60X/1.35 oil immersion UPlanSApo. The software used for image acquisition was Metamorph. Confocal microscopy was performed on a Leica TCS SP5 laser confocal scanner mounted on a Leica DMI 6000B inverted microscope equipped with HCX PL APO 63X/1.4NA oil immersion objective. The software used for image acquisitions was Leica LAS AF.

3.7.2. Primary cilium assembly/disassembly

hTERT-RPE1 cells were plated on coverlips coated with 0.2% gelatine. To allow cilium assembly, cells were cultured in medium with 0% serum (DMEM/F12 supplemented with 2 mM L-glutamine, 0.5 mM Na-Pyruvate, 15 mM Hepes pH 7.5). For cilium disassembly, complete medium was added to the cells (DMEM/F12 supplemented with 10% FBS, 2 mM L-glutamine, 0.5 mM Na-Pyruvate, 15 mM Hepes pH 7.5). Microtubules depolymerization was induced incubating the cells in PBS at +4 °C for 1 hour before Me-OH fixation. Then, IF was performed with anti-acetylated tubulin primary antibody.

3.7.3. Transmitted electron microscopy (TEM)

Cells were transfected with the indicated siRNA 96 hours before fixation and plated on MatTek dishes (P35G-1.5-14-C-GRID MatTek Corporation). The cells were then fixed and stained with anti-pericentrin antibody as described by Mironov and Besnoussenko (Mironov and Beznoussenko, 2013). In brief, cells were fixed with Fixative 1 (0.05% gluteraldehyde, 4% PFA in 0.15 M Hepes pH=7.2) for 5 minutes, and then with Fixative 2 (4% PFA in 0.15 M Hepes pH=7.2) three times for 10 minutes. Coverslips were washed

with 0.2 M Hepes pH=7.2 and incubated with Blocking solution (5% BSA, 1% Saponin, NH_4Cl in 0.2 M Hepes pH=7.2) for 30 minutes. Anti-pericentrin primary antibody was diluted in Blocking solution and the incubation was performed for 1 hour at RT. After three washes in 0.2 M Hepes pH=7.2, the cells were incubated with anti-mouse Alexa488 secondary antibody diluted in Blocking solution for 30 minutes at RT. The cells were then washed three times in 0.2 M Hepes pH=7.2. Images were acquired with a Leica inverted SP5 microscope with a laser-scanning confocal system. Pericentrin staining was used to identify the centrosomes, and Z-sections were performed in order to identify the section in which the centrosomes were present after resin embedding and cutting.

For electron microscopy, the cells were processed as previously described (Beznoussenko and Mironov, 2015; Polishchuk and Mironov, 2001). After image acquisition, the cells were fixed with 2.5% glutaraldehyde in 0.2 M sodium cacodylate pH 7.2 for 2 hours at RT. Afterwards, the cells were washed six times in 0.2 sodium cacodylate pH 7.2 at RT, followed by osmification: the cells were incubated for 1 hour at RT with a 1:1 mixture of 2% osmium tetraoxide in distilled water and 3% potassium ferrocyanide in 0.2 M sodium cacodylate (pH 6.9), rinsed six times for 5 minutes with the cacodylate buffer, and then treated with 0.3% Thiocarbohydrazide in 0.2 M cacodylate buffer (pH 6.9) for 10 minutes, washed three times with 0.2 M cacodylate buffer (pH 6.9) and treated with 1% OsO4 in 0.2 M cacodylate buffer (pH 6.9) for 30 minutes. The samples were then rinsed with 0.1 M sodium cacodylate (pH 6.9) buffer until all traces of the yellow osmium fixative had been removed. The samples were thereafter dehydrated: 3x10 minutes in 50% ethanol; 3x10 minutes in 70% ethanol; 3x10 minutes in 90% ethanol; and 3x10 minutes in 100% ethanol. The samples were subsequently incubated for 2 hours in 1:1 mixture of 100% ethanol and Epoxy resin (Epon) at RT. The mixture was then removed with a pipette and

finally the samples were embedded for 4 hours in Epoxy resin at RT. The resin was polymerized for at least 72 hours at 60°C in an oven.

The samples embedded into the resin were carefully picked and sectioned with diamond knife (Diatome, Switzerland) using Leica EM UC7 ultramicrotome. Sections (50-60 nm) were analyzed with a Tecnai 20 High Voltage EM (FEI, The Netherlands) operating at 200 kV.

3.7.4. Nuclei-centrosome distance

Cells were transfected with the indicated siRNA 96 hours before fixation and plated on coverslips coated with 0.2% gelatin. The cells were then fixed with 4% PFA and stained with anti-pericentrin and anti-giantin antibodies. F-actin was visualized with phalloidin reagent (Thermo Fisher Scientific) and the cells were mounted with VECTASHIELD® Antifade Mounting Medium containg DAPI to visualize the nuclei. Images were acquired every 0.3 µm of the focal plane using z-stack function with Ti inverted microscope (Nikon) equipped with the UltraVIEW VoX spinning-disc confocal unit (PerkinElmer) and Velocity software (PerkinElmer).

The images were processed using ImageJ software with custom-built plugins allowing automated image analysis (Infante et al., 2018). First, Z-stacks from all the channels were projected, then the nuclei were registered using a reference image. Then, the nuclei signal was subtracted using Otsu filter whereas the pericentrin channel was subtracted using the Yen filter. Finally, the custom-built plugin measured distance between the centrosome signal and the closest border of the nucleus. As an output, the custom-built plugin created a single file with color-coded nucleus and pericentrin allowing to check the quality of the analysis. Images with lacking pericentrin signal were excluded from the

analysis. All the data were summarized in the table that was imported to Prism (version 7.0d) where statistical analysis using Kruskal-Wallis test was performed.

3.7.5. Growth curve

Cells were transfected with the indicated siRNAs. After 24 hours, 10 000 cells were plated on a 6-well plate (day 0). From day 3 to 7 after plating, the cells were detached and counted using Beckman Multisizer 3 Coulter Counter. Cell counts were plotted to display the growth curve. During the experiments, the cells were split upon reaching 70% confluence to avoid slowdown of proliferation due to contact inhibition. Cell dilution was taken into consideration for the total cell count. Inhibitors were added to the cell culture media two days after transfection.

3.7.6. Bromodeoxyuridine (BrdU) incorporation assay

Cells were plated on coverslips and after 24 hours they were incubated in the cell culture incubator with 10 µg/ml BrdU for 20 minutes, 2 hours or 9 hours, as indicated. After the incubation, the cells were fixed with 4% PFA for 10 minutes. To denature the DNA and allow the anti-BrdU antibody to bind, cells were incubated with 2N HCl for 20 minutes. HCl was neutralized with 0.1 M sodium borate pH 8.5 for 5 minutes, and immunofluorescence was performed using anti-BrdU antibody. DAPI staining was used to detect the nuclei. The incorporation of BrdU was evaluated by calculating the percentage of cells that displayed BrdU staining in the nucleus, over the total number of cells stained with DAPI.

3.7.7. Multiparameter image cytometry analysis

Cells were transfected with the indicated siRNAs for the depletion of myosin VI and plated on coverslips coated with 0.2% gelatin. After 72 hours, the cells were fixed with 4% PFA and processed for the 5-parameter microscopy analysis. After blocking (5% BSA in PBS), the cells were incubated for 1 hour at RT with the following primary antibodies: anti-myosin VI (rabbit, 1296); anti-p21 (mouse, M7202, Dako); and anti-p53 (goat, sc-6243). After washing, the cells were incubated for 1 hour at RT with the secondary antibodies: anti-rabbit Cy3, anti-mouse A488 and anti-goat A647. The cells were then fixed again with 4% PFA, blocked with 5% BSA containing mouse-IgG and incubated for 1 hour with anti-Ki67 Pacific Blue-conjugated (mouse, Becton Dickinson). The DNA was counterstained with DAPI. Slides were then mounted in Mowiol-containing mounting media. Images were collected by a BX61 fully motorized Olympus fluorescence microscope controlled by Scan^R software (version 2.2.09, Olympus Germany). An oil-immersion 60X 1.3 NA objective was employed for image acquisition.

For the quantitative analysis of images, the computational platform A.M.I.CO. (Automated Microscopy for Image-Cytometry) was used, as described by Furia and colleagues (Furia et al., 2013a, b). Briefly, cell identification was based on segmentation of DAPI nuclei signals and, thus, the analysis of all acquired parameters was limited to nuclear expression and localization. Mean and maximum values of fluorescence per pixel were calculated, together with the integrated fluorescence intensity per cell. Then, the software creates a flow-cytometry like data-analysis interface, which was used to generate dot-plots of cell populations. The number of events analyzed was between 5 000 and 10 000 per sample.

To separate low and high range of expression of Ki67, p53 or p21, the distribution in each channel was fit by a Gaussian curve, and a threshold was set for each parameter at the

1% upper edge of the calculated distribution. After setting this gate, in samples in which a low-expressing population was identifiable (MyoVI depleted for Ki67, Mock for p53 and p21), the percentage of high- or low-expressing cells was calculated in all samples.

3.7.8. Flow cytometry analysis of cell cycle profile

Myosin VI shRNA expression was induced with 0.5 µg/ml doxycycline for ten days. The cells were then washed, detached and washed once in PBS. After centrifugation, cell pellets were resuspended in 250 µl 4°C-cold PBS and fixed by adding 750 µl 100% Et-OH (-20°C) dropwise while vortexing. The cells were left in the fixative for 1 hour on ice, washed in PBS-1% BSA, and resuspended in 1 ml PI (50 µg/ml) + RNAse (250 µg/ml). After incubation at 4°C overnight, flow cytometry was performed for cell cycle analysis. Sample acquisition was performed with FACSCanto II (Beckton Dickinson). Analysis of cell cycle distribution was performed with ModFitLT V3.1 software.

3.7.9. SA-β-gal assay

Cells were grown on coverslips, washed in PBS and fixed with 4% PFA for 10 minutes. Then, the cells were incubated with SA-β-gal staining solution containing 1 mg 5-bromo-4-chloro-3-indolyl β-D galactopyranoside (X-Gal) per ml, 40 mM citric acid/sodium phosphate pH 6.0, 5 mM potassium ferrocyanide, 5 mM potassium ferricyanide, 150 mM NaCl, and 2 mM MgCl2. After incubation at 37°C overnight, the cells were washed with PBS and mounted on glass slides using Mowiol Mounting Medium. Images were acquired with a digital camera connected to a white-light microscope. SA-β-gal activity was detected in senescent cells as local perinuclear blue precipitate.

3.7.10. Ionizing radiation

To induce DNA damage as positive control, cells were irradiated with 2 Gy or 5 Gy with ionizing radiation by a high-voltage X-rays generator tube (Faxitron X-Ray Corporation).

3.7.11. Time-lapse imaging

Cells were seeded on 6-well plates and transfected with the indicated siRNA for the depletion of myosin VI 24 hours before initiating the time-lapse. Live-cell imaging was performed with an ORCA-ER camera (Hamamatsu) on an Olympus IX81 automatic microscope equipped with closed heating and CO_2 perfusion devices. Brightfield and GFP images were acquired every 3 minutes for 72 hours. Data analysis was performed by calculating the number of cells undergoing mitosis during 12 hours, and by calculating the time occurring between chromosome condensation and decondensation after cell division.

3.8. CRISPR/Cas9 genome-wide screening

3.8.1. Genome-wide knock-out library generation

The Lentiviral Prep of the Human CRISPR Knockout Pooled Library (Brunello) was purchased from Addgene (#73178-LVC) (Doench et al., 2016). The Brunello library contains 76 441 sgRNAs targeting 19 114 genes and 1 000 non-targeting sgRNAs as controls.

hTERT-RPE1 Cas9 shUTR cells were transduced with the Brunello library via spinfection. A total of $90*10^6$ cells were mixed with 34 µl Lentiviral Prep (titer $5.3*10^5$ TU/ml, MOI~0.2), plated in 12-well plates ($2*10^6$ cells per well) and spinfected for 1 hour at 2 000 rpm. After spinfection, cells were returned to the incubator. On the following day, the cells were detached, plated in 15 cm plates ($9*10^6$ cells per plate) and selected with 3 µg/ml

puromycin. To calculate the actual MOI, cells were counted and $1*10^5$ cells were plated in duplicate wells. To one of the wells, 3 μg/ml puromycin was added for 3 days. After 3 days, cells were detached and counted, and the transduction percentage was calculated as the cell count from the replicate with puromycin divided by the cell count from the replicate without puromycin, and multiplied by 100. Calculated MOI was 0.08. Considering the MOI, the number of infected cells, and the number of sgRNAs contained in the library, each sgRNA was represented in ~75 cells.

After 7 days of puromycin selection, which allowed editing to proceed to completion, puromycin was removed from the medium. $8*10^6$ cells were frozen, divided in four vials, to be used for further experiments. The frozen library was used to analyze single cell clones (see below).

3.8.2. Cell cycle arrest rescued library

After selection with puromycin, the genome-wide knock-out library was treated with doxycycline to induce cell cycle arrest caused by the depletion of myosin VI. In particular, $8*10^6$ cells (~100 cells per each sgRNA) were seeded in 15 cm plates, 200 000 cells per plate, and treated with 0.5 μg/ml doxycycline. Fresh media was added every 3–4 days. After 15 days of doxycycline treatment, $20*10^6$ cells were collected and the genomic DNA was extracted. This library represents the cell cycle arrest rescued library and has been named “Treated library”.

As control, $20*10^6$ cells not treated with doxycycline were collected and the genomic DNA was extracted. This library represents the starting genome-wide knock-out library and has been named “Control library”.

3.8.3. Genomic DNA extraction, amplification and sequencing

Genomic DNA was extracted from Treated and Control library pellets right after that the cells were collected. The extraction of genomic DNA was performed using QIAGEN Genomic-tip 100/G and QIAGEN Genomic DNA Buffer Set according to the manufacturer's protocols (QIAGEN genomic DNA handbook).

To prepare the sgRNA library of each sample, PCR was performed to amplify the region containing the sgRNA cassette, at the same time adding appropriate sequencing adapters. Primers are specific to the sgRNA expression vector, and include both a variable length sequence to increase library complexity (stagger region, 0-8 nt) and an 8-bp barcode for multiplexing of different biological samples (as described in the Brunello library Addgene page).

The primers for Illumina sequencing are composed by the following sequences:

P5/P7 flowcell attachment sequence Illumina sequencing primer Stagger region/Barcode region Vector primer binding sequence

P5 (forward) primer sequence:

5'-AATGATACGGCGACCACCGAGATCTACACTCTTTCCCTACACGACGCTCTTCCGATCT [0-8 nt stagger] TTGTGGAAAGGACGAAACACCG-3'

P7 (reverse) primer sequence:

5'-CAAGCAGAAGACGGCATACGAGATNNNNNNNN[barcode]GTGACTGGAGTTCAGACGTGTG CTCTTCCGATCTTCTACTATTCTTTCCCCTGCACTGT-3'

The preparation of the PCR reaction was performed as follows:

Phusion DNA polymerase	0.5 µl
50mM $MgCl_2$	1 µl
5xGC buffer	10 µl
10 mM dNTP	1 µl
10 uM primer P7	2.5 µl
10 uM primer P5 mix	2.5 µl
Genomic DNA	1.3 µg
H2O	up to 50 µl

Assuming 6.6 pg DNA per cells, in order to obtain a 100x representation of sgRNAs for ~80 000 sgRNAs, the calculation would be $6.6*10^{-12}$g * 100 * 80 000 = 52.8 µg (43 PCR reactions).

The thermocycling parameters for the PCR were 98°C for 2 minutes; 24 cycles at 98°C for 5 seconds, 63°C for 30 seconds, and 72°C for 30 seconds; and 72°C for 10 minutes. The resulting amplicons for each sample were pooled and gel-purified with QIAGEN QIAquick gel extraction kit (following the manufacturer's protocol). The resulting sgRNA libraries were sequenced with MiSeq (Illumina) using MySeq® reagent Kit v3 (Illumina).

3.8.4. Bioinformatics analysis

The output reads derived from the Illumina sequencing were trimmed to leave only the 20bp sgRNA sequences. Reads shorter than 10bp were filtered out. The MAGeCK algorithm (Li et al., 2014) was used to align the sequences and to evaluate the enrichment of sgRNA in doxycycline-treated samples compared to the control not-induced knock-out cell library (Fig. 40). Trimmed reads were mapped to the designed sgRNA Brunello library, with a maximum of one mismatch per sgRNA. The sgRNA were then quantified by counting the number of reads per sgRNA, and normalized by the total number of reads of the sample. Finally, the sgRNA and their target genes were ranked according to the enrichment in the treated sample compared to the control.

3.8.5. Analysis of single cell clones

hTERT-RPE1 Cas9 shUTR cells were transduced with the Brunello library via spinfection with 17 µl Lentiviral Prep (titer $5.3*10^5$ TU/ml, MOI~0.1), with the same procedure described above. Actual MOI was 0.04. After 7 days of puromycin selection, which allowed editing to proceed to completion, puromycin was removed from the growth medium. Thereafter, the cell library was expanded for 2 days and then it was collected and frozen.

To pick single rescue clones, $2*10^6$ cells from the knock-out cell library were thawed (each sgRNA was represented in ~35 cells). After 2 days, cells were treated with 0.5 µg/ml doxycycline to induce the depletion of myosin VI and cell cycle arrest. After 4 days, $2*10^6$ cells were seeded in 10 cm plates (100 000 cells per plate) and kept under doxycycline treatment. After 9 days, single cell clones that were growing among the senescent cells were visible in the plates. The clones were detached by trypsinization in plastic cylinders and seeded into 48-well plates. From 312 clones that were picked from the plates, 92 were able to grow after the passage in 48-well plates. When the cells were confluent, they were lysed and the genomic DNA was extracted with DNA IQ™ Kits for Maxwell® 16 (Promega) following the manufacturer's instructions.

To amplify the region containing the sgRNA cassette, PCR was performed as follows:

GoTaq DNA polymerase	0.25 µl
5x buffer	10 µl
10 mM dNTP	1 µl
10 uM primer For	2.5 µl
10 uM primer Rev	2.5 µl
Genomic DNA	10-50 ng
H2O	up to 50 µl

For this PCR, the following primers were used for the amplification, annealing to the pLenti guide construct:

- Forward: 5’-AATGGACTATCATATGCTTACCGTAACTTGAAAGTATTTCG-3’
- Reverse: 5’-CTTTAGTTTGTATGTCTGTTGCTATTATGTCTACTATTCTTTCC-3’

The thermocycling parameters for the PCR were 98°C for 2 minutes; 24 cycles at 98°C for 5 seconds, 63°C for 30 seconds, and 72°C for 30 seconds; and 72°C for 10 minutes.

After amplification, the PCR product was sequenced by Sanger sequencing using the same Reverse primer used for the PCR. The sequences were then analyzed using Snapgene to identify the sgRNA and its related gene.

4. Results

4.1. Myosin VI interacts with proteins belonging to the centrosome compartment

Previous proteomic studies performed in our laboratory revealed that myosin VI short and long isoforms have two different interactomes (Wollscheid et al., 2016). These studies were performed with a mass spectrometry (MS) approach, using a myosin VI fragment spanning aminoacids 998–1131, in pulldown assays with HEK293T cellular lysates.

To characterize the full interactome of myosin VI, we decided to perform an IP of endogenous myosin VI using two antibodies that we generated against the full-length protein coupled with MS. In order to obtain a comprehensive view of the myosin VI interactome, the experiments were performed using different cell lines with different myosin VI isoform expression. A full description of these experiments and the findings is reported in the Appendix. When we analyzed the interactors with Gene Ontology for "Cellular Component" to identify enrichments in cell compartments, organelles or structures we found an enrichment in "microtubule organizing center" and "centrosome" cell components. These categories appeared in all of the IP/MS experiments performed, and Table 1 lists all the proteins belonging to the above-mentioned cell components that were found as myosin VI interactors in the different cell lines analyzed. These data suggest the involvement of myosin VI in centrosomal functions.

4.1.1. Myosin VI interacts with the centrosome and satellite protein OFD1

We focused our attention on OFD1, which was found as a specific interactor of myosin VI independently of the cell line used. OFD1 is a protein localized at the centrosome/basal body, as well as at the centriolar satellites, and it has a critical role in primary cilium

Gene name	Caco-2 sparse	Caco-2 confluent	HeLa	MCF10A sparse	MCF10A confluent	MDA-MB-231
OFD1	x	x	x	x	x	x
NUMA1	x	x	x	x	x	x
DYNC1H1	x	x		x		x
DYNC1I2	x	x				
DYNC1LI1	x	x				
NEK1	x	x				
KIF20B	x					
HSPA1A	x	x				
CDK11B	x	x				
DCTN1		x				
CALM1		x	x	x		x
PCNT			x	x	x	x
RAB11FIP1			x		x	x
CROCC						x
AKAP9				x	x	x
DIS3L				x		
FBF1				x		
PLEKHA7						x
CDK5RAP2				x	x	

Table 1: MTOC/centrosome proteins identified as myosin VI interactors in IP-MS experiments.

The table lists all proteins belonging to "MTOC" or "Centrosome" GO terms that were identified as myosin VI interactors in the IP-MS experiments described in the Appendix. The presence of the proteins in the interactome of a particular cell line is indicated with an 'x'.

formation (Ferrante et al., 2006; Lopes et al., 2011; Singla et al., 2010). To validate the interaction between myosin VI and OFD1, we immunoprecipitated endogenous myosin VI with two antibodies in HEK293T cells overexpressing Flag-tagged OFD1. Both anti-myosin VI antibodies were able to co-IP Flag-OFD1 (Fig. 10A), while anti-GST antibody, which was used as control, did not. To confirm this result, we overexpressed Flag-OFD1, or Flag alone as control, in HEK293T cells, and performed an IP with anti-Flag antibody conjugated beads. The anti-Flag beads were able to co-IP myosin VI only in the presence of Flag-OFD1, further validating the interaction between the two proteins (Fig. 10B). To better characterize this interaction, we aimed to understand if OFD1 is able to bind selectively one of the isoforms of myosin VI, and if this interaction involves its tail region,

which is usually deputed to the binding of the cargoes. HEK293T cells were transfected with different GFP-myosin VI constructs, coding for the tail region or the full-length (FL) protein of both isoforms (long and short), and with Flag-OFD1. GFP-myosin VI was then immunoprecipitated using anti-GFP nanobodies, and the interaction with OFD1 was assessed through an anti-Flag immunoblot. We found that Flag-OFD1 was co-immunoprecipitated with all the myosin VI constructs, demonstrating that myosin VI binds OFD1 through its tail domain, without isoform distinction (Fig. 10C).

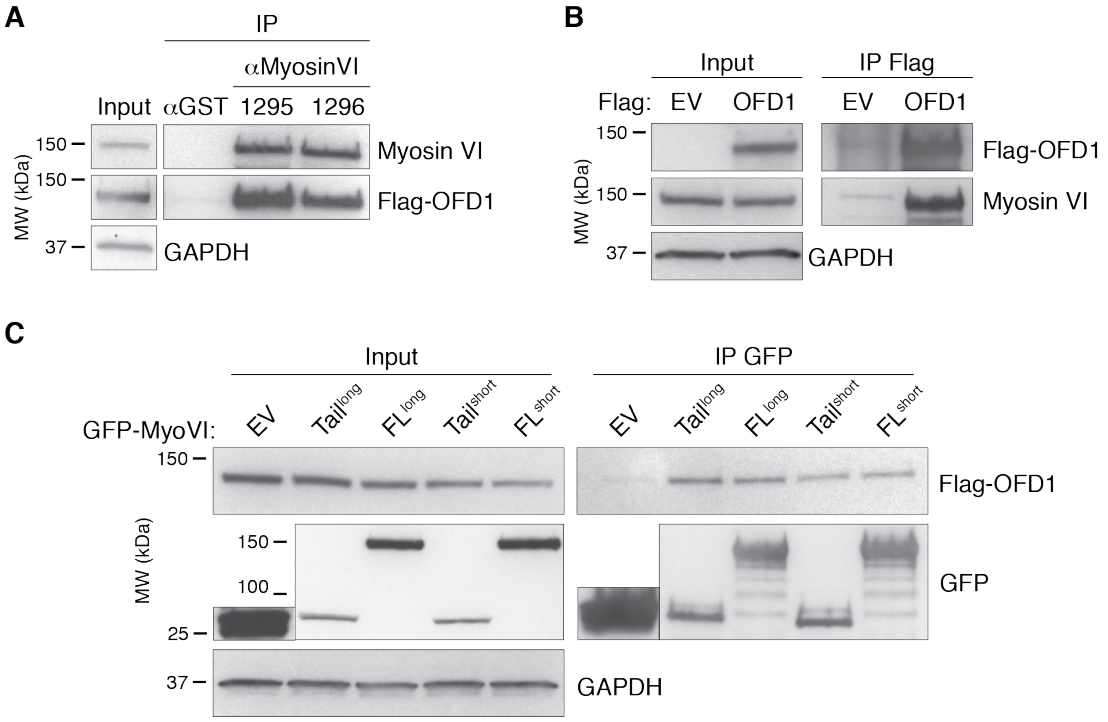

Figure 10: Myosin VI interacts with OFD1.

(A) Anti-myosin VI antibodies were used for IP in HEK-293T cells transfected with a Flag-OFD1 construct. Anti-GST rabbit polyclonal antibody was used as control. The co-IP of OFD1 was assessed by WB using an anti-Flag antibody. (B) Anti-Flag conjugated beads were used for IP in HEK-293T cells transfected with Flag-EV (as control) or Flag-OFD1 constructs. The co-IP of myosin VI was assessed by WB using an anti-Myosin VI antibody. (C) HEK-293T cells were transfected with GFP-tagged myosin VI Tail (998-1131) or full-length (FL) constructs, isoform long and short, together with Flag-OFD1. pEGFP-EV was used as control. GFP nanobodies were used for IP against total cell lysates. Proteins bound to GFP-beads were determined by WB using anti-Flag and anti-GFP antibodies.

4.2. Myosin VI has a role in centrosome structure maintenance

4.2.1. Myosin VI localization at the centrosomes

Given the interaction with OFD1, we investigated the possible role of myosin VI at the centrosome, taking advantage of the hTERT-immortalized retinal pigment epithelial cell line hTERT-RPE1. While cancer cells often have deregulation of centrosome number and structure, hTERT-RPE1 cells are widely used to study centrosomes and primary cilium because they are diploid, immortalized but non-tumoral cells, and show primary cilium formation upon serum starvation.

First, we assessed myosin VI localization. In growing conditions, myosin VI was localized at the centrosomes, marked with staining for pericentrin (Fig. 11A). To determine whether

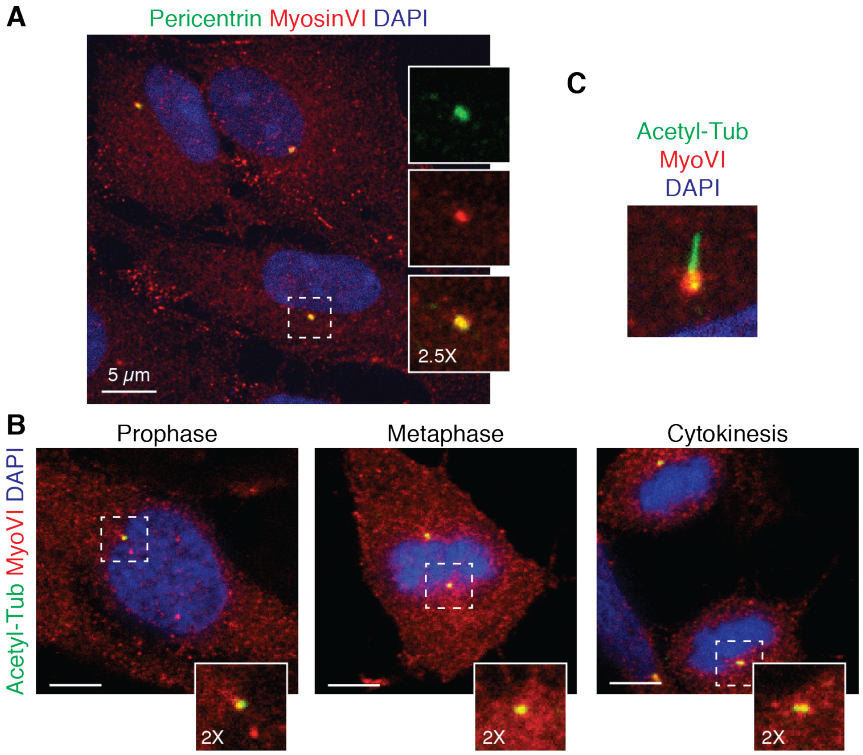

Figure 11: Myosin VI localizes at the centrosome.

(A) hTERT-RPE1 cells in growing conditions were fixed with methanol (Me-OH) and stained with anti-pericentrin and anti-myosin VI antibodies. Cell nuclei were stained with DAPI. (B) hTERT-RPE1 cells in growing condition were fixed with Me-OH, after MTs depolymerization, and stained with anti-myosin VI and anti-acetylated tubulin antibodies to mark the centrioles. DAPI staining was used to identify the nuclei in different phases of mitosis. (C) hTERT-RPE1 cells were serum starved for 48 hours to stimulate cilium assembly. The cells were then fixed with Me-OH, after MTs depolymerization, and stained with anti-myosin VI and anti-acetylated tubulin antibodies to mark the centrioles and primary cilium.

this localization changes during the cell cycle, we looked for cells displaying the typical chromatin shape of different cell cycle phases, and assessed myosin VI localization in the centrioles region. We found that myosin VI colocalizes with centrioles, marked with anti-acetylated tubulin, during all the phases of the cell cycle (Fig. 11B). The antibody against myosin VI stained also the basal body during primary cilium formation (Fig. 11C). These data suggest that the centrosomal localization of myosin VI is not regulated by cell cycle events.

Several antibodies display aspecific staining at the centrioles, particularly those produced in rabbits (personal communication by Brunella Franco). The home-made anti-myosin VI rabbit antibodies we generated are affinity purified and performed well in all assays used in the lab (Wollscheid et al. 2016). To assess the specificity of myosin VI staining at the centrosomes, hTERT-RPE1 cells were transfected with two different siRNAs for myosin VI and stained with the anti-myosin VI antibodies. As shown in Fig. 12A, upon myosin VI KD, the staining is greatly decreased throughout the cells but it is maintained at the centrosomes. Notably, even if the depletion seems to be almost complete (Fig. 12B), few dots at the periphery of the cells possibly corresponding to clathrin coated-pits remained

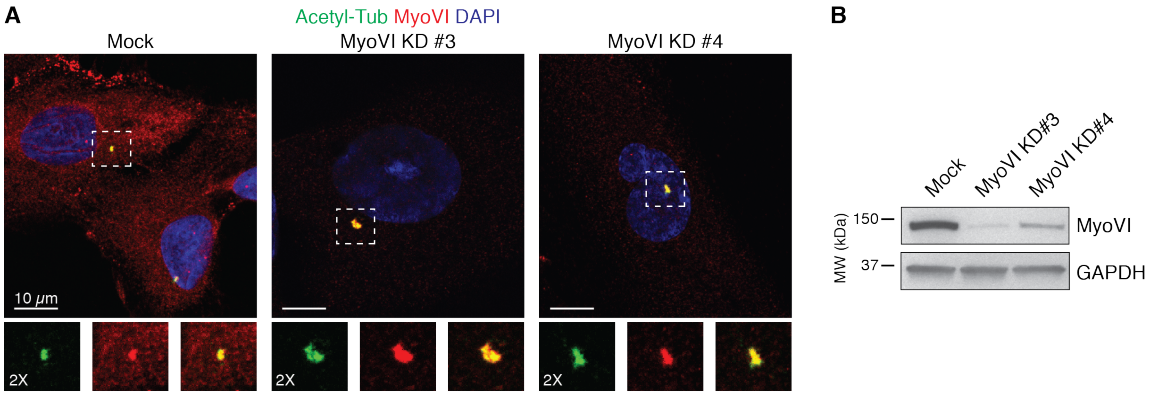

Figure 12: Anti-myosin VI antibody stains the centrioles also upon myosin VI depletion.

(A) hTERT-RPE1 cells in growing conditions were transfected with the indicated siRNAs for the depletion of myosin VI, fixed with Me-OH after MTs depolymerization, and stained with anti-myosin VI and anti-acetylated tubulin antibodies to mark the centrioles. Images were acquired with a confocal microscope with the same acquisition settings and subjected to the same contrast/brightness adjustments. (B) hTERT-RPE1 cells treated as in (A) were lysed and WB was performed to assess myosin VI depletion.

visible (Fig. 12A). Thus, with this result we were not able to confirm/exclude myosin VI centrosome localization.

To better clarify this issue, we took advantage of a modified HCT-116 cell line kindly provided us by Hans-Peter Wollscheid. In these cells, myosin VI is endogenously tagged with GFP at the C-terminus via CRISPR/Cas9 technology. The expression level of the tagged protein is similar to the one of untagged myosin VI in wild type (WT) cells (Fig. 13A), allowing us to check myosin VI localization at the centrosomes using an anti-GFP antibody that works well in methanol fixation. To control for anti-GFP specificity, the staining was performed in parallel in WT HCT-116. Results obtained further proved that myosin VI colocalizes with pericentrin at the centrosome (Fig. 13B).

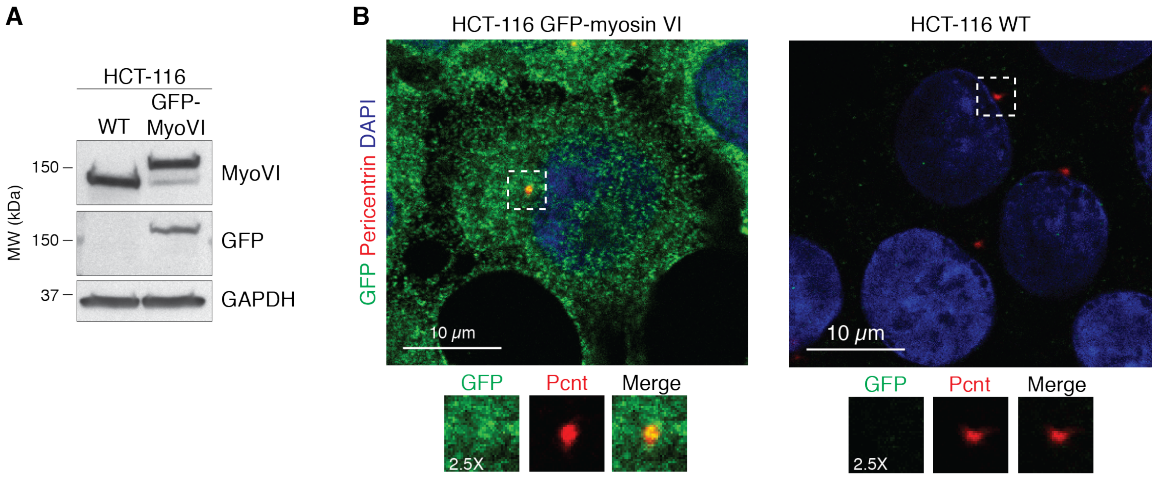

Figure 13: GFP-myosin VI colocalizes with pericentrin at the centrosomes.

(A) HCT-116 WT and GFP-myosin VI were lysed and WB was performed to assess GFP-myosin VI expression. (B) HCT-116 GFP-myosin VI and WT cells in growing condition were fixed with Me-OH and stained with anti-GFP and anti-pericentrin antibodies to mark the centrosomes. Images were acquired at confocal microscope with the same acquisition settings.

4.2.2. Myosin VI has a role in maintaining a correct structure and localization of the centrosome

Surprisingly, myosin VI-depleted cells showed the presence of multiple centrioles (Fig. 12A, MyoVI KD #3 condition). To investigate this phenotype, we transiently depleted

myosin VI with two siRNAs and calculated the percentage of cells that showed more than two centrioles. Indeed, a higher amount of myosin VI-depleted cells showed an increase of centriole number with respect to control cells (Fig. 14A). Likely, this was not due to the normal centriole duplication that occurs during S and G2 phase and shows a different morphology: while G2 cells usually displayed two centriole doublets, in which the newly-formed centriole is attached to the old one (as shown in the bottom panel of mock cells, Fig. 14B), myosin VI-depleted cells showed an increased number of centrioles that are separated from each other (Fig. 14B). Furthermore, myosin VI KD cells sometimes show more than four centrioles (shown in the bottom panel of MyoVI KD#3 cells, Fig. 14B).

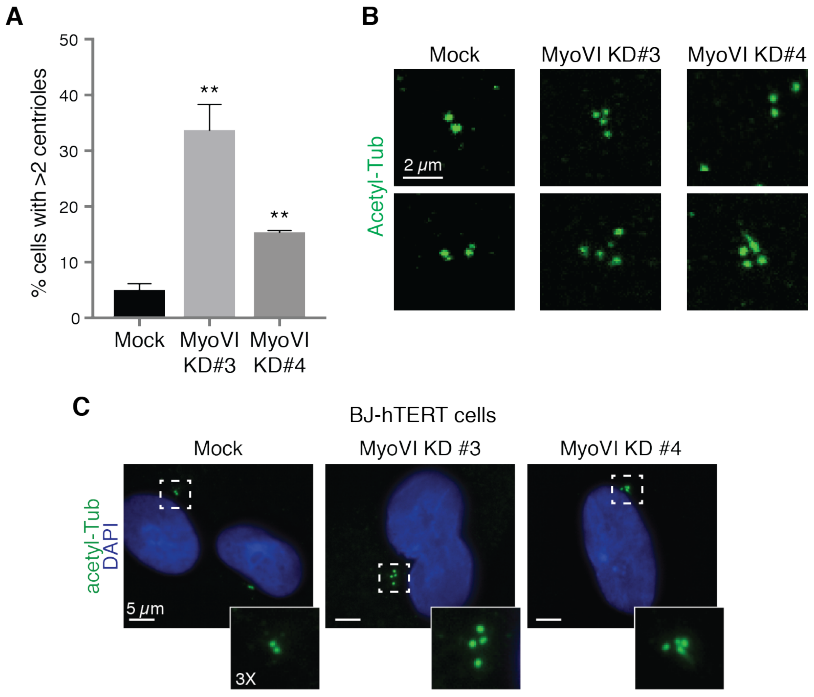

Figure 14: Depletion of myosin VI leads to centriole amplification.

(A) hTERT-RPE1 cells were transfected with the indicated siRNAs for the depletion of myosin VI. After 96 hours, the cells were fixed with Me-OH after MTs depolymerization and stained with an anti-acetylated tubulin antibody and DAPI to count the number of centrioles per cell. The graph shows the average +SEM of the percentage of cells with more than two centrioles, calculated from at least 230 cells per condition from three independent experiments. Statistical significance was calculated with student's T-test (N=3; **p<0,005). (B) Sample images of cells treated as in (A). Anti-acetylated tubulin staining is in green. (C) BJ-hTERT cells were transfected with the indicated siRNAs for the depletion of myosin VI. After 96 hours, the cells were fixed with Me-OH, after MTs depolymerization, and stained with an anti-acetylated tubulin antibody and DAPI to determine for centriole amplification.

These results suggest an unexpected role for myosin VI in centriole duplication. To validate that the observed effects are not only restricted to hTERT-RPE1 cells, we examined centriole number in another non-tumor cell line, namely the human fibroblast BJ-hTERT cells. As shown by anti-acetylated tubulin staining, the number of centrioles is increased upon the depletion of myosin VI with both siRNAs in BJ-hTERT cells (Fig. 14C), in line with the previous data.

To check in which phase of the cell cycle the centrosome amplification occurs, we generated hTERT-RPE1 cells bearing the FUCCI construct, which consists of different regulators of the cell cycle, cdt1 and geminin, fused with fluorescent markers, mCherry and YFP. During the cell cycle, these two proteins are ubiquitinated and degraded through the proteasome pathway in specific temporal phases: as a result, in the G1 phase only mCherry-Cdt1 is present, while YFP-geminin is present in S, G2 and M phases. Thanks to this system, we could demonstrate that amplified centrosomes are present in G1 cells (Fig. 15A). Interestingly, we found that the number of cells in G1 are greatly increased in myosin VI-depleted cells respect to control cells (Fig. 15C-D), suggesting that myosin VI depletion can alter the cell cycle. This phenotype and the experiments performed to investigate it are described in the next chapters.

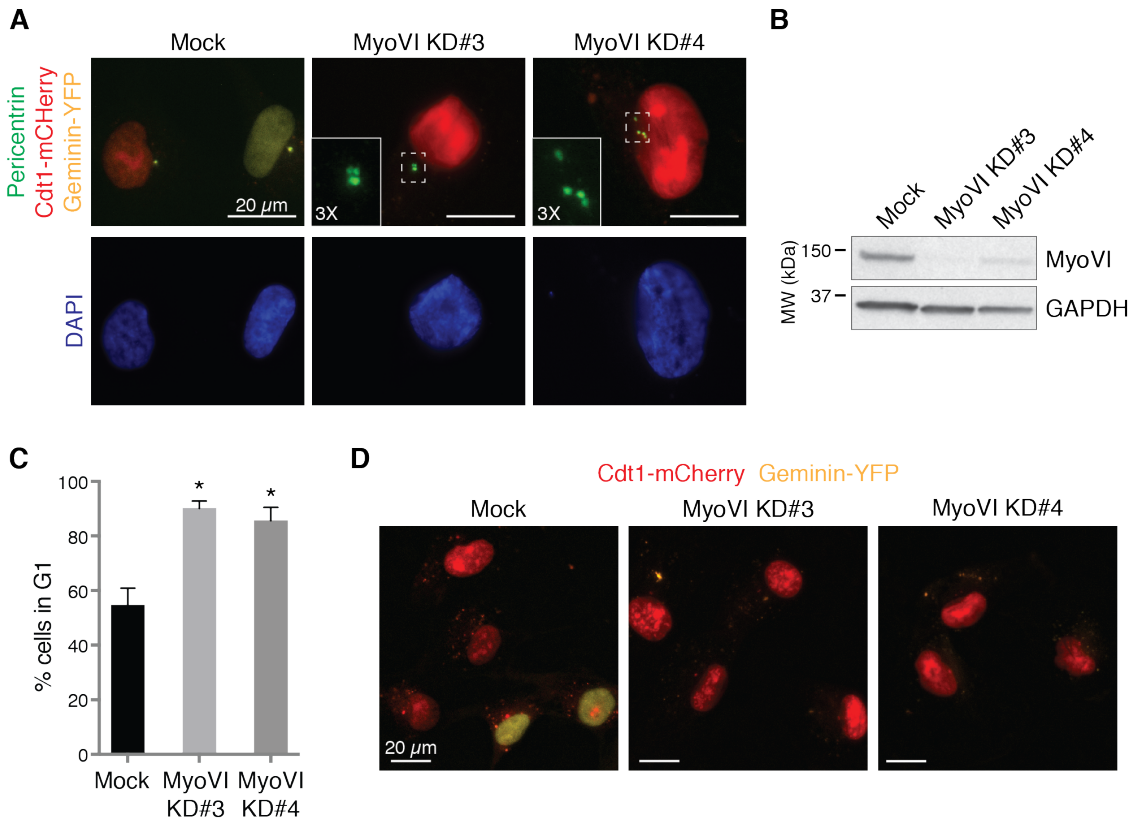

Figure 15: Centrosome amplification upon myosin VI depletion occurs in G1.

(A) hTERT-RPE1 FUCCI cells were transfected with the indicated siRNAs for myosin VI depletion, and after 96h were fixed with PFA and stained with anti-pericentrin antibody and DAPI to check for centriole amplification relative to the cell cycle phase. (B) hTERT-RPE1 FUCCI cells treated as in (A) were lysed and WB was performed to assess myosin VI depletion. (C) hTERT-RPE1 FUCCI cells were treated as in (A). The graph shows the average +SEM of the percentage of cells in G1, identified with nuclei showing only Cdt1-mCherry staining, calculated from at least 110 cells per condition from two technical replicates. Statistical significance was calculated with student's T-test (N=2; *p<0,05). (D) Sample images of cells treated as in (A) used for the quantification of G1 cells.

We next decided to extend our analysis, using electron microscopy to observe the ultrastructure of the centrioles. In collaboration with the electron microscopy facility at IFOM, we analyzed the structure of the centrioles in cells depleted of myosin VI and in control cells by TEM. Myosin VI KD cells did not show any alteration of the ultrastructure of the centrioles themselves that are well-organized with nine triplets of microtubules and a correct length (Fig. 16A, top, left panel). On the contrary, myosin VI depletion severely affects the centriole number and location (Fig. 16A). Confirming the data obtained by the IF analysis, centrosomes were amplified, separated, and not orthogonally

oriented (Fig. 16A). Furthermore, the distance between the single centrioles was increased and the matrix surrounding centrioles was narrower with no zone of exclusion between centriole and membrane organelles, which are found also between the two centrioles (Fig. 16A). None of these phenotypes are visible in control cells that contained two, well-structured and orthogonally oriented centrioles (Fig. 16B).

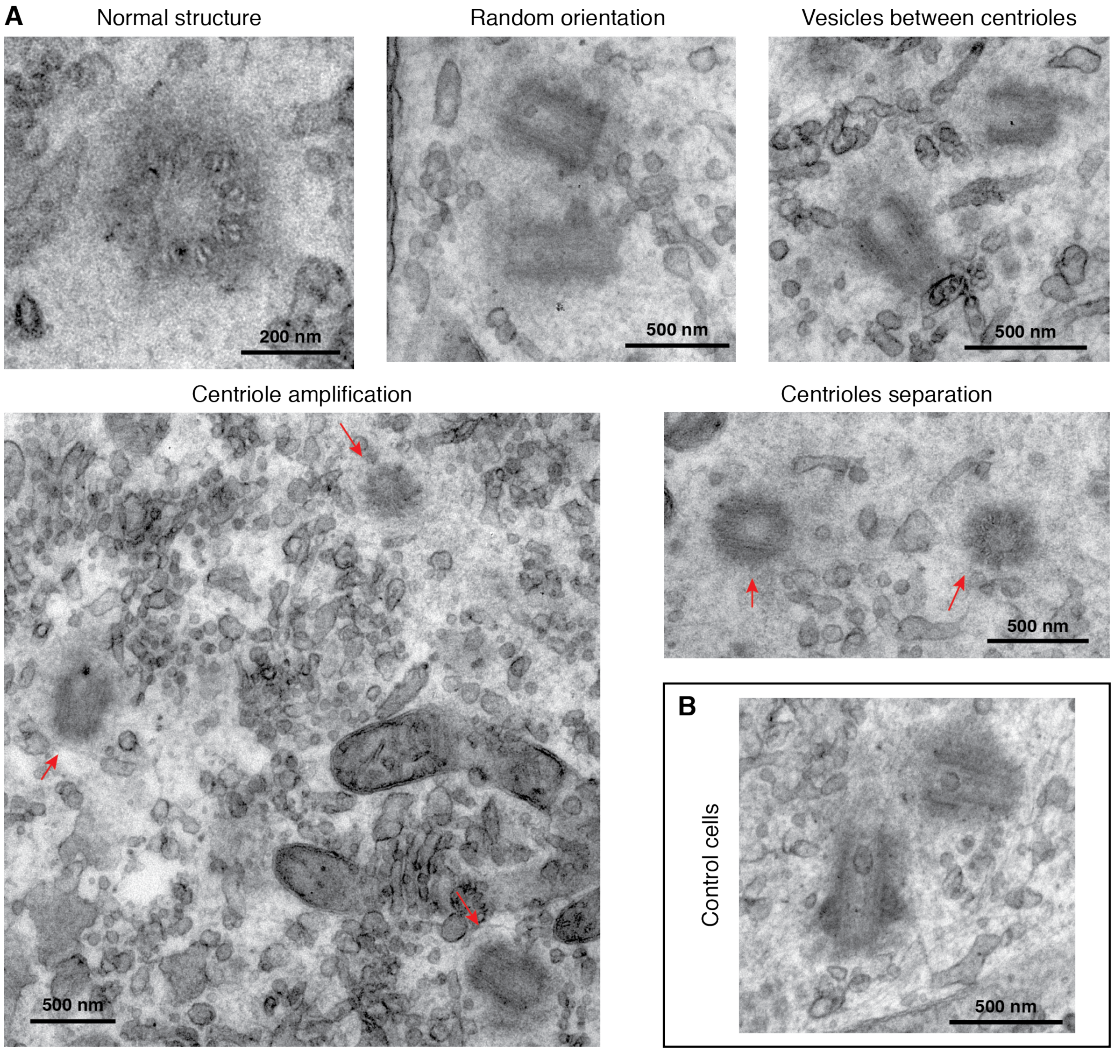

Figure 16: Myosin VI-depleted cells show alterations at the centrosomes.

hTERT-RPE1 cells were transfected with siRNA #3 for myosin VI KD, or with mock as control. After 96 hours, the cells were fixed with 4% PFA/Glutaraldehyde buffer and processed for EM acquisition. (A) Selected sections deriving from TEM analysis of hTERT-RPE myosin VI KD cells showing centrioles with different defects as indicated (red arrows). 20 cells were analyzed for centrosome structure. (B) Selected section deriving from TEM analysis of hTERT-RPE1 cells treated with mock shows centrioles in control cells. 21 cells were analyzed and none presented the phenotypes observed in myosin VI KD cells.

This qualitative TEM analysis also suggests that the subcellular localization of the centrosome might be altered upon myosin VI depletion, as the centrioles were found in a region far from the plasma membrane and the nuclear membrane. Thus, we decided to look deeper into centrosome localization in cells depleted of myosin VI. Control and myosin VI KD cells were stained with an anti-pericentrin antibody to visualize the centrosome, and XZ-section images of the cells were acquired. Using ImageJ, we calculated the distance between the centrosome and the cell cortex, stained with phalloidin. This experiment, confirming the initial observation of the TEM analysis, showed an increased centrosome-plasma membrane distance in myosin VI KD cells (Fig.17).

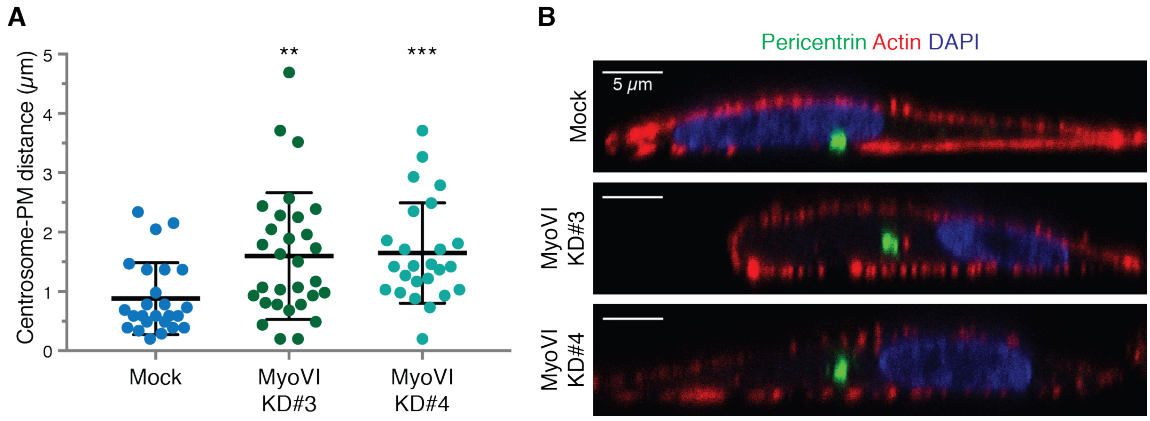

Figure 17: Depletion of myosin VI leads to displacement of the centrosome from the cell cortex.

hTERT-RPE1 cells were transfected with the indicated siRNAs for myosin VI depletion. After 96 hours, the cells were fixed and stained with anti-pericentrin and phalloidin-TRITC to mark actin. DAPI staining was used to mark the nuclei. Images along the XZ-axis of the cells were acquired with a confocal microscope. The dot plot represents the distance of the centrosome from the plasma membrane calculated using ImageJ from IF images along the XZ-axis of the cell. The mean distance ±SD is reported (N=25-30 cells from two independent experiments). Statistical significance was calculated with Kruskal-Wallis test, **p<0,005 ***p<0,001. (B) Sample images of cells treated as in (A) and used for the above-described analysis.

We then calculated the centrosome-nucleus distance by taking advantage of a software developed by the group of Paolo Maiuri in IFOM, which is able to automatically calculate the distance between the nuclear border and the centrosome in a high number of cells.

As expected, myosin VI-depleted cells showed a strong increase in the nucleus-centrosome distance (Fig. 18).

Altogether, these results suggest a role for myosin VI in the maintenance of the centrosome structure and in anchoring the centrosome to the nucleus and/or to the plasma membrane.

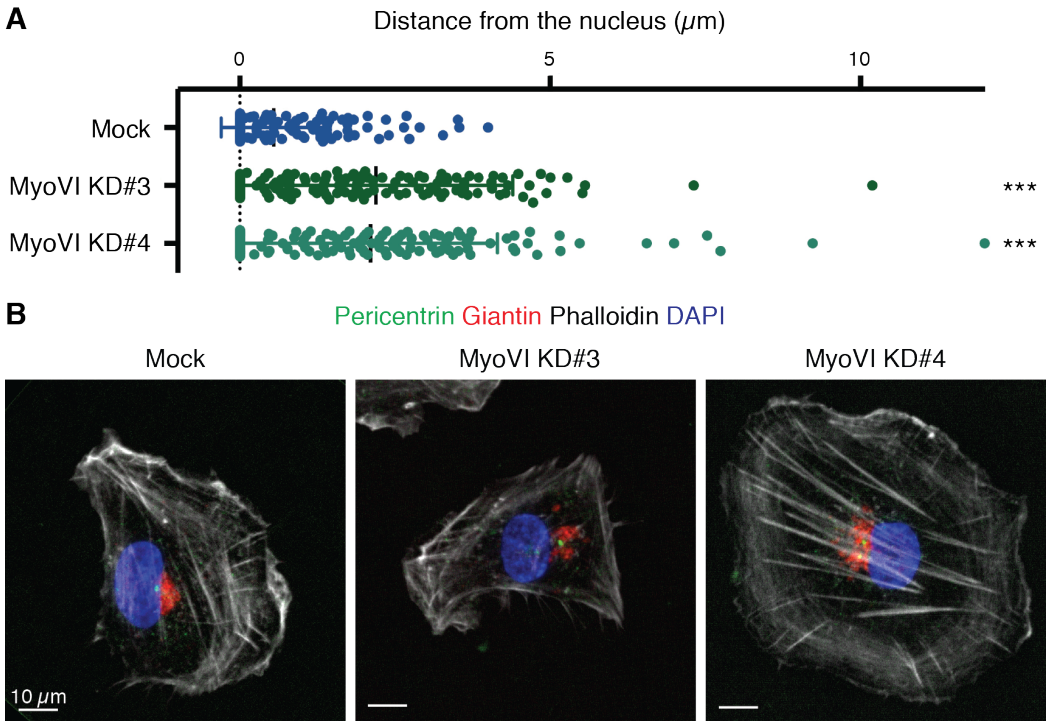

Figure 18: Myosin VI-depleted cells show an increased nucleus-centrosome distance.

(A) hTERT-RPE1 cells were transfected with the indicated siRNAs for myosin VI KD, or with mock as control. After 96 hours, the cells were fixed with 4% PFA and stained with anti-pericentrin and anti-golgin antibodies, FITC-phalloidin and DAPI. Images were acquired every 0.3 µm of the focal plane using z-stack function to visualize the entire cell. The images were processed using ImageJ software with custom-built plugins to measure the distance between the centrosome and the border of the nucleus. The dot plot represents the calculated distance in single cells (Mock N=174, MyoVI KD#3 N=137, MyoVI KD#4 N=130, from two independent experiments), displaying mean ±SD. Statistical significance was calculated with Kruskal-Wallis test (***p<0.0001). (B) Sample images of cells treated as in (A) and used for the above-described analysis.

4.2.3. Depletion of Myosin VI affects primary cilium elongation

The formation of the primary cilium is one of the main functions of the centrosome. Prompted by our results, we assessed the ability of the cells to assemble a primary cilium in the absence of myosin VI. To allow primary cilium formation, hTERT-RPE1 cells were

arrested in the G1 phase through serum starvation, after which the serum was added to the cell culture medium to induce primary cilium disassembly upon cell re-entry into the cell cycle. Myosin VI KD cells showed reduced cilium assembly abilities, as well as a delay in its readsorption respect to control cells (Fig. 19A-B). Furthermore, among the few myosin VI-depleted cells that were able to assemble a primary cilium, some showed alterations in its formation such as multiple or elongated cilia (Fig. 19C). The presence of multiple cilia could be ascribed to the centriole amplification reported above, meaning that more than one centriole is allowed to be converted into basal body at the same time.

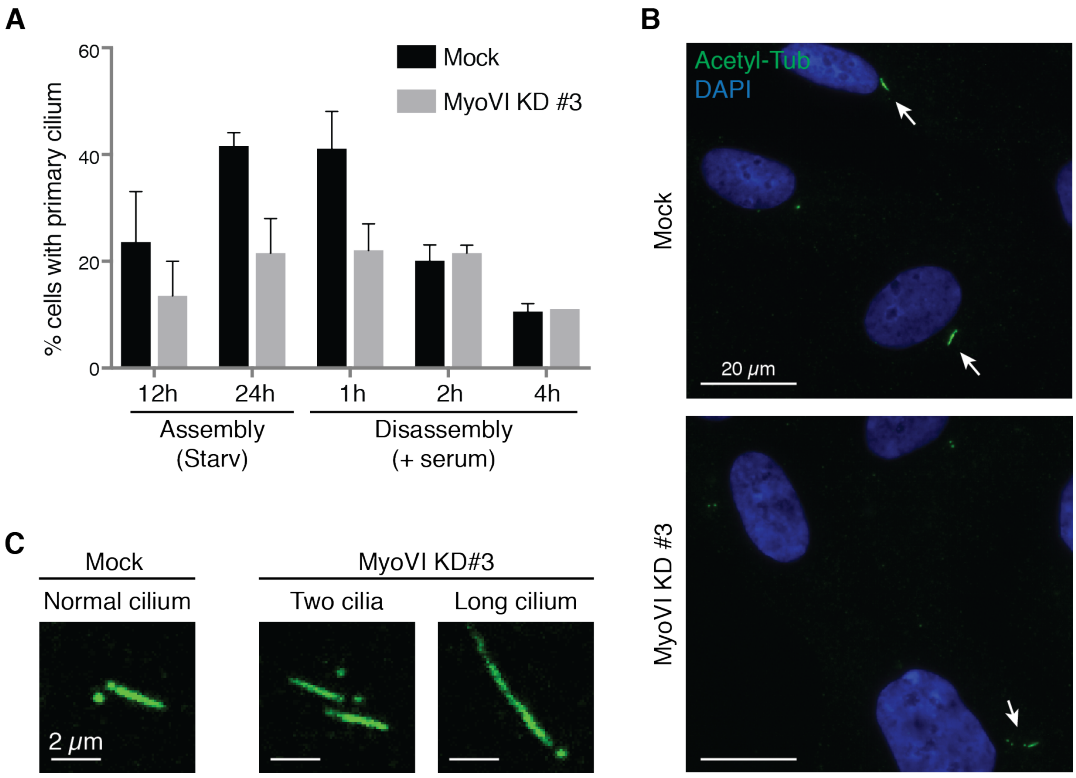

Figure 19: Myosin VI-depleted cells show impairment in the assembly of the primary cilium.

(A) hTERT-RPE1 cells were transfected with the indicated siRNA for myosin VI depletion. After 72 hours, the cells were serum starved for 12 or 24 hours to allow cilium assembly. After 24 hours of starvation, serum was added to the growth medium for the indicated hours to allow cilium disassembly. Then, the cells were fixed with Me-OH, after MTs depolymerization, and stained with an anti-acetylated tubulin antibody and DAPI to count the number of primary cilia per cell. The graph shows the average +SEM of the percentage of cells displaying a primary cilium, calculated from at least 150 cells per condition from two independent experiments. (B) Sample images of cells serum starved for 48 hours, treated as in (A). Arrows indicates the primary cilia. (C) Enlargements of primary cilia form cells treated as in (A) and serum starved for 48 hours, to show alterations of primary cilia in myosin VI KD cells with respect to control.

We also looked back at the TEM images of myosin VI KD cells taken in normal growing conditions, and in few cells we found an abnormal formation of primary cilia, with vesicles inside the ciliary pocket (Fig. 20) and two basal bodies docked to the plasma membrane (Fig. 20, left panel).

These data suggest that depletion of myosin VI has an impact not only on centrosome structure, but also on its functions.

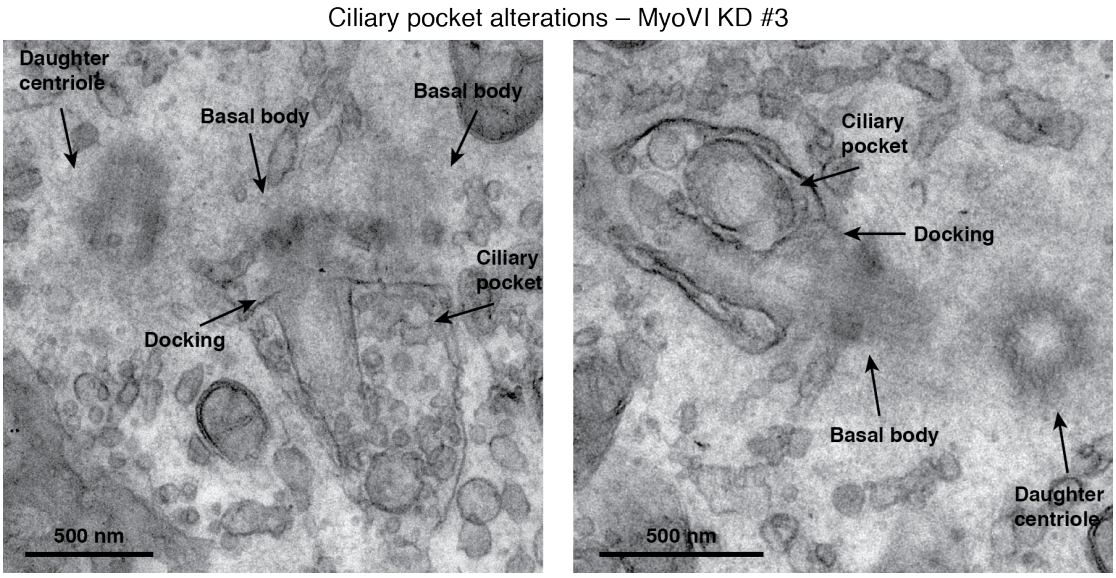

Figure 20: Depletion of myosin VI leads to ciliary pocket alterations.

hTERT-RPE1 cells were transfected with siRNA #3 for myosin VI KD. After 96 hours, the cells were fixed with 4 % PFA/Glutaraldehyde buffer and processed for EM acquisition. Selected sections deriving from TEM analysis show the basal body and the ciliary pocket. Arrows indicate the main centrosome and cilium structures present in the pictures. In the left panel, two basal bodies are docked to the membrane, but only one generates the primary cilium. In both images, the ciliary pocket appears wide and contains vesicles.

4.2.4. Myosin VI is important for OFD1 subcellular localization

We hypothesized that the deleterious effect of myosin VI depletion on centrosomes could be related to its interaction with OFD1. OFD1 is usually localized at the centrosomes and at the centriolar satellites, where it has a crucial role in suppressing primary ciliogenesis in growing condition (Tang et al., 2013). Its degradation, mediated by autophagy, is an essential step to promote primary cilium biogenesis (Tang et al., 2013). As showed in Fig.

21A, the depletion of myosin VI caused a drastic reduction of OFD1 cytosolic puncta, while its localization closed to the centrosome was retained.

The centriolar satellite localization of OFD1 is determined by PCM1 (Tang et al., 2013), which is one of the major components and a well-known marker of the satellites. Thus, we wondered if OFD1 altered localization was due to aberrant satellites distribution. Indeed, PCM-1 staining in myosin VI-depleted cells showed a decrease in the number of centriolar satellites (Fig. 21B). This phenotype was also visible in our TEM images (data not shown). Further experiments are needed to underpin the mechanism behind it.

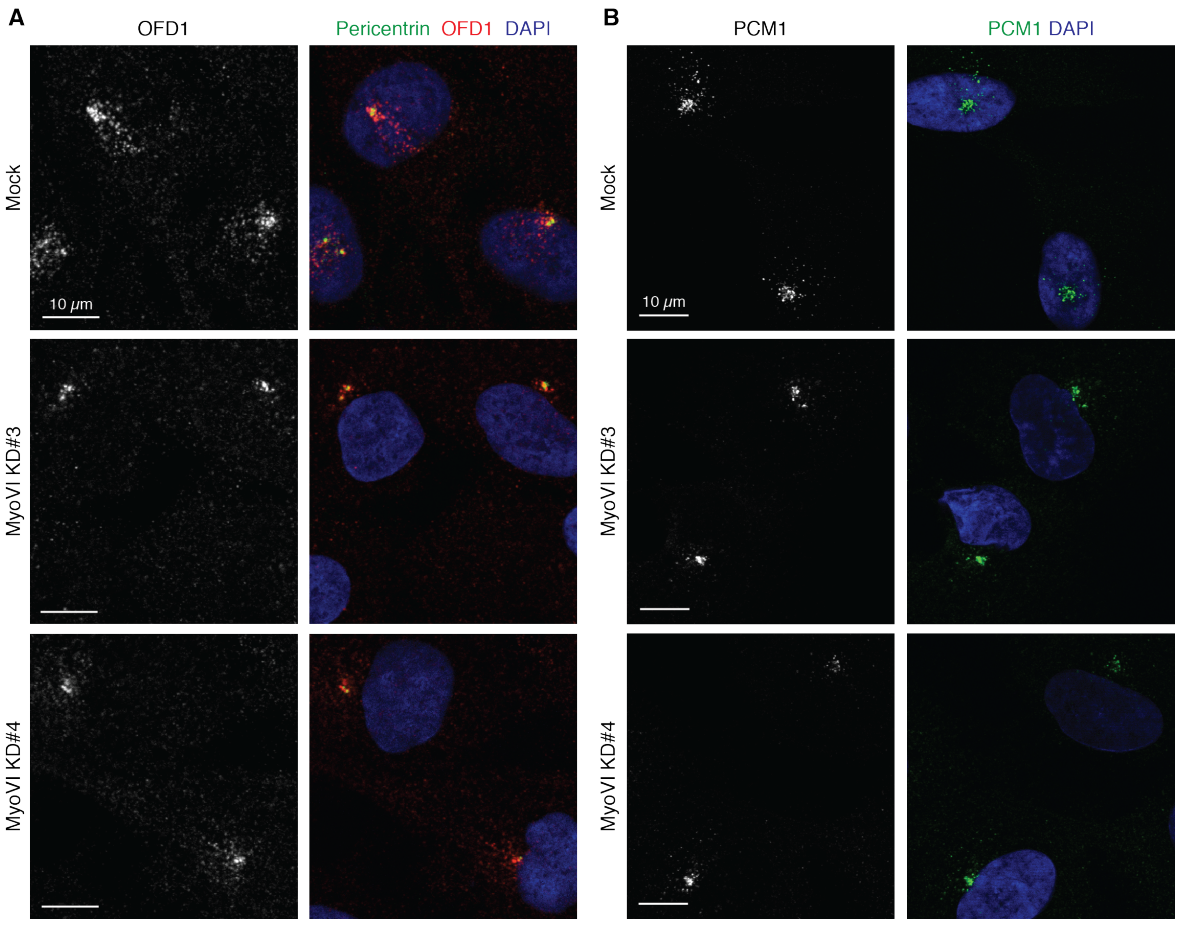

Figure 21: Myosin VI-depleted cells show OFD1 mis-localization and altered centriolar satellites distribution.

(A) hTERT-RPE1 cells were transfected with the indicated siRNAs for the depletion of myosin VI, fixed with 4% PFA after 4 days, and processed for OFD1 and pericentrin staining. OFD1 localization was determined using a confocal microscope. (B) hTERT-RPE1 cells were transfected with the indicated siRNAs for the depletion of myosin VI, fixed with 4% PFA after 4 days, and stained with anti-PCM-1 antibodies to determine satellites distribution. PCM1 localization was determined using a confocal microscope.

4.3. Myosin VI has a role in cell proliferation

4.3.1. Depletion of Myosin VI leads to cell cycle arrest in non-tumor cells

Human myosin VI has been studied mainly in cancer cell lines that, displaying a number of aberrations, differ from the normal tissues in terms of proliferative abilities, checkpoint activation and centrosome number. While working with non-tumor cells to study the centrosomal function of myosin VI in a physiological model, we realized soon that the depletion of myosin VI had a strong effect also on cell proliferation. In fact, prolonged depletion of myosin VI with both siRNAs led to a strong impairment in cell proliferation and a morphological change towards flattened and enlarged cells (Fig. 22). To try to understand in which phase of the cell cycle these cells are stuck, we determined the

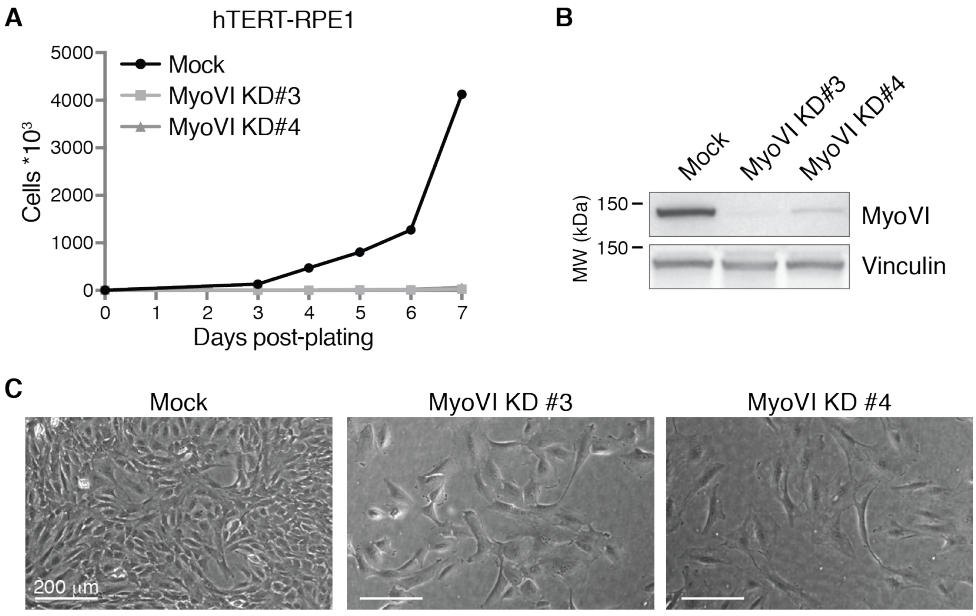

Figure 22: hTERT-RPE1 cells do not proliferate in the absence of myosin VI.

hTERT-RPE1 cells were transfected with the indicated siRNAs for the depletion of myosin VI, or mock-treated. (A) Growth curve of hTERT-RPE1 cells treated with siRNAs as indicated. One day after transfection, 10 000 cells were plated in 6-well plates (day 0). From day 3 to 7 after plating, cells from one well per condition were detached and counted with an automated cell counter. Cell counts are reported in the graph. A representative plot of one of the three experiments performed is shown. (B) Five days after transfection, cells were lysed and WB was performed with the indicated antibodies to determine myosin VI depletion. (C) Representative bright-field images of indicated hTERT-RPE1 cells five days after transfection.

levels of expression of Cyclin A, indicative of S/G2-phase, and of H3 phosphorylated in Ser10 (pH3-ser10), a M-phase marker. The WB analysis showed that both these markers were greatly reduced in the absence of myosin VI (Fig. 23).

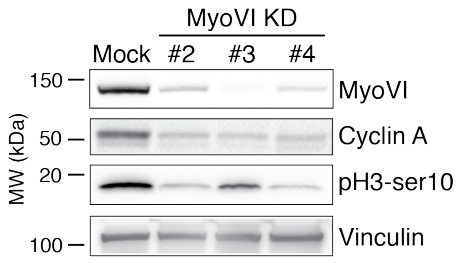

Figure 23: Myosin VI-depleted cells do not express cell cycle markers.

hTERT-RPE1 cells were transfected with the indicated siRNAs for the depletion of myosin VI, or mock-treated. Five days after transfection, the cells were lysed and WB was performed to assess the presence or the absence of markers for different cell cycle phases (Cyclin A as proxy for G2 phase, H3 phosphorylated on Ser10 as proxy for M phase).

Furthermore, we used a BrdU incorporation assay to check the ability of the cells to enter into the S-phase and duplicate their DNA. We incubated the cells with BrdU for 20 minutes, to have a snapshot of the percentage of cells that are in the S-phase, or for 9 hours, a prolonged incubation used to calculate the percentage of cells that are actively going through the cell cycle. This assay indicated that myosin VI depletion affected the ability of the cells to enter the S-phase and to duplicate their DNA (Fig. 24). These results suggest that myosin VI KD cells exit the cell cycle and enter into a resting phase.

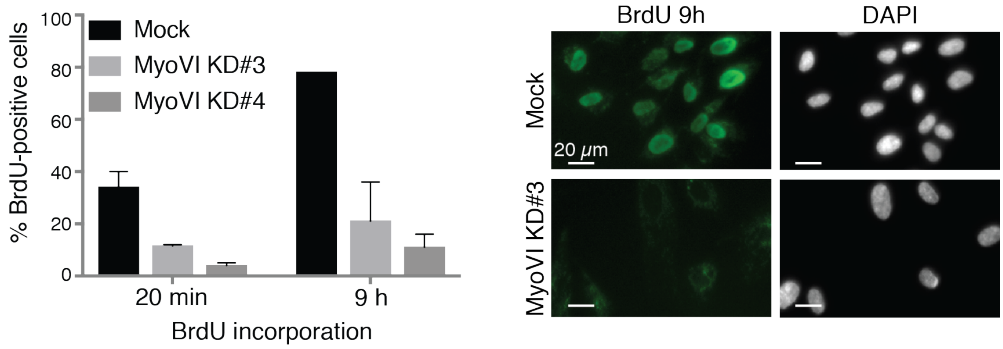

Figure 24: Myosin VI-depleted cells do not duplicate their DNA.

hTERT-RPE1 cells were transfected with the indicated siRNAs for the depletion of myosin VI, or mock-treated. Five days after transfection, the cells were incubated with BrdU as indicated. After immunostaining with anti-BrdU antibody and DAPI, random images were acquired with a wide-field microscope (shown in the right panel), and the percentage of BrdU-positive nuclei was quantified in myosin VI-depleted cells with respect to controls. Bars represent average of two independent experiments +SEM (counted >100 cells per sample per experiment).

To further confirm these results, we performed a multiparameter image cytometry analysis to evaluate the levels of Ki67, a widely-used marker of cell proliferation, in a high number of cells (Furia et al., 2013a). For each cell, we evaluated the intensity of Ki67 and the DAPI that directly correlates with the cell cycle profile (Fig. 25A-B). Then, we set a gate to distinguish high-expressing from low-expressing cells. While in the control cells more than 90% of cells showed high level of Ki67, upon myosin VI depletion the majority of the cells have low level of Ki67, indicating that they have exited the cell cycle (Fig. 25C).

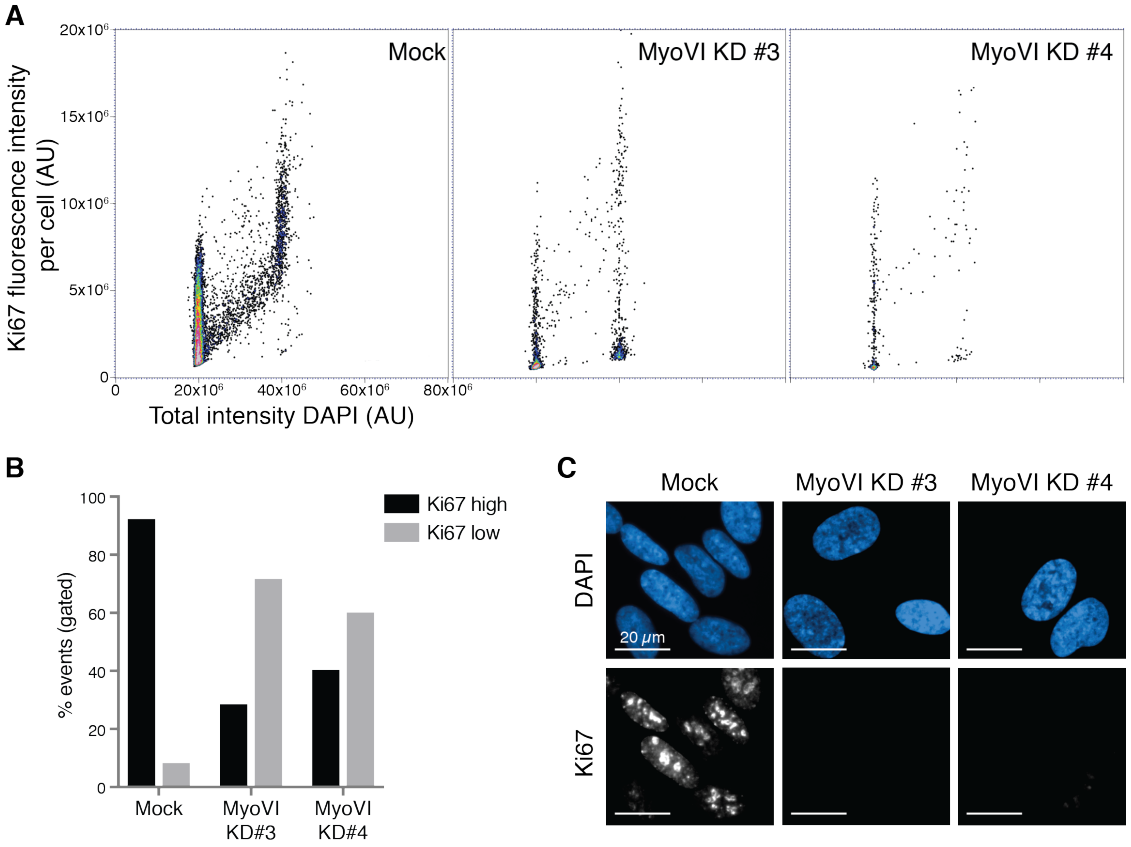

Figure 25: Depletion of myosin VI leads to a decrease in cell proliferation.

(A) hTERT-RPE1 cells were transfected with the indicated siRNAs for the depletion of myosin VI, or moc treated. After 72 hours, the cells were fixed with 4% PFA and stained with DAPI, to identify the nuclei, ai with anti-Ki67 antibody as a proliferation marker. Random images were acquired with confocal microscope. multiparameter image cytometry analysis was performed to correlate Ki67 intensity in the nucleus with tl cell cycle profile (DAPI intensity) in single cells. The dot plot shows the intensity of DAPI and Ki67 in single ce (a representative plot of one of the two experiments performed is shown). AU=arbitrary unit. (B) The ever calculated as in A were gated to distinguish between high and low Ki67 expression. The bars show tl percentage of cells with high or low levels of nuclear Ki67. (C) An example of the images used for the ima cytometry analysis, showing the reduction of Ki67 staining in the nuclei of myosin VI-depleted cells.

To assess if this effect of myosin VI depletion on cell proliferation is a common feature of non-tumor cells, we assessed the pro liferative abilities of BJ-hTERT cells and HeLa cells, a widely-used tumor cell line. Indeed, the depletion of myosin VI causes a strong impairment in the cell proliferation of BJ-hTERT but not that of HeLa cells. This latter cell line presented a small effect in the first days after transfection, but then the proliferation rate appears to be equal to the control (Fig. 26).

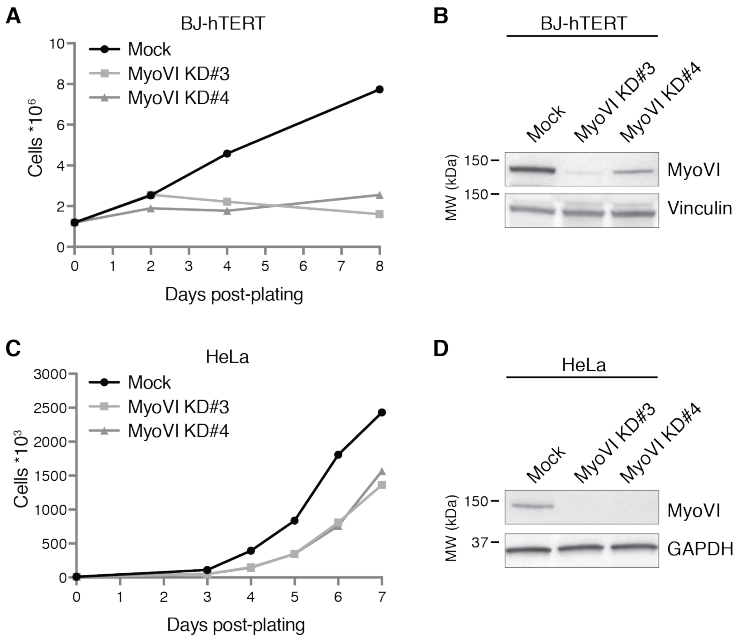

Figure 26: Only non-tumor cells show proliferation arrest upon depletion of myosin VI.

(A) BJ-hTERT cells were transfected with the indicated siRNAs for the depletion of myosin VI, or mock treated. On the day of the transfection, $1.2*10^6$ cells were plated in 10 cm dishes (day 0). On day 2, 4 and 8 cells were detached and counted with an automated cell counter. Cell counts are reported in the graph to show the growth curve. A representative plot of one of the two experiments performed is shown. (B) Four days after transfection, cells were lysed and WB was performed with the indicated antibodies to determine for myosin VI depletion. (C) HeLa cells were transfected with the indicated siRNAs for the depletion of myosin VI, or mock-treated. One day after transfection, 10 000 cells were plated in 6-well plates (day 0). From day 3 to 7 after plating, cells from one well per condition were detached and counted with an automated cell counter. Cell counts are reported in the graph to show the growth curve. A representative plot of one of the two experiments performed is shown. (D) Four days after transfection, cells were lysed and WB was performed with the indicated antibodies to determine for myosin VI depletion.

To better characterize the cell cycle arrest induced by myosin VI depletion, we moved to an inducible system, generating an hTERT-RPE1 cell line bearing a shRNA targeting myosin VI under the control of a TET-ON system. To control for a possible off-target effect, we

generated two cell lines expressing an shRNA targeting either the open reading frame (ORF) or the 5' untranslated region (UTR) of myosin VI. By single cell cloning, we obtained homogeneous populations and one clone for each shRNA was selected for further experiments. First, we determined the validity of this system, by evaluating the proliferative abilities of these cells in the absence or the presence of doxycycline. Confirming our previous results obtained with the siRNAs, cell proliferation was severely impaired upon shRNA induction in both clones (Fig. 27A). The depletion of myosin VI induced by doxycycline treatment was comparable in both clones and, after 10 days of depletion, both cell clones showed an enlarged and flattened morphology (Fig. 27B-C).

We then used these cells to assess the cell cycle phase in which the cells were blocked.

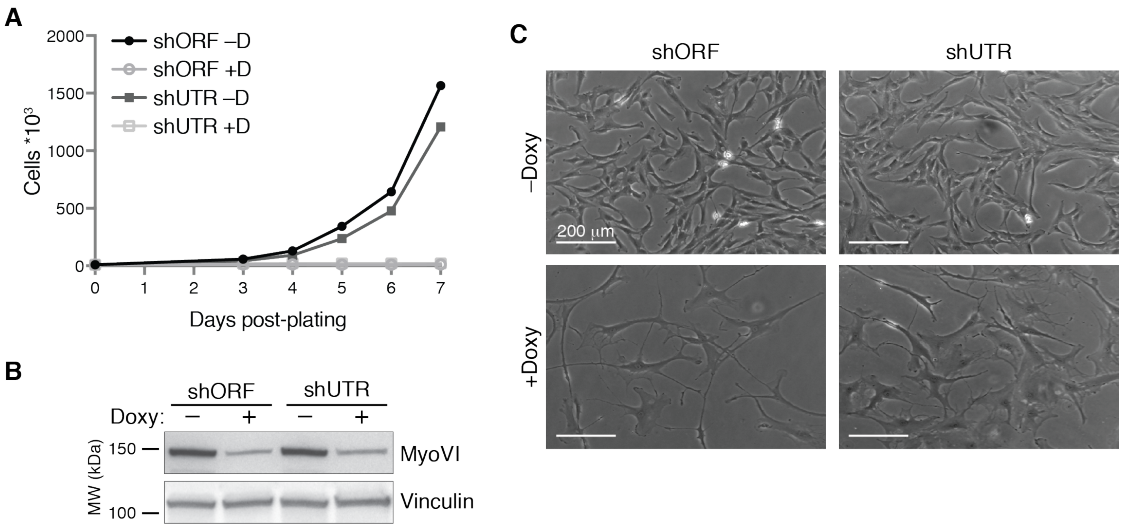

Figure 27: Characterization of hTERT-RPE1 cell clones expressing a shRNA targeting Myosin VI upon doxycycline induction.

hTERT-RPE1 cells were transduced with pSLIK-NEO containing shRNA targeting myosin VI mRNA in the ORF (shORF) or in the 5'UTR (shUTR), and single cell clones were chosen and characterized. (A) Growth curve of hTERT-RPE1 shORF and shUTR cells treated with doxycycline (D) to induce shRNA expression. One day after doxycycline induction, 10 000 cells were plated in 6-well plates (day 0). From day 3 to 7 after transfection, cells from one well per condition were detached and counted with an automated cell counter. Cell counts are reported in the graph. (B) WB of the same cells treated with doxycycline (Doxy) for 4 days to show the depletion of myosin VI. (C) Representative bright-field images of hTERT-RPE1 shORF and shUTR cells treated with doxycycline for 10 days.

After 10 days of myosin VI depletion, FACS analysis of the DNA content showed that >90% of the cells were in G0/G1 phase, in both clones (Fig. 28A). Prolonged cell cycle arrest can ultimately lead to senescence, an irreversible arrested state in which the cells display an increased cell size, the expression of SA-β-gal activity and altered patterns of gene expression (Debacq-Chainiaux et al., 2009; Dimri et al., 1995). The presence of SA-β-gal accumulation in myosin VI KD cells, together with their enlarged and flattened morphology, indicates that prolonged myosin VI KD ultimately leads to senescence (Fig. 28B).

Altogether, these data suggest that, in non-tumor cells, the depletion of myosin VI activates a cell cycle checkpoint, pushing the cells into a resting state, which, if prolonged, leads to senescence.

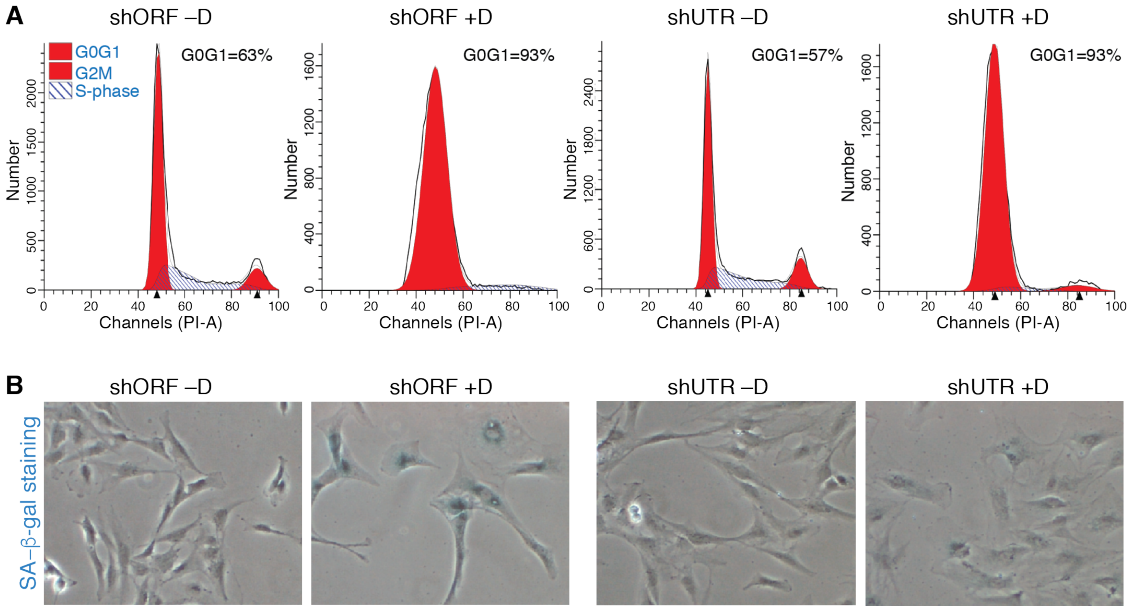

Figure 28: Depletion of myosin VI leads to cell cycle arrest in G0/G1 phase and senescence.

(A) shORF and shUTR cells were treated with doxycycline for 10 days to induce shRNA expression and myosin VI depletion. The cells were fixed with ethanol (Et-OH) and stained with propidium iodide (PI) to evaluate DNA content and calculate the percentage of cells in the different phases of the cell cycle. (B) Cells treated with doxycycline as in (A) were fixed with 4% PFA and treated to observe SA-β-gal accumulation as an indicator of senescence.

4.3.2. Depletion of Myosin VI leads to cell cycle arrest through the activation of the p53–p21 axis

Senescence can be induced by several stimuli that converge on p53 activation. Once activated, p53 induces the expression of the cyclin-dependent kinase inhibitor (CKI) p21, the effector that induces transient G1 arrest and then senescence or apoptosis (He et al., 2005). To elucidate the mechanism behind the cell cycle arrest induced by the depletion of myosin VI, we assessed the status of p53 and p21. When myosin VI is depleted from the cells through doxycycline induction, p53 is stabilized leading to p21 expression (Fig. 29A). Furthermore, while p53 activation decreases after several days of doxycycline induction, p21 expression is maintained, ensuring the maintenance of the cell cycle arrest (Fig. 29A). Transient depletion of myosin VI by siRNAs in both hTERT-RPE1 and BJ-hTERT cells further confirmed these results, indicating that what we observe is a general phenotype in non-tumor cells (Fig. 29B-C).

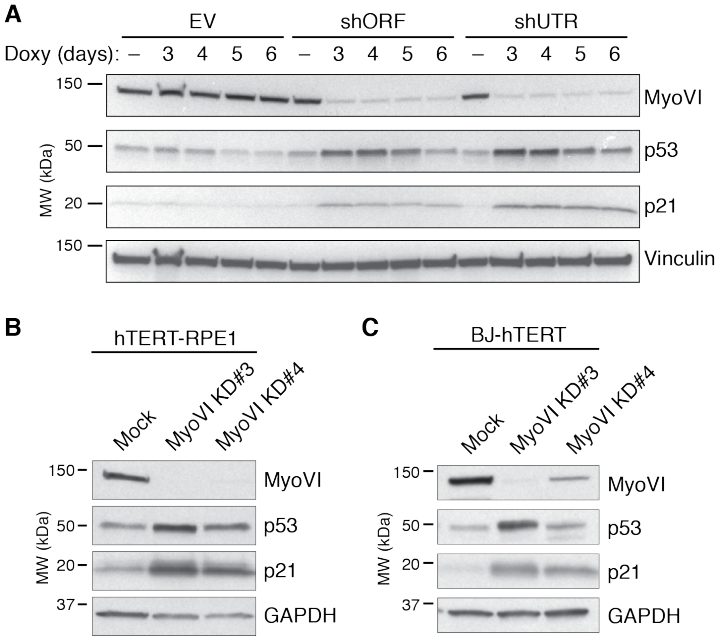

Figure 29: Depletion of myosin VI causes p53 and p21 activation.

hTERT-RPE1 shORF, shUTR and EV (as control) cells were treated with doxycycline as indicated to induce the depletion of myosin VI. The cells were lysed and WB was performed to assess p53 and p21 levels. (B) hTERT-RPE1 and (C) BJ-hTERT cells were transfected with the indicated siRNAs for the depletion of myosin VI, or mock-treated. Four days after transfection, cells were lysed and WB was performed to assess p53 and p21 levels.

To determine the increase in the nuclear levels of p53 and p21 at the single cell level, we used the multiparameter image cytometry analysis previously described (Furia et al., 2013b). hTERT-RPE1 cells were transfected with siRNAs for myosin VI KD and stained for p53, p21 and Ki67. DAPI staining was used by the software to identify the nuclei and calculate the intensity of the other signals in the nuclei area. Myosin VI staining was also performed to evaluate the efficiency of its depletion. Dot plots of single cells show that the population of myosin VI KD cells displayed an upper shift of p53 and p21 nuclear intensity compared to control cells (Fig. 30A and C). We then set a gate to distinguish cells expressing high levels of p53 or p21 in the nucleus from low-expressing cells. Indeed, 96.6% and 92.6% of cells transfected with siRNA #3 and #4, respectively, showed high nuclear p53 levels compared to 12.4% of control cells (Fig. 30B). Similarly, 95.3% and 92.2% of cells transfected with siRNA #3 and #4, respectively, showed high nuclear p21 levels compared to 36.8% of control cells (Fig. 30D). The increased levels of p53 and p21 in the nuclei also correlated with lower levels of Ki67 at the single cell level, further validating the absence of cell proliferation (Fig. 30E).

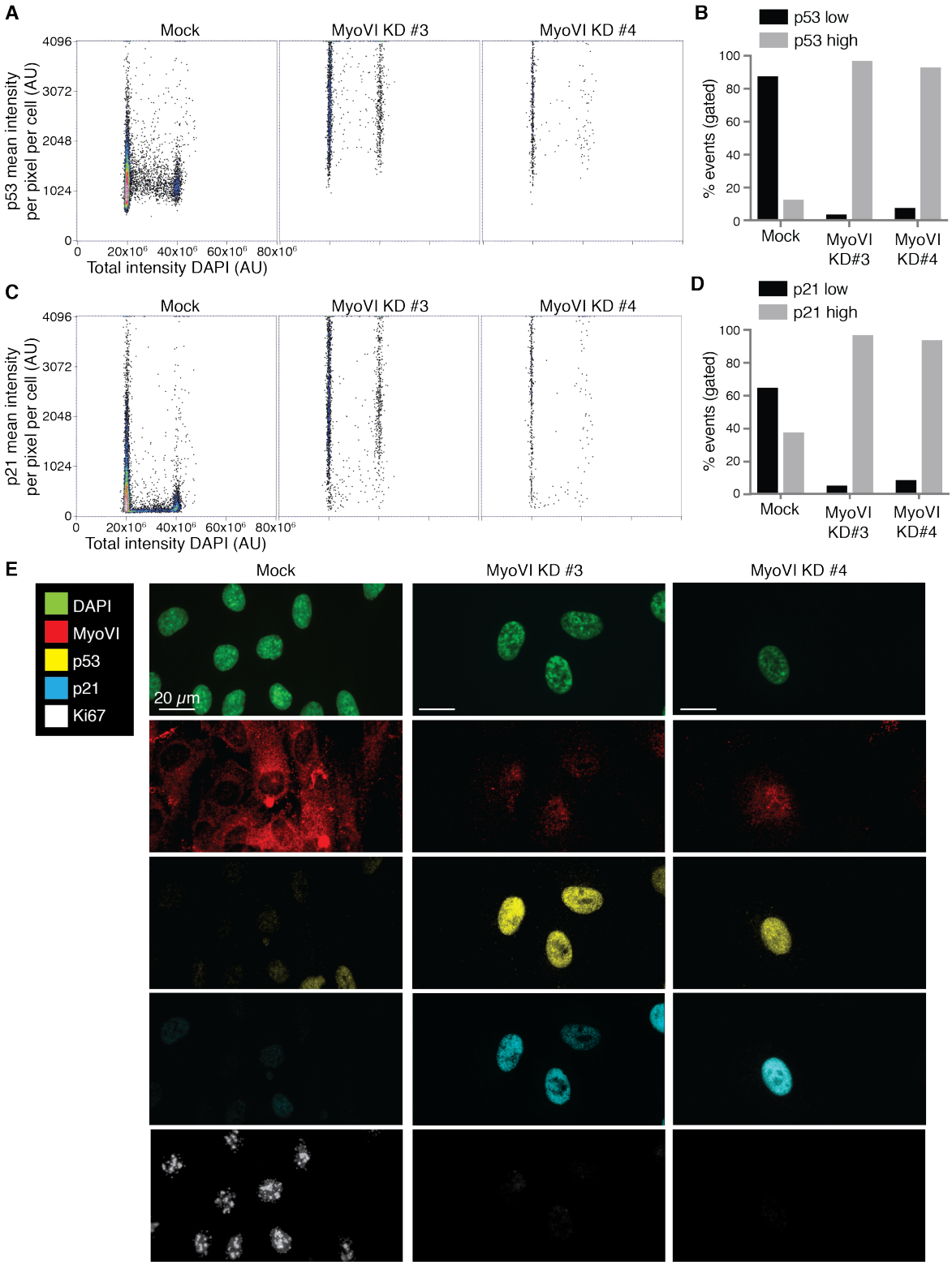

Figure 30: p53 and p21 nuclear levels are increased upon depletion of myosin VI.

hTERT-RPE1 cells were treated with the indicated siRNAs for the depletion of myosin VI, or mock-treated as control. After 72h, the cells were fixed with 4% PFA and stained with anti-p53 and anti-p21 antibodies to analyze their levels in the nuclei. DAPI staining was performed to identify the nuclei. Anti-Ki67 antibody was used as a proliferation marker. To determine for the depletion of myosin VI, an anti-myosin VI staining was performed. Random images were acquired with confocal microscope and a multiparameter image cytometry analysis was performed to correlate p53 or p21 intensity in the nucleus with the cell cycle profile

(DAPI intensity) in single cells. (A-C) The dot plots show the intensity of DAPI and p53 or p21 in the nuclei of single cells (a representative plot of one of the two experiments performed is shown). AU=arbitrary unit. (B-D) The events calculated in (A) and (C) were gated to distinguish between high and low p53 or p21 expression. The graphs show the percentage of cells with high or low levels of nuclear p53 and p21. (E) An example of the images used for the image cytometry analysis, showing the increase in the staining of p53 and p21 and the reduction of Ki67 staining in the nuclei of myosin VI-depleted cells.

We then wanted to understand if p53-p21 activation is required to induce cell cycle arrest caused by myosin VI KD. To this aim, we depleted p53 in myosin VI KD cells (Fig. 31C) and observed the behavior of the cells. As shown by the growth curve in Fig. 31A, the depletion of p53 rescued the proliferation impairment observed in myosin VI KD cells. Furthermore, p53 and myosin VI double KD cells showed no signs of a senescence-like morphology (Fig. 31B).

The sum of these results shows that the depletion of myosin VI induces p53-p21 activation, leading to subsequent cell cycle arrest and senescence.

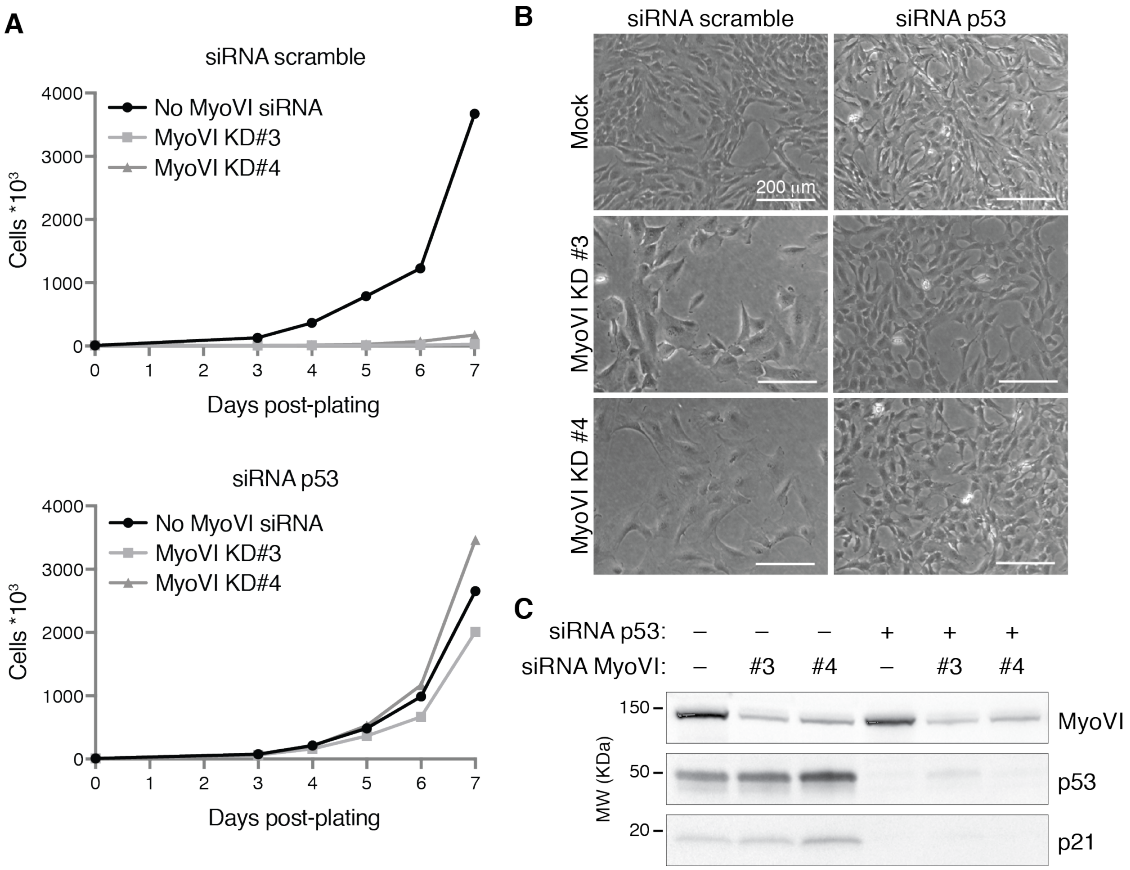

Figure 31: Depletion of p53 is sufficient to rescue myosin VI KD-induced cell cycle arrest.

hTERT-RPE1 cells were transfected with the indicated siRNAs for myosin VI and p53 depletion. (A) Growth curves of hTERT-RPE1 cells treated with the indicated siRNAs for myosin VI KD. Scramble or p53 siRNAs were co-transfected with myosin VI siRNAs (top and lower panel, respectively). One day after transfection, 10.000 cells were plated in 6-well plates (day 0). From day 3 to 7 after transfection, cells from one well per condition were detached and counted with an automated cell counter. Cell counts are reported in the graph. A representative plot of one of the two experiments performed is shown. (B) Representative bright-field images of indicated hTERT-RPE1 cells five days after transfection. (C) Five days after transfection, cells were lysed and WB was performed with the indicated antibodies to determine the depletion of myosin VI and p53.

4.3.3. DNA damage response is not involved in myosin VI-induced p53-p21 activation.

Since DNA damage is one of the best-known triggers of the p53-p21 axis activation, we investigated the possible involvement of the DDR in the myosin VI KD-induced cell cycle arrest. To analyze the presence of DNA damage foci in myosin VI-depleted cells, we used the well-known marker γH2AX, which accumulates at the sites of double-strand breaks. As a positive control, cells were irradiated with ionizing radiation (X-rays) that, causing DNA damage, promotes the generation of γH2AX foci (Fig. 32, right panel). As visible in Figure 32, myosin VI-depleted cells showed no increase of γH2AX foci in comparison to control cells.

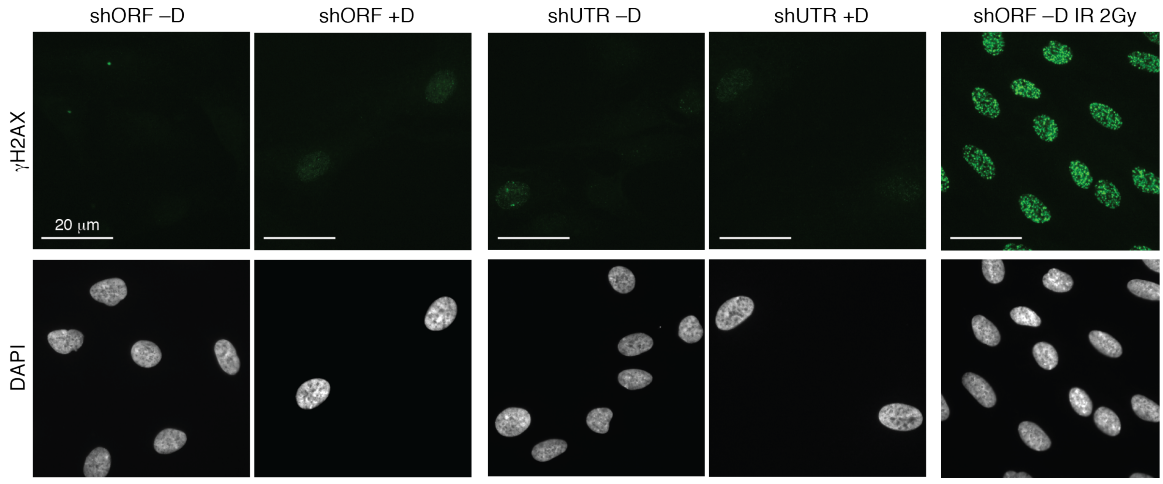

Figure 32: Myosin VI KD cells do not show DNA damage foci.

hTERT-RPE1 shORF and shUTR cells were treated with doxycycline for four days to induce the depletion of myosin VI. Positive control cells for DNA damage were irradiated as indicated (right panel). Cells were fixed with 4% PFA and stained with anti-γH2AX antibody and DAPI. All images were acquired with a wide-field microscope with the same parameter settings and the contrast/brightness enhancement was homogeneous for all images.

This result was confirmed by WB analysis. Levels of γH2AX was measured at different time points after myosin VI depletion induced by doxycycline. While irradiated cells showed an increase in the levels of this marker, the same did not occur after myosin VI KD (Fig. 33). In agreement with these results, p53 phosphorylation on Ser15, primary target of the DDR pathways, is clearly visible upon ionizing radiation, but not in myosin VI-depleted cells (Fig. 33).

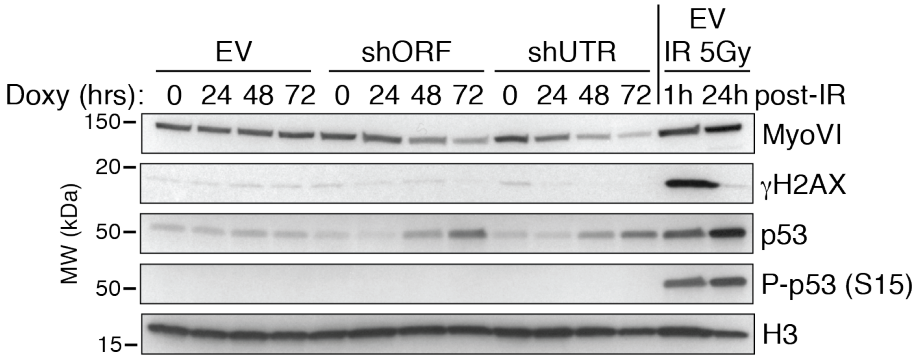

Figure 33: Myosin VI-depleted cells do not express markers of DNA damage response activation.

hTERT-RPE1 shORF, shUTR and EV (as control) cells were treated with doxycycline as indicated to induce the depletion of myosin VI. Positive control cells for DNA damage were irradiated as indicated and cells were collected at the indicated time points after irradiation. The cells were lysed and WB was performed to assess γH2AX activation (marker for DNA damage foci) and p53 phosphorylation on Ser15 (marker for DDR activation). An anti-H3 antibody was used as loading control.

Finally, we determined whether the DDR kinases were somehow involved in the myosin VI-induced cell cycle arrest. We treated control and myosin VI-depleted cells with inhibitors of the upstream mediators of DDR, DNA-PK, ATR and ATM kinases. None of the three inhibitors was able to rescue the proliferative impairment of myosin VI KD cells (Fig. 34).

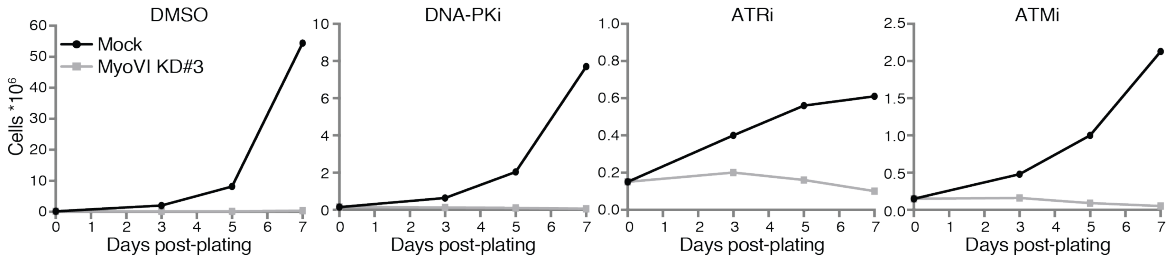

Figure 34: Inhibition of DDR pathways does not rescue myosin VI KD-induced cell cycle arrest.

hTERT-RPE1 cells were transfected with siRNA #3 for myosin VI depletion, or mock-treated as control. After 48h, the indicated inhibitors for DDR kinases were added to the medium and 150 000 cells were plated in 6 cm petri dishes (day 0). The inhibitors used for this assay are: DNA-PK inhibitor, NU7441 1µm; ATR inhibitor, ETP46464 2µm; ATM inhibitor, KU60019 10µm. DMSO was used as control at 1:500 dilution, which is the lowest dilution used among the three inhibitors. On day 3, 5 and 7, cells from one plate per condition were detached and counted with automated cell counter. Cell counts are reported is the graph.

Taken together, these data show that the cell cycle arrest induced by the depletion of myosin VI is not caused by DNA damage and is not mediated by the activation of the DDR pathways.

4.3.4. Myosin VI KD-induced cell cycle arrest is not mediated by centrosome surveillance pathways

As shown so far, the depletion of myosin VI in hTERT-RPE1 cells leads to centrosome alterations and cell cycle arrest due to p53-p21 activation. Therefore, we wondered whether these two phenotypes are linked to each other. It is noteworthy that different centrosomal defects have been linked to the activation of a possible "centrosome surveillance pathway", which is able to sense alterations in the number or the structure of the centrosome, leading to p53/p21 activation and subsequent cell cycle arrest (Fig. 8) (Fong et al., 2016; Ganem et al., 2014; Lambrus et al., 2016; Mikule et al., 2007). Therefore, we hypothesized the involvement of this pathway in the myosin VI KD-induced cell cycle arrest.

The depletion of many centrosome proteins arrests human diploid cells in G1 via activation of a p38-p53-p21 axis. The p38-MAPK stress response, activated in response to structural alterations of the centrosome, leads to p53 phosphorylation on serine 33 and its subsequent activation (Mikule et al., 2007). A well-known sign of the activation of this pathway is the phosphorylation of the serine/threonine p38 kinase on T180/Y182. Thus, we evaluated the status of the p38 kinase in myosin VI-depleted cells. As positive control, cells were treated with Nocodazole that arrests cells in the M phase by disruption of the mitotic spindle (Takenaka et al., 1998). While in this condition p38-MAPK phosphorylation is clearly visible, no sign of activation was evident in the doxycycline-induced cells (Fig.

35A). Similar to the shRNA, myosin VI depletion through siRNA transfection did not lead to p38-MAPK phosphorylation (Fig. 35).

Another pathway that is known to be activated following tetraploidy or centrosome amplification is the Hippo pathway (Ganem et al., 2014). Therefore, we used YAP phosphorylation and cytoplasm relocalization as readout of the Hippo pathway activation to understand if it is involved in the cell cycle arrest induced by myosin VI KD. As shown in Fig. 36A, YAP phosphorylation was slightly decreased right after doxycycline addition and did not increase when myosin VI was depleted, indicating that the Hippo pathway was off. To confirm this data, we determined YAP localization by IF. As positive control, we

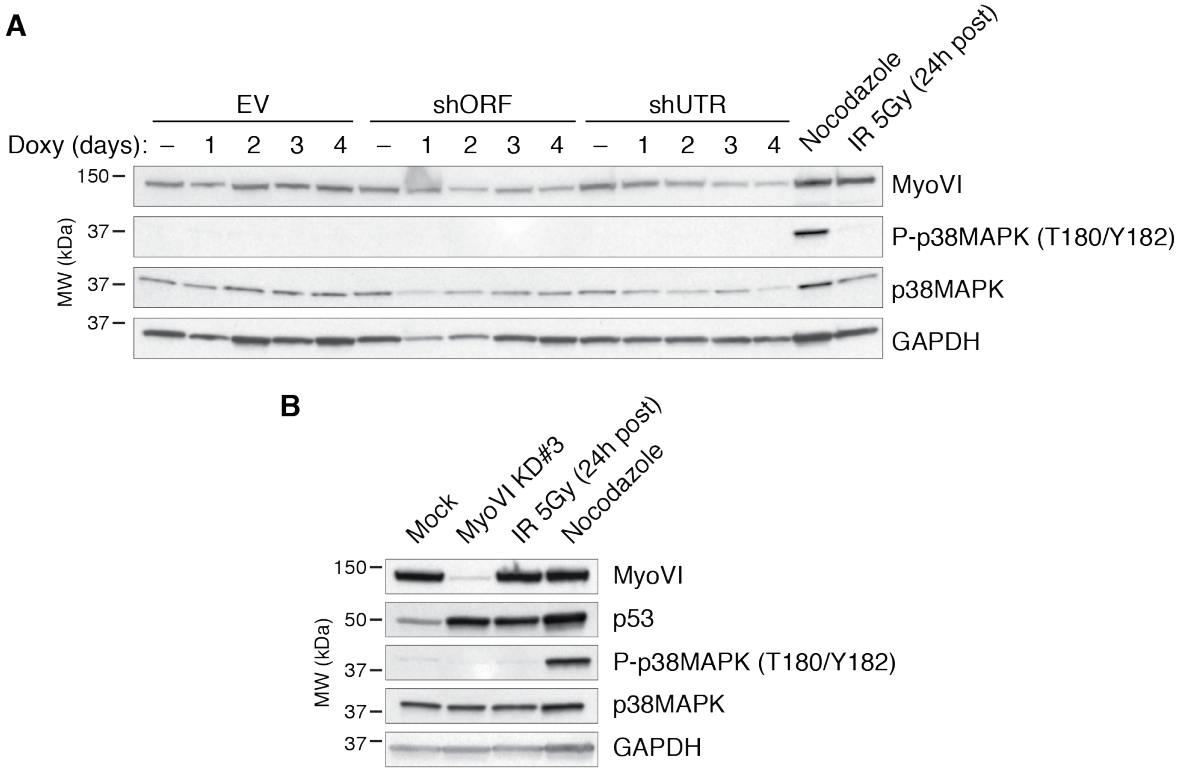

Figure 35: The p38-MAPK pathway is not involved in myosin VI KD-induced p53 activation and cell cycle arrest.

hTERT-RPE1 were treated with shRNA or siRNA for myosin VI depletion. (A) shORF, shUTR and EV (as control) cells were treated with doxycycline as indicated. (B) hTERT-RPE1 cells were transfected with siRNA #3 for myosin VI depletion or mock-treated as control. As positive control for p38-MAPK activation, EV or mock cells were treated with Nocodazole 50 ng/ml for 24 hours. As negative control, EV or mock cells were irradiated as indicated and cells were collected 24 hours after irradiation. The cells were then lysed and WB was performed to assess p38-MAPK phosphorylation on T180/Y182 as a marker of its activation.

used cells grown for few days after reaching confluency, a condition that activates the Hippo pathway, with YAP relocalized in cytoplasm (Fig. 36B, right panel). On the contrary, myosin VI-depleted cells, as well as control cells, displayed nuclear localization of YAP (Fig. 36B), confirming the non-phosphorylated status of YAP and thus the off status of the Hippo pathway.

Centrosomal alterations could lead to a defective mitosis, given the importance of the centrosome for the formation of the mitotic spindle. A recently discovered pathway

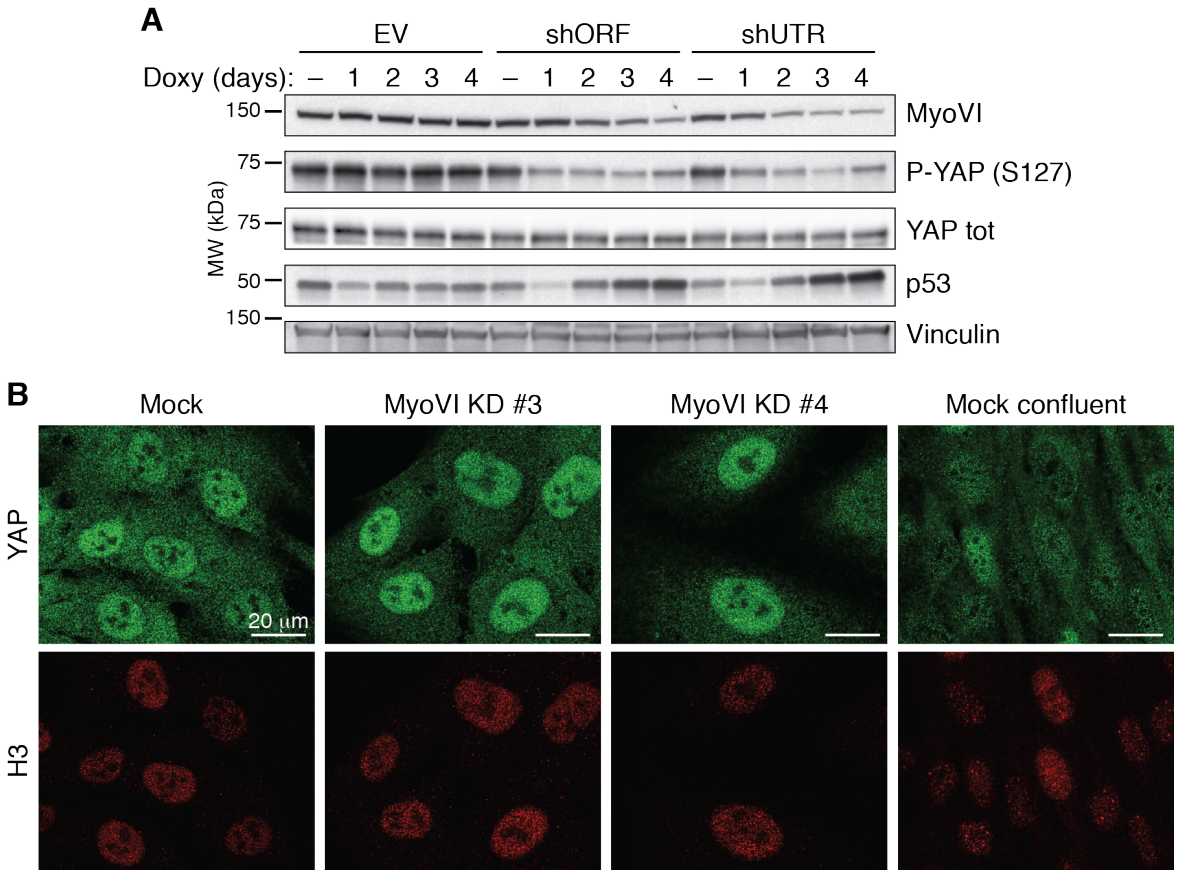

Figure 36: The Hippo pathway is not activated upon depletion of myosin VI.

(A) hTERT-RPE1 shORF, shUTR and EV (as control) cells were treated with doxycycline as indicated to induce the depletion of myosin VI. The cells were then lysed and WB was performed to assess YAP phosphorylation on S127 as a sign of its inactivation and cytoplasm translocation. (B) hTERT-RPE1 cells were transfected with the indicated siRNAs for the depletion of myosin VI, fixed with 4% PFA after 4 days, and stained with anti-YAP and anti-H3 (as a positive control for nuclear staining) antibodies. Positive control cells for the activation of the Hippo pathway (cytoplasmic YAP, inactive) were cultured in confluency for three days. All images were acquired with the same parameter settings and the contrast/brightness enhancement was homogeneous for all images.

involves USP28 and 53BP1 in the stabilization of p53 following centrosome depletion or prolonged mitosis. This pathway is activated when mitosis length overcomes a threshold that has been called “mitotic timer”, described as 90 minutes for hTERT-RPE1 cells (Fong et al., 2016; Lambrus et al., 2016). Since our previous results show that the depletion of myosin VI leads to several defects at the centrosomes, we assessed mitosis duration before the occurrence of cell cycle arrest. For this purpose, we generated hTERT-RPE1 cells stably expressing H2B-GFP as a marker for chromosomes, that allowed us to follow cell division. After 24 hours from transfection with siRNA for myosin VI, we performed time-lapse analysis to follow the cell division for 72 hours. Then, we calculated the number of mitosis occurring in a 12-hours timeframe, and the duration of mitosis. As expected, cells depleted of myosin VI underwent a decreased number of mitosis after siRNA transfection, reaching a complete cell cycle arrest 72 hours after siRNA transfection (Fig. 37A). On the other hand, the duration of mitosis was only slightly increased upon myosin VI KD (Fig. 37B), with an average of 39 minutes in myosin VI-depleted cells in comparison to 33 minutes in control cells. This small increase is not sufficient to reach the threshold of 90 minutes and to activate the “mitotic timer” required for the cell cycle arrest.

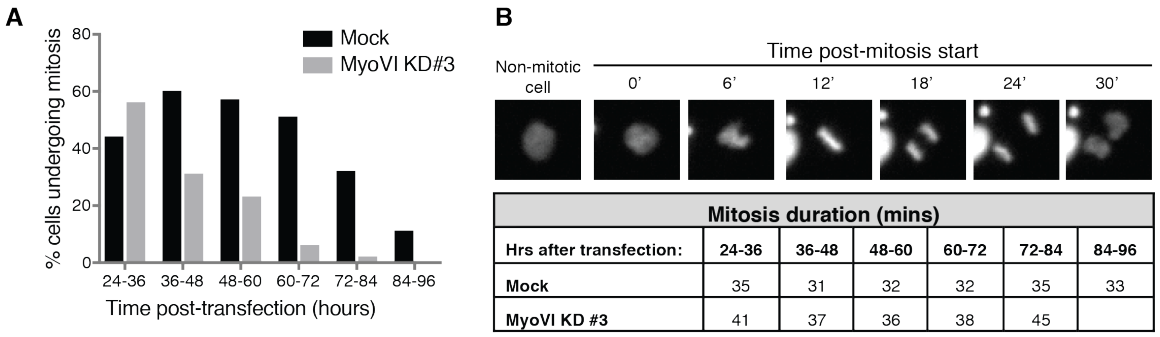

Mitosis duration (mins)						
Hrs after transfection:	**24-36**	**36-48**	**48-60**	**60-72**	**72-84**	**84-96**
Mock	35	31	32	32	35	33
MyoVI KD #3	41	37	36	38	45	

Figure 37: Myosin VI KD cells do not show an increased mitotic duration.

(A) hTERT-RPE1 cells expressing H2B-GFP as reporter were transfected with siRNA #3 for myosin VI KD and used for time-lapse imaging. Bars represent the percentage of cells undergoing mitosis during 12 hours timeframes after siRNA treatment. (B) Representative images of the time-lapse during a mitosis used to calculate its duration. The table reports the average duration of mitosis, from chromosomes condensation to decondensation, during 12 hours timeframes after siRNA treatment.

To further analyze the possible involvement of the 53BP1-USP28 pathway in p53 activation and cell cycle arrest induced by myosin VI depletion, we depleted the two main players on top of myosin VI KD. Neither 53BP1 (Fig. 38) nor USP28 (Fig. 39) depletion was able to rescue the proliferation impairment due to myosin VI depletion, as shown by the growth curve and the BrdU incorporation assays, respectively (Fig. 38A and 39A). Furthermore, in both cases, the cells retained a senescence-like morphology (Fig. 38B and 39B).

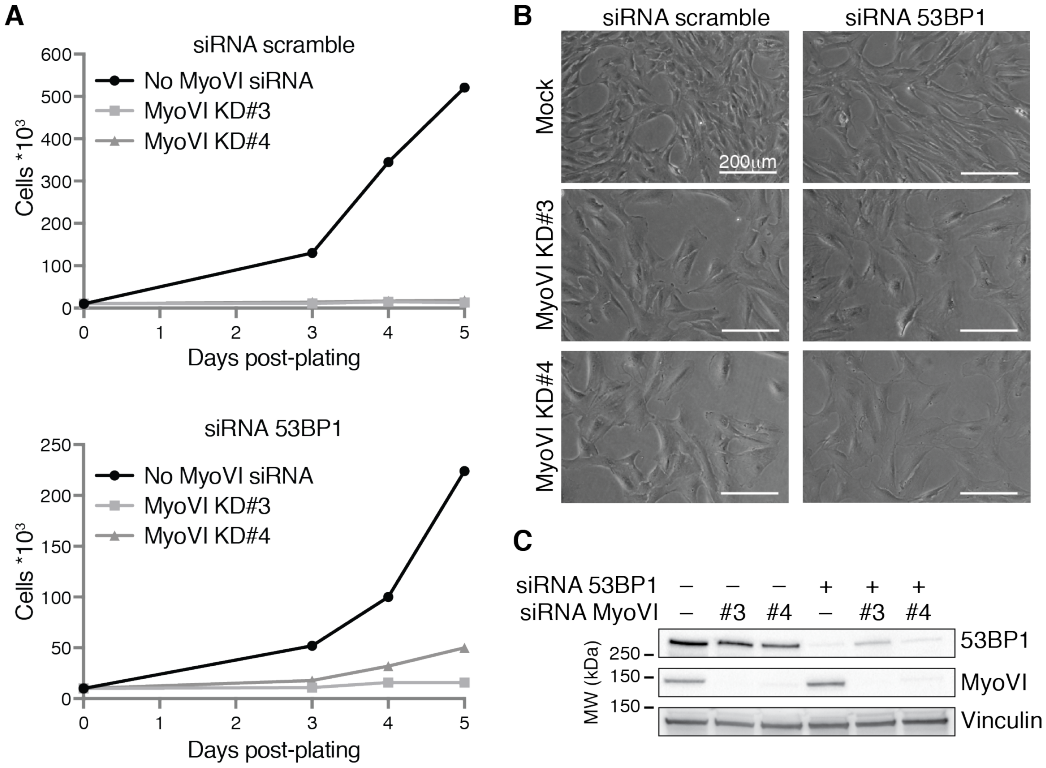

Figure 38: Depletion of 53BP1 is not sufficient to rescue myosin VI KD-induced cell cycle arrest.

hTERT-RPE1 cells were transfected with the indicated siRNAs for the depletion of myosin VI and 53BP1, or mock-treated as control. (A) Growth curves of hTERT-RPE1 cells treated with the indicated siRNAs for myosin VI KD. Scramble or 53BP1 siRNAs were co-transfected with myosin VI siRNAs (top and lower panel, respectively). One day after the transfection, 10000 cells were plated in 6-well plates plate (day 0). From day 3 to 7, cells from one well per condition were detached and counted with an automated cell counter. Cell counts are reported in the graph. Representative plots of one of the two experiments performed is shown. (B) Representative bright-field images of indicated hTERT-RPE1 cells five days after transfection. (C) Five days after transfection, cells were lysed and WB was performed with the indicated antibodies to determine the depletion of myosin VI and 53BP1.

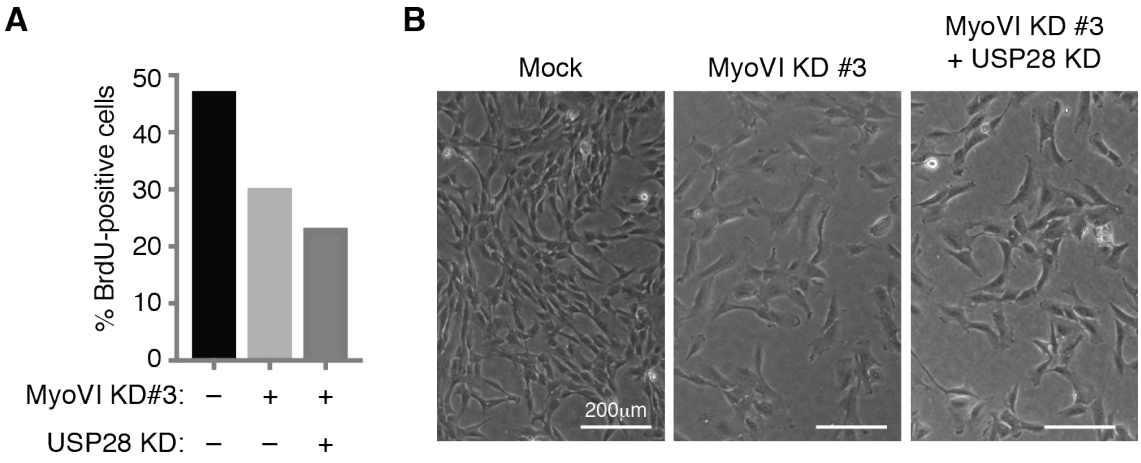

Figure 39: Depletion of USP28 is not sufficient to rescue myosin VI KD-induced cell cycle arrest.

(A) hTERT-RPE1 cells were transfected with the indicated siRNAs for the depletion of myosin VI and USP28, or mock-treated as control. Four days after transfection, cells were incubated with BrdU for 2 hours. After immunostaining with anti-BrdU antibody and DAPI, random images were acquired with a wide-field microscope, and the percentage of BrdU-positive nuclei was quantified. (B) Representative bright-field images of hTERT-RPE1 cells treated with the indicated siRNAs, acquired four days after transfection.

4.3.5. p53-dependent cell cycle arrest and centrosome alteration are not functionally linked

Prompted by these negative results, we went back to evaluate if the centrosome alterations are linked to the p53 activation in myosin VI-depleted cells.

First, we evaluated if the absence of p53 may rescue the centrosome alterations detectable upon siRNA-induced myosin VI depletion. As shown in Fig. 40A, hTERT-RPE1 cells in which both p53 and myosin VI are depleted do not show an increase in the distance between the centrosome and the nucleus in comparison to p53-depleted cells. Furthermore, only a small number of the double KD cells presented supernumerary centrioles (Fig. 40C). We used TEM to deeply analyze the ultrastructure of the centrosomes, but did not find any difference between p53-myosin VI double KD cells and control cells, depleted of p53 only (Fig. 40D).

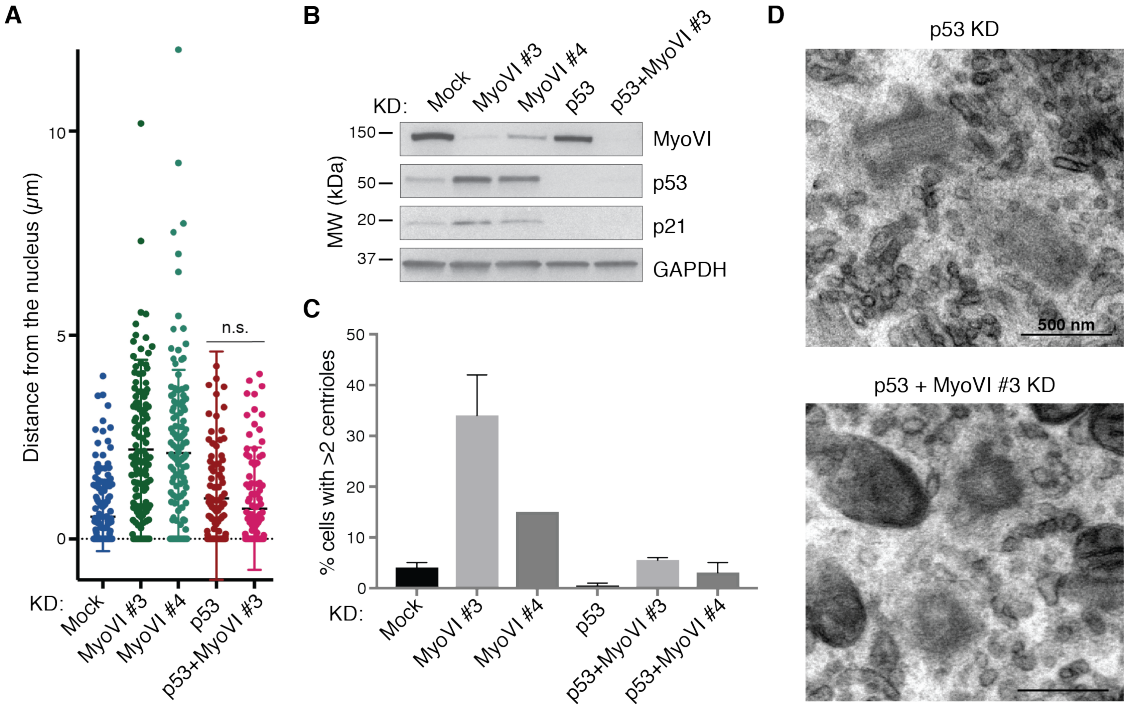

Figure 40: Depletion of p53 partially rescue myosin VI-KD induced centrosomal defects.

(A) hTERT-RPE1 cells were transfected with the indicated siRNAs for myosin VI and p53 KD, or mock-treated as control. After four days, the cells were fixed with 4% PFA and stained with anti-pericentrin and anti-golgin antibodies, FITC-phalloidin and DAPI. Images were acquired every 0.3 µm of the focal plane using z-stack function to visualize the entire cell. The images were processed using ImageJ software with custom-built plugins to measure the distance between the centrosome and the border of the nucleus. The dot plot represents the calculated distance in single cells (Mock N=174, MyoVI KD#3 N=137, MyoVI KD#4 N=130, p53 KD N=136, KD p53+MyoVI#3 N=134) from two independent experiments, displaying average ±SD. Statistical significance was calculated with Kruskal-Wallis test (n.s.=not significant). (B) Four days after transfection, cells were lysed and WB was performed with the indicated antibodies to determine the depletion of myosin VI and p53. (C) hTERT-RPE1 cells were transfected with the indicated siRNAs for myosin VI and p53 depletion. After four days, cells were fixed with Me-OH, after MTs depolymerisation, and stained with anti-acetylated tubulin antibody and DAPI to count the number of centrioles per cell. The graph shows the average +SEM of the percentage of cells with more than two centrioles, calculated from at least 150 cells per condition from two independent experiments. (D) hTERT-RPE1 cells were transfected with siRNA for p53 KD in addition to siRNA #3 for myosin VI KD, or with p53 siRNA as control. After four days, cells were fixed with 4% PFA/Glutaraldehyde buffer and processed for EM acquisition. Selected sections deriving from TEM analysis show the centrioles. 26 cells were analyzed for p53 KD and 21 cells were analyzed for p53+MyoVI KD.

Next, we assessed if we could observe the centrosome alterations also in the doxycycline-induced myosin VI depletion. It is worth noting that the levels of myosin VI KD vary

between the different siRNAs and shRNA. In fact, while the siRNA transfection results in >80% of KD efficiency, shRNA induction reaches only 65% of KD efficiency (Fig. 41B). Differently from the siRNA treated cells, doxycycline-induced myosin VI-depleted cells did not show any alteration at the level of the centrosomes. We did not observe an increase in centriole number or alterations in the centrosome-nucleus distance in doxycycline-

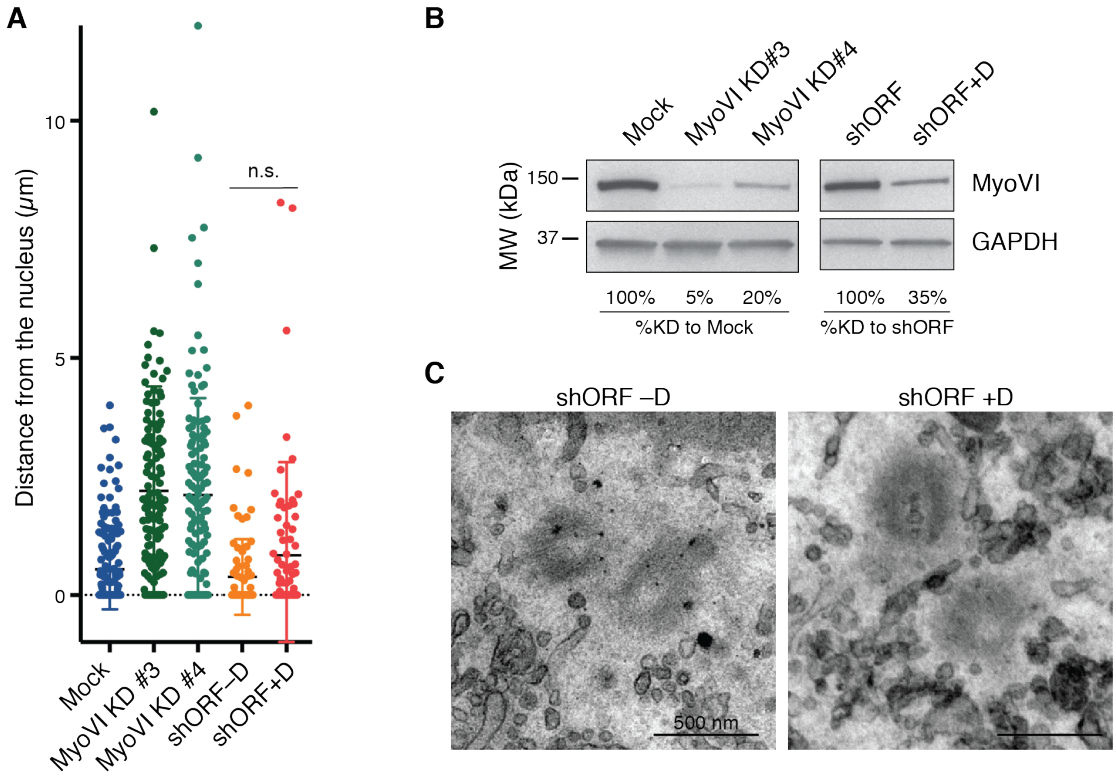

Figure 41: shORF cells do not show centrosome aberrations upon doxycycline induction.

(A) hTERT-RPE1 shORF cells were treated with doxycycline (D) for four days to induce the depletion of myosin VI. Then, cells were fixed with 4% PFA and stained with anti-pericentrin and anti-golgin antibodies, FITC-phalloidin and DAPI. Images were acquired every 0.3 µm of the focal plane using z-stack function to visualize the entire cell. The images were processed using ImageJ software with custom-built plugins to measure the distance between the centrosome and border of the nucleus. The dot plot represents the calculated distance in single cells (Mock N=174, MyoVI KD#3 N=137, MyoVI KD#4 N=130, shORF–D N=87, shORF+ D N=94), displaying average ±SD. Statistical significance was calculated with Kruskal-Wallis test (n.s.=not significant). (B) Cells treated with the indicated siRNAs or shRNA were lysed and WB was performed with the indicated antibodies to compare myosin VI KD levels. The % of myosin VI expression in myosin VI depleted cells relative to control cells was quantified as band intensity with Image Lab software. (C) hTERT-RPE1 shORF cells were treated with doxycycline (D) for four days to induce the depletion of myosin VI. Then, cells were fixed with 4% PFA/Glutaraldehyde buffer and processed for EM acquisition. Selected sections deriving from the TEM analysis show the centrioles. Six cells were analyzed for the control condition (not induced) and 12 cells were analyzed for doxycycline-induced cells.

induced cells with respect to control cells (Fig. 41A). Furthermore, the ultrastructure of the centrosome of doxycycline-induced cells appears normal (Fig. 41C). These data indicate that p53 activation and the centrosome alterations induced by the depletion of myosin VI are not linked.

4.3.6. A genome-wide CRISPR/Cas9 screening to identify genes involved in the myosin VI KD-induced cell cycle arrest

The candidate approaches we used to clarify the trigger of p53 activation in myosin VI-depleted cells was unsuccessful. Given the wide range of possible p53 activating pathways and the number of functions in which myosin VI is involved, we decided to take advantage of an unbiased approach. Therefore, we set-out a genome-wide, loss-of-function CRISPR/Cas9 screen in order to identify genes whose inactivation enables myosin VI-depleted cells to proliferate. This approach would allow us to identify components acting upstream or downstream of the p53-p21 axis in response to myosin VI depletion. As reported in the scheme (Fig. 42A), we generated hTERT-RPE1 cells that stably express Cas9 together with an inducible shRNA for myosin VI depletion. In order to obtain a homogeneous population, we selected single cell clones which showed, upon doxycycline induction and myosin VI depletion, an increment in the levels of p53 and p21, and a senescence-like morphology (Fig. 42B). The screening was performed using the Brunello library (Doench et al., 2016), a pooled lentivirus sgRNA library covering the entire human genome, in which each gene is targeted by 4 different sgRNAs (77441 gene-targeting sgRNAs + 1000 non-targeting sgRNAs as control). The library was used to infect shUTR cl.8 cells with a MOI of 0.08 to avoid the infection of the same cell from more than one virus. Cells were selected with puromycin for 6 days and then $8*10^6$ cells were left untreated (control), while $8*10^6$ cells were induced with doxycycline for 15 days.

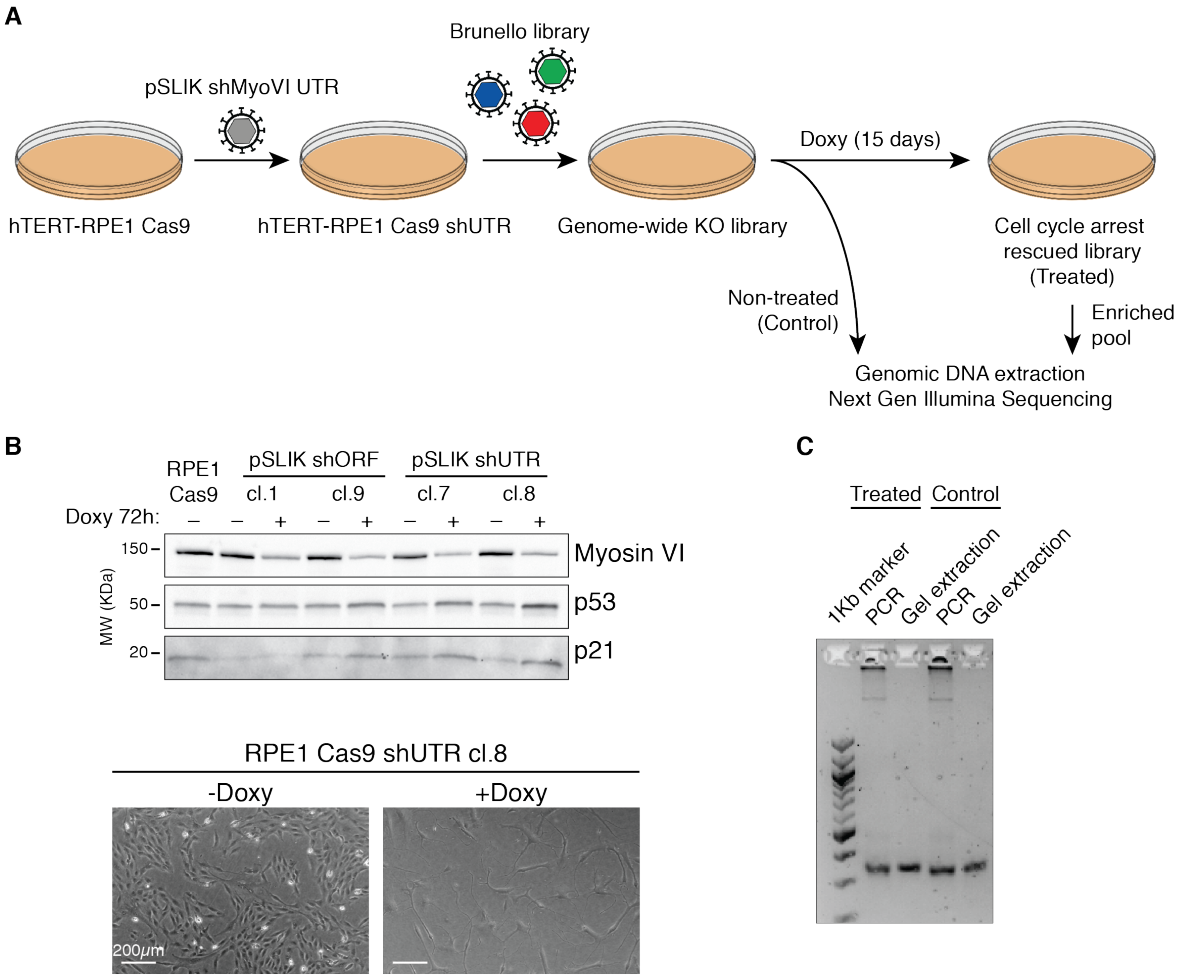

Figure 42: The genome-wide CRISPR/Cas9 screen to identify proteins involved in the cell cycle arrest induced by depletion of myosin VI.

(A) Scheme of the screening procedure. hTERT-RPE1 cells stably expressing Cas9 were transduced with pSLIK-NEO containing shRNA targeting the mRNA of myosin VI in the ORF (shORF) or in the 5'UTR (shUTR), and single cell clones were chosen and characterized (see examples in (B), top panel). The obtained cells were transduced with the Brunello library of lentiviruses containing pLentiGuide plasmids encoding for 77441 sgRNAs. The resulting genome-wide knockout cell library was treated with doxycycline for two weeks to induce the depletion of myosin VI and cell cycle arrest. Cells lacking genes required for the cell cycle arrest were expected to proliferate, generating a rescued library. All the cells were collected, genomic DNA was extracted and the region encoding for the sgRNA was amplified by PCR. The resulting sgRNA library was sequenced with next generation Illumina sequencing. As control, non-treated genome-wide knock-out library was harvested and processed as above. (B) Examples of the characterization of hTERT-RPE1 Cas9 shMyoVI clones, showing an increase in the levels of p53 and p21 upon doxycycline induction (top panel), and senescence-like morphology of the clone selected for the screening (lower panel). (C) After genomic DNA extraction of treated and non-treated (Control) cell libraries, PCR products before and after gel extraction (performed to remove genomic DNA from the sample) were loaded on a 2% agarose gel and stained with Syber Safe to visualize the DNA.

Cells that lacked genes critical for cell cycle arrest were expected to proliferate in the absence of myosin VI and enrich in the doxycycline–treated population compared with untreated controls. Genomic DNAs of the two cell populations were extracted, purified and subjected to PCR to amplify the inserted region encoding for the sgRNAs. This process was followed by gel extraction and purification to remove the genomic DNA (Fig. 42C). The obtained DNA libraries (Control and Treated) were then sequenced with Next Generation Illumina sequencing to identify the sgRNAs. Finally, each sgRNA enrichment was calculated using MAGeCK algorithm (Fig. 43).

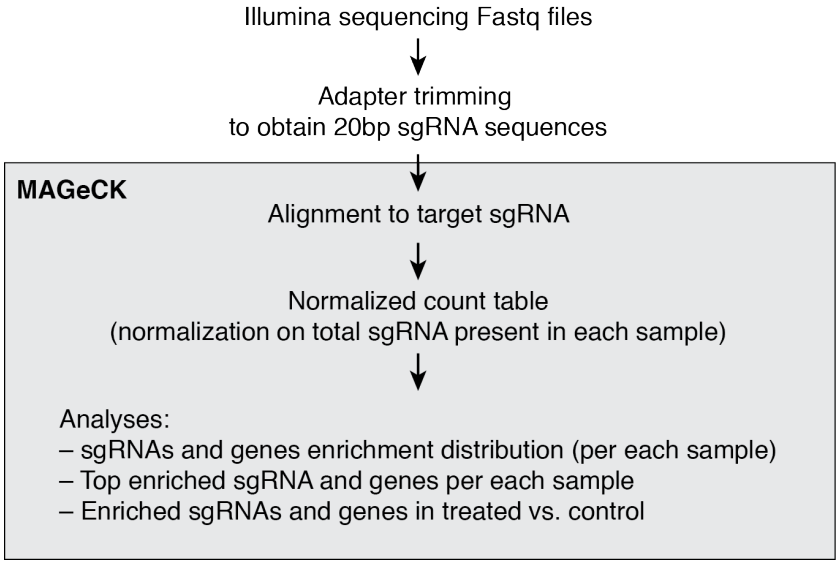

Figure 43: Bioinformatics analysis for the identification of enriched genes in the cell cycle arrest rescue library.

A scheme of the steps performed to identify genes enriched in the cell cycle arrest rescue library (treated with doxycycline) in comparison to not-induced knock-out cell library. Once the 20bp sequences of the sgRNAs were obtained performing adapter trimming of the raw Illumina reads, the MAGeCK algorithm was used to perform all the downstream steps as reported in the grey box.

In both samples, >80% of the sequencing reads mapped to target sgRNAs present in the Brunello library, meaning that all of the steps performed retained a good amount of information (Table 2). The Gini index (G.I.) was calculated in order to measure the evenness of the read count distribution of each sample. This index can assume values between 0 and 1 with smaller values indicating higher evenness. The control library

showed a more even distribution (G.I.=0.49) while the treated library had a Gini index of 0.71. The distribution of the sgRNAs frequency in Treated and Control libraries are shown in Fig. 44A and B. In the control sample 25% of the sgRNAs were not represented, meaning that in the process of infection and initial selection many cells did not proliferate or died. This could be only partially explained by genes essential for cell proliferation, whose deletion leads to apoptosis or senescence. In contrast, 56% of the sgRNAs were missing in the doxycycline treated library suggesting that a selection took place upon treatment with doxycycline (Table 2).

Condition	Total number of reads	Reads after trimming (length>10bp)	Reads mapped to target sgRNAs (%)	Reads mapped to non-targeting sgRNAs (%)	Total sgRNAs	Zero Counts	Gini Index
Control	2126063	2125842	86.86%	3.71%	77441	19036	0.49
Treated	2709150	2709029	82.99%	2.85%	77441	43170	0.71

Table 2: Quality assessment of sgRNAs library after Illumina sequencing of control and sample.
The "number of reads after trimming" indicates the total number of reads that were used for the analysis with MAGeCK algorithm. The percentage of reads mapping to sgRNAs of the Brunello library are reported, as well as the percentage of reads mapping to non-targeting sgRNAs. Zero Counts: total number of missing sgRNAs (sgRNAs of the Brunello library that have 0 counts). Gini Index: the Gini Index of the read count distribution. A smaller value indicates more evenness of the count distribution.

Finally, we examined the significantly enriched genes in Sample vs. Ctrl. Strikingly, p53 and p21 were among the highest-ranking genes (Fig. 44C) (false discovery rate, FDR <0.002), validating the entire procedure and our previous findings. Other two genes showed an FDR<0.1 are ATF7IP and SETDB1 and are considered strong candidates (Fig. 44C). Interestigly, they have been recently reported to be part of the same complex (Timms et al., 2016). We considered for further validation also a fifth gene, STAMBPL1, whose FDR was slightly above the threshold (Fig. 44C).

We also looked at the status of the DDR kinases ATM, ATR and PRKDC, of the proteins involved in centrosome surveillance pathways (53BP1 and USP28, p38-MAPK) and of the

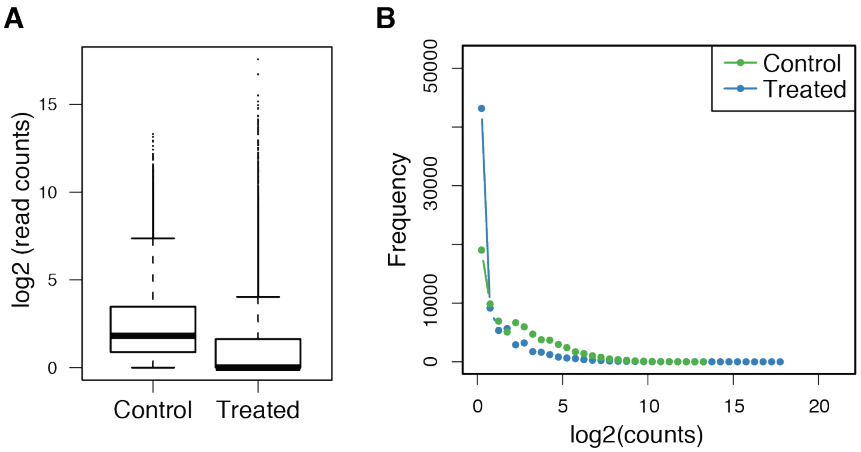

Gene	FDR
TP53	0,002
ATF7IP	0,002
CDKN1A	0,002
SETDB1	0,011
STAMBPL1	0,120

Figure 44: sgRNA reads count distribution in doxycycline-treated and control samples.

(A) Boxplots representing the distribution of the sgRNAs counts normalized by the total reads of the sample. The bottom and top of the rectangle indicate the first and third quartiles, the line inside is the median value. Upper and lower whiskers represent 1.5 times below or above the interquartile range. (B) Graph showing the number of sgRNAs relative to their frequency in the samples. (C) The table shows the top five enriched genes in the cell cycle arrest rescue library compared to control library. False discovery rate (FDR) was calculated to show statistical significance of gene enrichment.

Hippo pathway (LATS2). None of the listed genes was enriched in our screening, even though they could be detected in the baseline reads in both Control and Treated samples. This result confirmed that these genes are not involved in myosin VI-induced cell cycle arrest.

In a parallel approach, we also extracted the DNA from single clones that popped-out after two weeks of doxycycline-treatment. Indeed, cells that were proliferating in the absence of myosin VI generated single cell clones visible among the senescent cells (Fig. 45B). These clones were selected and cultured in presence of doxycycline. After genomic DNA extraction, the region encoding for the sgRNA was amplified by PCR (Fig. 45C) and sequenced in order to identify the gene target. Among the 312 clones that were initially picked, only 92 survived to the clone expansion. All of them contained a single sgRNA, confirming the validity of the procedure.

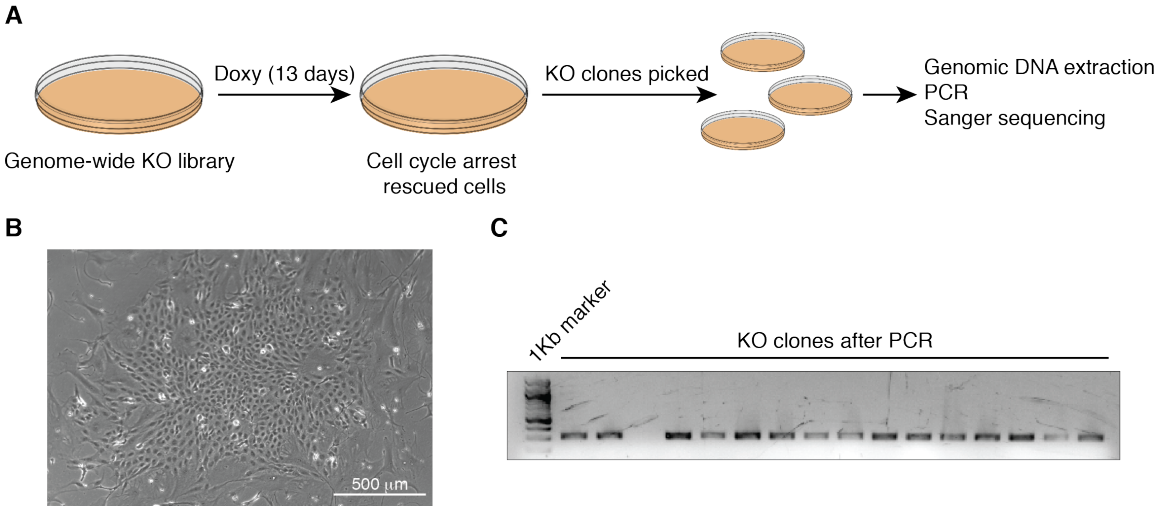

Figure 45: Analysis of single cell clones that bypass the myosin VI-induced cell cycle arrest.

(A) A scheme of the procedure used to identify single cell clones that proliferate despite the depletion of myosin VI. The previously made genome-wide knock-out cell library was treated for 13 days with doxycycline to induce the depletion of myosin VI and cell cycle arrest. Proliferating clones (see example in (B)) were expanded to reach a sufficient number of cells for genomic DNA extraction. The region encoding for the sgRNA was amplified by PCR (see examples in (C)) and the sgRNA was identified by Sanger sequencing.

Table 3 lists the genes we identified. As expected, most of the clones contained a sgRNA targeting p53. Strikingly, we found one clone containing a sgRNA against ATF7IP, further suggesting that this protein is involved in myosin VI KD-induced cell cycle arrest or that cells depleted of ATF7IP are able to bypass the p53-mediated arrest.

Finally, we compared the list of genes identified via direct sequencing with the list of statistically enriched single sgRNAs and we identified another potential candidate, MAPKAPK2. Indeed, one sgRNA targeting this gene was found as significantly enriched in the Treated sample by the bioinformatics analysis.

In summary, the two different approaches generated a list of candidates that could be involved in the myosin VI KD-induced cell cycle arrest, either upstream or downstream of p53 activation.

Genes (alias)	Protein name	Description	Number of clones identified
TP53	Cellular tumor antigen p53	Transcription factor whose protein levels and post-translational modification state alter in response to cellular stress. Tumor suppressor.	56
ATF7IP (MCAF1)	ATF7-interacting protein	Multifunctional nuclear protein that associates with heterochromatin. It can act as a transcriptional coactivator or corepressor.	1
MAPKAPK2	MAPK-activated protein kinase 2	Stress-activated serine/threonine-protein kinase involved in cytokine production, endocytosis, reorganization of the cytoskeleton, cell migration, cell cycle control, chromatin remodeling, DNA damage response and transcriptional regulation.	1
ARL6IP6 (PFAAP1)	ARL-6-interacting protein 6		1
BATF2	B-ATF-2	AP-1 family transcription factor that controls the differentiation of lineage-specific cells in the immune system	1
CACNG2	Voltage-dependent calcium channel gamma-2 subunit	Regulates the trafficking and gating properties of AMPA-selective glutamate receptors (AMPARs).	1
ECHDC2	Enoyl-CoA hydratase domain-containing protein2, mitochondrial		1
ETS2	Protein C-ets-2	Transcription factor activating transcription. Binds specifically the DNA GGAA/T core motif.	1
FBXL22	F-box and leucine-rich protein 22	Substrate-recognition component of the SCF (SKP1-CUL1-F-box protein)-type E3 ubiquitin ligase complex.	1
GALP	Galanin-like peptide	Member of the galanin family of neuropeptides. Involved in hypothalamic regulation of metabolism and reproduction.	1
GRINA (LFG1-NMDARA1-TMBIM3)	Protein lifeguard 1	Glutamate Receptor, NMDA Subtype, Glutamate-Binding Subunit	1
IL31RA (CRL3-GPL)	IL-31 receptor subunit alpha	Type I cytokine receptor. It is expressed on monocytes, and is involved in IL-31 signaling via activation of STAT-3 and STAT-5.	1
JAK2	Tyrosine-protein kinase JAK2	Non-receptor tyrosine kinase involved in various processes such as cell growth, development, differentiation or histone modifications.	1
MBD2	Methyl-CpG-binding domain protein 2	Functions as a scaffold protein, targeting GATAD2A and GATAD2B to chromatin to promote repression.	1
MRC1 (CLEC13D)	Macrophage mannose receptor 1	Mediates the endocytosis of glycoproteins by macrophages.	1
NIPSNAP3A	NipSnap3A	It belongs to a family of proteins with putative roles in vesicular transport	1
NRP1 (VEGF165R)	Neuropilin-1	Neuropilins ind many ligands and various types of co-receptors (like VEGF); they affect cell survival, migration, and attraction	1
OR4C15	Olfactory receptor 4C15	Odorant receptor.	1
OSER1	Oxidative stress-responsive protein 1		1
OTUD6B (DUBA5)	Deubiquitinase OTUD6B	Iso1: Deubiquitinating enzyme that may play a role in the ubiquitin-dependent regulation of	1

		protein synthesis, downstream of mTORC1. Iso2: Stimulates protein synthesis.	
PA2G4 (EBP1)	Proliferation-associated protein 2G4	RNA-binding protein that is involved in growth regulation.	2
PTBP3 (ROD1)	Polypyrimidine tract-binding protein 3	RNA-binding protein that mediates pre-mRNA alternative splicing regulation.	1
PTCHD1	Patched Domain Containing 1	Required for the development and function of the thalamic reticular nucleus (TRN)	1
RRAGB	Ras-related GTP-binding protein B	Guanine nucleotide-binding protein that plays a crucial role in the cellular response to amino acid availability through regulation of the mTORC1 signaling cascade.	1
S100A7A	Protein S100-A7A	May be involved in epidermal differentiation and inflammation	1
SLC12A4 (KCC1)	Solute carrier family 12 member 4	Mediates electroneutral potassium-chloride cotransport when activated by cell swelling.	2
SMIM24	Small integral membrane protein 24		1
TFPT	TCF3 fusion partner	Appears to promote apoptosis in a p53/TP53-independent manner.	1
ZNF662	Zinc finger protein 662		1

Table 3: List of the genes identified in cells that rescue the myosin VI KD-induced cell cycle arrest.

sgRNAs identified through Sanger sequencing in cells derived from knock-out library that were able to proliferate in the presence of doxycycline. The number of clones identified per sgRNA is reported. The rows in grey indicate the genes that show at least one significantly enriched sgRNA also in the Illumina sequencing screening.

4.3.7. STAMBPL1 is involved in myosin VI KD-induced cell cycle arrest

To validate the results obtained with the genome-wide CRISPR/Cas9 screening described above, we need to generate individual knock-out cell lines and assess their growth in the absence of myosin VI. While these experiments are on-going, we started validating STAMBPL1, also called AMSH-like protein (AMSH-LP), for which we have in house functional siRNAs (Savio et al., 2016). Thus, we transiently depleted AMSH-LP together with myosin VI in hTERT-RPE1 cells. As shown by the growth curve in Fig. 46A, the depletion of AMSH-LP partially rescued the proliferation impairment observed in myosin VI KD cells. Furthermore, AMSH-LP and myosin VI double KD cells showed no signs of a senescence-like morphology (Fig. 46B).

To understand if AMSH-LP acts up or downstream p53 following myosin VI depletion, we checked p53 and p21 levels. As shown in Fig. 46C, double KD cells show a reduction of p53 and p21 levels compared to myosin VI KD cells. This result has also been confirmed by the analysis of p21 mRNA level, which is decreased in double KD cells compared to myosin VI KD cells, even if it is not able to reach the basal level of control cells (Fig. 46D). This partial rescue of cell cycle arrest and p53-p21 activation could be easily ascribed to the incomplete depletion of AMSH-LP, visible at the mRNA levels (Fig. 46D) and should be confirmed in the validation procedure that relies in the generation of full knock-out clones.

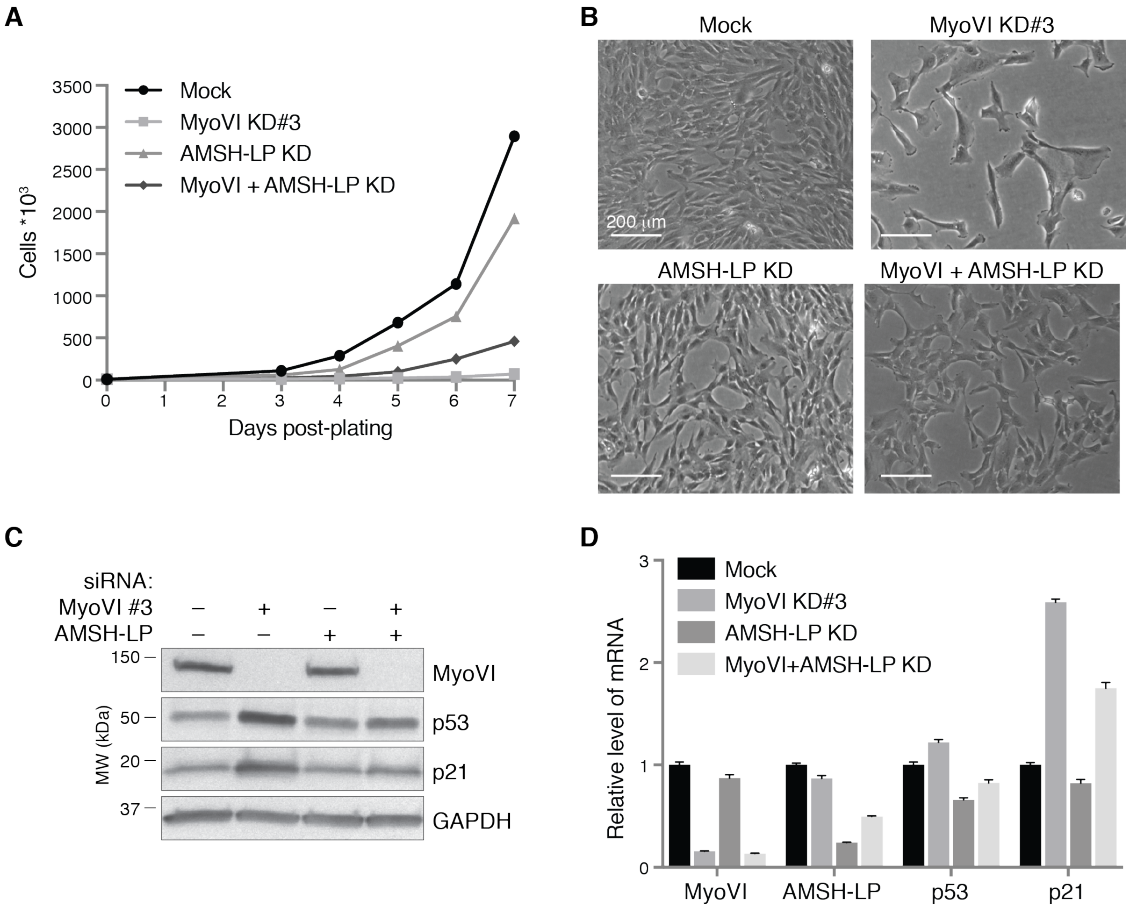

Figure 46: The depletion of AMSH-LP is sufficient to rescue myosin VI KD-induced cell cycle arrest and p53-p21 activation.

hTERT-RPE1 cells were transfected with the indicated siRNAs for myosin VI and AMSH-LP depletion, or mock-treated as control. (A) Growth curves of hTERT-RPE1 cells treated with the indicated siRNAs for myosin VI KD. One day after transfection, 10000 cells were plated in 6-well plates (day 0). From day 3 to 7 after transfection, cells from one well per condition were detached and counted with an automated cell counter. Cell counts are reported in the graph. A representative plot of one of the two experiments performed is shown. (B) Representative bright-field images of indicated hTERT-RPE1 cells five days after transfection. (C) Five days after transfection, cells were lysed and WB was performed with the indicated antibodies to determine the depletion of myosin VI and the levels of expression of p53 and p21. (D) Five days after transfection, cells were lysed and RNA was extracted. Retro-transcription was performed to obtain the cDNA of the samples. Quantitative PCR was performed to determine the depletion of myosin VI and AMSH-LP, and the expression levels of p53 and p21.

5. Discussion

Previous studies aimed at understanding the functions of myosin VI have been performed mainly in cancer cell lines, in which cell cycle progression and centrosomes are frequently altered and myosin VI itself is deregulated. In fact, myosin VI_{short} is upregulated in ovarian and other invasive cancers, where it has a role in cancer cell migration (Wollscheid et al., 2016). The present study started addressing the role of myosin VI in physiological conditions using non-tumor cells. Our results unveil an unprecedented involvement of myosin VI in the regulation of the cell cycle and in the maintenance of centrosome structure and number.

5.1. New functions of myosin VI in non-tumor cells

Myosin VI has been implicated in several cellular functions. The diversity of the functions of myosin VI derives from its interactions with multiple cargo adaptors, which mediate the targeting of myosin VI to different cellular locations (Tumbarello et al., 2013). Moreover, the cargoes that bind myosin VI play a role in the switch between the motor or anchor properties of the protein, further regulating its properties (Altman et al., 2004; Chuan et al., 2011).

Recently, our laboratory performed various experiments with the purpose of identifying novel myosin VI interactors, with particular attention on the isoform-specific binders (Appendix) (Wollscheid et al., 2016). Among well-known myosin VI interactors, we found enrichment of proteins belonging to the MTOC. Among the identified proteins, the centrosome protein OFD1 was found in all tested cell lines, suggesting that OFD1 is a reliable interactor of the motor protein. Indeed, IP assays not only confirmed the interaction between the two proteins, but also showed that both myosin VI_{long} and myosin VI_{short} interact with OFD1, in line with the fact that the interaction was found in

cells expressing different isoforms. As expected, myosin VI binds OFD1 through its tail domain, which is normally deputed to cargo binding. Further experiments will allow us to precisely identify the region of interaction between the two proteins. Of note, an interactome that was recently described for endogenous myosin VI further validated OFD1 as myosin VI interactor (O'Loughlin et al., 2018).

Given the fact that OFD1 is a centrosome/basal body protein involved in centriole elongation and primary cilium formation (Ferrante et al., 2006; Singla et al., 2010; Tang et al., 2013), we hypothesized that myosin VI could play a role in the regulation of centriole structure and function. To analyze this possibility, we used hTERT-RPE1, a diploid non-tumor cell line that is widely used as a cellular model for primary cilium and centrosome assays. Interestingly, depletion of myosin VI in these cells resulted in centrosome amplification, confirming a new role of myosin VI in this organelle. Unexpectedly, we soon realized that myosin VI depletion had also a strong effect on cell proliferation. These findings prompted us to analyze the two phenotypes and to assess whether there is a connection between the two.

5.2. Myosin VI depletion leads to centrosome amplification possibly by uncoupling the centrosome cycle from the cell cycle

Centrosomes are key organelles of the cells, and their main function is to organize microtubules during interphase and mitosis. Centrosomes are composed of two orthogonally oriented centrioles, connected by a protein linker, surrounded by the pericentriolar matrix (Loncarek and Bettencourt-Dias, 2018). Centrosome duplication is semi-conservative and follows the cell cycle, starting in late G1, under the control of CDKs. A tight control of this process ensures that duplication occurs only once per cell

cycle (Loncarek and Bettencourt-Dias, 2018). Our results show different alterations of the centrosomes upon myosin VI depletion, which affect both its structure and functions.

In particular, myosin VI depletion causes centrosome amplification in cells that are arrested in G1. In the literature, it is reported that centrosome amplification could be caused by the upregulation of Plk4, STIL or SAS-6, key factors that drive procentriole assembly, leading to the production of flower-like centrioles around the mother centriole (Habedanck et al., 2005; Kleylein-Sohn et al., 2007; Leidel et al., 2005; Vulprecht et al., 2012). Centrioles over elongation and fragmentation has been indicated as another source for centrosome amplification. Indeed, deregulation of centriole length could lead to overly long centrioles, that can fragment and ectopically form procentrioles (Marteil et al., 2018). Differently from the above-mentioned publication, myosin VI-depleted cells do not show neither overly long centrioles, nor centriole fragments, but nonetheless present an abnormal number of fully-formed centrioles that are not engaged with the mother centriole, as seen by TEM images.

Interestingly, myosin VI-depleted cells sporadically show two primary cilia, indicating that more than one centriole is able to be converted to basal body. The centrioles acquire the distal and subdistal appendages, and thus the ability to dock to the plasma membrane and to grow a primary cilium, only after one and a half cycle from their birth (Loncarek and Bettencourt-Dias, 2018). The presence of multiple primary cilia imply that more than one centriole possesses the appendages. This observation is even more interesting if we take into consideration that myosin VI-depleted cells are arrested in G1, suggesting that a decoupling between the cell and the centrosome cycle is occurring. It is worth mentioning that the impaired ability of myosin VI cells to generate primary cilia could lead to an underestimation of the number of mother centrioles that are present. In the near future, we intend to use specific markers in order to assess more precisely the number of mother

and daughter centrioles present in each cell to understand when the uncoupling of the centrosome cycle from the cell cycle is occurring.

5.3. Centrosome alterations and cell cycle arrest induced by myosin VI depletion are not linked

CDK2 is a key player in the coordination of the cell cycle and the centrosome cycle, and plays a major role in the initiation of centrosome duplication (Fukasawa, 2008). When p53 is activated, CDK2 is inhibited through upregulation of p21, thus creating an environment that is not permissive for centriole duplication. This evidence is in contrast with our data, in which myosin VI-depleted cells show both p53 activation and centrosome amplification, suggesting that the two phenotypes observed in myosin VI-depleted cells are not linked, and that centrosome amplification could occur before or regardless of the inhibition of CDK2 by p21. In this scenario, the decoupling of the centrosome cycle from the cell cycle in myosin VI-depleted cells is exacerbated by the cell cycle arrest in the G0/G1 phase. Cells depleted of p53 and myosin VI are able to cycle and undergo mitosis, thus impeding the accumulation of amplified centrosomes in the cell.

Other evidences suggest that the centrosome alteration found in myosin VI-depleted cells does not derive from cell cycle arrest. In fact, myosin VI depletion through inducible shRNA leads to cell cycle arrest but not to detectable centrosomal alterations, which could be explained by the different levels of knock-down obtained by the use of siRNAs or shRNAs. In fact, while siRNAs can deplete >85% of myosin VI, shRNAs can induce only 65% of depletion. The latter level of depletion could be enough to induce cell cycle arrest, but not centrosome alterations. A similar scenario occurs in the case of OFD1: the phenotypes observed in OFD1-depleted cells are present only when a high level of depletion is achieved (personal communication by Brunella Franco). These findings support the

hypothesis that centrosome alterations and cell cycle arrest derived from the depletion of myosin VI are two independent phenomena.

Interestingly, centrosome amplification has been shown to induce activation of p53 and cell cycle arrest through the Hippo pathway, which leads to phosphorylation of p53 mediated by LATS2, or by the activation of the PIDDosome (Fava et al., 2017; Ganem et al., 2014). Our data show that the Hippo pathway is not activated by the depletion of myosin VI. To further complete the picture, we intend to evaluate if the activation of the PIDDosome could possibly be the trigger of the cell cycle arrest, although its involvement is unlikely, considering the data discussed above.

5.4. Myosin VI depletion affects centrosome structure and position

Centrosome cohesion is maintained during interphase by a proteinaceous linker called G1-G2 tether, whose main components are rootletin and Cep68, which compose the fibrous linker, and c-Nap1 that connects the linker to the proximal part of the centrioles (Bahe et al., 2005; Flanagan et al., 2017; Fry et al., 1998; Mayor et al., 2000; Yang et al., 2006b). At the onset of mitosis, Nek2A phosphorylates the linker components, triggering the dissolution of the linker and thus allowing the separation of the centrioles (Agircan et al., 2014; Bahe et al., 2005; Fry et al., 1998; Helps et al., 2000; Mardin et al., 2011). The dissolution of the linker can be caused also by DNA damage (Inanc et al., 2010; Saladino et al., 2009), which also triggers centrosome amplification by un unknown mechanisms (Bourke et al., 2007; Dodson et al., 2004), but the connection between amplification and centriole splitting is still controversial. In fact, the deletion of c-Nap1 causes centriole splitting which is not associated with centriole amplification, and also reduces DNA damage-induced amplification (Flanagan et al., 2017). Myosin VI-depleted cells show both centrosome amplification and centriole splitting, as shown by TEM images, a phenotype

that is not induced by DNA damage. Interestingly, overexpression of Nek2A leads to premature centrosome splitting independently of the cell cycle phase (Flanagan et al., 2017), suggesting that, in myosin VI-depleted cells, the uncoupling between centrosome and cell cycle could be responsible for the premature centriole separation observed.

Furthermore, myosin VI could have an active role in the maintenance of centrosome cohesion. In fact, the actin cytoskeleton is important for centriole disjunction at the onset of mitosis as it provides the forces required to split the centrosomes through GAS2L1, a microtubule- and actin-binding protein (Au et al., 2017; Goriounov et al., 2003; Stroud et al., 2014). Interestingly, overexpression of GAS2L1 triggers premature centrosome separation, with a concomitant increase in actin density around the centrosome (Au et al., 2017). Myosin VI could be required as an actin motor or tether, providing the force to counteract the separation of the centrioles (Fig. 47-1). Interestingly, it has recently been published that myosin VI initiates the assembly of actin cages surrounding damaged mitochondria, forming a barrier that prevents their re-fusion, and promoting their clearance by autophagy (Kruppa and Buss, 2018). These evidences suggest that myosin VI could be required to organize the actin network that surrounds the centrosomes (Fig. 47-2). To verify these hypotheses, we will analyse the actin network surrounding the centrioles in myosin VI-depleted cells. Furthermore, we will deeply characterize the localization of myosin VI at the centrosome through super-resolution microscopy or immuno-gold EM analysis in order to verify its possible localization in the proximity of the linker.

After mitosis, centrioles are disengaged and the G1-G2 tether is established, even if the mechanism required for this latter event has still to be clarified. Another interesting possibility is that myosin VI could be required for the establishment of the linker after

mitosis. Experiments aimed at characterizing the linker proteins in myosin VI-depleted cells are needed to uncover the mechanism behind centriole splitting.

To summarize, our data point to a role of myosin VI in the coordination between the centrosome cycle and the cell cycle, and a possible involvement in the establishment/maintenance of the centriole linker, but the mechanistic details are yet to be defined.

Another interesting possibility to explore is the requirement of the motor abilities of myosin VI to transport proteins inside or outside the actin meshwork that surrounds the centrosome (Fig. 47-3). Depletion of centrosomal proteins, like pericentrin, leads to alterations at the level of centrosome structure and function, resulting in p53 activation and cell cycle arrest (Mikule et al., 2007; Srsen et al., 2006). Given the similar phenotypes obtained upon myosin VI depletion, its localization at the centrosomes and the interaction with centrosomal proteins, we can hypothesize that the absence of myosin VI could have an impact on the localization of important centrosomal proteins, and consequently on the assembly of a functional centrosome.

In addition, myosin VI could be required to tether the centrosome to the actin network, thus maintaining its position (Fig. 47-4). Centrosomes are usually found in the proximity of the nucleus, and some studies suggest the existence of a structural link between the two organelles. This connection could be mediated by the interaction between dynein-dynactin and the nuclear pore complex (Bolhy et al., 2011; Splinter et al., 2010), or by proteins that span the nuclear membrane, such as the LINC complex or the protein emerin (Salpingidou et al., 2007; Zhang et al., 2009). Our results suggest that myosin VI is important for the correct localization of centrosomes at the interface between the nucleus and the plasma membrane. The tethering functions of myosin VI could be required to anchor centrosomal proteins to the nuclear membrane through actin. Indeed,

actin is required to maintain the nucleus-centrosome complex (Hubert et al., 2011; Shay et al., 1974), and centrosomes themselves are able to nucleate actin (Farina et al., 2016), but this kind of association has been poorly characterized. Furthermore, myosin VI could function as a tether to connect the centrosomes to the actin cortex that is found at the plasma membrane. In this picture, the nature of the cargo that connects the centrosome to myosin VI is still unknown, but a valuable candidate for this job would be OFD1, which binds to the myosin VI tail.

Another possibility is that the centrosomal alterations observed upon myosin VI depletion may be secondary due to defects in organelle trafficking. Indeed, myosin VI is involved in the secretion processes and in the maintenance of the Golgi structure (Bond et al., 2011). Furthermore, Golgi proteins are required for ciliogenesis (Follit et al., 2008; Follit et al., 2006) and for centrosome polarization during migration (Bisel et al., 2008). Thus, impaired trafficking from the Golgi complex to centrosomes could affect the PCM in myosin VI-depleted cells, with subsequent centrosomal alterations.

5.5. Myosin VI plays a role in primary cilium formation and satellites maintenance

Our preliminary data suggest a novel function for myosin VI in primary cilium formation. The assembly of the primary cilium occurs during the G1 phase and requires that the mother centriole is converted to a basal body, using the distal appendages to dock to the plasma membrane, from which the cilium emanate (Satir et al., 2010). In hTERT-RPE1 cells, this process starts in the cytoplasm, where a ciliary vesicle is formed before its fusion with the plasma membrane. In this case, the primary cilium remains partially embedded in the cell, forming the ciliary pocket (Benmerah, 2013; Molla-Herman et al., 2010; Sorokin, 1968).

The lower number of assembled primary cilia in cells depleted of myosin VI is even more striking considering that these cells are blocked in the G0/G1 phase of the cell cycle, in which the primary cilium is normally assembled. This impairment in primary cilium formation following myosin VI depletion could be due to a defective docking of the basal body to the ciliary vesicle. Interestingly, the formation of the distal appendages requires the recruitment of OFD1 and C2cd3, and OFD1 deletion affects primary cilium formation (Ye et al., 2014). Given the interaction between myosin VI and OFD1, we could speculate that the two proteins act together in basal body docking and primary cilium assembly. Myosin VI could link OFD1 to the surrounding actin cytoskeleton, thus facilitating the transport of proteins toward the ciliary vesicle (Fig. 47-5).

A fundamental role in primary cilium formation and functions is played by the actin cytoskeleton. Actin is involved in anchoring the basal body to the cells cortex (Boisvieux-Ulrich et al., 1990; Dawe et al., 2009; Hirota et al., 2010; Pan et al., 2007; Panizzi et al., 2007), and in maintaining the correct shape of the ciliary pocket (Rattner et al., 2010). In fact, the ciliary pocket is a docking site for actin cables (Ghossoub et al., 2011; Molla-Herman et al., 2010). Myosin VI-depleted cells show not only a decreased ability of cells to form primary cilia, but also an alteration of the ciliary pocket, which becomes wider and contains vesicles. Interestingly, it has been shown that actin polymerization negatively controls ciliogenesis (Kim et al., 2010), which could be ascribed to alterations in the vesicle trafficking, as a dense actin mesh can act as a physical barrier for transport. In this picture, myosin VI could be required to facilitate the movement of the vesicles through the actin network that surrounds the ciliary pocket (Fig. 47-6).

To better understand this mechanism, we will use markers of the distal appendages to analyze if the loss of primary cilia is due to an incomplete formation of the docking

structures. Furthermore, immune-gold EM analyses will allow us to clarify if myosin VI localizes at the distal appendages and at the ciliary pocket during cilia formation.

Intriguingly, an interplay exists between the primary cilium and centriolar satellites. During ciliogenesis, centriolar satellite distribution is altered (Loffler et al., 2013; Tollenaere et al., 2015; Villumsen et al., 2013). Our preliminary experiments show that myosin VI depletion affects the distribution of centriolar satellites in the cell. This phenotype is reflected in the decrease of the distribution of OFD1 puncta in the cytoplasm, which likely correspond to the satellites. The reduced dispersion of OFD1 in the cytoplasm could contribute to the phenotype observed at the primary cilium in myosin VI-depleted cells. Indeed, the relative abundance of OFD1 in the satellites or the centrosome is important for primary cilium formation, and this relative distribution is controlled by autophagy (Tang et al., 2013).

One of the main functions of the centriolar satellites is to act as storage sites for centrosome proteins, preventing their uncontrolled degradation, thus maintaining centrosome homeostasis (Tollenaere et al., 2015). An alteration of the distribution of the satellites could thus cause of centrosome alterations, due to impaired targeting of fundamental centrosomal proteins. In fact, several studies implicated centriolar satellite densities in the control of centrosome overduplication (Kodani et al., 2015; Loffler et al., 2013; Prosser et al., 2009). These hints are particularly interesting considering the plethora of phenotypes caused by myosin VI depletion. Whether myosin VI acts to ensure a correct trafficking of proteins between satellites and the centrosome is a hypothesis to evaluate (Fig. 47-7). Interestingly, satellites are required to ensure the centrosomal recruitment of proteins like Nek2A, which is important for centriole disjunction and is thus fundamental also in the maintenance of the coupling between the centrosome cycle and the cell cycle (Hames et al., 2005). Satellites also regulate the recruitment of

pericentrin to the centrosome (Dammermann and Merdes, 2002), which is cleaved by separase at the end of mitosis to promote disengagement (Lee and Rhee, 2012; Matsuo et al., 2012).

Although preliminary, our data about OFD1 and satellites distribution in myosin VI-depleted cells fit into the picture of the centrosome and primary cilium alterations. We intend to evaluate the hypotheses described above by studying the mechanistic details of the possible roles that myosin VI plays in centrosome biology (Fig. 47).

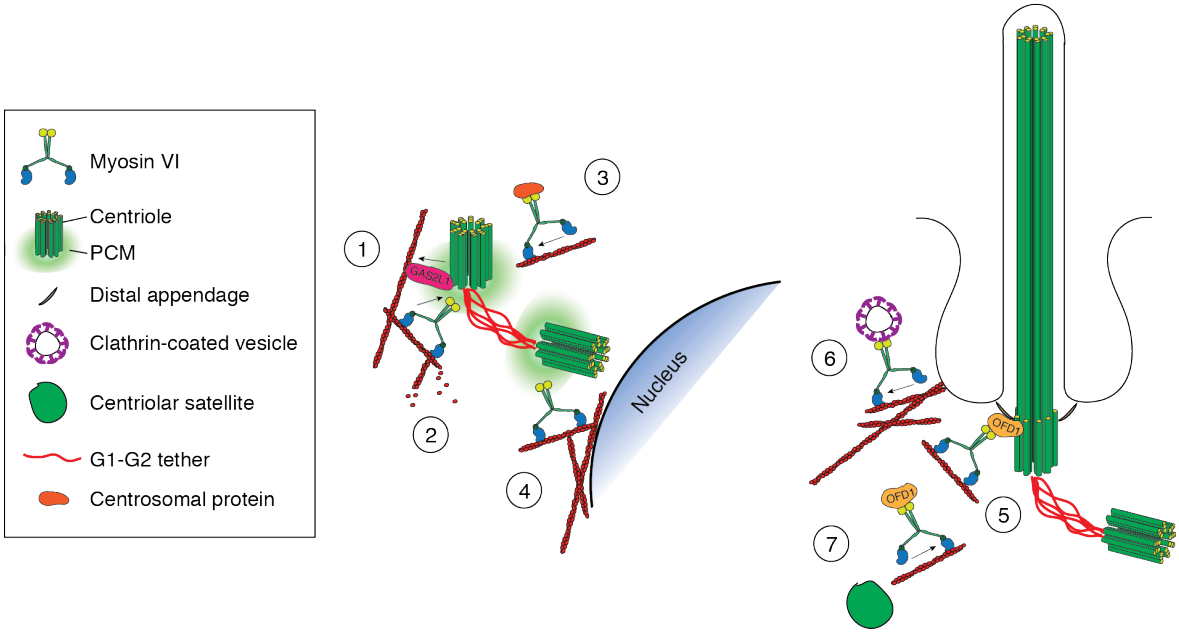

Figure 47: The possible functions of myosin VI in centrosome biology.

The scheme represents the possible roles that myosin VI can play at the centrosome, as described in the text. (1) Myosin VI could be required to counteract centriole separation. (2) Myosin VI could have a role in actin organization around the centrosome. (3) Myosin VI's motor abilities could be required for protein transport in/outside the actin meshwork surrounding the centrioles. (4) Myosin VI could tether the centrosome to the actin network that surrounds the nuclear envelope or to the cell cortex. (5) Myosin VI could connect OFD1 to the actin cytoskeleton. (6) Myosin VI could be important for the transport of vesicles at the ciliary pocket. (7) Myosin VI could be involved in the traffic of proteins between satellites and the centrosome.

5.6. Myosin VI plays a role in cell cycle regulation

A role for myosin VI in cell cycle progression has recently been suggested by few reports showing that the silencing of myosin VI leads to a slight slowdown of the cell cycle in a variety of cancer cell lines, including melanoma, gastric cancer, breast cancer, lung cancer and hepatocellular carcinoma (Li et al., 2015; Ma et al., 2015; Wang et al., 2015a; Wang et al., 2016; You et al., 2016; Yu et al., 2015). These observations were not corroborated by mechanistic insights.

Our results show that myosin VI depletion in non-tumor cells leads to a complete block of the cell cycle, which finally leads to senescence. This is caused by the activation of the p53-p21 axis, which is frequently altered in cancer cells (Leroy et al., 2014), thus explaining the observed difference between cancer and non-cancer cell lines. Indeed, depletion of p53 in hTERT-RPE1 cells can restore the cells' ability to proliferate in the absence of myosin VI, demonstrating that the activation of p53 activation is required for myosin VI KD-induced cell cycle arrest.

The analysis of DNA content by flow cytometry and the usage of hTERT-RPE1 FUCCI cells show that myosin VI-depleted cells arrest in the G0/G1 phase. The arrest in G0 can be caused by several kinds of stress. In particular, we analysed the implication of DDR, which is the best-known inducer of p53 activation. After DDR activation, p53 is phosphorylated on Ser15 and Ser20 by two kinases, CHK1 and CHK2, that act downstream of ATM, ATR and DNA-PK (Appella and Anderson, 2001; Sulli et al., 2012). Our results show that p53 is not phosphorylated on the above-mentioned sites following myosin VI depletion, which is in line with the absence of detectable DNA damage. Furthermore, the inhibition of the DDR kinases is not able to rescue the cell cycle arrest induced by myosin VI depletion. However, it is difficult to conclude that the lack of rescue is due to the specific inhibition of the DDR kinases, since these inhibitors are *per se* toxic for the hTERT-RPE1 cells.

Nevertheless, the other experiments performed are sufficient to exclude the activation of the DDR caused by myosin VI depletion.

As mentioned above, our results also exclude that the centrosome alterations caused by the depletion of myosin VI are the cause of the concomitant cell cycle arrest.

5.7. Potential candidates that mediate the cell cycle arrest induced by myosin VI depletion

The induction of p53-p21 activation can be caused by several stimuli, such as DNA damage, oncogene activation, nutrient deprivation, hypoxia, oxidative stress, ribosomal stress, adhesion loss and centrosome alterations (Horn and Vousden, 2007; Levine et al., 2006). Despite the centrosome alterations observed in myosin VI-depleted cells, we did not find a correlation with the activation of p53. Furthermore, the DDR is not activated upon myosin VI KD, excluding its involvement in p53 activation. In the absence of other obvious candidates, we chose to pursue an unbiased approach to uncover the triggers of the cell cycle arrest induced by myosin VI depletion. The genome-wide CRISPR/Cas9 screening was successfully used by recent studies, uncovering the proteins involved in the so called “mitotic surveillance pathway” (Fong et al., 2016; Lambrus et al., 2016; Meitinger et al., 2016; Nigg and Holland, 2018). This approach could allow us to find the proteins that are involved in the cell cycle arrest caused by myosin VI depletion, acting upstream or downstream the activation of p53. Our data suggested that, during the experiment, the majority of the sgRNAs was lost, possibly due to a selection process that occurred during the amplification of the cell library. It has recently been shown that CRISPR/Cas9-mediated editing of the genome causes the activation of a DDR, due to the single strand breaks generated by the Cas9. The DDR activation then leads to the activation of p53 and to a transient cells cycle arrest until the damage is repaired.

Therefore, cells deleted of p53 or p21 have a growth advantage over cells deleted of other proteins, and are thus positively selected (Haapaniemi et al., 2018).

Unfortunately, due to technical problems, we were not able to collect the cell library shortly after the puromycine selection to control for the homogeneous distribution of the sgRNAs in the population. Nevertheless, the comparison of the distribution of the sgRNAs enrichment between control and treated samples shows that a selection occurred upon doxycycline treatment, since less sgRNAs were identified. Moreover, the distribution of the identified genes in the treated sample is less even, with few genes showing a high level of enrichment among the sgRNA population, which is indicative of a selection process, in which the most enriched sgRNAs are the ones involved in the cell cycle arrest mediated by myosin VI depletion, such as TP53 and CDKN1A.

The other two genes that were identified as enriched in the treated sample, with an FDR below 0.1, are ATF7IP and SETDB1. Interestingly, ATF7IP knock-out cells were identified in the single cell clone analysis, confirming it as a reliable candidate. ATF7IP and SETDB1 encode for two proteins involved in histone methylation. In particular, SETDB1 (also known as ESET) is a methyltransferase responsible for the methylation of lysine 9 of histone H3 (H3K9me), a hallmark of repressed chromatin that is involved in the transcriptional silencing of euchromatic genes and retroelements (Becker et al., 2016; Li et al., 2006; Matsui et al., 2010; Schultz et al., 2002). Strikingly, SETDB1 interacts with ATF7IP (also known as MCAF1) (Fujita et al., 2003; Wang et al., 2003), which protects SETDB1 from proteasomal degradation in the nucleus (Timms et al., 2016). The two proteins are functionally co-dependent: in fact, the knock-out of SETDB1 or ATF7IP leads to an almost identical effect on the distribution of H3K9me3, confirming that the two proteins act in a complex for the deposition of H3K9me3 (Timms et al., 2016). Since the deletion of one of the two proteins leads to destabilization of the other one (Timms et al.,

2016), the functionality of the complex is impaired in an equal manner in the absence of SETDB1 and ATF7IP, further supporting the validity of the results we obtained from the CRISPR/Cas9 screening.

In the near future, we will validate the results obtained from the CRISPR/Cas9 screening by creating individual knock-out cell lines of the candidate genes and assessing their growth in the absence of myosin VI. Being active in the repression of transcription, it is possible that deletion of SETDB1 and ATF7IP impede cell cycle arrest by acting on the expression of genes required for establishing the arrest. Therefore, we will clarify if these genes act upstream or downstream the p53-p21 axis in inducing the cell cycle arrest caused by myosin VI depletion, by assessing whether doxycycline induction caused an increment in the levels of p53 and p21 in the individual knock-out cell lines. Interestingly, it has been shown that SETDB1 can directly methylate p53, leading to an increase in p53 stability (Fei et al., 2015). To assess if this mechanism is involved in the stabilization of p53, we will check its methylation status in the presence or absence of SETDB1.

Given the low number of candidates with FDR below 0.1 found at the end of the CRISPR/Cas9 screening, we decided to extend our analysis and to take into account also genes with FDR near the threshold of 0.1. In fact, during the period of selection with doxycycline, the sgRNAs that provided a modest growth advantage to the myosin VI-depleted cells could have been outcompeted by the faster growth of cells lacking p53, p21, ATF7IP or SETDB1. Only one gene, STAMBPL1, showed an FDR of 0.12, while all the other genes showed an FDR above 0.35. We validated this candidate gene through silencing using a siRNA that was already used in our laboratory. Our results show that the depletion of AMSH-LP, the protein coded by STAMBPL1, is able to partially rescue the cell cycle arrest induced by myosin VI depletion. The partial rescue obtained is possibly due to the low efficiency of the siRNA used for AMSH-LP depletion, as shown by the qPCR

analysis. Nevertheless, the levels of p53 and p21 are decreased in cells depleted of myosin VI and AMSH-LP compared to the cells depleted only of myosin VI, suggesting that AMSH-LP acts to induce p53 activation after myosin VI KD. To overcome the problem of partial depletion of the candidate protein, these results will be further validated by deleting AMSH-LP through CRISPR/Cas9 and assessing the growth and p53 status of the cells in the absence of myosin VI.

AMSH-LP is a poorly studied deubiquitinase protein that specifically cleaves K63-linked polyubiquitin chains (Sato et al., 2008). It has been shown that AMSH-LP can interact with clathrin and that this interaction targets this protein to the early endosomes (Nakamura et al., 2006). Furthermore, localization of AMSH-LP in the nucleus has been detected (Nakamura et al., 2006), even if its possible function is unknown.

The interplay between myosin VI and AMSH-LP will be the object of the next studies. Interestingly, myosin VI_{short} interacts with K63-linked ubiquitin through its MyUb domain, providing a possible connection with AMSH-LP. One possibility is that the binding of myosin VI could protect K63-linked polyubiquitin chains from cleavage by AMSH-LP, by masking the chains or by transporting the ubiquitinated protein to a different compartment.

Collectively, our data uncover new physiological roles for myosin VI in non-tumor cells. The control of cell cycle progression and maintenance of centrosome structure are fundamental steps to avoid the onset of tumors, by assuring proper chromosome segregation and cell division. The role of myosin VI in carcinogenesis has already been studied, in particular regarding tumor cell migration and invasion. It will be interesting to understand if these new functions of myosin VI could contribute to its role in tumor onset and/or progression.

6. Appendix: functional insights into myosin VI isoforms

6.1. Background

Myosin VI has been implicated in several cellular functions. The diversity of the roles of myosin VI derives from interactions with multiple cargo adaptors, which mediate the targeting of myosin VI to different cellular locations. Moreover, the cargoes that bind myosin VI play a role in the switch between the motor or anchor properties of the protein, further regulating its properties.

An interesting level of regulation of the activity of myosin VI is given by the alternative splicing of the region called long insert, which generates myosin VI_{long} and myosin VI_{short} isoforms (Wollscheid et al., 2016). Notably, the inclusion or the skipping of the large insert causes different structural conformations of myosin VI that in turn determines mutually exclusive interactomes of the two isoforms (Wollscheid et al., 2016). As a consequence, the two isoforms are involved in different biological functions, such as endocytosis (long) and cell migration (short). This finding is relevant to cancer where myosin VI alternative splicing is deregulated and exon skipping dictates addiction to myosin VI_{short} for tumour cell migration. Interestingly, a switch from the short to the long isoform expression occurs once the cell reach confluency (Buss et al., 2001). We recently extended this observation showing that epithelial cells expressing both isoforms can switch on/off their expression according to the culture conditions: in sparse condition they express mainly the short isoform, while the long isoform is expressed when a polarized status is reached (unpublished data of the lab). In addition, the disaggregation of polarized cells that express myosin VI_{long} leads to the opposite effect, with a gradual switch to the short isoform (unpublished data of the lab).

6.2. Myosin VI long and short isoforms identification through specific antibodies

The published data about myosin VI interactome were obtained with a mass spectrometry approach using GST-tagged fragments of myosin VI spanning amino acids 998–1131 in pulldown assays with HEK293T cellular lysates (Wollscheid et al., 2016). We were then interested in studying the interactomes of the different isoforms in an endogenous setting.

To this end, we developed two antibodies that specifically recognize the long or short isoforms of myosin VI. Specific peptides were produced for rabbits' immunization (Appendix Fig. 1A), and the resulting sera were affinity purified using the same peptides. To check for the specificity of the affinity purified antibodies, we took advantage of two

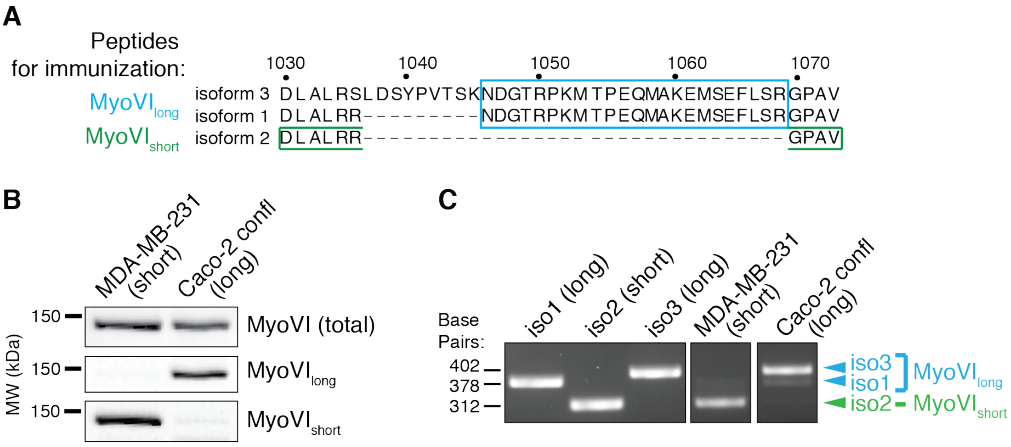

Appendix Figure 1: Generation of antibodies specific for myosin VI short or long isoforms.

(A) The scheme shows the sequences of the peptides used for rabbits' immunization, specific for the long or short isoforms of myosin VI (boxed in pale blue and green, respectively). (B) Affinity purified antibodies were used for WB against whole cell lysates of cell lines expressing selectively myosin VI_{short} (MDA-MB-231) or myosin VI_{long} (Caco-2 confluent). Both the antibodies are able to specifically recognize the respective myosin VI isoform. An antibody anti total myosin VI was used as control for myosin VI expression. (C) RT-PCR from cDNA prepared from the cell lines used for antibodies validation, using primers flanking the long insert to distinguish the myosin VI isoforms. PCR controls are from plasmids carrying different isoforms of myosin VI.

cell lines that express selectively myosin VI short or long isoforms: MDA-MB-231 cells, that express only the short, and Caco-2 cells grown in confluent condition for 5 days, that

express only the long (Appendix Fig. 1C). The western blot using the two affinity purified antibodies against these cell lysates show that they specifically recognize the respective myosin VI isoform (Appendix Fig. 1B).

Since different tumor cell lines express different myosin VI isoforms, and this has an impact on the function of the protein (Wollscheid et al., 2016), we wanted to have a wider view of the isoform expressed by the tumor cells. So, we used the isoform specific antibodies to check myosin VI expression in the cell lines belonging to the NCI-60 Human Tumor Cell Lines, which represent nine cancer types. As shown in Appendix Fig. 2, the majority of the cell lines express mainly the short isoform, while only few express the long isoforms. This confirms that myosin VI_{long} is expressed mainly in cells that maintain their epithelial polarization.

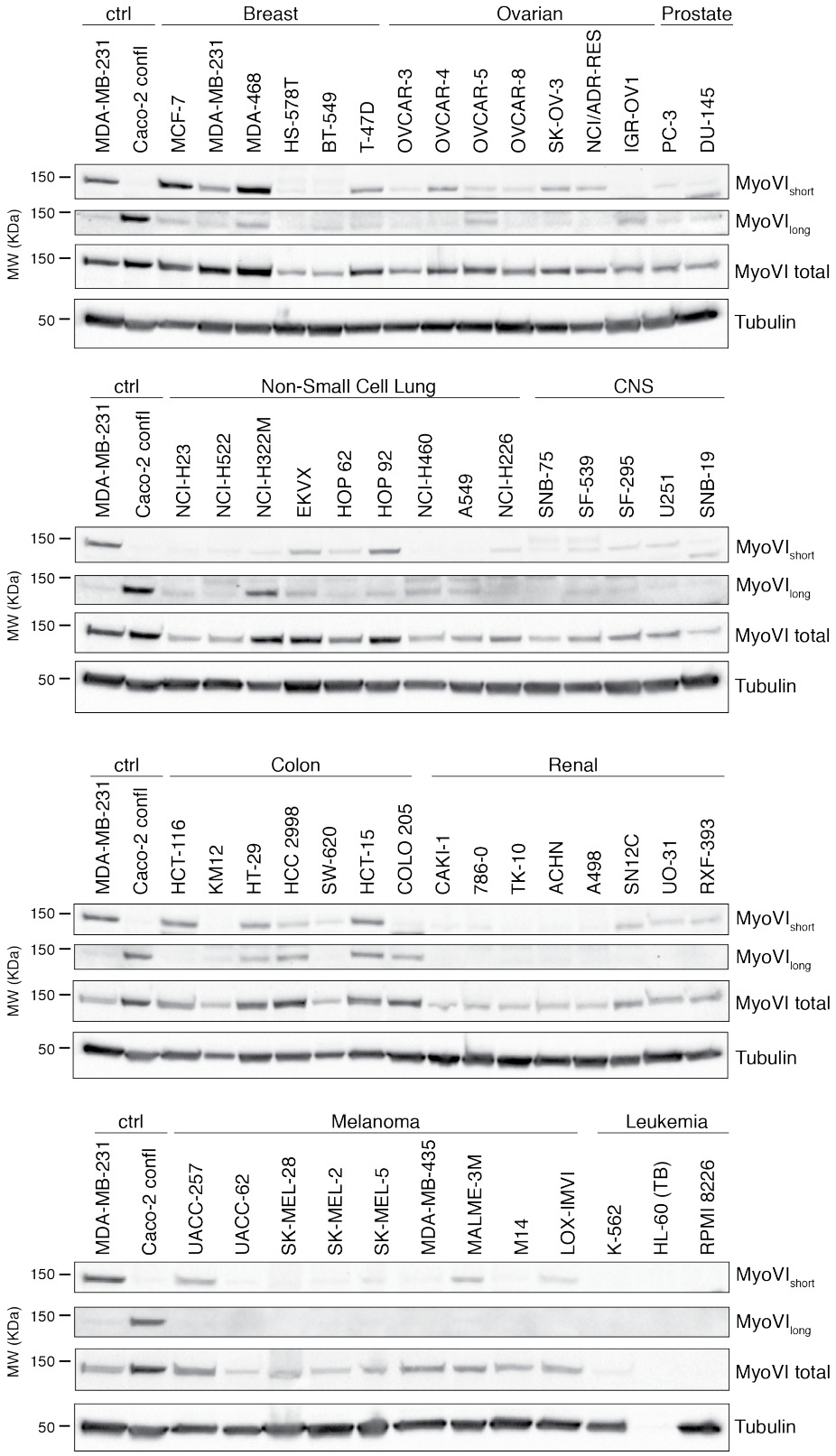

Appendix Figure 2: Myosin VI expression in NCI-60 cancer cell lines.

NCI-60 cell lines pellets were collected from Cell Culture Facility. Total cell lysates were analysed by WB with myosin VI isoform-specific antibodies as well as anti-total myosin VI antibody as control for myosin VI expression. MDA-MB-231 and Caco-2 confluent cells were used as control for specific isoforms expression.

6.3. Ovarian cancers express selectively myosin VI_{short}

The overexpression of myosin VI was reported in ovarian and prostate cancers, in which it was linked to bad prognosis (Dunn et al., 2006; Yoshida et al., 2004). Our lab recently demonstrated that the majority of the tumors preferentially express myosin VI_{short} (Wollscheid et al., 2016). In particular, we analysed the myosin VI isoform expression in high-grade primary ovarian cancer cells cultured *in vitro* for two passages. This analysis showed that ovarian tumors almost exclusively express myosin VI_{short}, compared to normal tissue derived from ovarian surface epithelium (OSE), which express different myosin VI isoforms (Appendix Fig. 3A). We recently confirmed these data by immunohistochemistry analysis. We compared the expression of myosin VI isoforms, using the specific antibodies we generated, in ovarian tumors and normal ovarian epithelium (OSE). Indeed, while the normal sample shows mainly the expression of myosin VI_{long} in the surface epithelium, tumor samples show high expression of myosin VI_{short}, and no expression of myosin VI_{long} (Appendix Fig. 3B). These results validated the concept of a positive selection for myosin VI_{short} during tumor progression, possibly connected to epithelial to mesenchymal transition (EMT).

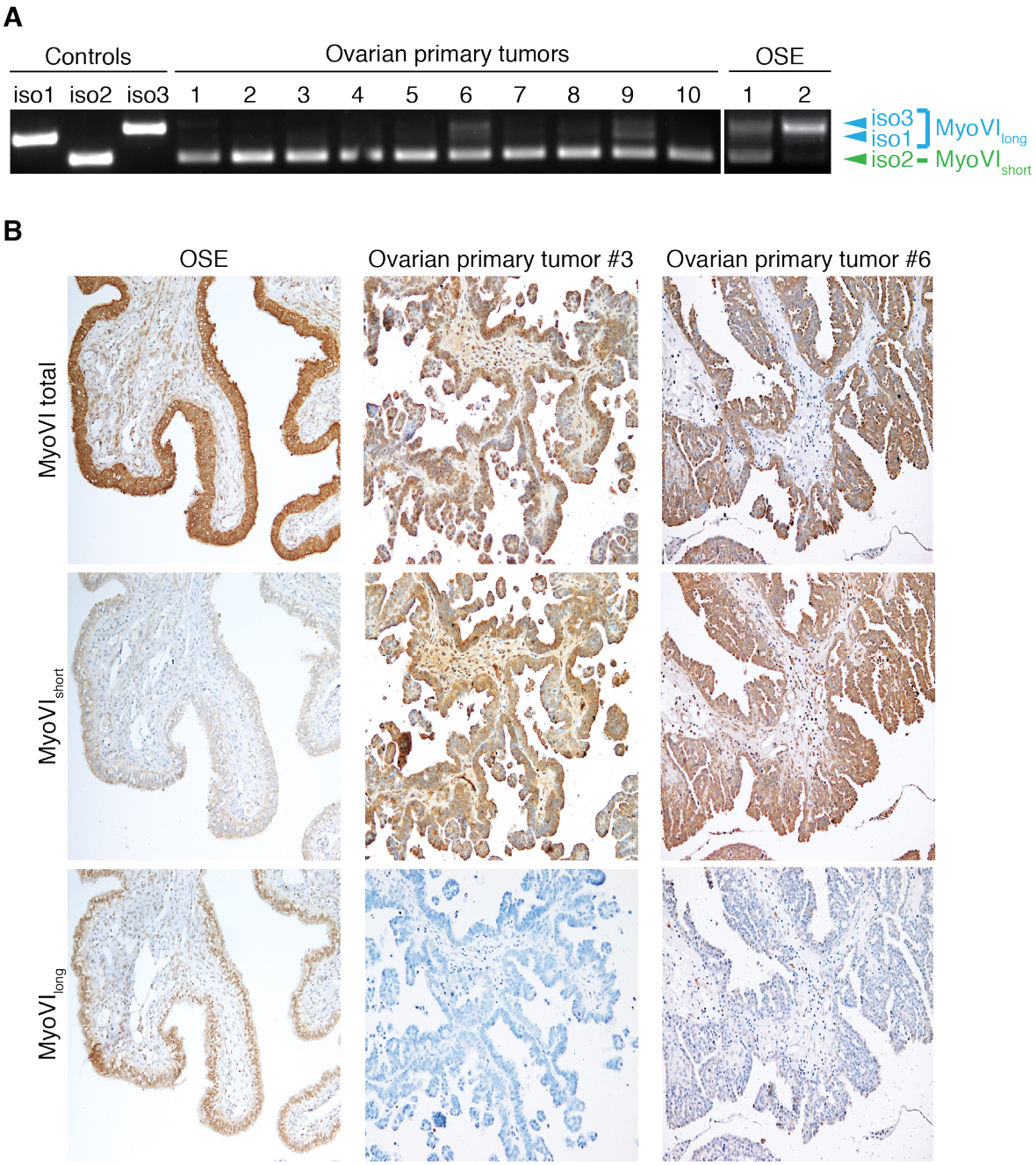

Appendix Figure 3: Myosin VI short is overexpressed in ovarian cancers.

(A) RT-PCR from cDNA prepared from the indicated primary cells. PCR controls are from plasmids carrying myosin VI of the different isoforms. Cells from normal tissue (OSE-Ovarian Surface Epithelium), were used as control to compare myosin VI isoform expression in cancer and normal tissues. These results are included in *Wollscheid et al., Nature Structural and Molecular Biology, 2016*. (B) Ovarian primary tumors and normal tissue (OSE, as control) were embedded in paraffin and sections were cut for IHC analysis. The sections were stained with antibodies specific for myosin VI total (1296), myosin VI_{short} or myosin VI_{long} to compare their expression in the tumor and normal tissues.

6.4. Characterization of myosin VI interactors in different cell lines

With the isoform-specific antibodies we generated, we sought to compare the interactomes of the two isoforms in an endogenous setting. We first characterized the ability of these antibodies to IP myosin VI in cells expressing selectively short (MDA-MB-231) or long (Caco-2 confluent) myosin VI. An antibody anti-total myosin VI was used as control. As shown in Appendix Fig. 4, the anti-myosin VI_{short} antibody did not work for IP in MDA-MB-231 cells. On the contrary, the anti-myosin VI_{long} antibody was able to IP myosin VI selectively in Caco-2 confluent cells (Appendix Fig. 4). The specificity of the immunoprecipitated isoform was confirmed by immunoblot against myosin VI_{long}. Since anti-myosin VI_{short} antibody was not working for IP, it was not possible to compare the interactomes of the myosin VI isoforms in the same cell line expressing both isoforms.

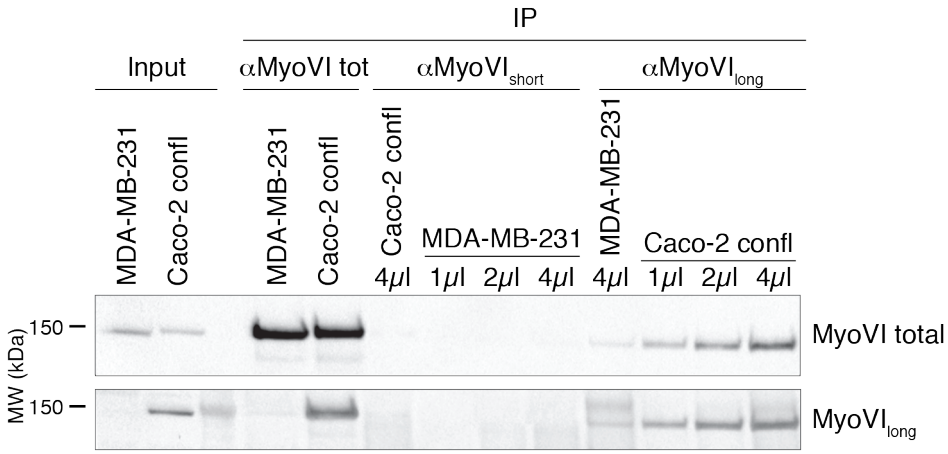

Appendix Figure 4: IP test of isoform-specific anti-myosin VI antibodies.

Affinity purified antibodies were tested for immunoprecipitation (IP) against 300µg of total cell lysates from cell lines expressing selectively myosin VI_{short} (MDA-MB-231) or myosin VI_{long} (Cac o-2 confluent). Different amounts of antibodies were tested as indicated. Antibody anti-myosin VI total was used as control for IP. The IP was then assessed through WB using anti-total myosin VI and myosin VI_{long} antibodies.

To bypass this problem, we decided to take advantage of cell lines that express different myosin VI isoforms, and to use for IP the anti-myosin VI total antibody. In order to obtain a comprehensive view of the myosin VI interactome, the experiments were performed using different cell lines: HeLa cells, which express mainly myosin VI_{long}; MDA-MB-231

cells, which express myosin VI_{short}; MCF10A cells in sparse cell growth conditions, which express the short isoform, or MCF10A in confluent cell growth conditions in which the expression of myosin VI_{long} is increased (Appendix Fig. 5). To identify the specific interactors, we analyzed the anti-myosin VI IP through MS, comparing it to an IP performed with a control antibody.

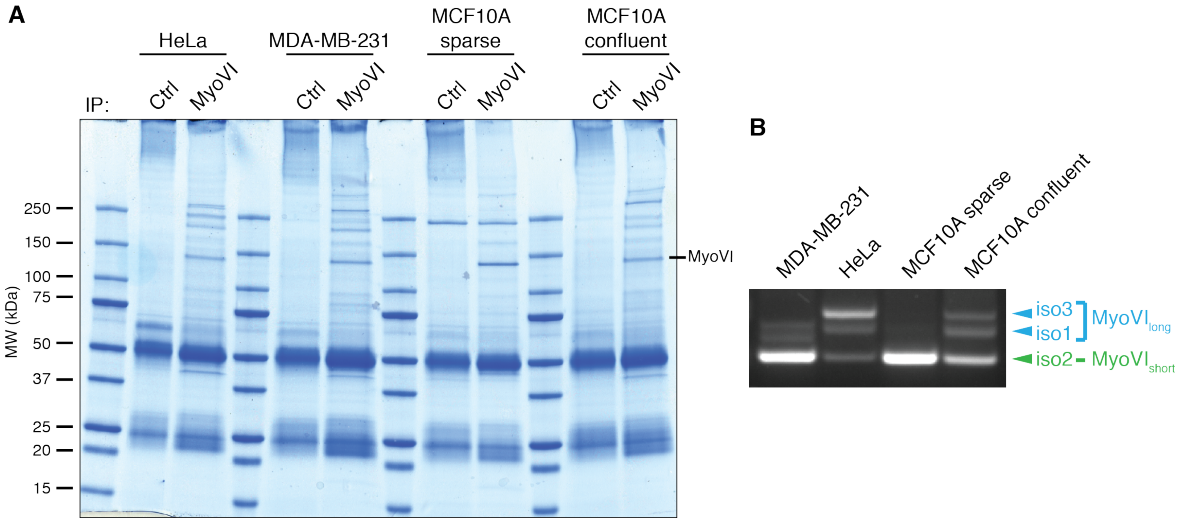

Appendix Figure 5: IP performed for MS analysis of myosin VI interactors.

(A) Colloidal blue-stained SDS-PAGE of the IP performed with anti-myosin VI affinity purified antibody (1295) or a control antibody against total cell lysates from HeLa, MDA-MB-231 cells, and MCF10A cells in sparse growth conditions or after 5 days of confluency. For mass spectrometry identification, the entire lanes were cut in different pieces, digested and loaded on the analyzer. The presence of the bait (MyoVI) in the sample IP with anti-myosin VI antibodies is indicated. (B) RT-PCR from cDNA prepared from the cell lines used for the IP-MS analysis, using primers flanking the long insert to distinguish the myosin VI isoforms.

We identified 48, 51, 41 and 39 interactors, respectively, in HeLa, MDA-MB-231, MCF10A in sparse or confluent condition, considering as positive hits the proteins that were identified with at least three peptides, and that showed three times more identified peptides in the anti-myosin VI IP compared to the control IP. Appendix Table 1 lists the top hit candidates. Interestingly, the list shows the presence of proteins belonging to the desmosomes (desmoplakin, plectin, periplakin, envoplakin) and to the centrosome (pericentrin, OFD1, NUMA1), as well as nuclear proteins (SFPQ, PRKDC, MCM4, MCM6, NUP205). For these groups of proteins, there is no clear enrichment in some cell lines

compared to the others, suggesting that they do not show isoform specificity for myosin VI interaction.

	HeLa		MDA-MB-231		MCF10A sparse		MCF10A confluent	
Gene	**Ctrl**	**MyoVI**	**Ctrl**	**MyoVI**	**Ctrl**	**MyoVI**	**Ctrl**	**MyoVI**
DSP	48	184	22	201	2	36	21	205
NUMA1	4	155	0	141	0	84	4	124
PLEC	0	69	0	218	21	110	21	134
PPL	0	102	4	142	0	0	3	104
PRKDC	0	35	0	93	2	2	3	30
MYH9	2	30	2	74	142	142	11	66
GIGYF2	0	34	0	39	0	44	0	33
SLC12A4	0	32	0	26	0	23	0	26
SPTBN2	6	75	0	25	0	0	0	10
SPTAN1	2	75	0	24	0	0	0	3
PCNT	0	31	0	16	0	44	0	5
GCC2	0	14	0	22	0	19	0	19
OFD1	0	20	0	6	0	20	0	27
MAP4K4	0	6	0	29	0	17	0	21
SFPQ	0	18	0	16	0	17	5	21
DTX3L	0	15	0	15	0	7	0	24
EIF3A	0	6	0	25	0	15	0	8
KIAA1468	0	9	0	12	0	26	0	1
PARP9	0	13	0	8	0	7	0	18
NUDC	0	6	0	14	0	12	0	14
NUP155	0	20	0	7	0	10	0	5
ENAH	0	7	0	7	0	6	0	11
MYH10	0	14	0	15	85	78	0	3
RAB11FIP1	0	6	0	16	0	0	0	3
MCM4	0	15	0	0	0	4	0	3
NUP205	0	7	0	5	0	0	0	2
MCM6	0	7	0	0	0	4	0	2

Appendix Table 1: List of the interactors of myosin VI identified in the IP-MS analysis as myosin VI interactors in the different cell lines tested.

The number of peptides identified per each protein is shown per each IP condition. Among all the proteins identified in the experiment, the list shows the proteins that were identified with the highest number of peptides.

To complete the analysis, we performed further IP-MS experiments in Caco-2 cells in sparse and confluent growth conditions. Caco-2 cancer epithelial cells polarize upon confluency, with the formation of microvilli in the apical side of the cells, and show a complete switch from expressing all the myosin VI isoforms to selective myosin VI_{long} expression during this process (Appendix Fig. 6B). Total myosin VI was immunoprecipitated using two antibodies raised against total myosin VI, namely 1295 and 1296 (Appendix Fig. 6A), and an anti-GST rabbit antibody was used as a control. The IP was loaded on SDS-PAGE, stained with colloidal blue and processed for the identification of the interactors through MS (Appendix Fig. 6A). The MS analysis performed in Caco-2 sparse or confluent cells identified, respectively, 44 and 75 interactors, considering as positive hits the proteins that were identified with at least three unique peptides, and that showed three times more identified peptides in the anti-

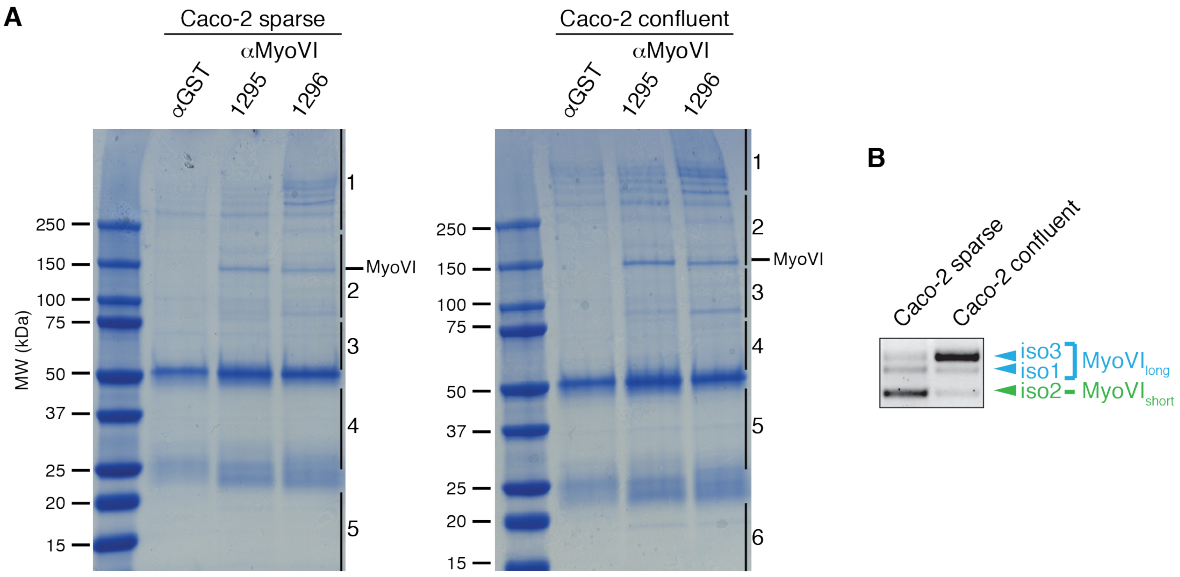

Appendix Figure 6: IP performed for MS analysis of myosin VI interactors in Caco-2 cells

(A) Colloidal blue-stained SDS-PAGE of the IP performed with two anti-myosin VI affinity purified antibodies (1295 and 1296) or a control antibody (anti-GST rabbit polyclonal) against total cell lysates from Caco-2 cells, in sparse growth conditions or after 8 days of confluency to induce polarization. For mass spectrometry identification, the entire lanes were cut in different pieces as indicated, digested and loaded on the analyzer. The presence of the bait (MyoVI) in the sample IP with anti-myosin VI antibodies is indicated. (B) RT-PCR from cDNA prepared from the cell lines used for the IP-MS analysis, using primers flanking the long insert to distinguish the myosin VI isoforms.

myosin VI IP compared to the control IP. Appendix Table 2 lists the myosin VI interactors that were found with the highest number of peptides compared to the control antibody in at least one cell line. The list contains some previously published interactors, clathrin, DOCK7, TOM1 and ubiquitin. Interestingly, this analysis confirms the presence of proteins belonging to the centrosome or centrosome-related functions (OFD1, NUMA1, dynein heavy chain, dynein light chain 1). Also in this case, the presence of these interactors in both Caco-2 sparse or confluent suggests no isoform specificity of the interaction.

	Caco-2 sparse			Caco-2 confluent		
Gene name	**Ctrl**	**αMyoVI 1295**	**αMyoVI 1296**	**Ctrl**	**αMyoVI 1295**	**αMyoVI 1296**
DYNC1H1	0	2	91	0	0	67
DTX3L	0	25	39	0	29	37
PARP9	0	15	20	0	27	26
CLTC	4	24	19	5	26	21
DOCK7	0	1	15	0	2	33
SFPQ	2	7	6	1	17	15
NONO	1	11	12	3	9	11
DNM1L	0	0	14	0	0	18
DBNL	0	19	0	0	10	0
SLC12A4	0	17	0	0	12	0
DOCK6	0	0	4	0	0	23
UBB	1	8	7	1	7	6
SEC31A	0	6	5	0	10	5
TTK	0	4	14	0	1	7
GART	0	0	9	0	0	16
TOM1L2	0	7	5	0	6	6
NUMA1	0	8	0	0	15	0
ENAH	0	12	1	0	9	0
OFD1	0	10	0	0	11	0
CCDC6	0	0	10	0	0	9
RAB11FIP1	0	10	3	0	4	1
TOLLIP	0	4	2	0	6	6
STRN3	0	0	6	0	1	11
ELMSAN1	0	0	0	0	0	17
OTUD4	0	0	9	0	0	8
DYNC1LI1	0	0	10	0	0	6
VARS2	0	0	2	0	0	14
TCERG1	0	0	4	0	1	11
GIGYF2	0	11	0	0	4	0
NEK1	0	2	1	0	4	7
TOM1	0	3	2	0	4	4
TBC1D2B	0	0	0	0	11	2
DSP	1	4	0	1	9	1
EZR	0	0	0	2	0	14

Appendix Table 2: List of the interactors of myosin VI in Caco-2 cells grown in different conditions.

The number of peptides identified per each protein is shown per each IP condition. Among all the proteins identified in the experiment, the list shows the proteins that were identified with the highest number of peptides. In grey are reported the proteins that were identified as highest ranked in the previous IP-MS experiment.

6.5. Conclusions

The presented data show that ovarian tumors selectively overexpress myosin VI_{short}, while silencing the expression of the long isoform. During cancer progression, a fundamental step is EMT, that allows epithelial cells to be converted to migratory and invasive cells. EMT occurs through transcriptional reprogramming, and alternative splicing provides an additional layer of regulation (De Craene and Berx, 2013). Our data suggest that myosin VI_{short} overexpression could provide a migratory advantage to cancer cells. This isoform switch could thus be part of the reprogramming of tumor cells during EMT, contributing to cancer invasiveness and metastasis.

Our experiment aimed at evaluating the interactomes of myosin VI in an endogenous setting failed to uncover strong differences between the different cell lines. Nevertheless, this approach revealed a new set of interactors that belong to the centrosome compartment, whose characterization is the subject of the presented thesis.

6.6. Appendix methods

6.6.1. Cell lines

Caco-2 cells (DSMZ) were maintained in Minimum Essential Medium (MEM, Gibco), supplemented with 20% FBS, 0.1 mM non-essential amino acids, 2 mM L-glutamine and 1 mM Na-Pyruvate.

HeLa cells (ATCC) were maintained in MEM, supplemented with 10% FBS, 0.1 mM non-essential amino acids, 2 mM L-glutamine and 1 mM Na-Pyruvate.

MCF10A cells (ATCC) were cultured in DMEM/F12 (Gibco), supplemented with 5% horse serum, hydrocortisone (0.5 µg/ml), insulin (10 µg/ml), cholera toxin (50 ng/ml) and EGF (20 ng/ml).

MDA-MB-231 cells (NCI-60) were maintained in RPMI-1640 (Lonza) containing 10% FBS and 2 mM L-glutamine.

All cell lines were authenticated at each batch freezing by STR profiling (StemElite ID System, Promega). All cell lines were tested for mycoplasma at each batch freezing with both PCR and a biochemical test (MycoAlert, Lonza).

6.6.2. Myosin VI isoforms detection by PCR

The expression of myosin VI isoforms in various cell lines was assessed by PCR. Messenger RNA was isolated from cells grown on plastic dishes using TRIzol reagent (Invitrogen) and RNeasy Mini Kit (Qiagen) according to the manufacturer's protocols. Genomic DNA and RNA retro-transcription was performed with QuantiTect Reverse Transcription Kit (Qiagen). The obtained cDNA was used in PCR reactions with primers flanking the spliced region:

For: 5′-CCGAGCTCATCAGTGATGAGGC-3′

Rev: 5′-CCAAGCATGATACACTTTTAGTCTCC-3′

6.6.3. Isolation, culture and processing of primary epithelial ovarian cancer cells

Patient-derived tissue samples were collected with the approval of the Ethical Committee of the European Institute of Oncology. Fresh biopsies of ovarian cancer were obtained from patients with high-grade epithelial ovarian serous carcinoma who underwent surgical tumour debulking. Fresh biopsies of normal ovaries were obtained upon informed consent from patients undergoing adnexectomy for non- ovarian gynaecological pathologies.

All tumours were digested in DMEM/F12 medium (Gibco) containing 2 mM glutamine, 1% Penicillin/Streptomycin, 200 U/ml collagenase IA and 100 U/ml hyaluronidase. Normal ovaries were digested in 5U/ml Dispase for 30 minutes at 37°C and then the organ surfaces were scraped to isolate the epithelial cells. The derived primary epithelial cells were maintained in monolayer adherent cultures in collagen I Cellware coated flask (Corning) in DMEM/F12 medium (Gibco) containing 1% FBS, 2 mM glutamine, 1% Penicillin/Streptomycin, 0.2% gentamicin, 0.2% amphotericin, 10 mg/ml transferrin, 1 mg/ml insulin, 1 mg/ml hydrocortisone, 10 mM HEPES pH 7.5, 50 mM ascorbic acid, 15 nM sodium selenite, 50 ng/ml cholera toxin, 10 nM EGF, 35 mg/ml bovine pituary extract, 10 nM T3, 10 nM β-estradiol. For RNA extraction, $5x10^6$ primary cells were washed in PBS and the cell pellets were snap frozen in dry ice.

6.6.4. Immunohistochemistry (IHC)

The human samples described above were fixed in 4% paraformaldehyde and embedded in paraffin by Leica automatic processator. Then, 4 µm-thick serial sections were dissected using microtome. For IHC analysis on paraffin sections, paraffin was removed with xylene and the sections were rehydrated in graded alcohol. Antigen retrieval was

carried out with preheated target retrieval solution (Sodium Citrate Buffer: 10mM Sodium Citrate, 0.05% Tween 20, pH 6.0) for 45 minutes. Tissue sections were stained with H_2O_2 (DAB Substrate Kit peroxidase, Vector Lab) for quenching of endogenous peroxidases, blocked with FBS serum in PBS for 60 min and incubated overnight with primary antibodies (anti-Myosin VI 1296 1:500, anti-Myosin VI_{long} 1:400, anti-Myosin VI_{short} 1:200). The antibody binding was detected using a polymer detection kit (GAR-HRP, Microtech) followed by a diaminobenzidine chromogen reaction (Peroxidase substrate kit, DAB, SK-4100; Vector Lab). All sections were counterstained with Mayer's hematoxylin and visualized using a bright-field microscope.

6.6.5. Antibodies generation

For the production of the anti-myosin VI_{long} specific antibody, a synthetic peptide corresponding to the α2-linker, present only in the isoforms 1 and 3 of myosin VI (Fig. 1A) was produced by Mimotopes. The lyophilized peptide was resuspended in PBS and sent to Eurogentech S.A. for the immunization of two rabbits.

For the production of the anti-myosin VI_{short} specific antibody, a synthetic peptide corresponding to aminoacids 1030-1073, missing the aminoacids 1036-1069 that are not present in the isoform 2 of myosin VI (Appendix Fig. 1A) was produced by Genecust. The peptide was used by Genecust for the immunization of two rabbits.

Rabbits bleedings were tested by WB for the recognition of myosin VI_{long} or myosin VI_{short} in Caco-2 confluent or MDA-MB-231 lysates, respectively. Rabbits sera were affinity purified by Cogentech with the same peptides used for immunization. The affinity purified antibodies were validated for the use in WB and IP.

6.6.6. Immunoprecipitation (IP)

For the validation of anti-myosin VI_{long} and anti-myosin VI_{short} antibodies, MDA-MB-231 and Caco-2 confluent cells were lysed in JS buffer and incubated for 20' on ice. Lysates were cleared by centrifugation at 16 000 g for 20 min at 4°C. Anti-myosin VI_{long} and anti-myosin VI_{short} IP was performed incubating 1 mg of lysates with 1, 2 or 4 µl of antibody for 2h at 4°C. Then, protein A sepharose beads were added to the IP and incubated for an additional hour. Precipitated immunocomplexes were washed, loaded on a precast gradient gel (4–20% TGX precast gel, Bio-Rad) and analyzed by WB.

6.6.7. IP-Mass spectrometry (MS)

To identify myosin VI interactors, anti-myosin VI IP was performed in HeLa, MDA-MB-231, MCF10A grown in sparse or confluent conditions and Caco-2 grown in sparse or confluent conditions. 3 mg of lysates were incubated with anti-myosin VI antibodies (1295 or 1296) or a rabbit control antibody as negative control. After 2 hours of incubation at 4°C, protein A sepharose beads were added to the IP and the mixture was incubated for an additional hour. Precipitated immunocomplexes were washed, loaded on a precast gradient gel (4–20% TGX precast gel, Bio-Rad) and stained with colloidal blue (Colloidal Blue Staining Kit, Invitrogen).

6.6.7.1. Liquid chromatography–tandem MS (LC–MS/MS) analysis

Slices of interest were cut from gels and trypsinized as previously described by Shevchenko and colleagues (Shevchenko et al., 1996). Peptides were desalted as described by Rappsilber and colleagues (Rappsilber et al., 2003), dried in a Speed-Vac and resuspended in 10 µL of solvent A (2% ACN, 0.1% formic acid). 3 µL were injected on a quadrupole Orbitrap Q-Exactive mass spectrometer (Thermo Scientific) coupled with an

UHPLC Easy-nLC 1000 (Thermo Scientific), with a 25 cm fused-silica emitter of 75 µm inner diameter. Columns were packed in-house with ReproSil-Pur C18-AQ beads (Dr. Maisch Gmbh, Ammerbuch, Germany), 1.9 µm of diameter, using a high-pressure bomb loader (Proxeon, Odense, Denmark). Peptide separation was achieved with a linear gradient from 95% solvent A (2% ACN, 0.1% formic acid) to 40% solvent B (80% acetonitrile, 0.1% formic acid) over 30 minutes and from 40% to 100% solvent B in 2 minutes at a constant flow rate of 0.25 µL/minute, with a single run time of 33 minutes. MS data were acquired using a data-dependent top 12 method, and the survey full scan MS spectra (300–1750 Th) were acquired in the Orbitrap with 70000 resolution, AGC target 1e6, IT 120 ms. For HCD spectra, the resolution was set to 35000, AGC target 1e5, IT 120 ms; normalized collision energy 25% and isolation width of 3.0 m/z

6.6.7.2. Protein identification

For protein identification, the raw data were processed using Proteome Discoverer (version 1.4.0.288, Thermo Fischer Scientific). MS2 spectra were searched with Mascot engine against uniprot_human_20150401 database (90411 entries), with the following parameters: enzyme Trypsin, maximum missed cleavage 2, fixed modification carbamidomethylation (C), variable modification oxidation (M) and protein N-terminal acetylation, peptide tolerance 10 ppm, MS/MS tolerance 20 mmu. Peptide Spectral Matches (PSM) were filtered using percolator based on q-values at a 0.01 FDR (high confidence). Proteins were considered identified with 2 unique high confident peptides (Kall et al., 2007). Scaffold (version Scaffold_4.3.4, Proteome Software Inc., Portland, OR) was used to validate MS/MS based peptide and protein identifications. Peptide identifications were accepted if they could be established at a probability greater than 95.0% by the Peptide Prophet algorithm (Keller et al., 2002) with Scaffold delta-mass

correction. Protein identifications were accepted if they could be established at a probability greater than 99.0% and contained at least 2 identified peptides. Protein probabilities were assigned by the Protein Prophet algorithm (Nesvizhskii et al., 2003). Proteins that contained similar peptides and that could not be differentiated based on MS/MS analysis alone were grouped to satisfy the principles of parsimony. Proteins sharing significant peptide evidence were grouped into clusters.

7. References

Acconcia, F., Sigismund, S., and Polo, S. (2009). Ubiquitin in trafficking: the network at work. Exp Cell Res *315*, 1610-1618.

Acharya, B.R., Nestor-Bergmann, A., Liang, X., Gupta, S., Duszyc, K., Gauquelin, E., Gomez, G.A., Budnar, S., Marcq, P., Jensen, O.E.*, et al.* (2018). A Mechanosensitive RhoA Pathway that Protects Epithelia against Acute Tensile Stress. Developmental cell.

Acosta, J.C., Banito, A., Wuestefeld, T., Georgilis, A., Janich, P., Morton, J.P., Athineos, D., Kang, T.W., Lasitschka, F., Andrulis, M.*, et al.* (2013). A complex secretory program orchestrated by the inflammasome controls paracrine senescence. Nature cell biology *15*, 978-990.

Acosta, J.C., O'Loghlen, A., Banito, A., Guijarro, M.V., Augert, A., Raguz, S., Fumagalli, M., Da Costa, M., Brown, C., Popov, N.*, et al.* (2008). Chemokine signaling via the CXCR2 receptor reinforces senescence. Cell *133*, 1006-1018.

Agircan, F.G., Schiebel, E., and Mardin, B.R. (2014). Separate to operate: control of centrosome positioning and separation. Philos Trans R Soc Lond B Biol Sci *369*.

Al-Haddad, A., Shonn, M.A., Redlich, B., Blocker, A., Burkhardt, J.K., Yu, H., Hammer, J.A., 3rd, Weiss, D.G., Steffen, W., Griffiths, G.*, et al.* (2001). Myosin Va bound to phagosomes binds to F-actin and delays microtubule-dependent motility. Mol Biol Cell *12*, 2742-2755.

Altman, D., Sweeney, H.L., and Spudich, J.A. (2004). The Mechanism of Myosin VI Translocation and Its Load-Induced Anchoring. Cell *116*, 737–749.

Alves-Cruzeiro, J.M., Nogales-Cadenas, R., and Pascual-Montano, A.D. (2014). CentrosomeDB: a new generation of the centrosomal proteins database for Human and Drosophila melanogaster. Nucleic Acids Res *42*, D430-436.

Ameen, N., and Apodaca, G. (2007). Defective CFTR apical endocytosis and enterocyte brush border in myosin VI-deficient mice. Traffic *8*, 998-1006.

Andersen, J.S., Wilkinson, C.J., Mayor, T., Mortensen, P., Nigg, E.A., and Mann, M. (2003). Proteomic characterization of the human centrosome by protein correlation profiling. Nature *426*, 570-574.

Appella, E., and Anderson, C.W. (2001). Post-translational modifications and activation of p53 by genotoxic stresses. Eur J Biochem *268*, 2764-2772.

Arden, S.D., Puri, C., Au, J.S.-Y., Kendrick-Jones, J., and Buss, a.F. (2007). Myosin VI Is Required for Targeted Membrane Transport during Cytokinesis. Molecular Biology of the Cell

Vol. 18, 4750–4761.

Arquint, C., Gabryjonczyk, A.M., Imseng, S., Bohm, R., Sauer, E., Hiller, S., Nigg, E.A., and Maier, T. (2015). STIL binding to Polo-box 3 of PLK4 regulates centriole duplication. eLife *4*.

Arquint, C., and Nigg, E.A. (2014). STIL microcephaly mutations interfere with APC/C-mediated degradation and cause centriole amplification. Current biology : CB *24*, 351-360.

Arquint, C., and Nigg, E.A. (2016). The PLK4-STIL-SAS-6 module at the core of centriole duplication. Biochemical Society transactions *44*, 1253-1263.

Arquint, C., Sonnen, K.F., Stierhof, Y.D., and Nigg, E.A. (2012). Cell-cycle-regulated expression of STIL controls centriole number in human cells. Journal of cell science *125*, 1342-1352.

Aschenbrenner, L., Lee, T., and Hasson, T. (2003). Myo6 Facilitates the Translocation of Endocytic Vesicles from Cell Peripheries. Molecular Biology of the Cell *14*, 2728–2743.

Aschenbrenner, L., Naccache, S.N., and Hasson*, T. (2004). Uncoated Endocytic Vesicles Require the Unconventional Myosin, Myo6, for Rapid Transport through Actin Barriers. Molecular Biology of the Cell *15*, 2253-2263.

Ashcroft, M., Kubbutat, M.H., and Vousden, K.H. (1999). Regulation of p53 function and stability by phosphorylation. Molecular and cellular biology *19*, 1751-1758.
Au, F.K., Jia, Y., Jiang, K., Grigoriev, I., Hau, B.K., Shen, Y., Du, S., Akhmanova, A., and Qi, R.Z. (2017). GAS2L1 Is a Centriole-Associated Protein Required for Centrosome Dynamics and Disjunction. Developmental cell *40*, 81-94.
Au, J.S., Puri, C., Ihrke, G., Kendrick-Jones, J., and Buss, F. (2007). Myosin VI is required for sorting of AP-1B-dependent cargo to the basolateral domain in polarized MDCK cells. The Journal of cell biology *177*, 103-114.
Avraham, K.B., Hasson, T., Sobe, T., Balsara, B., Testa, J.R., Skvorak, A.B., Morton, C.C., Copeland, N.G., and Jenkins, N.A. (1997). Characterization of unconventional MYO6 , the human homologue of the gene responsible for deafness in Snell's waltzer mice. Human molecular genetics *6*, 1225–1231.
Avraham., K.B., T, H., KP, S., DM, K., LB, R., MS, M., NG, C., and NA., J. (1995). The mouse Snell's waltzer deafness gene encodes an unconventional myosin required for structural integrity of the inner ear hair. Nature Genetics *11*, 369-375.
Aylon, Y., and Oren, M. (2016). The Paradox of p53: What, How, and Why? Cold Spring Harbor perspectives in medicine *6*.
Baboolal, T.G., Sakamoto, T., Forgacs, E., White, H.D., Jackson, S.M., Takagi, Y., Farrow, R.E., Molloy, J.E., Knight, P.J., Sellers, J.R.*, et al.* (2009). The SAH domain extends the functional length of the myosin lever. Proceedings of the National Academy of Sciences of the United States of America *106*, 22193-22198.
Bahe, S., Stierhof, Y.D., Wilkinson, C.J., Leiss, F., and Nigg, E.A. (2005). Rootletin forms centriole-associated filaments and functions in centrosome cohesion. The Journal of cell biology *171*, 27-33.
Baker, J.P., and Titus, M.A. (1997). A Family of Unconventional Myosins from the Nematode Caenorhabditis elegans. Journal of Molecular Biology *272*, 523-535.
Barnes, B.G. (1961). Ciliated secretory cells in the pars distalis of the mouse hypophysis. J Ultrastruct Res *5*, 453-467.
Barnum, K.J., and O'Connell, M.J. (2014). Cell cycle regulation by checkpoints. Methods Mol Biol *1170*, 29-40.
Barros, T.P., Kinoshita, K., Hyman, A.A., and Raff, J.W. (2005). Aurora A activates D-TACC-Msps complexes exclusively at centrosomes to stabilize centrosomal microtubules. The Journal of cell biology *170*, 1039-1046.
Bartek, J., Bartkova, J., and Lukas, J. (1996). The retinoblastoma protein pathway and the restriction point. Current opinion in cell biology *8*, 805-814.
Basto, R., Brunk, K., Vinadogrova, T., Peel, N., Franz, A., Khodjakov, A., and Raff, J.W. (2008). Centrosome amplification can initiate tumorigenesis in flies. Cell *133*, 1032-1042.
Bates, S., Phillips, A.C., Clark, P.A., Stott, F., Peters, G., Ludwig, R.L., and Vousden, K.H. (1998). p14ARF links the tumour suppressors RB and p53. Nature *395*, 124-125.
Batters, C., Brack, D., Ellrich, H., Averbeck, B., and Veigel, C. (2016). Calcium can mobilize and activate myosin-VI. Proceedings of the National Academy of Sciences of the United States of America *113*, E1162-1169.
Bazzi, H., and Anderson, K.V. (2014). Acentriolar mitosis activates a p53-dependent apoptosis pathway in the mouse embryo. Proceedings of the National Academy of Sciences of the United States of America *111*, E1491-1500.
Beausejour, C.M., Krtolica, A., Galimi, F., Narita, M., Lowe, S.W., Yaswen, P., and Campisi, J. (2003). Reversal of human cellular senescence: roles of the p53 and p16 pathways. EMBO J *22*, 4212-4222.
Becker, J.S., Nicetto, D., and Zaret, K.S. (2016). H3K9me3-Dependent Heterochromatin: Barrier to Cell Fate Changes. Trends Genet *32*, 29-41.

Benmerah, A. (2013). The ciliary pocket. Current opinion in cell biology *25*, 78-84.
Berbari, N.F., O'Connor, A.K., Haycraft, C.J., and Yoder, B.K. (2009). The primary cilium as a complex signaling center. Current biology : CB *19*, R526-535.
Bettencourt-Dias, M., and Glover, D.M. (2007). Centrosome biogenesis and function: centrosomics brings new understanding. Nature reviews Molecular cell biology *8*, 451-463.
Bettencourt-Dias, M., Rodrigues-Martins, A., Carpenter, L., Riparbelli, M., Lehmann, L., Gatt, M.K., Carmo, N., Balloux, F., Callaini, G., and Glover, D.M. (2005). SAK/PLK4 is required for centriole duplication and flagella development. Current biology : CB *15*, 2199-2207.
Beznoussenko, G.V., and Mironov, A.A. (2015). Correlative video-light-electron microscopy of mobile organelles. Methods Mol Biol *1270*, 321-346.
Bisel, B., Wang, Y., Wei, J.H., Xiang, Y., Tang, D., Miron-Mendoza, M., Yoshimura, S., Nakamura, N., and Seemann, J. (2008). ERK regulates Golgi and centrosome orientation towards the leading edge through GRASP65. The Journal of cell biology *182*, 837-843.
Blackford, A.N., and Jackson, S.P. (2017). ATM, ATR, and DNA-PK: The Trinity at the Heart of the DNA Damage Response. Molecular cell *66*, 801-817.
Boisvieux-Ulrich, E., Laine, M.C., and Sandoz, D. (1990). Cytochalasin D inhibits basal body migration and ciliary elongation in quail oviduct epithelium. Cell Tissue Res *259*, 443-454.
Bolhy, S., Bouhlel, I., Dultz, E., Nayak, T., Zuccolo, M., Gatti, X., Vallee, R., Ellenberg, J., and Doye, V. (2011). A Nup133-dependent NPC-anchored network tethers centrosomes to the nuclear envelope in prophase. The Journal of cell biology *192*, 855-871.
Bonazzi, M., Kuhbacher, A., Toledo-Arana, A., Mallet, A., Vasudevan, L., Pizarro-Cerda, J., Brodsky, F.M., and Cossart, P. (2012). A common clathrin-mediated machinery co-ordinates cell-cell adhesion and bacterial internalization. Traffic *13*, 1653-1666.
Bonazzi, M., Vasudevan, L., Mallet, A., Sachse, M., Sartori, A., Prevost, M.C., Roberts, A., Taner, S.B., Wilbur, J.D., Brodsky, F.M*., et al.* (2011). Clathrin phosphorylation is required for actin recruitment at sites of bacterial adhesion and internalization. The Journal of cell biology *195*, 525-536.
Bond, L.M., Brandstaetter, H., Sellers, J.R., Kendrick-Jones, J., and Buss, F. (2011). Myosin motor proteins are involved in the final stages of the secretory pathways. Biochemical Society transactions *39*, 1115-1119.
Bond, L.M., Peden, A.A., Kendrick-Jones, J., Sellers, J.R., and Buss, F. (2010). Myosin VI and its binding partner optineurin are involved in secretory vesicle fusion at the plasma membrane. Molecular biology of the cell *22*, 54-65.
Bornens, M. (1977). Is the centriole bound to the nuclear membrane? Nature *270*, 80-82.
Bourke, E., Dodson, H., Merdes, A., Cuffe, L., Zachos, G., Walker, M., Gillespie, D., and Morrison, C.G. (2007). DNA damage induces Chk1-dependent centrosome amplification. EMBO reports *8*, 603-609.
Bower, J.J., Vance, L.D., Psioda, M., Smith-Roe, S.L., Simpson, D.A., Ibrahim, J.G., Hoadley, K.A., Perou, C.M., and Kaufmann, W.K. (2017). Patterns of cell cycle checkpoint deregulation associated with intrinsic molecular subtypes of human breast cancer cells. NPJ Breast Cancer *3*, 9.
Brandstaetter, H., Kishi-Itakura, C., Tumbarello, D.A., Manstein, D.J., and Buss, F. (2014). Loss of functional MYO1C/myosin 1c, a motor protein involved in lipid raft trafficking, disrupts autophagosome-lysosome fusion. Autophagy *10*, 2310-2323.
Brugarolas, J., Moberg, K., Boyd, S.D., Taya, Y., Jacks, T., and Lees, J.A. (1999). Inhibition of cyclin-dependent kinase 2 by p21 is necessary for retinoblastoma protein-mediated G1 arrest after gamma-irradiation. Proceedings of the National Academy of Sciences of the United States of America *96*, 1002-1007.

Bryant, Z., Altman, D., and Spudich, J.A. (2007). The power stroke of myosin VI and the basis of reverse directionality. Proceedings of the National Academy of Sciences of the United States of America *104*, 772-777.
Bunn, R.C., Jensen, M.A., and Reed, B.C. (1999). Protein Interactions with the Glucose Transporter Binding Protein GLUT1CBP That Provide a Link between GLUT1 and the Cytoskeleton. Molecular Biology of the Cell *10*.
Bunz, F., Dutriaux, A., Lengauer, C., Waldman, T., Zhou, S., Brown, J.P., Sedivy, J.M., Kinzler, K.W., and Vogelstein, B. (1998). Requirement for p53 and p21 to sustain G2 arrest after DNA damage. Science *282*, 1497-1501.
Buss, F., D.Arden, S., Lindsay, M., Luzio, J.P., and Kendrick-Jones, J. (2001). Myosin VI isoform localized to clathrin-coated vesicles with a role in clathrin-mediated endocytosis. The EMBO Journal *14*, 3676-3684.
Buss, F., Kendrick-Jones, J., Lionne, C., Knight, A.E., Côté, G.P., and Luzio, J.P. (1998). The Localization of Myosin VI at the Golgi Complex and Leading Edge of Fibroblasts and Its Phosphorylation and Recruitment into Membrane Ruffles of A431 Cells after Growth Factor Stimulation. The Journal of cell biology *143*, 1535–1545.
Buss, F., Luzio, J.P., and Kendrick-Jones, J. (2002). Myosin VI, an actin motor for membrane traffic and cell migration. Traffic *3*, 851-858.
Campisi, J. (2005). Senescent cells, tumor suppression, and organismal aging: good citizens, bad neighbors. Cell *120*, 513-522.
Campisi, J. (2011). Cellular senescence: putting the paradoxes in perspective. Curr Opin Genet Dev *21*, 107-112.
Campisi, J., and d'Adda di Fagagna, F. (2007). Cellular senescence: when bad things happen to good cells. Nature reviews Molecular cell biology *8*, 729-740.
Chamling, X., Seo, S., Searby, C.C., Kim, G., Slusarski, D.C., and Sheffield, V.C. (2014). The centriolar satellite protein AZI1 interacts with BBS4 and regulates ciliary trafficking of the BBSome. PLoS genetics *10*, e1004083.
Chan, H.M., Narita, M., Lowe, S.W., and Livingston, D.M. (2005). The p400 E1A-associated protein is a novel component of the p53 --> p21 senescence pathway. Genes & development *19*, 196-201.
Chan, J.Y. (2011). A clinical overview of centrosome amplification in human cancers. Int J Biol Sci *7*, 1122-1144.
Chen, Q., and Ames, B.N. (1994). Senescence-like growth arrest induced by hydrogen peroxide in human diploid fibroblast F65 cells. Proceedings of the National Academy of Sciences of the United States of America *91*, 4130-4134.
Chibalina, M.V., Poliakov, A., Kendrick-Jones, J., and Buss, F. (2010). Myosin VI and optineurin are required for polarized EGFR delivery and directed migration. Traffic *11*, 1290-1303.
Chibalina, M.V., Puri, C., Kendrick-Jones, J., and Buss, F. (2009). Potential roles of myosin VI in cell motility. Biochemical Society transactions *37*, 966-970.
Chibalina, M.V., Seaman, M.N., Miller, C.C., Kendrick-Jones, J., and Buss, F. (2007). Myosin VI and its interacting protein LMTK2 regulate tubule formation and transport to the endocytic recycling compartment. Journal of cell science *120*, 4278-4288.
Cho, K.A., Ryu, S.J., Oh, Y.S., Park, J.H., Lee, J.W., Kim, H.P., Kim, K.T., Jang, I.S., and Park, S.C. (2004). Morphological adjustment of senescent cells by modulating caveolin-1 status. The Journal of biological chemistry *279*, 42270-42278.
Chuan, P., Spudich, J.A., and Dunn, A.R. (2011). Robust mechanosensing and tension generation by myosin VI. Journal of molecular biology *405*, 105-112.
Ciccia, A., and Elledge, S.J. (2010). The DNA damage response: making it safe to play with knives. Molecular cell *40*, 179-204.

Coelho, P.A., Bury, L., Shahbazi, M.N., Liakath-Ali, K., Tate, P.H., Wormald, S., Hindley, C.J., Huch, M., Archer, J., Skarnes, W.C.*, et al.* (2015). Over-expression of Plk4 induces centrosome amplification, loss of primary cilia and associated tissue hyperplasia in the mouse. Open biology *5*, 150209.
Collaco, A., Jakab, R., Hegan, P., Mooseker, M., and Ameen, N. (2010). Alpha-AP-2 directs myosin VI-dependent endocytosis of cystic fibrosis transmembrane conductance regulator chloride channels in the intestine. The Journal of biological chemistry *285*, 17177-17187.
Comartin, D., Gupta, G.D., Fussner, E., Coyaud, E., Hasegan, M., Archinti, M., Cheung, S.W., Pinchev, D., Lawo, S., Raught, B.*, et al.* (2013). CEP120 and SPICE1 cooperate with CPAP in centriole elongation. Current biology : CB *23*, 1360-1366.
Conduit, P.T., Feng, Z., Richens, J.H., Baumbach, J., Wainman, A., Bakshi, S.D., Dobbelaere, J., Johnson, S., Lea, S.M., and Raff, J.W. (2014). The centrosome-specific phosphorylation of Cnn by Polo/Plk1 drives Cnn scaffold assembly and centrosome maturation. Developmental cell *28*, 659-669.
Coppe, J.P., Patil, C.K., Rodier, F., Sun, Y., Munoz, D.P., Goldstein, J., Nelson, P.S., Desprez, P.Y., and Campisi, J. (2008). Senescence-associated secretory phenotypes reveal cell-nonautonomous functions of oncogenic RAS and the p53 tumor suppressor. PLoS Biol *6*, 2853-2868.
Corbit, K.C., Shyer, A.E., Dowdle, W.E., Gaulden, J., Singla, V., Chen, M.H., Chuang, P.T., and Reiter, J.F. (2008). Kif3a constrains beta-catenin-dependent Wnt signalling through dual ciliary and non-ciliary mechanisms. Nature cell biology *10*, 70-76.
Courtois, A., Schuh, M., Ellenberg, J., and Hiiragi, T. (2012). The transition from meiotic to mitotic spindle assembly is gradual during early mammalian development. The Journal of cell biology *198*, 357-370.
Cuella-Martin, R., Oliveira, C., Lockstone, H.E., Snellenberg, S., Grolmusova, N., and Chapman, J.R. (2016). 53BP1 Integrates DNA Repair and p53-Dependent Cell Fate Decisions via Distinct Mechanisms. Molecular cell *64*, 51-64.
Dai, M.S., and Lu, H. (2004). Inhibition of MDM2-mediated p53 ubiquitination and degradation by ribosomal protein L5. The Journal of biological chemistry *279*, 44475-44482.
Dammermann, A., and Merdes, A. (2002). Assembly of centrosomal proteins and microtubule organization depends on PCM-1. The Journal of cell biology *159*, 255-266.
Dawe, H.R., Adams, M., Wheway, G., Szymanska, K., Logan, C.V., Noegel, A.A., Gull, K., and Johnson, C.A. (2009). Nesprin-2 interacts with meckelin and mediates ciliogenesis via remodelling of the actin cytoskeleton. Journal of cell science *122*, 2716-2726.
De Craene, B., and Berx, G. (2013). Regulatory networks defining EMT during cancer initiation and progression. Nature reviews Cancer *13*, 97-110.
Debacq-Chainiaux, F., Erusalimsky, J.D., Campisi, J., and Toussaint, O. (2009). Protocols to detect senescence-associated beta-galactosidase (SA-betagal) activity, a biomarker of senescent cells in culture and in vivo. Nat Protoc *4*, 1798-1806.
DeGregori, J., Leone, G., Miron, A., Jakoi, L., and Nevins, J.R. (1997). Distinct roles for E2F proteins in cell growth control and apoptosis. Proceedings of the National Academy of Sciences of the United States of America *94*, 7245-7250.
Desnos, C., Huet, S., Fanget, I., Chapuis, C., Bottiger, C., Racine, V., Sibarita, J.B., Henry, J.P., and Darchen, F. (2007). Myosin va mediates docking of secretory granules at the plasma membrane. The Journal of neuroscience : the official journal of the Society for Neuroscience *27*, 10636-10645.
Dick, F.A., and Rubin, S.M. (2013). Molecular mechanisms underlying RB protein function. Nature reviews Molecular cell biology *14*, 297-306.

Dilley, T.K., Bowden, G.T., and Chen, Q.M. (2003). Novel mechanisms of sublethal oxidant toxicity: induction of premature senescence in human fibroblasts confers tumor promoter activity. Exp Cell Res *290*, 38-48.
Dimri, G.P., Lee, X., Basile, G., Acosta, M., Scott, G., Roskelley, C., Medrano, E.E., Linskens, M., Rubelj, I., Pereira-Smith, O.*, et al.* (1995). A biomarker that identifies senescent human cells in culture and in aging skin in vivo. Proceedings of the National Academy of Sciences of the United States of America *92*, 9363-9367.
Dippold, H.C., Ng, M.M., Farber-Katz, S.E., Lee, S.K., Kerr, M.L., Peterman, M.C., Sim, R., Wiharto, P.A., Galbraith, K.A., Madhavarapu, S.*, et al.* (2009). GOLPH3 bridges phosphatidylinositol-4- phosphate and actomyosin to stretch and shape the Golgi to promote budding. Cell *139*, 337-351.
Dodson, H., Bourke, E., Jeffers, L.J., Vagnarelli, P., Sonoda, E., Takeda, S., Earnshaw, W.C., Merdes, A., and Morrison, C. (2004). Centrosome amplification induced by DNA damage occurs during a prolonged G2 phase and involves ATM. EMBO J *23*, 3864-3873.
Doench, J.G., Fusi, N., Sullender, M., Hegde, M., Vaimberg, E.W., Donovan, K.F., Smith, I., Tothova, Z., Wilen, C., Orchard, R.*, et al.* (2016). Optimized sgRNA design to maximize activity and minimize off-target effects of CRISPR-Cas9. Nat Biotechnol *34*, 184-191.
Douthwright, S., and Sluder, G. (2014). Link between DNA damage and centriole disengagement/reduplication in untransformed human cells. J Cell Physiol *229*, 1427-1436.
Dunn, T.A., Chen, S., Faith, D.A., Hicks, J.L., Platz, E.A., Chen, Y., Ewing, C.M., Sauvageot, J., Isaacs, W.B., De Marzo, A.M.*, et al.* (2006). A novel role of myosin VI in human prostate cancer. The American journal of pathology *169*, 1843-1854.
Dutertre, S., Cazales, M., Quaranta, M., Froment, C., Trabut, V., Dozier, C., Mirey, G., Bouche, J.P., Theis-Febvre, N., Schmitt, E.*, et al.* (2004). Phosphorylation of CDC25B by Aurora-A at the centrosome contributes to the G2-M transition. Journal of cell science *117*, 2523-2531.
Dzhindzhev, N.S., Tzolovsky, G., Lipinszki, Z., Schneider, S., Lattao, R., Fu, J., Debski, J., Dadlez, M., and Glover, D.M. (2014). Plk4 phosphorylates Ana2 to trigger Sas6 recruitment and procentriole formation. Current biology : CB *24*, 2526-2532.
Faragher, A.J., and Fry, A.M. (2003). Nek2A kinase stimulates centrosome disjunction and is required for formation of bipolar mitotic spindles. Mol Biol Cell *14*, 2876-2889.
Farina, F., Gaillard, J., Guerin, C., Coute, Y., Sillibourne, J., Blanchoin, L., and Thery, M. (2016). The centrosome is an actin-organizing centre. Nature cell biology *18*, 65-75.
Fava, L.L., Schuler, F., Sladky, V., Haschka, M.D., Soratroi, C., Eiterer, L., Demetz, E., Weiss, G., Geley, S., Nigg, E.A.*, et al.* (2017). The PIDDosome activates p53 in response to supernumerary centrosomes. Genes & development *31*, 34-45.
Fei, Q., Shang, K., Zhang, J., Chuai, S., Kong, D., Zhou, T., Fu, S., Liang, Y., Li, C., Chen, Z.*, et al.* (2015). Histone methyltransferase SETDB1 regulates liver cancer cell growth through methylation of p53. Nature communications *6*, 8651.
Ferrante, M.I., Zullo, A., Barra, A., Bimonte, S., Messaddeq, N., Studer, M., Dolle, P., and Franco, B. (2006). Oral-facial-digital type I protein is required for primary cilia formation and left-right axis specification. Nat Genet *38*, 112-117.
Fili, N., Hari-Gupta, Y., Dos Santos, A., Cook, A., Poland, S., Ameer-Beg, S.M., Parsons, M., and Toseland, C.P. (2017). NDP52 activates nuclear myosin VI to enhance RNA polymerase II transcription. Nature communications *8*, 1871.
Fisk, H.A., Mattison, C.P., and Winey, M. (2003). Human Mps1 protein kinase is required for centrosome duplication and normal mitotic progression. Proceedings of the National Academy of Sciences of the United States of America *100*, 14875-14880.
Fisk, H.A., and Winey, M. (2001). The mouse Mps1p-like kinase regulates centrosome duplication. Cell *106*, 95-104.

Flanagan, A.M., Stavenschi, E., Basavaraju, S., Gaboriau, D., Hoey, D.A., and Morrison, C.G. (2017). Centriole splitting caused by loss of the centrosomal linker protein C-NAP1 reduces centriolar satellite density and impedes centrosome amplification. Mol Biol Cell *28*, 736-745.
Follit, J.A., San Agustin, J.T., Xu, F., Jonassen, J.A., Samtani, R., Lo, C.W., and Pazour, G.J. (2008). The Golgin GMAP210/TRIP11 anchors IFT20 to the Golgi complex. PLoS genetics *4*, e1000315.
Follit, J.A., Tuft, R.A., Fogarty, K.E., and Pazour, G.J. (2006). The intraflagellar transport protein IFT20 is associated with the Golgi complex and is required for cilia assembly. Mol Biol Cell *17*, 3781-3792.
Fong, C.S., Kim, M., Yang, T.T., Liao, J.C., and Tsou, M.F. (2014). SAS-6 assembly templated by the lumen of cartwheel-less centrioles precedes centriole duplication. Developmental cell *30*, 238-245.
Fong, C.S., Mazo, G., Das, T., Goodman, J., Kim, M., O'Rourke, B.P., Izquierdo, D., and Tsou, M.F. (2016). 53BP1 and USP28 mediate p53-dependent cell cycle arrest in response to centrosome loss and prolonged mitosis. eLife *5*.
Foth, B.J., Goedecke, M.C., and Soldati, D. (2006). New insights into myosin evolution and classification. Proceedings of the National Academy of Sciences of the United States of America *103*, 3681-3686.
Fry, A.M., Mayor, T., Meraldi, P., Stierhof, Y.D., Tanaka, K., and Nigg, E.A. (1998). C-Nap1, a novel centrosomal coiled-coil protein and candidate substrate of the cell cycle-regulated protein kinase Nek2. The Journal of cell biology *141*, 1563-1574.
Fu, J., Hagan, I.M., and Glover, D.M. (2015). The centrosome and its duplication cycle. Cold Spring Harbor perspectives in biology *7*, a015800.
Fu, J., Lipinszki, Z., Rangone, H., Min, M., Mykura, C., Chao-Chu, J., Schneider, S., Dzhindzhev, N.S., Gottardo, M., Riparbelli, M.G.*, et al.* (2016). Conserved molecular interactions in centriole-to-centrosome conversion. Nature cell biology *18*, 87-99.
Fujita, N., Watanabe, S., Ichimura, T., Ohkuma, Y., Chiba, T., Saya, H., and Nakao, M. (2003). MCAF mediates MBD1-dependent transcriptional repression. Molecular and cellular biology *23*, 2834-2843.
Fukasawa, K. (2008). P53, cyclin-dependent kinase and abnormal amplification of centrosomes. Biochimica et biophysica acta *1786*, 15-23.
Furia, L., Pelicci, P.G., and Faretta, M. (2013a). A computational platform for robotized fluorescence microscopy (I): high-content image-based cell-cycle analysis. Cytometry A *83*, 333-343.
Furia, L., Pelicci, P.G., and Faretta, M. (2013b). A computational platform for robotized fluorescence microscopy (II): DNA damage, replication, checkpoint activation, and cell cycle progression by high-content high-resolution multiparameter image-cytometry. Cytometry A *83*, 344-355.
Gabrielli, B., Brooks, K., and Pavey, S. (2012). Defective cell cycle checkpoints as targets for anti-cancer therapies. Front Pharmacol *3*, 9.
Ganem, N.J., Cornils, H., Chiu, S.Y., O'Rourke, K.P., Arnaud, J., Yimlamai, D., Thery, M., Camargo, F.D., and Pellman, D. (2014). Cytokinesis failure triggers hippo tumor suppressor pathway activation. Cell *158*, 833-848.
Ganem, N.J., Godinho, S.A., and Pellman, D. (2009). A mechanism linking extra centrosomes to chromosomal instability. Nature *460*, 278-282.
Ganem, N.J., Storchova, Z., and Pellman, D. (2007). Tetraploidy, aneuploidy and cancer. Curr Opin Genet Dev *17*, 157-162.
Geisbrecht, E.R., and Montell, D.J. (2002). Myosin VI is required for E-cadherin-mediated border cell migration. Nature cell biology *4*, 616-620.

Ghossoub, R., Molla-Herman, A., Bastin, P., and Benmerah, A. (2011). The ciliary pocket: a once-forgotten membrane domain at the base of cilia. Biol Cell *103*, 131-144.
Giacinti, C., and Giordano, A. (2006). RB and cell cycle progression. Oncogene *25*, 5220-5227.
Giet, R., McLean, D., Descamps, S., Lee, M.J., Raff, J.W., Prigent, C., and Glover, D.M. (2002). Drosophila Aurora A kinase is required to localize D-TACC to centrosomes and to regulate astral microtubules. The Journal of cell biology *156*, 437-451.
Godinho, S.A., and Pellman, D. (2014). Causes and consequences of centrosome abnormalities in cancer. Philos Trans R Soc Lond B Biol Sci *369*.
Godinho, S.A., Picone, R., Burute, M., Dagher, R., Su, Y., Leung, C.T., Polyak, K., Brugge, J.S., Thery, M., and Pellman, D. (2014). Oncogene-like induction of cellular invasion from centrosome amplification. Nature *510*, 167-171.
Goetz, S.C., Liem, K.F., Jr., and Anderson, K.V. (2012). The spinocerebellar ataxia-associated gene Tau tubulin kinase 2 controls the initiation of ciliogenesis. Cell *151*, 847-858.
Goriounov, D., Leung, C.L., and Liem, R.K. (2003). Protein products of human Gas2-related genes on chromosomes 17 and 22 (hGAR17 and hGAR22) associate with both microfilaments and microtubules. Journal of cell science *116*, 1045-1058.
Gotoh, N., Yan, Q., Du, Z., Biemesderfer, D., Kashgarian, M., Mooseker, M.S., and Wang, T. (2010). Altered renal proximal tubular endocytosis and histology in mice lacking myosin-VI. Cytoskeleton *67*, 178-192.
Gottlieb, T.A., Ivanov, I.E., Adesnik, M., and Sabatini, D.D. (1993). Actin microfilaments play a critical role in endocytosis at the apical but not the basolateral surface of polarized epithelial cells. The Journal of cell biology *120*, 695-710.
Gouveia, S.M., Zitouni, S., Kong, D., Duarte, P., Gomes, B.F., Sousa, A.L., Tranfield, E.M., Hyman, A., Loncarek, J., and Bettencourt-Dias, M. (2018). PLK4 is a microtubule-associated protein that self assembles promoting de novo MTOC formation. Journal of cell science.
Gromley, A., Jurczyk, A., Sillibourne, J., Halilovic, E., Mogensen, M., Groisman, I., Blomberg, M., and Doxsey, S. (2003). A novel human protein of the maternal centriole is required for the final stages of cytokinesis and entry into S phase. The Journal of cell biology *161*, 535-545.
Guderian, G., Westendorf, J., Uldschmid, A., and Nigg, E.A. (2010). Plk4 trans-autophosphorylation regulates centriole number by controlling betaTrCP-mediated degradation. Journal of cell science *123*, 2163-2169.
Gueth-Hallonet, C., Antony, C., Aghion, J., Santa-Maria, A., Lajoie-Mazenc, I., Wright, M., and Maro, B. (1993). gamma-Tubulin is present in acentriolar MTOCs during early mouse development. Journal of cell science *105 (Pt 1)*, 157-166.
Guichard, P., Chretien, D., Marco, S., and Tassin, A.M. (2010). Procentriole assembly revealed by cryo-electron tomography. EMBO J *29*, 1565-1572.
Guichard, P., Desfosses, A., Maheshwari, A., Hachet, V., Dietrich, C., Brune, A., Ishikawa, T., Sachse, C., and Gonczy, P. (2012). Cartwheel architecture of Trichonympha basal body. Science *337*, 553.
Gupta, G.D., Coyaud, E., Goncalves, J., Mojarad, B.A., Liu, Y., Wu, Q., Gheiratmand, L., Comartin, D., Tkach, J.M., Cheung, S.W.*, et al.* (2015). A Dynamic Protein Interaction Landscape of the Human Centrosome-Cilium Interface. Cell *163*, 1484-1499.
Gurel, P.S., Hatch, A.L., and Higgs, H.N. (2014). Connecting the cytoskeleton to the endoplasmic reticulum and Golgi. Current biology : CB *24*, R660-672.
Haapaniemi, E., Botla, S., Persson, J., Schmierer, B., and Taipale, J. (2018). CRISPR-Cas9 genome editing induces a p53-mediated DNA damage response. Nat Med *24*, 927-930.
Habedanck, R., Stierhof, Y.D., Wilkinson, C.J., and Nigg, E.A. (2005). The Polo kinase Plk4 functions in centriole duplication. Nature cell biology *7*, 1140-1146.

Hames, R.S., Crookes, R.E., Straatman, K.R., Merdes, A., Hayes, M.J., Faragher, A.J., and Fry, A.M. (2005). Dynamic recruitment of Nek2 kinase to the centrosome involves microtubules, PCM-1, and localized proteasomal degradation. Mol Biol Cell *16*, 1711-1724.
Hammer, J.A., 3rd, and Sellers, J.R. (2011). Walking to work: roles for class V myosins as cargo transporters. Nature reviews Molecular cell biology *13*, 13-26.
Han, Y.G., Kim, H.J., Dlugosz, A.A., Ellison, D.W., Gilbertson, R.J., and Alvarez-Buylla, A. (2009). Dual and opposing roles of primary cilia in medulloblastoma development. Nat Med *15*, 1062-1065.
Harper, J.W., Elledge, S.J., Keyomarsi, K., Dynlacht, B., Tsai, L.H., Zhang, P., Dobrowolski, S., Bai, C., Connell-Crowley, L., Swindell, E.*, et al.* (1995). Inhibition of cyclin-dependent kinases by p21. Mol Biol Cell *6*, 387-400.
Hartman, M.A., and Spudich, J.A. (2012). The myosin superfamily at a glance. Journal of cell science *125*, 1627-1632.
Hasson, T., Gillespie, P.G., Garcia, J.A., MacDonald, R.B., Zhao, Y.-d., Yee, A.G., Mooseker, M.S., and Corey, D.P. (1997). Unconventional Myosins in Inner-Ear Sensory Epithelia. The Journal of Cell Biology, *137*, 1287–1307.
Hasson, T., and Mooseker, M.S. (1994). Porcine Myosin-VI- Characterization of a New Mammalian Unconventional Myosin. The Journal of cell biology *127*, 425-440.
Haupt, Y., Maya, R., Kazaz, A., and Oren, M. (1997). Mdm2 promotes the rapid degradation of p53. Nature *387*, 296-299.
Hayflick, L. (1965). The Limited in Vitro Lifetime of Human Diploid Cell Strains. Exp Cell Res *37*, 614-636.
He, F., Wollscheid, H.P., Nowicka, U., Biancospino, M., Valentini, E., Ehlinger, A., Acconcia, F., Magistrati, E., Polo, S., and Walters, K.J. (2016). Myosin VI Contains a Compact Structural Motif that Binds to Ubiquitin Chains. Cell reports *14*, 2683-2694.
He, G., Siddik, Z.H., Huang, Z., Wang, R., Koomen, J., Kobayashi, R., Khokhar, A.R., and Kuang, J. (2005). Induction of p21 by p53 following DNA damage inhibits both Cdk4 and Cdk2 activities. Oncogene *24*, 2929-2943.
Hegan, P.S., Giral, H., Levi, M., and Mooseker, M.S. (2012). Myosin VI is required for maintenance of brush border structure, composition, and membrane trafficking functions in the intestinal epithelial cell. Cytoskeleton *69*, 235-251.
Hegan, P.S., Lanahan, A.A., Simons, M., and Mooseker, M.S. (2015). Myosin VI and cardiomyopathy: Left ventricular hypertrophy, fibrosis, and both cardiac and pulmonary vascular endothelial cell defects in the Snell's waltzer mouse. Cytoskeleton *72*, 373-387.
Heissler, S.M., and Sellers, J.R. (2014). Myosin light chains: Teaching old dogs new tricks. Bioarchitecture *4*, 169-188.
Helps, N.R., Luo, X., Barker, H.M., and Cohen, P.T. (2000). NIMA-related kinase 2 (Nek2), a cell-cycle-regulated protein kinase localized to centrosomes, is complexed to protein phosphatase 1. Biochem J *349*, 509-518.
Hemerly, A.S., Prasanth, S.G., Siddiqui, K., and Stillman, B. (2009). Orc1 controls centriole and centrosome copy number in human cells. Science *323*, 789-793.
Herbig, U., Jobling, W.A., Chen, B.P., Chen, D.J., and Sedivy, J.M. (2004). Telomere shortening triggers senescence of human cells through a pathway involving ATM, p53, and p21(CIP1), but not p16(INK4a). Molecular cell *14*, 501-513.
Hertzano, R., Shalit, E., Rzadzinska, A.K., Dror, A.A., Song, L., Ron, U., Tan, J.T., Shitrit, A.S., Fuchs, H., Hasson, T.*, et al.* (2008). A Myo6 mutation destroys coordination between the myosin heads, revealing new functions of myosin VI in the stereocilia of mammalian inner ear hair cells. PLoS genetics *4*, e1000207.
Hilbert, M., Noga, A., Frey, D., Hamel, V., Guichard, P., Kraatz, S.H., Pfreundschuh, M., Hosner, S., Fluckiger, I., Jaussi, R.*, et al.* (2016). SAS-6 engineering reveals interdependence

between cartwheel and microtubules in determining centriole architecture. Nature cell biology *18*, 393-403.
Hinchcliffe, E.H., Li, C., Thompson, E.A., Maller, J.L., and Sluder, G. (1999). Requirement of Cdk2-cyclin E activity for repeated centrosome reproduction in Xenopus egg extracts. Science *283*, 851-854.
Hirota, Y., Meunier, A., Huang, S., Shimozawa, T., Yamada, O., Kida, Y.S., Inoue, M., Ito, T., Kato, H., Sakaguchi, M.*, et al.* (2010). Planar polarity of multiciliated ependymal cells involves the anterior migration of basal bodies regulated by non-muscle myosin II. Development *137*, 3037-3046.
Holland, A.J., Fachinetti, D., Zhu, Q., Bauer, M., Verma, I.M., Nigg, E.A., and Cleveland, D.W. (2012). The autoregulated instability of Polo-like kinase 4 limits centrosome duplication to once per cell cycle. Genes & development *26*, 2684-2689.
Holland, A.J., Lan, W., Niessen, S., Hoover, H., and Cleveland, D.W. (2010). Polo-like kinase 4 kinase activity limits centrosome overduplication by autoregulating its own stability. The Journal of cell biology *188*, 191-198.
Hori, A., Barnouin, K., Snijders, A.P., and Toda, T. (2016). A non-canonical function of Plk4 in centriolar satellite integrity and ciliogenesis through PCM1 phosphorylation. EMBO reports *17*, 326-337.
Hori, A., and Toda, T. (2017). Regulation of centriolar satellite integrity and its physiology. Cellular and molecular life sciences : CMLS *74*, 213-229.
Horn, H.F., and Vousden, K.H. (2007). Coping with stress: multiple ways to activate p53. Oncogene *26*, 1306-1316.
Hu, M., Gu, L., Li, M., Jeffrey, P.D., Gu, W., and Shi, Y. (2006). Structural basis of competitive recognition of p53 and MDM2 by HAUSP/USP7: implications for the regulation of the p53-MDM2 pathway. PLoS Biol *4*, e27.
Hu, S., Wang, Y., Gong, Y., Liu, J., Li, Y., and Pan, L. (2018). Mechanistic Insights into Recognitions of Ubiquitin and Myosin VI by Autophagy Receptor TAX1BP1. Journal of molecular biology.
Hubackova, S., Krejcikova, K., Bartek, J., and Hodny, Z. (2012). IL1- and TGFbeta-Nox4 signaling, oxidative stress and DNA damage response are shared features of replicative, oncogene-induced, and drug-induced paracrine 'bystander senescence'. Aging (Albany NY) *4*, 932-951.
Hubert, T., Vandekerckhove, J., and Gettemans, J. (2011). Actin and Arp2/3 localize at the centrosome of interphase cells. Biochemical and biophysical research communications *404*, 153-158.
Iacovoni, J.S., Caron, P., Lassadi, I., Nicolas, E., Massip, L., Trouche, D., and Legube, G. (2010). High-resolution profiling of gammaH2AX around DNA double strand breaks in the mammalian genome. EMBO J *29*, 1446-1457.
Inanc, B., Dodson, H., and Morrison, C.G. (2010). A centrosome-autonomous signal that involves centriole disengagement permits centrosome duplication in G2 phase after DNA damage. Mol Biol Cell *21*, 3866-3877.
Infante, E., Castagnino, A., Ferrari, R., Monteiro, P., Aguera-Gonzalez, S., Paul-Gilloteaux, P., Domingues, M.J., Maiuri, P., Raab, M., Shanahan, C.M.*, et al.* (2018). LINC complex-Lis1 interplay controls MT1-MMP matrix digest-on-demand response for confined tumor cell migration. Nature communications *9*, 2443.
Inoue, A., Sato, O., Homma, K., and Ikebe, M. (2002). DOC-2/DAB2 is the binding partner of myosin VI. Biochemical and biophysical research communications *292*, 300-307.
Jackman, M., Lindon, C., Nigg, E.A., and Pines, J. (2003). Active cyclin B1-Cdk1 first appears on centrosomes in prophase. Nature cell biology *5*, 143-148.

Jackman, M.R., Shurety, W., Ellis, J.A., and Luzio, J.P. (1994). Inhibition of apical but not basolateral endocytosis of ricin and folate in Caco-2 cells by cytochalasin D. Journal of cell science *107 (Pt 9)*, 2547-2556.
Jakobsen, L., Vanselow, K., Skogs, M., Toyoda, Y., Lundberg, E., Poser, I., Falkenby, L.G., Bennetzen, M., Westendorf, J., Nigg, E.A.*, et al.* (2011). Novel asymmetrically localizing components of human centrosomes identified by complementary proteomics methods. EMBO J *30*, 1520-1535.
Janke, C. (2014). The tubulin code: molecular components, readout mechanisms, and functions. The Journal of cell biology *206*, 461-472.
Joachim, J., Razi, M., Judith, D., Wirth, M., Calamita, E., Encheva, V., Dynlacht, B.D., Snijders, A.P., O'Reilly, N., Jefferies, H.B.J.*, et al.* (2017). Centriolar Satellites Control GABARAP Ubiquitination and GABARAP-Mediated Autophagy. Current biology : CB *27*, 2123-2136 e2127.
Jones, R.G., Plas, D.R., Kubek, S., Buzzai, M., Mu, J., Xu, Y., Birnbaum, M.J., and Thompson, C.B. (2005). AMP-activated protein kinase induces a p53-dependent metabolic checkpoint. Molecular cell *18*, 283-293.
Kaksonen, M., Toret, C.P., and Drubin, D.G. (2006). Harnessing actin dynamics for clathrin-mediated endocytosis. Nature reviews Molecular cell biology *7*, 404-414.
Kall, L., Canterbury, J.D., Weston, J., Noble, W.S., and MacCoss, M.J. (2007). Semi-supervised learning for peptide identification from shotgun proteomics datasets. Nat Methods *4*, 923-925.
Karolczak, J., Weis, S., Ehler, E., Kierdaszuk, B., Berdynski, M., Zekanowski, C., Kaminska, A.M., and Redowicz, M.J. (2014). Myosin VI localization and expression in striated muscle pathology. Anat Rec (Hoboken) *297*, 1706-1713.
Kastenhuber, E.R., and Lowe, S.W. (2017). Putting p53 in Context. Cell *170*, 1062-1078.
Keller, A., Nesvizhskii, A.I., Kolker, E., and Aebersold, R. (2002). Empirical statistical model to estimate the accuracy of peptide identifications made by MS/MS and database search. Anal Chem *74*, 5383-5392.
Keller, D., Orpinell, M., Olivier, N., Wachsmuth, M., Mahen, R., Wyss, R., Hachet, V., Ellenberg, J., Manley, S., and Gonczy, P. (2014). Mechanisms of HsSAS-6 assembly promoting centriole formation in human cells. The Journal of cell biology *204*, 697-712.
Kellerman, K.A., and Miller, K.G. (1992). An Unconventional Myosin Heavy Chain Gene from Drosophila melanogaster. The Journal of cell biology *119*, 823-834.
Khodjakov, A., Cole, R.W., Oakley, B.R., and Rieder, C.L. (2000). Centrosome-independent mitotic spindle formation in vertebrates. Current biology : CB *10*, 59-67.
Khodjakov, A., and Rieder, C.L. (2001). Centrosomes enhance the fidelity of cytokinesis in vertebrates and are required for cell cycle progression. The Journal of cell biology *153*, 237-242.
Khodjakov, A., Rieder, C.L., Sluder, G., Cassels, G., Sibon, O., and Wang, C.L. (2002). De novo formation of centrosomes in vertebrate cells arrested during S phase. The Journal of cell biology *158*, 1171-1181.
Kim, J., Lee, J.E., Heynen-Genel, S., Suyama, E., Ono, K., Lee, K., Ideker, T., Aza-Blanc, P., and Gleeson, J.G. (2010). Functional genomic screen for modulators of ciliogenesis and cilium length. Nature *464*, 1048-1051.
Kim, K., and Rhee, K. (2011). The pericentriolar satellite protein CEP90 is crucial for integrity of the mitotic spindle pole. Journal of cell science *124*, 338-347.
Kim, M., O'Rourke, B.P., Soni, R.K., Jallepalli, P.V., Hendrickson, R.C., and Tsou, M.B. (2016). Promotion and Suppression of Centriole Duplication Are Catalytically Coupled through PLK4 to Ensure Centriole Homeostasis. Cell reports *16*, 1195-1203.

Kim, S., and Dynlacht, B.D. (2013). Assembling a primary cilium. Current opinion in cell biology *25*, 506-511.
Kinoshita, K., Noetzel, T.L., Pelletier, L., Mechtler, K., Drechsel, D.N., Schwager, A., Lee, M., Raff, J.W., and Hyman, A.A. (2005). Aurora A phosphorylation of TACC3/maskin is required for centrosome-dependent microtubule assembly in mitosis. The Journal of cell biology *170*, 1047-1055.
Kitagawa, D., Vakonakis, I., Olieric, N., Hilbert, M., Keller, D., Olieric, V., Bortfeld, M., Erat, M.C., Fluckiger, I., Gonczy, P.*, et al.* (2011). Structural basis of the 9-fold symmetry of centrioles. Cell *144*, 364-375.
Kleylein-Sohn, J., Westendorf, J., Le Clech, M., Habedanck, R., Stierhof, Y.D., and Nigg, E.A. (2007). Plk4-induced centriole biogenesis in human cells. Developmental cell *13*, 190-202.
Klos Dehring, D.A., Vladar, E.K., Werner, M.E., Mitchell, J.W., Hwang, P., and Mitchell, B.J. (2013). Deuterosome-mediated centriole biogenesis. Developmental cell *27*, 103-112.
Kochanski, R.S., and Borisy, G.G. (1990). Mode of centriole duplication and distribution. The Journal of cell biology *110*, 1599-1605.
Kodani, A., Yu, T.W., Johnson, J.R., Jayaraman, D., Johnson, T.L., Al-Gazali, L., Sztriha, L., Partlow, J.N., Kim, H., Krup, A.L.*, et al.* (2015). Centriolar satellites assemble centrosomal microcephaly proteins to recruit CDK2 and promote centriole duplication. eLife *4*.
Komander, D., and Rape, M. (2012). The ubiquitin code. Annu Rev Biochem *81*, 203-229.
Kramer, A., Mailand, N., Lukas, C., Syljuasen, R.G., Wilkinson, C.J., Nigg, E.A., Bartek, J., and Lukas, J. (2004). Centrosome-associated Chk1 prevents premature activation of cyclin-B-Cdk1 kinase. Nature cell biology *6*, 884-891.
Kratz, A.S., Barenz, F., Richter, K.T., and Hoffmann, I. (2015). Plk4-dependent phosphorylation of STIL is required for centriole duplication. Biology open *4*, 370-377.
Krause, A., and Hoffmann, I. (2010). Polo-like kinase 2-dependent phosphorylation of NPM/B23 on serine 4 triggers centriole duplication. PloS one *5*, e9849.
Krtolica, A., Parrinello, S., Lockett, S., Desprez, P.Y., and Campisi, J. (2001). Senescent fibroblasts promote epithelial cell growth and tumorigenesis: a link between cancer and aging. Proceedings of the National Academy of Sciences of the United States of America *98*, 12072-12077.
Krueger, L.E., Wu, J.C., Tsou, M.F., and Rose, L.S. (2010). LET-99 inhibits lateral posterior pulling forces during asymmetric spindle elongation in C. elegans embryos. The Journal of cell biology *189*, 481-495.
Kruppa, A.J., and Buss, F. (2018). Actin cages isolate damaged mitochondria during mitophagy. Autophagy, 1-2.
Kruppa, A.J., Kendrick-Jones, J., and Buss, F. (2016). Myosins, Actin and Autophagy. Traffic *17*, 878-890.
Kubbutat, M.H., Jones, S.N., and Vousden, K.H. (1997). Regulation of p53 stability by Mdm2. Nature *387*, 299-303.
Kubo, A., and Tsukita, S. (2003). Non-membranous granular organelle consisting of PCM-1: subcellular distribution and cell-cycle-dependent assembly/disassembly. Journal of cell science *116*, 919-928.
Kuilman, T., Michaloglou, C., Mooi, W.J., and Peeper, D.S. (2010). The essence of senescence. Genes & development *24*, 2463-2479.
Kuilman, T., Michaloglou, C., Vredeveld, L.C., Douma, S., van Doorn, R., Desmet, C.J., Aarden, L.A., Mooi, W.J., and Peeper, D.S. (2008). Oncogene-induced senescence relayed by an interleukin-dependent inflammatory network. Cell *133*, 1019-1031.
Kuilman, T., and Peeper, D.S. (2009). Senescence-messaging secretome: SMS-ing cellular stress. Nature reviews Cancer *9*, 81-94.

Kurz, D.J., Decary, S., Hong, Y., and Erusalimsky, J.D. (2000). Senescence-associated (beta)-galactosidase reflects an increase in lysosomal mass during replicative ageing of human endothelial cells. Journal of cell science *113 (Pt 20)*, 3613-3622.
Kwon, M., Godinho, S.A., Chandhok, N.S., Ganem, N.J., Azioune, A., Thery, M., and Pellman, D. (2008). Mechanisms to suppress multipolar divisions in cancer cells with extra centrosomes. Genes & development *22*, 2189-2203.
La Terra, S., English, C.N., Hergert, P., McEwen, B.F., Sluder, G., and Khodjakov, A. (2005). The de novo centriole assembly pathway in HeLa cells: cell cycle progression and centriole assembly/maturation. The Journal of cell biology *168*, 713-722.
Laakso, J.M., Lewis, J.H., Shuman, H., and Ostap, E.M. (2008). Myosin I can act as a molecular force sensor. Science *321*, 133-136.
Lacey, K.R., Jackson, P.K., and Stearns, T. (1999). Cyclin-dependent kinase control of centrosome duplication. Proceedings of the National Academy of Sciences of the United States of America *96*, 2817-2822.
Lambrus, B.G., Daggubati, V., Uetake, Y., Scott, P.M., Clutario, K.M., Sluder, G., and Holland, A.J. (2016). A USP28-53BP1-p53-p21 signaling axis arrests growth after centrosome loss or prolonged mitosis. The Journal of cell biology *214*, 143-153.
Lambrus, B.G., Uetake, Y., Clutario, K.M., Daggubati, V., Snyder, M., Sluder, G., and Holland, A.J. (2015). p53 protects against genome instability following centriole duplication failure. The Journal of cell biology *210*, 63-77.
Lane, H.A., and Nigg, E.A. (1996). Antibody microinjection reveals an essential role for human polo-like kinase 1 (Plk1) in the functional maturation of mitotic centrosomes. The Journal of cell biology *135*, 1701-1713.
Lawo, S., Hasegan, M., Gupta, G.D., and Pelletier, L. (2012). Subdiffraction imaging of centrosomes reveals higher-order organizational features of pericentriolar material. Nature cell biology *14*, 1148-1158.
Lee, B.Y., Han, J.A., Im, J.S., Morrone, A., Johung, K., Goodwin, E.C., Kleijer, W.J., DiMaio, D., and Hwang, E.S. (2006). Senescence-associated beta-galactosidase is lysosomal beta-galactosidase. Aging Cell *5*, 187-195.
Lee, J.Y., Koga, H., Kawaguchi, Y., Tang, W., Wong, E., Gao, Y.S., Pandey, U.B., Kaushik, S., Tresse, E., Lu, J*., et al.* (2010). HDAC6 controls autophagosome maturation essential for ubiquitin-selective quality-control autophagy. EMBO J *29*, 969-980.
Lee, K., and Rhee, K. (2011). PLK1 phosphorylation of pericentrin initiates centrosome maturation at the onset of mitosis. The Journal of cell biology *195*, 1093-1101.
Lee, K., and Rhee, K. (2012). Separase-dependent cleavage of pericentrin B is necessary and sufficient for centriole disengagement during mitosis. Cell Cycle *11*, 2476-2485.
Leidel, S., Delattre, M., Cerutti, L., Baumer, K., and Gonczy, P. (2005). SAS-6 defines a protein family required for centrosome duplication in C. elegans and in human cells. Nature cell biology *7*, 115-125.
Leroy, B., Girard, L., Hollestelle, A., Minna, J.D., Gazdar, A.F., and Soussi, T. (2014). Analysis of TP53 mutation status in human cancer cell lines: a reassessment. Hum Mutat *35*, 756-765.
Levine, A.J., Hu, W., and Feng, Z. (2006). The P53 pathway: what questions remain to be explored? Cell Death Differ *13*, 1027-1036.
Levine, M.S., Bakker, B., Boeckx, B., Moyett, J., Lu, J., Vitre, B., Spierings, D.C., Lansdorp, P.M., Cleveland, D.W., Lambrechts, D*., et al.* (2017). Centrosome Amplification Is Sufficient to Promote Spontaneous Tumorigenesis in Mammals. Developmental cell *40*, 313-322 e315.

Li, A., Saito, M., Chuang, J.Z., Tseng, Y.Y., Dedesma, C., Tomizawa, K., Kaitsuka, T., and Sung, C.H. (2011). Ciliary transition zone activation of phosphorylated Tctex-1 controls ciliary resorption, S-phase entry and fate of neural progenitors. Nature cell biology *13*, 402-411.
Li, H., Rauch, T., Chen, Z.X., Szabo, P.E., Riggs, A.D., and Pfeifer, G.P. (2006). The histone methyltransferase SETDB1 and the DNA methyltransferase DNMT3A interact directly and localize to promoters silenced in cancer cells. The Journal of biological chemistry *281*, 19489-19500.
Li, H., Zhou, F., Wang, H., Lin, D., Chen, G., Zuo, X., Sun, L., Zhang, X., and Yang, S. (2015). Knockdown of myosin VI by lentivirus-mediated short hairpin RNA suppresses proliferation of melanoma. Mol Med Rep *12*, 6801-6806.
Li, W., Xu, H., Xiao, T., Cong, L., Love, M.I., Zhang, F., Irizarry, R.A., Liu, J.S., Brown, M., and Liu, X.S. (2014). MAGeCK enables robust identification of essential genes from genome-scale CRISPR/Cas9 knockout screens. Genome Biol *15*, 554.
Lin, Y.N., Wu, C.T., Lin, Y.C., Hsu, W.B., Tang, C.J., Chang, C.W., and Tang, T.K. (2013). CEP120 interacts with CPAP and positively regulates centriole elongation. The Journal of cell biology *202*, 211-219.
Lindstrom, M.S., Jin, A., Deisenroth, C., White Wolf, G., and Zhang, Y. (2007). Cancer-associated mutations in the MDM2 zinc finger domain disrupt ribosomal protein interaction and attenuate MDM2-induced p53 degradation. Molecular and cellular biology *27*, 1056-1068.
Lister, I., Schmitz, S., Walker, M., Trinick, J., Buss, F., Veigel, C., and Kendrick-Jones, J. (2004). A monomeric myosin VI with a large working stroke. The EMBO journal *23*, 1729-1738.
Loffler, H., Fechter, A., Liu, F.Y., Poppelreuther, S., and Kramer, A. (2013). DNA damage-induced centrosome amplification occurs via excessive formation of centriolar satellites. Oncogene *32*, 2963-2972.
Loncarek, J., and Bettencourt-Dias, M. (2018). Building the right centriole for each cell type. The Journal of cell biology *217*, 823-835.
Loncarek, J., Hergert, P., and Khodjakov, A. (2010). Centriole reduplication during prolonged interphase requires procentriole maturation governed by Plk1. Current biology : CB *20*, 1277-1282.
Loncarek, J., Hergert, P., Magidson, V., and Khodjakov, A. (2008). Control of daughter centriole formation by the pericentriolar material. Nature cell biology *10*, 322-328.
Lopes, C.A., Jana, S.C., Cunha-Ferreira, I., Zitouni, S., Bento, I., Duarte, P., Gilberto, S., Freixo, F., Guerrero, A., Francia, M.*, et al.* (2015). PLK4 trans-Autoactivation Controls Centriole Biogenesis in Space. Developmental cell *35*, 222-235.
Lopes, C.A., Prosser, S.L., Romio, L., Hirst, R.A., O'Callaghan, C., Woolf, A.S., and Fry, A.M. (2011). Centriolar satellites are assembly points for proteins implicated in human ciliopathies, including oral-facial-digital syndrome 1. Journal of cell science *124*, 600-612.
Ma, X., Yan, J., Chen, W., Du, P., Xie, J., Yu, H., and Wu, H. (2015). Knockdown of Myosin VI Inhibits Proliferation of Hepatocellular Carcinoma Cells In Vitro. Chemical biology & drug design *86*, 723-730.
Macurek, L., Lindqvist, A., Lim, D., Lampson, M.A., Klompmaker, R., Freire, R., Clouin, C., Taylor, S.S., Yaffe, M.B., and Medema, R.H. (2008). Polo-like kinase-1 is activated by aurora A to promote checkpoint recovery. Nature *455*, 119-123.
Maddugoda, M.P., Crampton, M.S., Shewan, A.M., and Yap, A.S. (2007). Myosin VI and vinculin cooperate during the morphogenesis of cadherin cell cell contacts in mammalian epithelial cells. The Journal of cell biology *178*, 529-540.
Mahen, R., Jeyasekharan, A.D., Barry, N.P., and Venkitaraman, A.R. (2011). Continuous polo-like kinase 1 activity regulates diffusion to maintain centrosome self-organization

during mitosis. Proceedings of the National Academy of Sciences of the United States of America *108*, 9310-9315.
Mahjoub, M.R., and Stearns, T. (2012). Supernumerary centrosomes nucleate extra cilia and compromise primary cilium signaling. Current biology : CB *22*, 1628-1634.
Mahjoub, M.R., Xie, Z., and Stearns, T. (2010). Cep120 is asymmetrically localized to the daughter centriole and is essential for centriole assembly. The Journal of cell biology *191*, 331-346.
Majewski, L., Nowak, J., Sobczak, M., Karatsai, O., Havrylov, S., Lenartowski, R., Suszek, M., Lenartowska, M., and Redowicz, M.J. (2018). Myosin VI in the nucleus of neurosecretory PC12 cells: Stimulation-dependent nuclear translocation and interaction with nuclear proteins. Nucleus *9*, 125-141.
Majewski, L., Sobczak, M., and Rędowicz, M.J. (2010). Myosin VI is associated with secretory granules and is present in the nucleus in adrenal medulla chromaffin cells. Acta Biochimica Polonica *57*, 109–114.
Malumbres, M., and Barbacid, M. (2001). To cycle or not to cycle: a critical decision in cancer. Nature reviews Cancer *1*, 222-231.
Malumbres, M., and Barbacid, M. (2009). Cell cycle, CDKs and cancer: a changing paradigm. Nature reviews Cancer *9*, 153-166.
Mangold, S., Norwood, S.J., Yap, A.S., and Collins, B.M. (2012). The juxtamembrane domain of the E-cadherin cytoplasmic tail contributes to its interaction with Myosin VI. Bioarchitecture *2*, 185-188.
Mardin, B.R., Agircan, F.G., Lange, C., and Schiebel, E. (2011). Plk1 controls the Nek2A-PP1gamma antagonism in centrosome disjunction. Current biology : CB *21*, 1145-1151.
Marteil, G., Guerrero, A., Vieira, A.F., de Almeida, B.P., Machado, P., Mendonca, S., Mesquita, M., Villarreal, B., Fonseca, I., Francia, M.E*., et al.* (2018). Over-elongation of centrioles in cancer promotes centriole amplification and chromosome missegregation. Nature communications *9*, 1258.
Masters, T.A., Tumbarello, D.A., Chibalina, M.V., and Buss, F. (2017). MYO6 Regulates Spatial Organization of Signaling Endosomes Driving AKT Activation and Actin Dynamics. Cell reports *19*, 2088-2101.
Matsui, T., Leung, D., Miyashita, H., Maksakova, I.A., Miyachi, H., Kimura, H., Tachibana, M., Lorincz, M.C., and Shinkai, Y. (2010). Proviral silencing in embryonic stem cells requires the histone methyltransferase ESET. Nature *464*, 927-931.
Matsumoto, Y., Hayashi, K., and Nishida, E. (1999). Cyclin-dependent kinase 2 (Cdk2) is required for centrosome duplication in mammalian cells. Current biology : CB *9*, 429-432.
Matsuo, K., Ohsumi, K., Iwabuchi, M., Kawamata, T., Ono, Y., and Takahashi, M. (2012). Kendrin is a novel substrate for separase involved in the licensing of centriole duplication. Current biology : CB *22*, 915-921.
Mayo, L.D., Dixon, J.E., Durden, D.L., Tonks, N.K., and Donner, D.B. (2002). PTEN protects p53 from Mdm2 and sensitizes cancer cells to chemotherapy. The Journal of biological chemistry *277*, 5484-5489.
Mayor, T., Stierhof, Y.D., Tanaka, K., Fry, A.M., and Nigg, E.A. (2000). The centrosomal protein C-Nap1 is required for cell cycle-regulated centrosome cohesion. The Journal of cell biology *151*, 837-846.
Megraw, T.L., Kilaru, S., Turner, F.R., and Kaufman, T.C. (2002). The centrosome is a dynamic structure that ejects PCM flares. Journal of cell science *115*, 4707-4718.
Meitinger, F., Anzola, J.V., Kaulich, M., Richardson, A., Stender, J.D., Benner, C., Glass, C.K., Dowdy, S.F., Desai, A., Shiau, A.K*., et al.* (2016). 53BP1 and USP28 mediate p53 activation and G1 arrest after centrosome loss or extended mitotic duration. The Journal of cell biology *214*, 155-166.

Melchionda, S., Ahituv, N., Bisceglia, L., Sobe, T., Glaser, F., Rabionet, R., Arbones, M.L., Notarangelo, A., Di Iorio, E., Carella, M.*, et al.* (2001). MYO6, the human homologue of the gene responsible for deafness in Snell's waltzer mice, is mutated in autosomal dominant nonsyndromic hearing loss. American journal of human genetics *69*, 635-640.
Mennella, V., Keszthelyi, B., McDonald, K.L., Chhun, B., Kan, F., Rogers, G.C., Huang, B., and Agard, D.A. (2012). Subdiffraction-resolution fluorescence microscopy reveals a domain of the centrosome critical for pericentriolar material organization. Nature cell biology *14*, 1159-1168.
Meraldi, P., Lukas, J., Fry, A.M., Bartek, J., and Nigg, E.A. (1999). Centrosome duplication in mammalian somatic cells requires E2F and Cdk2-cyclin A. Nature cell biology *1*, 88-93.
Meunier, A., and Azimzadeh, J. (2016). Multiciliated Cells in Animals. Cold Spring Harbor perspectives in biology *8*.
Mi, N., Chen, Y., Wang, S., Chen, M., Zhao, M., Yang, G., Ma, M., Su, Q., Luo, S., Shi, J.*, et al.* (2015). CapZ regulates autophagosomal membrane shaping by promoting actin assembly inside the isolation membrane. Nature cell biology *17*, 1112-1123.
Michaloglou, C., Vredeveld, L.C., Soengas, M.S., Denoyelle, C., Kuilman, T., van der Horst, C.M., Majoor, D.M., Shay, J.W., Mooi, W.J., and Peeper, D.S. (2005). BRAFE600-associated senescence-like cell cycle arrest of human naevi. Nature *436*, 720-724.
Mikule, K., Delaval, B., Kaldis, P., Jurcyzk, A., Hergert, P., and Doxsey, S. (2007). Loss of centrosome integrity induces p38-p53-p21-dependent G1-S arrest. Nature cell biology *9*, 160-170.
Mironov, A.A., and Beznoussenko, G.V. (2013). Correlative microscopy. Methods Cell Biol *113*, 209-255.
Mohiddin, S.A., Ahmed, Z.M., Griffith, A.J., Tripodi, D., Friedman, T.B., Fananapazir, L., and Morell, R.J. (2004). Novel association of hypertrophic cardiomyopathy, sensorineural deafness, and a mutation in unconventional myosin VI (MYO6). Journal of Medical Genetics *41*, 309-314.
Molla-Herman, A., Ghossoub, R., Blisnick, T., Meunier, A., Serres, C., Silbermann, F., Emmerson, C., Romeo, K., Bourdoncle, P., Schmitt, A.*, et al.* (2010). The ciliary pocket: an endocytic membrane domain at the base of primary and motile cilia. Journal of cell science *123*, 1785-1795.
Mooren, O.L., Galletta, B.J., and Cooper, J.A. (2012). Roles for actin assembly in endocytosis. Annu Rev Biochem *81*, 661-686.
Mori, D., Yano, Y., Toyo-oka, K., Yoshida, N., Yamada, M., Muramatsu, M., Zhang, D., Saya, H., Toyoshima, Y.Y., Kinoshita, K.*, et al.* (2007). NDEL1 phosphorylation by Aurora-A kinase is essential for centrosomal maturation, separation, and TACC3 recruitment. Molecular and cellular biology *27*, 352-367.
Morris, S.M., Arden, S.D., Roberts, R.C., Kendrick-Jones, J., Cooper, J.A., Luzio, P., and Buss, F. (2002). Myosin VI Binds to and Localises with Dab2, Potentially Linking Receptor-Mediated Endocytosis and the Actin Cytoskeleton. Traffic *2*, 331-341.
Morris, S.M., and Cooper, J.A. (2001). Disabled-2 Colocalizes with the LDLR in Clathrin-Coated Pits and Interacts with AP-2. Traffic *2*, 111-123.
Morriswood, B., Ryzhakov, G., Puri, C., Arden, S.D., Roberts, R., Dendrou, C., Kendrick-Jones, J., and Buss, F. (2007). T6BP and NDP52 are myosin VI binding partners with potential roles in cytokine signalling and cell adhesion. Journal of cell science *120*, 2574-2585.
Moyer, T.C., Clutario, K.M., Lambrus, B.G., Daggubati, V., and Holland, A.J. (2015). Binding of STIL to Plk4 activates kinase activity to promote centriole assembly. The Journal of cell biology *209*, 863-878.

Mukherjea, M., Ali, M.Y., Kikuti, C., Safer, D., Yang, Z., Sirkia, H., Ropars, V., Houdusse, A., Warshaw, D.M., and Sweeney, H.L. (2014). Myosin VI must dimerize and deploy its unusual lever arm in order to perform its cellular roles. Cell reports *8*, 1522-1532.
Mukherjea, M., Llinas, P., Kim, H., Travaglia, M., Safer, D., Menetrey, J., Franzini-Armstrong, C., Selvin, P.R., Houdusse, A., and Sweeney, H.L. (2009). Myosin VI dimerization triggers an unfolding of a three-helix bundle in order to extend its reach. Molecular cell *35*, 305-315.
Murray-Zmijewski, F., Slee, E.A., and Lu, X. (2008). A complex barcode underlies the heterogeneous response of p53 to stress. Nature reviews Molecular cell biology *9*, 702-712.
Naccache, S.N., and Hasson, T. (2006). Myosin VI altered at threonine 406 stabilizes actin filaments in vivo. Cell motility and the cytoskeleton *63*, 633-645.
Nachury, M.V., Loktev, A.V., Zhang, Q., Westlake, C.J., Peranen, J., Merdes, A., Slusarski, D.C., Scheller, R.H., Bazan, J.F., Sheffield, V.C*., et al.* (2007). A core complex of BBS proteins cooperates with the GTPase Rab8 to promote ciliary membrane biogenesis. Cell *129*, 1201-1213.
Nadezhdina, E.S., Fais, D., and Chentsov, Y.S. (1979). On the association of centrioles with the interphase nucleus. Eur J Cell Biol *19*, 109-115.
Nakamura, M., Tanaka, N., Kitamura, N., and Komada, M. (2006). Clathrin anchors deubiquitinating enzymes, AMSH and AMSH-like protein, on early endosomes. Genes to cells : devoted to molecular & cellular mechanisms *11*, 593-606.
Narita, M., Nunez, S., Heard, E., Narita, M., Lin, A.W., Hearn, S.A., Spector, D.L., Hannon, G.J., and Lowe, S.W. (2003). Rb-mediated heterochromatin formation and silencing of E2F target genes during cellular senescence. Cell *113*, 703-716.
Nash, J.E., Appleby, V.J., Correa, S.A., Wu, H., Fitzjohn, S.M., Garner, C.C., Collingridge, G.L., and Molnar, E. (2010). Disruption of the interaction between myosin VI and SAP97 is associated with a reduction in the number of AMPARs at hippocampal synapses. Journal of neurochemistry *112*, 677-690.
Nelson, S.R., Ali, M.Y., Trybus, K.M., and Warshaw, D.M. (2009). Random walk of processive, quantum dot-labeled myosin Va molecules within the actin cortex of COS-7 cells. Biophysical journal *97*, 509-518.
Nesvizhskii, A.I., Keller, A., Kolker, E., and Aebersold, R. (2003). A statistical model for identifying proteins by tandem mass spectrometry. Anal Chem *75*, 4646-4658.
Nigg, E.A. (2007). Centrosome duplication: of rules and licenses. Trends in cell biology *17*, 215-221.
Nigg, E.A., and Holland, A.J. (2018). Once and only once: mechanisms of centriole duplication and their deregulation in disease. Nature reviews Molecular cell biology *19*, 297-312.
Nigg, E.A., and Raff, J.W. (2009). Centrioles, centrosomes, and cilia in health and disease. Cell *139*, 663-678.
Noguchi, T., Lenartowska, M., and Miller, K.G. (2006). Myosin VI Stabilizes an Actin Network during Drosophila Spermatid Individualization. Molecular Biology of the Cell *17*, 2559–2571.
Novak, Z.A., Wainman, A., Gartenmann, L., and Raff, J.W. (2016). Cdk1 Phosphorylates Drosophila Sas-4 to Recruit Polo to Daughter Centrioles and Convert Them to Centrosomes. Developmental cell *37*, 545-557.
O'Loughlin, T., Masters, T.A., and Buss, F. (2018). The MYO6 interactome reveals adaptor complexes coordinating early endosome and cytoskeletal dynamics. EMBO reports *19*.
Odronitz, F., and Kollmar, M. (2007). Drawing the tree of eukaryotic life based on the analysis of 2,269 manually annotated myosins from 328 species. Genome Biol *8*, R196.

Oguchi, Y., Mikhailenko, S.V., Ohki, T., Olivares, A.O., De La Cruz, E.M., and Ishiwata, S. (2008). Load-dependent ADP binding to myosins V and VI: implications for subunit coordination and function. Proceedings of the National Academy of Sciences of the United States of America *105*, 7714-7719.
Ohta, M., Ashikawa, T., Nozaki, Y., Kozuka-Hata, H., Goto, H., Inagaki, M., Oyama, M., and Kitagawa, D. (2014). Direct interaction of Plk4 with STIL ensures formation of a single procentriole per parental centriole. Nature communications *5*, 5267.
Ohta, M., Watanabe, K., Ashikawa, T., Nozaki, Y., Yoshiba, S., Kimura, A., and Kitagawa, D. (2018). Bimodal Binding of STIL to Plk4 Controls Proper Centriole Copy Number. Cell reports *23*, 3160-3169 e3164.
Okoshi, R., Ozaki, T., Yamamoto, H., Ando, K., Koida, N., Ono, S., Koda, T., Kamijo, T., Nakagawara, A., and Kizaki, H. (2008). Activation of AMP-activated protein kinase induces p53-dependent apoptotic cell death in response to energetic stress. The Journal of biological chemistry *283*, 3979-3987.
Okuda, M., Horn, H.F., Tarapore, P., Tokuyama, Y., Smulian, A.G., Chan, P.K., Knudsen, E.S., Hofmann, I.A., Snyder, J.D., Bove, K.E*., et al.* (2000). Nucleophosmin/B23 is a target of CDK2/cyclin E in centrosome duplication. Cell *103*, 127-140.
Oshimori, N., Li, X., Ohsugi, M., and Yamamoto, T. (2009). Cep72 regulates the localization of key centrosomal proteins and proper bipolar spindle formation. EMBO J *28*, 2066-2076.
Osterweil, E., Wells, D.G., and Mooseker, M.S. (2005). A role for myosin VI in postsynaptic structure and glutamate receptor endocytosis. The Journal of cell biology *168*, 329-338.
Paintrand, M., Moudjou, M., Delacroix, H., and Bornens, M. (1992). Centrosome organization and centriole architecture: their sensitivity to divalent cations. J Struct Biol *108*, 107-128.
Pan, J., You, Y., Huang, T., and Brody, S.L. (2007). RhoA-mediated apical actin enrichment is required for ciliogenesis and promoted by Foxj1. Journal of cell science *120*, 1868-1876.
Panizzi, J.R., Jessen, J.R., Drummond, I.A., and Solnica-Krezel, L. (2007). New functions for a vertebrate Rho guanine nucleotide exchange factor in ciliated epithelia. Development *134*, 921-931.
Park, H., Li, A., Chen, L.Q., Houdusse, A., Selvin, P.R., and Sweeney, H.L. (2007). The unique insert at the end of the myosin VI motor is the sole determinant of directionality. Proceedings of the National Academy of Sciences of the United States of America *104*, 778-783.
Park, H., Ramamurthy, B., Travaglia, M., Safer, D., Chen, L.Q., Franzini-Armstrong, C., Selvin, P.R., and Sweeney, H.L. (2006). Full-length myosin VI dimerizes and moves processively along actin filaments upon monomer clustering. Molecular cell *21*, 331-336.
Pathak, D., Sepp, K.J., and Hollenbeck, P.J. (2010). Evidence that myosin activity opposes microtubule-based axonal transport of mitochondria. The Journal of neuroscience : the official journal of the Society for Neuroscience *30*, 8984-8992.
Pedersen, L.B., and Rosenbaum, J.L. (2008). Intraflagellar transport (IFT) role in ciliary assembly, resorption and signalling. Curr Top Dev Biol *85*, 23-61.
Penengo, L., Mapelli, M., Murachelli, A.G., Confalonieri, S., Magri, L., Musacchio, A., Di Fiore, P.P., Polo, S., and Schneider, T.R. (2006). Crystal structure of the ubiquitin binding domains of rabex-5 reveals two modes of interaction with ubiquitin. Cell *124*, 1183-1195.
Phichith, D., Travaglia, M., Yang, Z., Liu, X., Zong, A.B., Safer, D., and Sweeney, H.L. (2009). Cargo binding induces dimerization of myosin VI. Proceedings of the National Academy of Sciences of the United States of America *106*, 17320-17324.
Piehl, M., Lehmann, C., Gumpert, A., Denizot, J.-P., Segretain, D., and Falk, a.M.M. (2007). Internalization of Large Double-Membrane Intercellular Vesicles by a Clathrin-dependent Endocytic Process. Molecular Biology of the Cell *18*, 337–347,.

Pike, A.N., and Fisk, H.A. (2011). Centriole assembly and the role of Mps1: defensible or dispensable? Cell Div *6*, 9.
Polishchuk, R.S., and Mironov, A.A. (2001). Correlative video light/electron microscopy. Curr Protoc Cell Biol *Chapter 4*, Unit 4 8.
Polo, S.E., and Jackson, S.P. (2011). Dynamics of DNA damage response proteins at DNA breaks: a focus on protein modifications. Genes & development *25*, 409-433.
Prosser, S.L., Straatman, K.R., and Fry, A.M. (2009). Molecular dissection of the centrosome overduplication pathway in S-phase-arrested cells. Molecular and cellular biology *29*, 1760-1773.
Provance, D.W., Jr., Addison, E.J., Wood, P.R., Chen, D.Z., Silan, C.M., and Mercer, J.A. (2008). Myosin-Vb functions as a dynamic tether for peripheral endocytic compartments during transferrin trafficking. BMC cell biology *9*, 44.
Pugacheva, E.N., Jablonski, S.A., Hartman, T.R., Henske, E.P., and Golemis, E.A. (2007). HEF1-dependent Aurora A activation induces disassembly of the primary cilium. Cell *129*, 1351-1363.
Puklowski, A., Homsi, Y., Keller, D., May, M., Chauhan, S., Kossatz, U., Grunwald, V., Kubicka, S., Pich, A., Manns, M.P*., et al.* (2011). The SCF-FBXW5 E3-ubiquitin ligase is regulated by PLK4 and targets HsSAS-6 to control centrosome duplication. Nature cell biology *13*, 1004-1009.
Pylypenko, O., Song, L., Squires, G., Liu, X., Zong, A.B., Houdusse, A., and Sweeney, H.L. (2011). Role of insert-1 of myosin VI in modulating nucleotide affinity. The Journal of biological chemistry *286*, 11716-11723.
Quintero, O.A., DiVito, M.M., Adikes, R.C., Kortan, M.B., Case, L.B., Lier, A.J., Panaretos, N.S., Slater, S.Q., Rengarajan, M., Feliu, M*., et al.* (2009). Human Myo19 is a novel myosin that associates with mitochondria. Current biology : CB *19*, 2008-2013.
Quintyne, N.J., Reing, J.E., Hoffelder, D.R., Gollin, S.M., and Saunders, W.S. (2005). Spindle multipolarity is prevented by centrosomal clustering. Science *307*, 127-129.
Rappsilber, J., Ishihama, Y., and Mann, M. (2003). Stop and go extraction tips for matrix-assisted laser desorption/ionization, nanoelectrospray, and LC/MS sample pretreatment in proteomics. Anal Chem *75*, 663-670.
Rattner, J.B., Sciore, P., Ou, Y., van der Hoorn, F.A., and Lo, I.K. (2010). Primary cilia in fibroblast-like type B synoviocytes lie within a cilium pit: a site of endocytosis. Histol Histopathol *25*, 865-875.
Richards, T.A., and Cavalier-Smith, T. (2005). Myosin domain evolution and the primary divergence of eukaryotes. Nature *436*, 1113-1118.
Riley, T., Sontag, E., Chen, P., and Levine, A. (2008). Transcriptional control of human p53-regulated genes. Nature reviews Molecular cell biology *9*, 402-412.
Rodier, F., and Campisi, J. (2011). Four faces of cellular senescence. The Journal of cell biology *192*, 547-556.
Rodier, F., Coppe, J.P., Patil, C.K., Hoeijmakers, W.A., Munoz, D.P., Raza, S.R., Freund, A., Campeau, E., Davalos, A.R., and Campisi, J. (2009). Persistent DNA damage signalling triggers senescence-associated inflammatory cytokine secretion. Nature cell biology *11*, 973-979.
Rodier, F., Munoz, D.P., Teachenor, R., Chu, V., Le, O., Bhaumik, D., Coppe, J.P., Campeau, E., Beausejour, C.M., Kim, S.H*., et al.* (2011). DNA-SCARS: distinct nuclear structures that sustain damage-induced senescence growth arrest and inflammatory cytokine secretion. Journal of cell science *124*, 68-81.
Rodrigues-Martins, A., Riparbelli, M., Callaini, G., Glover, D.M., and Bettencourt-Dias, M. (2007). Revisiting the role of the mother centriole in centriole biogenesis. Science *316*, 1046-1050.

Rogakou, E.P., Pilch, D.R., Orr, A.H., Ivanova, V.S., and Bonner, W.M. (1998). DNA double-stranded breaks induce histone H2AX phosphorylation on serine 139. The Journal of biological chemistry *273*, 5858-5868.
Rogat, A.D., and Miller, K.G. (2002). A role for myosin VI in actin dynamics at sites of membrane remodeling during Drosophila spermatogenesis. Journal of cell science *115*, 4855-4865.
Sahlender, D.A., Roberts, R.C., Arden, S.D., Spudich, G., Taylor, M.J., Luzio, J.P., Kendrick-Jones, J., and Buss, F. (2005). Optineurin links myosin VI to the Golgi complex and is involved in Golgi organization and exocytosis. The Journal of cell biology *169*, 285-295.
Saladino, C., Bourke, E., Conroy, P.C., and Morrison, C.G. (2009). Centriole separation in DNA damage-induced centrosome amplification. Environ Mol Mutagen *50*, 725-732.
Salisbury, J.L. (2003). Centrosomes: coiled-coils organize the cell center. Current biology : CB *13*, R88-90.
Salpingidou, G., Smertenko, A., Hausmanowa-Petrucewicz, I., Hussey, P.J., and Hutchison, C.J. (2007). A novel role for the nuclear membrane protein emerin in association of the centrosome to the outer nuclear membrane. The Journal of cell biology *178*, 897-904.
Sancar, A., Lindsey-Boltz, L.A., Unsal-Kacmaz, K., and Linn, S. (2004). Molecular mechanisms of mammalian DNA repair and the DNA damage checkpoints. Annu Rev Biochem *73*, 39-85.
Sarraf, S.A., Raman, M., Guarani-Pereira, V., Sowa, M.E., Huttlin, E.L., Gygi, S.P., and Harper, J.W. (2013). Landscape of the PARKIN-dependent ubiquitylome in response to mitochondrial depolarization. Nature *496*, 372-376.
Satir, P., Pedersen, L.B., and Christensen, S.T. (2010). The primary cilium at a glance. Journal of cell science *123*, 499-503.
Sato, Y., Yoshikawa, A., Yamagata, A., Mimura, H., Yamashita, M., Ookata, K., Nureki, O., Iwai, K., Komada, M., and Fukai, S. (2008). Structural basis for specific cleavage of Lys 63-linked polyubiquitin chains. Nature *455*, 358-362.
Savio, M.G., Wollscheid, N., Cavallaro, E., Algisi, V., Di Fiore, P.P., Sigismund, S., Maspero, E., and Polo, S. (2016). USP9X Controls EGFR Fate by Deubiquitinating the Endocytic Adaptor Eps15. Current biology : CB *26*, 173-183.
Schmidt, T.I., Kleylein-Sohn, J., Westendorf, J., Le Clech, M., Lavoie, S.B., Stierhof, Y.D., and Nigg, E.A. (2009). Control of centriole length by CPAP and CP110. Current biology : CB *19*, 1005-1011.
Schnerch, D., and Nigg, E.A. (2016). Structural centrosome aberrations favor proliferation by abrogating microtubule-dependent tissue integrity of breast epithelial mammospheres. Oncogene *35*, 2711-2722.
Schockel, L., Mockel, M., Mayer, B., Boos, D., and Stemmann, O. (2011). Cleavage of cohesin rings coordinates the separation of centrioles and chromatids. Nature cell biology *13*, 966-972.
Schultz, D.C., Ayyanathan, K., Negorev, D., Maul, G.G., and Rauscher, F.J., 3rd (2002). SETDB1: a novel KAP-1-associated histone H3, lysine 9-specific methyltransferase that contributes to HP1-mediated silencing of euchromatic genes by KRAB zinc-finger proteins. Genes & development *16*, 919-932.
Seki, A., Coppinger, J.A., Jang, C.Y., Yates, J.R., and Fang, G. (2008). Bora and the kinase Aurora a cooperatively activate the kinase Plk1 and control mitotic entry. Science *320*, 1655-1658.
Self, T., Sobe, T., Copeland, N.G., Jenkins, N.A., Avraham, K.B., and Steel, a.K.P. (1999). Role of Myosin VI in the Differentiation of Cochlear Hair Cells. Developmental biology *214*, 331-341.

Seo, M.Y., Jang, W., and Rhee, K. (2015). Integrity of the Pericentriolar Material Is Essential for Maintaining Centriole Association during M Phase. PloS one *10*, e0138905.
Serrano, M., Lin, A.W., McCurrach, M.E., Beach, D., and Lowe, S.W. (1997). Oncogenic ras provokes premature cell senescence associated with accumulation of p53 and p16INK4a. Cell *88*, 593-602.
Shay, J.W., Porter, K.R., and Prescott, D.M. (1974). The surface morphology and fine structure of CHO (Chinese hamster ovary) cells following enucleation. Proceedings of the National Academy of Sciences of the United States of America *71*, 3059-3063.
Shevchenko, A., Wilm, M., Vorm, O., and Mann, M. (1996). Mass spectrometric sequencing of proteins silver-stained polyacrylamide gels. Anal Chem *68*, 850-858.
Shieh, S.Y., Ikeda, M., Taya, Y., and Prives, C. (1997). DNA damage-induced phosphorylation of p53 alleviates inhibition by MDM2. Cell *91*, 325-334.
Shurety, W., and Luzio, J.P. (1995). Differential modulation of apical and basolateral endocytosis in Caco-2 cells. Biochemical Society transactions *23*, 184S.
Silkworth, W.T., Nardi, I.K., Scholl, L.M., and Cimini, D. (2009). Multipolar spindle pole coalescence is a major source of kinetochore mis-attachment and chromosome mis-segregation in cancer cells. PloS one *4*, e6564.
Sillibourne, J.E., Tack, F., Vloemans, N., Boeckx, A., Thambirajah, S., Bonnet, P., Ramaekers, F.C., Bornens, M., and Grand-Perret, T. (2010). Autophosphorylation of polo-like kinase 4 and its role in centriole duplication. Mol Biol Cell *21*, 547-561.
Singla, V., Romaguera-Ros, M., Garcia-Verdugo, J.M., and Reiter, J.F. (2010). Ofd1, a human disease gene, regulates the length and distal structure of centrioles. Developmental cell *18*, 410-424.
Sladitschek, H.L., and Neveu, P.A. (2015). MXS-Chaining: A Highly Efficient Cloning Platform for Imaging and Flow Cytometry Approaches in Mammalian Systems. PloS one *10*, e0124958.
Song, M.S., Song, S.J., Kim, S.Y., Oh, H.J., and Lim, D.S. (2008). The tumour suppressor RASSF1A promotes MDM2 self-ubiquitination by disrupting the MDM2-DAXX-HAUSP complex. EMBO J *27*, 1863-1874.
Sonnen, K.F., Schermelleh, L., Leonhardt, H., and Nigg, E.A. (2012). 3D-structured illumination microscopy provides novel insight into architecture of human centrosomes. Biology open *1*, 965-976.
Sorokin, S. (1962). Centrioles and the formation of rudimentary cilia by fibroblasts and smooth muscle cells. The Journal of cell biology *15*, 363-377.
Sorokin, S.P. (1968). Reconstructions of centriole formation and ciliogenesis in mammalian lungs. Journal of cell science *3*, 207-230.
Spassky, N., and Meunier, A. (2017). The development and functions of multiciliated epithelia. Nature reviews Molecular cell biology *18*, 423-436.
Spink, B.J., Sivaramakrishnan, S., Lipfert, J., Doniach, S., and Spudich, J.A. (2008). Long single alpha-helical tail domains bridge the gap between structure and function of myosin VI. Nature structural & molecular biology *15*, 591-597.
Splinter, D., Tanenbaum, M.E., Lindqvist, A., Jaarsma, D., Flotho, A., Yu, K.L., Grigoriev, I., Engelsma, D., Haasdijk, E.D., Keijzer, N*., et al.* (2010). Bicaudal D2, dynein, and kinesin-1 associate with nuclear pore complexes and regulate centrosome and nuclear positioning during mitotic entry. PLoS Biol *8*, e1000350.
Spudich, G., Chibalina, M.V., Au, J.S., Arden, S.D., Buss, F., and Kendrick-Jones, J. (2007). Myosin VI targeting to clathrin-coated structures and dimerization is mediated by binding to Disabled-2 and PtdIns(4,5)P2. Nature cell biology *9*, 176-183.

Srsen, V., Gnadt, N., Dammermann, A., and Merdes, A. (2006). Inhibition of centrosome protein assembly leads to p53-dependent exit from the cell cycle. The Journal of cell biology *174*, 625-630.
Starr, D.A. (2009). A nuclear-envelope bridge positions nuclei and moves chromosomes. Journal of cell science *122*, 577-586.
Stowe, T.R., Wilkinson, C.J., Iqbal, A., and Stearns, T. (2012). The centriolar satellite proteins Cep72 and Cep290 interact and are required for recruitment of BBS proteins to the cilium. Mol Biol Cell *23*, 3322-3335.
Strnad, P., Leidel, S., Vinogradova, T., Euteneuer, U., Khodjakov, A., and Gonczy, P. (2007). Regulated HsSAS-6 levels ensure formation of a single procentriole per centriole during the centrosome duplication cycle. Developmental cell *13*, 203-213.
Stroud, M.J., Nazgiewicz, A., McKenzie, E.A., Wang, Y., Kammerer, R.A., and Ballestrem, C. (2014). GAS2-like proteins mediate communication between microtubules and actin through interactions with end-binding proteins. Journal of cell science *127*, 2672-2682.
Stucke, V.M., Sillje, H.H., Arnaud, L., and Nigg, E.A. (2002). Human Mps1 kinase is required for the spindle assembly checkpoint but not for centrosome duplication. EMBO J *21*, 1723-1732.
Sulli, G., Di Micco, R., and d'Adda di Fagagna, F. (2012). Crosstalk between chromatin state and DNA damage response in cellular senescence and cancer. Nature reviews Cancer *12*, 709-720.
Swiatecka-Urban, A., Boyd, C., Coutermarsh, B., Karlson, K.H., Barnaby, R., Aschenbrenner, L., Langford, G.M., Hasson, T., and Stanton, B.A. (2004). Myosin VI regulates endocytosis of the cystic fibrosis transmembrane conductance regulator. The Journal of biological chemistry *279*, 38025-38031.
Szalai, P., Hagen, L.K., Saetre, F., Luhr, M., Sponheim, M., Overbye, A., Mills, I.G., Seglen, P.O., and Engedal, N. (2015). Autophagic bulk sequestration of cytosolic cargo is independent of LC3, but requires GABARAPs. Exp Cell Res *333*, 21-38.
Takenaka, K., Moriguchi, T., and Nishida, E. (1998). Activation of the protein kinase p38 in the spindle assembly checkpoint and mitotic arrest. Science *280*, 599-602.
Takizawa, P.A., and Vale, R.D. (2000). The myosin motor, Myo4p, binds Ash1 mRNA via the adapter protein, She3p. Proceedings of the National Academy of Sciences of the United States of America *97*, 5273-5278.
Tang, C.J., Fu, R.H., Wu, K.S., Hsu, W.B., and Tang, T.K. (2009). CPAP is a cell-cycle regulated protein that controls centriole length. Nature cell biology *11*, 825-831.
Tang, H.W., Wang, Y.B., Wang, S.L., Wu, M.H., Lin, S.Y., and Chen, G.C. (2011). Atg1-mediated myosin II activation regulates autophagosome formation during starvation-induced autophagy. EMBO J *30*, 636-651.
Tang, Z., Lin, M.G., Stowe, T.R., Chen, S., Zhu, M., Stearns, T., Franco, B., and Zhong, Q. (2013). Autophagy promotes primary ciliogenesis by removing OFD1 from centriolar satellites. Nature *502*, 254-257.
Terada, Y., Uetake, Y., and Kuriyama, R. (2003). Interaction of Aurora-A and centrosomin at the microtubule-nucleating site in Drosophila and mammalian cells. The Journal of cell biology *162*, 757-763.
Terrak, M., Rebowski, G., Lu, R.C., Grabarek, Z., and Dominguez, R. (2005). Structure of the light chain-binding domain of myosin V. Proceedings of the National Academy of Sciences of the United States of America *102*, 12718-12723.
Timms, R.T., Tchasovnikarova, I.A., Antrobus, R., Dougan, G., and Lehner, P.J. (2016). ATF7IP-Mediated Stabilization of the Histone Methyltransferase SETDB1 Is Essential for Heterochromatin Formation by the HUSH Complex. Cell reports *17*, 653-659.

Tokuo, H., Mabuchi, K., and Ikebe, M. (2007). The motor activity of myosin-X promotes actin fiber convergence at the cell periphery to initiate filopodia formation. The Journal of cell biology *179*, 229-238.
Tollenaere, M.A., Mailand, N., and Bekker-Jensen, S. (2015). Centriolar satellites: key mediators of centrosome functions. Cellular and molecular life sciences : CMLS *72*, 11-23.
Tomatis, V.M., Papadopulos, A., Malintan, N.T., Martin, S., Wallis, T., Gormal, R.S., Kendrick-Jones, J., Buss, F., and Meunier, F.A. (2013). Myosin VI small insert isoform maintains exocytosis by tethering secretory granules to the cortical actin. The Journal of cell biology *200*, 301-320.
Tsou, M.F., Wang, W.J., George, K.A., Uryu, K., Stearns, T., and Jallepalli, P.V. (2009). Polo kinase and separase regulate the mitotic licensing of centriole duplication in human cells. Developmental cell *17*, 344-354.
Tumbarello, D.A., Kendrick-Jones, J., and Buss, F. (2013). Myosin VI and its cargo adaptors - linking endocytosis and autophagy. Journal of cell science *126*, 2561-2570.
Tumbarello, D.A., Manna, P.T., Allen, M., Bycroft, M., Arden, S.D., Kendrick-Jones, J., and Buss, F. (2015). The Autophagy Receptor TAX1BP1 and the Molecular Motor Myosin VI Are Required for Clearance of Salmonella Typhimurium by Autophagy. PLoS Pathog *11*, e1005174.
Tumbarello, D.A., Waxse, B.J., Arden, S.D., Bright, N.A., Kendrick-Jones, J., and Buss, F. (2012). Autophagy receptors link myosin VI to autophagosomes to mediate Tom1-dependent autophagosome maturation and fusion with the lysosome. Nature cell biology *14*, 1024-1035.
Tyska, M.J., and Warshaw, D.M. (2002). The Myosin Power Stroke. Cell motility and the cytoskeleton *51*, 1–15.
Uetake, Y., Loncarek, J., Nordberg, J.J., English, C.N., La Terra, S., Khodjakov, A., and Sluder, G. (2007). Cell cycle progression and de novo centriole assembly after centrosomal removal in untransformed human cells. The Journal of cell biology *176*, 173-182.
Valdembri, D., Caswell, P.T., Anderson, K.I., Schwarz, J.P., Konig, I., Astanina, E., Caccavari, F., Norman, J.C., Humphries, M.J., Bussolino, F.*, et al.* (2009). Neuropilin-1/GIPC1 signaling regulates alpha5beta1 integrin traffic and function in endothelial cells. PLoS Biol *7*, e25.
Varsano, T., Dong, M.Q., Niesman, I., Gacula, H., Lou, X., Ma, T., Testa, J.R., Yates, J.R., 3rd, and Farquhar, M.G. (2006). GIPC is recruited by APPL to peripheral TrkA endosomes and regulates TrkA trafficking and signaling. Molecular and cellular biology *26*, 8942-8952.
Villumsen, B.H., Danielsen, J.R., Povlsen, L., Sylvestersen, K.B., Merdes, A., Beli, P., Yang, Y.G., Choudhary, C., Nielsen, M.L., Mailand, N.*, et al.* (2013). A new cellular stress response that triggers centriolar satellite reorganization and ciliogenesis. EMBO J *32*, 3029-3040.
Vousden, K.H., and Ryan, K.M. (2009). p53 and metabolism. Nature reviews Cancer *9*, 691-700.
Vreugde, S., Ferrai, C., Miluzio, A., Hauben, E., Marchisio, P.C., Crippa, M.P., Bussi, M., and Biffo, S. (2006). Nuclear myosin VI enhances RNA polymerase II-dependent transcription. Molecular cell *23*, 749-755.
Vulprecht, J., David, A., Tibelius, A., Castiel, A., Konotop, G., Liu, F., Bestvater, F., Raab, M.S., Zentgraf, H., Izraeli, S.*, et al.* (2012). STIL is required for centriole duplication in human cells. Journal of cell science *125*, 1353-1362.
Wagner, W., Brenowitz, S.D., and Hammer, J.A., 3rd (2011). Myosin-Va transports the endoplasmic reticulum into the dendritic spines of Purkinje neurons. Nature cell biology *13*, 40-48.
Wang, G., Chen, Q., Zhang, X., Zhang, B., Zhuo, X., Liu, J., Jiang, Q., and Zhang, C. (2013). PCM1 recruits Plk1 to the pericentriolar matrix to promote primary cilia disassembly before mitotic entry. Journal of cell science *126*, 1355-1365.

Wang, H., An, W., Cao, R., Xia, L., Erdjument-Bromage, H., Chatton, B., Tempst, P., Roeder, R.G., and Zhang, Y. (2003). mAM facilitates conversion by ESET of dimethyl to trimethyl lysine 9 of histone H3 to cause transcriptional repression. Molecular cell *12*, 475-487.
Wang, H., Wang, B., Zhu, W., and Yang, Z. (2015a). Lentivirus-Mediated Knockdown of Myosin VI Inhibits Cell Proliferation of Breast Cancer Cell. Cancer Biother Radiopharm *30*, 330-335.
Wang, W.J., Acehan, D., Kao, C.H., Jane, W.N., Uryu, K., and Tsou, M.F. (2015b). De novo centriole formation in human cells is error-prone and does not require SAS-6 self-assembly. eLife *4*.
Wang, W.J., Soni, R.K., Uryu, K., and Tsou, M.F. (2011). The conversion of centrioles to centrosomes: essential coupling of duplication with segregation. The Journal of cell biology *193*, 727-739.
Wang, X., Taplick, J., Geva, N., and Oren, M. (2004). Inhibition of p53 degradation by Mdm2 acetylation. FEBS Lett *561*, 195-201.
Wang, Z., Edwards, J.G., Riley, N., Provance, D.W., Jr., Karcher, R., Li, X.D., Davison, I.G., Ikebe, M., Mercer, J.A., Kauer, J.A.*, et al.* (2008). Myosin Vb mobilizes recycling endosomes and AMPA receptors for postsynaptic plasticity. Cell *135*, 535-548.
Wang, Z., Ying, M., Wu, Q., Wang, R., and Li, Y. (2016). Overexpression of myosin VI regulates gastric cancer cell progression. Gene *593*, 100-109.
Warner, C.L., Stewart, A., Luzio, J.P., Steel, K.P., Libby, R.T., Kendrick-Jones, J., and Buss, F. (2003). Loss of myosin VI reduces secretion and the size of the Golgi in fibroblasts from Snell's waltzer mice. The EMBO journal *22*, 569-579.
Waxse, B.J., Sengupta, P., Hesketh, G.G., Lippincott-Schwartz, J., and Buss, F. (2017). Myosin VI facilitates connexin 43 gap junction accretion. Journal of cell science *130*, 827-840.
Weber, J.D., Taylor, L.J., Roussel, M.F., Sherr, C.J., and Bar-Sagi, D. (1999). Nucleolar Arf sequesters Mdm2 and activates p53. Nature cell biology *1*, 20-26.
Wells, A.L., Lin, A.W., Chen, L.-Q., Safer, D., Cain, S.M., Hasson, T., Carragher, B.O., Milligan, R.A., and Sweeney, H.L. (1999). Myosin VI is an actin-based motor that moves backwards. Nature *401*.
Westermann, S., and Weber, K. (2003). Post-translational modifications regulate microtubule function. Nature reviews Molecular cell biology *4*, 938-947.
Wiese, C., and Zheng, Y. (2006). Microtubule nucleation: gamma-tubulin and beyond. Journal of cell science *119*, 4143-4153.
Winey, M., and O'Toole, E. (2014). Centriole structure. Philos Trans R Soc Lond B Biol Sci *369*.
Wollscheid, H.P., Biancospino, M., He, F., Magistrati, E., Molteni, E., Lupia, M., Soffientini, P., Rottner, K., Cavallaro, U., Pozzoli, U.*, et al.* (2016). Diverse functions of myosin VI elucidated by an isoform-specific alpha-helix domain. Nature structural & molecular biology *23*, 300-308.
Wong, C., and Stearns, T. (2003). Centrosome number is controlled by a centrosome-intrinsic block to reduplication. Nature cell biology *5*, 539-544.
Wong, S.Y., Seol, A.D., So, P.L., Ermilov, A.N., Bichakjian, C.K., Epstein, E.H., Jr., Dlugosz, A.A., and Reiter, J.F. (2009). Primary cilia can both mediate and suppress Hedgehog pathway-dependent tumorigenesis. Nat Med *15*, 1055-1061.
Wong, Y.L., Anzola, J.V., Davis, R.L., Yoon, M., Motamedi, A., Kroll, A., Seo, C.P., Hsia, J.E., Kim, S.K., Mitchell, J.W.*, et al.* (2015). Cell biology. Reversible centriole depletion with an inhibitor of Polo-like kinase 4. Science *348*, 1155-1160.
Woodruff, J.B., Wueseke, O., and Hyman, A.A. (2014). Pericentriolar material structure and dynamics. Philos Trans R Soc Lond B Biol Sci *369*.

Woolner, S., and Bement, W.M. (2009). Unconventional myosins acting unconventionally. Trends in cell biology *19*, 245-252.
Wu, X., Bowers, B., Rao, K., Wei, Q., and Hammer, J.A., 3rd (1998). Visualization of melanosome dynamics within wild-type and dilute melanocytes suggests a paradigm for myosin V function In vivo. The Journal of cell biology *143*, 1899-1918.
Xiong, Y., Hannon, G.J., Zhang, H., Casso, D., Kobayashi, R., and Beach, D. (1993). p21 is a universal inhibitor of cyclin kinases. Nature *366*, 701-704.
Xue, W., Zender, L., Miething, C., Dickins, R.A., Hernando, E., Krizhanovsky, V., Cordon-Cardo, C., and Lowe, S.W. (2007). Senescence and tumour clearance is triggered by p53 restoration in murine liver carcinomas. Nature *445*, 656-660.
Yang, G., Rosen, D.G., Zhang, Z., Bast, R.C., Jr., Mills, G.B., Colacino, J.A., Mercado-Uribe, I., and Liu, J. (2006a). The chemokine growth-regulated oncogene 1 (Gro-1) links RAS signaling to the senescence of stromal fibroblasts and ovarian tumorigenesis. Proceedings of the National Academy of Sciences of the United States of America *103*, 16472-16477.
Yang, J., Adamian, M., and Li, T. (2006b). Rootletin interacts with C-Nap1 and may function as a physical linker between the pair of centrioles/basal bodies in cells. Mol Biol Cell *17*, 1033-1040.
Yang, N.C., and Hu, M.L. (2005). The limitations and validities of senescence associated-beta-galactosidase activity as an aging marker for human foreskin fibroblast Hs68 cells. Exp Gerontol *40*, 813-819.
Ye, X., Zeng, H., Ning, G., Reiter, J.F., and Liu, A. (2014). C2cd3 is critical for centriolar distal appendage assembly and ciliary vesicle docking in mammals. Proceedings of the National Academy of Sciences of the United States of America *111*, 2164-2169.
Ye, X., Zerlanko, B., Zhang, R., Somaiah, N., Lipinski, M., Salomoni, P., and Adams, P.D. (2007). Definition of pRB- and p53-dependent and -independent steps in HIRA/ASF1a-mediated formation of senescence-associated heterochromatin foci. Molecular and cellular biology *27*, 2452-2465.
Yoshida, H., Cheng, W., Hung, J., Montell, D., Geisbrecht, E., Rosen, D., Liu, J., and Naora, H. (2004). Lessons from border cell migration in the Drosophila ovary: A role for myosin VI in dissemination of human ovarian cancer. Proceedings of the National Academy of Sciences of the United States of America *101*, 8144-8149.
You, W., Tan, G., Sheng, N., Gong, J., Yan, J., Chen, D., Zhang, H., and Wang, Z. (2016). Downregulation of myosin VI reduced cell growth and increased apoptosis in human colorectal cancer. Acta Biochim Biophys Sin (Shanghai) *48*, 430-436.
Yu, C., Feng, W., Wei, Z., Miyanoiri, Y., Wen, W., Zhao, Y., and Zhang, M. (2009). Myosin VI undergoes cargo-mediated dimerization. Cell *138*, 537-548.
Yu, H., Zhu, Z., Chang, J., Wang, J., and Shen, X. (2015). Lentivirus-Mediated Silencing of Myosin VI Inhibits Proliferation and Cell Cycle Progression in Human Lung Cancer Cells. Chemical biology & drug design.
Zalzali, H., Nasr, B., Harajly, M., Basma, H., Ghamloush, F., Ghayad, S., Ghanem, N., Evan, G.I., and Saab, R. (2015). CDK2 transcriptional repression is an essential effector in p53-dependent cellular senescence-implications for therapeutic intervention. Mol Cancer Res *13*, 29-40.
Zhang, Q., Ragnauth, C.D., Skepper, J.N., Worth, N.F., Warren, D.T., Roberts, R.G., Weissberg, P.L., Ellis, J.A., and Shanahan, C.M. (2005). Nesprin-2 is a multi-isomeric protein that binds lamin and emerin at the nuclear envelope and forms a subcellular network in skeletal muscle. Journal of cell science *118*, 673-687.
Zhang, W., Chan, H.M., Gao, Y., Poon, R., and Wu, Z. (2007). BS69 is involved in cellular senescence through the p53-p21Cip1 pathway. EMBO reports *8*, 952-958.

Zhang, X., Lei, K., Yuan, X., Wu, X., Zhuang, Y., Xu, T., Xu, R., and Han, M. (2009). SUN1/2 and Syne/Nesprin-1/2 complexes connect centrosome to the nucleus during neurogenesis and neuronal migration in mice. Neuron *64*, 173-187.
Zhang, Y., Wolf, G.W., Bhat, K., Jin, A., Allio, T., Burkhart, W.A., and Xiong, Y. (2003). Ribosomal protein L11 negatively regulates oncoprotein MDM2 and mediates a p53-dependent ribosomal-stress checkpoint pathway. Molecular and cellular biology *23*, 8902-8912.
Zhao, H., Zhu, L., Zhu, Y., Cao, J., Li, S., Huang, Q., Xu, T., Huang, X., Yan, X., and Zhu, X. (2013). The Cep63 paralogue Deup1 enables massive de novo centriole biogenesis for vertebrate multiciliogenesis. Nature cell biology *15*, 1434-1444.
Zilfou, J.T., and Lowe, S.W. (2009). Tumor suppressive functions of p53. Cold Spring Harbor perspectives in biology *1*, a001883.
Zitouni, S., Francia, M.E., Leal, F., Montenegro Gouveia, S., Nabais, C., Duarte, P., Gilberto, S., Brito, D., Moyer, T., Kandels-Lewis, S*., et al.* (2016). CDK1 Prevents Unscheduled PLK4-STIL Complex Assembly in Centriole Biogenesis. Current biology : CB *26*, 1127-1137.
Zorca, C.E., Kim, L.K., Kim, Y.J., Krause, M.R., Zenklusen, D., Spilianakis, C.G., and Flavell, R.A. (2015). Myosin VI regulates gene pairing and transcriptional pause release in T cells. Proceedings of the National Academy of Sciences of the United States of America *112*, E1587-1593.

Acknowledgment

I would like to thank Simona Polo for encouraging me in working on this challenging project, and for the energy that she constantly transmits to us.

My gratitude goes to all the members of the Polo's group, for the technical and moral help, for the discussions, and for the tea breaks. A special thanks to Elena Maspero, which is always present no matter what you need, a reagent, a suggestion or only ears that listen to you.

I would like to thank all the new friends that I met at the campus: life is easier if you have someone to sing with.

I am grateful to all my friends, with who I share talks and experiences, and who made this path easier.

My biggest thank goes to my family for having always supported me, and for being always interested in my work asking me "What did you discover?".

Il grazie più grande va alla mia famiglia per avermi sempre supportato, e per essersi interessata al mio lavoro chiedendomi "Cosa hai scoperto?".

I have to thank AIRC for the trust they put in supporting my project.

I would like also to thank the ENABLE team, for the wonderful and challenging experience.